



Nanocellulose based materials for Cell Culture

Megan Smyth

► To cite this version:

Megan Smyth. Nanocellulose based materials for Cell Culture. Chemical and Process Engineering. Université Grenoble Alpes, 2017. English. NNT : 2017GREAI027 . tel-01691100

HAL Id: tel-01691100

<https://theses.hal.science/tel-01691100>

Submitted on 23 Jan 2018

HAL is a multi-disciplinary open access archive for the deposit and dissemination of scientific research documents, whether they are published or not. The documents may come from teaching and research institutions in France or abroad, or from public or private research centers.

L'archive ouverte pluridisciplinaire **HAL**, est destinée au dépôt et à la diffusion de documents scientifiques de niveau recherche, publiés ou non, émanant des établissements d'enseignement et de recherche français ou étrangers, des laboratoires publics ou privés.

THÈSE

Pour obtenir le grade de

DOCTEUR DE LA COMMUNAUTE UNIVERSITE GRENOBLE ALPES

Spécialité : **2MGE : Matériaux, Mécanique, Génie civil, Electrochimie**

Arrêté ministériel : 25 mai 2016

Présentée par

Megan SMYTH

Thèse dirigée par **Julien BRAS**, Maître de Conférences, Grenoble-INP

préparée au sein du **Laboratoire de Genie des Procédés Papetiers**
dans l'**École Doctorale Ingénierie - Matériaux, Mécanique,**
Environnement, Énergétique, Procédés, Production (I-MEP2).

Matrice à base de nanocellulose pour croissance de cellules

Thèse soutenue publiquement le **27 Juin 2017**,
devant le jury composé de :

Pr. Catherine PICART

Professor de Grenoble-INP, Présidente

Pr. Kristin SYVERUD

Professor de NTNU, Rapporteur

Dr. Tanja ZIMMERMANN

Directeur de Recherche à EMPA, Rapporteur

Dr. Claire ROME

Maître de conférences de Grenoble Institut des Neurosciences, Examineur

Dr. Johan FOSTER

Professeur associé de Virginia Tech, Examineur



But the Hebrew word, the word Timsbel - 'Thou mayest' - that gives a choice.

It might be the most important word in the world.

That says the way is open.

John Steinbeck, *East of Eden*

To my parents and their unwavering support and encouragement

Acknowledgements

I have never thought I would have the opportunity to live abroad, let alone complete my thesis in a country that was not my own. Throughout my time in France I have developed relationships and friendships that will last a lifetime. I would like to take the time to thank a few of the numerous people who have made my life and research here successful.

First, I would like to thank my supervisors Julien Bras and Johan Foster for providing me with the opportunity to complete my thesis at LGP2, and teaching me about a material I have never heard about before - nanocellulose. Thank you Julien for assisting me in my move across the Atlantic Ocean, for being patient with me during my first months here during my acclimation to the life and culture here in France, and for providing support thereafter. To Johan, my fellow North American, for always being an email away in assisting me with whatever question I may have, and for teaching me the importance of telling a story in scientific writing. Without the both of you I would not have been able to gain the confidence and skills necessary to complete my Ph.D. research.

To Marie-Stella and Chris for being amazing stagiaires or interns and assisting me in completing research. I would not have been able to complete my thesis without the two of you, and you also taught me the importance of communication within scientific research. To Cécile for all of her assistance within the lab regarding the numerous experimental devices. To LabEx Tec21 for providing the funding for this scientific research (Investissements d'Avenir –grant agreement no. ANR-11-LABX-0030).

To Catherine Picart for allowing me to collaborate and conduct experiments at LMGP. Without this I would have never been able to discover how cells react to nanocellulose, and to all of my colleagues at LMGP, especially Antalya, Mirasbek, Vincent, and Paul. Thank you Carole for all of your valuable advice in regards to cell-based experiments, and your patience and encouragement.

Thank you to my fellow doctoral students at LGP2 for your support and kindness. Most importantly my fellow officemates in B120, Hippolyte, Erwan, and Charlène, for the conversations and laughter necessary to provide motivation during the hectic time that is Ph.D. studies. Without the three of you to commiserate and laugh together my time at LGP2 would not have been as wonderful as it was. Also to all of the other wonderful people who have provided me with friendship and kindness these past three years - Elsa, Marcos, Seema, Ara, Luis, Daniele, Carolina, and many more. Also, thank you to service technique and the administrative staff for helping me

with whatever I may need, and being patient when I attempted to communicate in French. Thank you for welcoming me into the LGP2 community.

I would like to thank the people outside of the lab who have made my life in France more enjoyable. To Bea and Rachel for always being wonderful friends who are always there for me (and Xabi). For travelling with me and discovering this continent that is so different from our own. You two have provided me with the friendship (and beers and wine) necessary to make it through this little thing called life in France. To all of my friends at home in the States and abroad for your continued friendship and support - Arlesa, Arielle, Alex, Alejandro, Alyssa, Ben, Solie, Sabrina, and many more. To Pascal, Clément, Chloé, and especially Lisa for welcoming me and providing me with familial support in France that I would have never imagined I would have when moving here. Your warmth and kindness, even if we do not speak the same language, has given me so much that words cannot express how thankful I am to all of you. To Quentin, who has provided me with so much these past two years. I never could have imagined I would have met a person like you when I got on the plane to come to France, and having you in my life has changed it for the better. It is difficult to put into words how much you meant to me during this time, and will continue to mean to me.

Finally, I would like to thank my family – Mom, Dad, Trent, Paige, Gramma, Pop-Pop, Grandma, Auntie Tish, Antho, Cassandra, Justin, Maddie, Marci, and everyone else. To Trent and Paige for being my favorite brother and sister, and not thinking I was crazy to leave the U.S. to study. To my grandparents for inspiring me to see the world and igniting my scientific curiosity. Most importantly to my parents for always encouraging me to achieve my dreams ever since I was a little girl; for never saying I could not do something. Thank you for being such supportive parents and cultivating a confidence within me since I was child to be able to do something as challenging as moving to a small city in the French Alpes without knowing a word of French. To always being a phone call away and continuing to reassure me whenever I got frustrated with either research or adjustment to French culture. All of the work in the following pages are dedicated to you two. Without your love and support this research would not exist.

Table of Contents

Scientific Communications	1
Abbreviations	3
 General Introduction	 7
 Chapter 1. Literature Review	 15
1. Current Trends of Biomaterials	17
2. Nanocellulose: Production, Characterization, and Applications	28
3. Tissue Engineering and Nanocellulose.....	50
4. Conclusions and Perspectives	73
 Chapter 2. Extraction and Process Analysis of High Aspect Ratio Cellulose Nanocrystals from Corn (<i>Zea mays</i>) Agricultural Residue	 99
 Chapter 3. Nanocellulose-Based Materials in Physiological Conditions	 131
1. Effect of Hydration on the Material and Mechanical Properties of Cellulose Nanocrystal-Alginate Composites	133
2. Characterization and Mechanical Properties of Ultraviolet Stimuli-Responsive Functionalized Cellulose Nanocrystal -Alginate Composites	165
3. Incorporation and Release of Bovine Serum Albumin from Cellulose Nanofiber Films for Growth Factor Release Applications	191
4. Mechanical Properties of Thin Cellulose Nanofiber Films in Liquid	211
 Chapter 4. The Influence of Nanocellulose on Stem Cell Behavior in Culture	 229
1. Modulation of Mechanical Properties of Cellulose Nanocrystal Composites for use in Stem Cell Culture	231
2. Tunable Structural and Mechanical Properties of Cellulose Nanofiber Substrates in Liquid for Stem Cell Culture	255
 Conclusions and Perspectives	 287
 Abstract – English Version	 297
Résumé -Version Française.....	311
Appendix A: Scientific Posters	325
Appendix B: Supplementary Materials and Methods	327

Scientific Communications

The scientific communications presented were conducted from 2014-2017 as a collaboration between three research units. Two based in Grenoble (France), Laboratoire de Génie des Procédés Papetiers (LGP2) and Laboratoire des Matériaux et du Génie Physique (LMGP), and Macromolecules and Interfaces Institute, Department of Materials Science & Engineering at Virginia Tech (USA). LGP2 is part of the LabEx Tec 21 (Investissements d'Avenir - grant agreement n°ANR-11-LABX-0030) and of the PolyNat Carnot Institut (Investissements d'Avenir - grant agreement n°ANR-11-CARN-030-01). LMGP is part of the LabEx Centre of Excellence of Multifunctional Architected Materials "CEMAM" (ANR 10-LABX-44-01). The author was financed by the LabEx Tec 21 (Investissements d'Avenir - grant agreement n°ANR-11-LABX-0030).

Scientific Publications

Megan Smyth, Araceli García, Chris Rader, E. Johan Foster, Julien Bras. *Extraction and characterization of cellulose nanocrystals from corn (Zea mays) agricultural residue*. **Industrial Crops and Products**. (2017).

Megan Smyth, Carole Fournier, Carlos Driemeier, Catherine Picart, E. Johan Foster, Julien Bras. *Tuning of Mechanical Properties of Cellulose Nanofiber Films in Aqueous Conditions for Cell Culture*. **Biomacromolecules**. (2017).

Megan Smyth, Julien Bras, Marie-Stella M'Bengue, Maxime Terrien, Catherine Picart, E. Johan Foster. *The effect of hydration on the material and mechanical properties of cellulose nanocrystal-alginate composites*. **Carbohydrate Polymers**. Under Revision.

Megan Smyth, Chris Rader, Julien Bras, E. Johan Foster. *Characterization and Mechanical Properties of Ultraviolet Stimuli-Responsive Functionalized Cellulose Nanocrystal Alginate Composites*. **Journal of Polymer Science**. Submitted.

Oral Communications

Megan Smyth, Carole Fournier, Catherine Picart, Johan Foster, Julien Bras. *The Potential of Nanocellulose for Cell Culture*. Glyco@Alps Morning Event. Grenoble, France. May 2017.

Megan Smyth, Johan Foster, Julien Bras. *A study of the effect of hydration on the mechanical properties of alginate-cellulose nanocrystal composites*. 2016 International Conference on Nanotechnology for Renewable Materials. Grenoble, France. June 2016.

Megan Smyth, Carole Fournier, Catherine Picart, Johan Foster, Julien Bras. *CELLDIFF: Stimuli Responsive Nanocellulose based Matrices for Differentiating Cell Growth*. 251st American Chemical Society National Meeting and Exposition. San Diego, California, United States. March 2016.

Megan Smyth, Johan Foster, Julien Bras. *New Nanocellulose Based Materials for Stem Cell Culture*. 2015 International Conference on Nanotechnology for Renewable Materials. Atlanta, Georgia, United States. June 2015.

Poster Communications

Megan Smyth, Carole Fournier, Carlos Driemeier, Catherine Picart, Johan Foster, Julien Bras. *Tuning of Mechanical Properties of Cellulose Nanofiber Films for Cell Culture*. 6th Seminar on Recent Advances in Cellulose Nanotechnology Research. Trondheim, Norway. October 2016. Poster Presentation.

Megan Smyth, Lisias Pereira Novo, Araceli Garcia, Julien Bras. *Comparison of cellulose nanocrystals properties extracted from agricultural residues*. 4th EPNOE International Polysaccharides Conference. October 2015. Warsaw, Poland. Poster Presentation.

Abbreviations

Chapter 1

IUPAC	International Union of Pure and Applied Chemistry	ClChCl	Chlorocholine Chloride
TGF- β	Transforming Growth Factor – Beta	EPTMAC	2,3-epoxypropyltrimethylammonium
PEG	Polyethylene Glycol	NaBr	Sodium Bromide
GF	Growth Factors	NaClO	Sodium Hypochlorite
ECM	Extracellular Matrix	NaClO ₂	Sodium Chlorite
M-Chain	β -D-mannouronate	HPMC	Hydroxypropyl Methylcellulose
G-Chain	α -L-gulonate	WAXD	Wide Angle X-Ray Diffraction
Chitin	poly(β -(1-4)-N-acetyl-d-glucosamine)	CNC-Ts	TEMPO-oxidized CNCs
GAGs	glycosaminoglycans	CPs	Cellulose Nanoparticles
BNC	Bacterial Nanocellulose	EO-EPI	1:1 Ethyleneoxide/Epichlorohydrin Co-Polymer
CNC	Cellulose Nanocrystals	UPy	Ureidopyrimidone
CNF	Cellulose Nanofibers, Cellulose Nanofibrils	Mebip	2,6-bis(1'-methylbenzimidazolyl) pyridine
BMP-2	Bone Morphogenic Protein-2	BSA	Bovine Serum Albumin
hEGF	Human Epidermal Growth Factor	ESCs	Embryonic Stem Cells
Cellobiose	D-glucopyranosyl- α -1,4-D-glucopyranose	iPSCs	Induced Pluripotent Stem Cells
NaOH	Sodium Hydroxide	MSCs	Mesenchymal Stem Cells
MFC	Microfibrillated Cellulose	RGD	Arginine-Lysine-Aspartic
DLS	Dynamic Light Scattering	PLA	Polylactic Acid
¹³ C NMR	13-Carbon Nuclear Magnetic Resonance	hMSCs	Human Mesenchymal Stem Cells
AFM	Atomic Force Microscopy	hDFCs	Human Dental Follicle Cells
SEM	Scanning Electron Microscopy	PLGA	poly(lactic-co-glycolic acid)
FEG-SEM	Field Emission SEM	FTTC	Fluorescein Isothiocyanate Conjugated
TEM	Transmission Electron Microscopy	PVA	Polyvinyl Alcohol
UV	Ultraviolet	P-CNCs	Phosphoric Acid Derived CNCs
XRD	X-Ray Diffraction	S-CNCs	Sulfuric Acid Derived CNCs
TEMPO	2,2,6,6-tetramethylpiperidine-1-oxyl radical	LDH	Lactate Dehydrogenase
DMA	Dynamic Mechanical Analysis	LPS	Lipopolysaccharide
GT	Girard's Reagent T, (2-hydrazinyl-2-oxoethyl)trimethylazanium chloride	MTT	Thiazolyl Blue Tetrazolium Bromide
		TMX	Thermanox ® Resistant Plastic
		CMF	Cellulose Macrofibers

Chapter 2

CNCs	Cellulose Nanocrystals
m-CNCs	Maize CNCs
DLS	Dynamic Light Scattering
TGA	Thermogravimetric Analysis
XRD	X-Ray Diffraction
NREL	National Renewable Energy Laboratory
FTIR	Fourier Transform Infrared Spectroscopy
NaClO ₂	Sodium Chlorite
HCl	Hydrochloric Acid
NaOH	Sodium Chloride
C ₂ H ₆ O	Ethanol
H ₂ SO ₄	Sulfuric Acid
w-CNC	Wood CNCs
NR	Natural Rubber
DI-H ₂ O	Deionized Water
AFM	Atomic Force Microscopy
DMA	Dynamic Mechanical Analysis
PDI	Polydispersion Index
co-CNCs	Cotton CNCs
t-CNCs	Tunicate CNCs
s-CNCs	Sugarcane Bagasse CNCs
a-CNCs	Agave CNCs
b-CNC	Banana Psuedostems CNCs
br-CNCs	Barley CNCs

Chapter 3

CNCs	Cellulose Nanocrystals
CNC-Ts	TEMPO Oxidized CNCs
PBS	Phosphate Buffer Solution
M-Chain	β -D-mannuronate
G-Chain	α -L-guluronate
BC	Bacterial Cellulose
MFC	Microfibrillated Cellulose
CNF	Cellulose Nanofibers, Cellulose Nanofibrils
CaCl ₂	Calcium Chloride
D-PBS	Dubecco's Phosphate Buffer Solution
TEMPO	(2,2,6,6-tetramethylpiperidin-1-yl)oxyl
EDTA	Ethylenediaminetetraacetic Acid
NaOH	Sodium Hydroxide
AFM	Atomic Force Microscopy
XRD	X-Ray Diffraction
DI-H ₂ O	Deionized Water
UV-Vis	Ultraviolet-Visible
Ca ²⁺	Calcium Ions
Mg ²⁺	Magnesium Ions
UV	Ultraviolet
PA-g-CNCs	4-Pentenoic acid-g-CNCs
¹³ C NMR	13-Carbon Nuclear Magnetic Resonance
EDC	1-Ethyl-3-(3-dimethylaminopropyl)carbodiimide
NHS	N-Hydroxysuccinimide
EO-EPI	1:1 ethyleneoxide/epichlorohydrin copolymer
ACVA	4,4'-Azobis(4-cyanovaleric acid)
TGA	Thermogravimetric Analysis
BSA	Bovine Serum Albumin
BNC	Bacterial Nanocellulose
BCA	Bicinchoninic Acid
MSCs	Mesenchymal Stem Cells

α MEM Minimum Essential Eagle Medium
 DAPI 4,6-Diaminidino-2-phenylindole-dilactate
 Phalloidin phalloidintetramethylrhod B isothiocyanate
 AC-CNF As-cast CNF
 2hC-CNF 2 hour cured Cast CNF
 DMA Dynamic Mechanical Analysis

Chapter 4

CNCs Cellulose Nanocrystals
 CNC-Ts TEMPO-Oxidized CNCs
 MSCs Mesenchymal Stem Cells
 M-Chain β -D-mannuronate
 G-Chain α -L-guluronate
 TGF- β Transforming Growth Factor-Beta
 DMA Dynamic Mechanical Analysis
 CaCl₂ Calcium Chloride
 D-PBS Dubecco's Phosphate Buffer Solution
 TEMPO (2,2,6,6-tetramethylpiperidin-1-yl)oxyl
 α MEM Minimum Essential Eagle Medium
 Phalloidin phalloidintetramethylrhod B isothiocyanate dyes
 TBS Tris Buffer Saline
 MTT Thiazolyl Blue Tetrazolium Bromide
 DMSO Dimethyl Sulfoxide
 FBS Fetal Bovine Serum
 AFM Atomic Force Microscopy
 D1 MSCs BALB/c D1 Murine Mesenchymal Stem Cells
 DI-H₂O Deionized Water
 TCPS Tissue Culture Polystyrene
 CNF Cellulose Nanofibers, Cellulose Nanofibrils
 BNC Bacterial Nanocellulose
 PDMS Polydimethylsiloxane
 DAPI 4,6-Diaminidino-2-phenylindole-dilactate
 AC-CNF As-Cast CNF
 1hC-CNF 1 hour cured Cast CNF
 2hC-CNF 2 hour cured Cast CNF
 SEM Scanning Electron Microscopy
 DSC Differential Scanning Calorimetry
 TGA Thermogravimetric Analysis

General Introduction

A biocompatible material, or biomaterial, can be anything from a bandage to a three-dimensional scaffold for tissue engineering, or more precisely a biomaterial is any material that comes in contact with microorganisms, organisms, or living tissue according to the International Union of Pure and Applied Chemistry (IUPAC) [1]. Traditional biomaterials include metals, ceramics, and polymers. Recent interest has now turned to bio-sourced materials for a variety of reasons including biomimicry for use in tissue engineered constructs [2, 3] to sustainability and biocompatibility in the case of nanocellulose [4-6]. The interest in nanocellulose as a biomaterial has gained more interest in recent years with some very recent reviews covering the topic [4-6] and published during the course of Ph.D. research, but the use of nanocellulose as a biomaterial is still not widely used by researchers. Since the start of the 21st century, only less than 0.5% of published articles dedicated to biomaterials research the use of nanocellulose as seen in Figure 1.

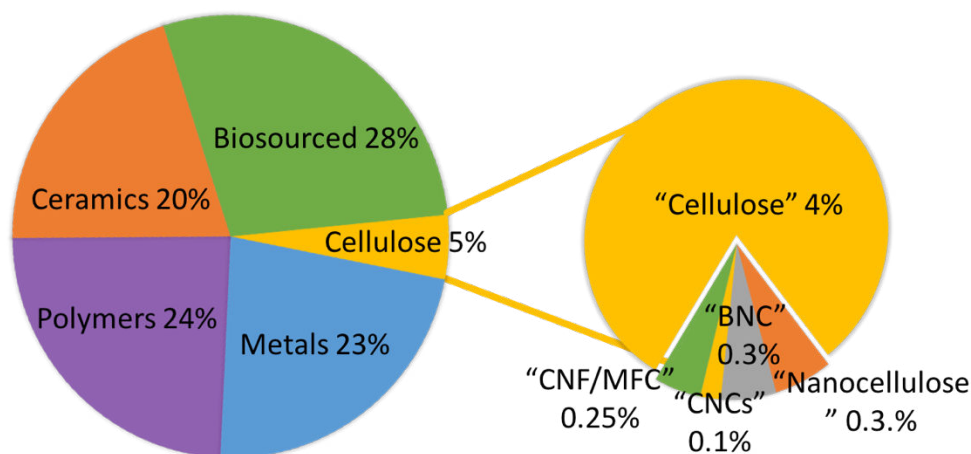


Figure 1. Number of publications from 2000-2017 with keywords “biomaterial” and cellulose= “cellulose,” “nanocellulose,” “bacterial nanocellulose” “cellulose nanocrystals,” “cellulose nanofibers,” “microfibrillated cellulose,” metal = “metal,” “titanium,” “magnesium,” “stainless steel,” “polymer,” ceramics = “ceramics,” “hydroxyapatite,” “bioglass,” biopolymer = “alginate,” “chitin,” “chitosan,” “collagen,” “fibrin,” and “fibronectin” on *SciFinder*

The biodegradability, biocompatibility, sustainability, and numerous functionalization or adsorption capabilities of nanocellulose makes it a promising biomaterial for the future, especially for tissue engineering applications.

Meanwhile, the use of cells in regenerative medicine has been one of the most promising advancements of the medical field in recent years and is more easily defined as tissue engineering. Tissue engineering usually requires the use of cells in combination with biomaterials. The cell and biomaterial choice by researchers are ultimately dependent on the final application of the tissue engineered construct. Some materials and cells are more suitable for bone regeneration, while others are more appropriate for soft-tissue repair or cell-based therapy. One of the most common types of cells used for tissue engineering is stem cells. While there are numerous types of stem cells; the main characteristics of stem cells are their ability to self-renew, differentiate, and are immortal *in vivo* [7]. Stem cells can have differing levels of potency or differentiation potential depending on the source. Differentiation is a process in which a stem cell changes its phenotype or function based on differential gene expression [8]. Differentiation of stem cells can be controlled through biomaterial design. Most commonly through topographical, chemical, and mechanical property modification. In seminal work by Engler et al. it was shown that the mechanical properties alone of a cell culture polymer substrate, without any other stimulation factors, could determine stem cell differentiation [9]. This finding was the basis of the thesis to determine if mechanically adaptive nanocellulose substrates could influence stem cells in a similar manner.

As stated previously the use of nanocellulose for biomedical applications, and more specifically tissue engineering or cell differentiation is minimal. Nanocellulose can be obtained through different sources which can impart differing characteristics depending on the source [10]. Nanocellulose can be grouped into three distinct families with differing characteristics: bacterial nanocellulose (BNC), cellulose nanocrystals (CNCs), and cellulose nanofibers (CNFs). The use of nanocellulose in biomedical applications in the past has focused on BNC, with more recent interest gaining in the use of vegetal-sourced nanocellulose. This focus on BNC can be attributed to the purity or lack of lignin or hemicellulose, high crystallinity, and controllable water content [11]. But a major drawback of BNC is the production requirements including time and material requirements which are not favorable for industrialization, but also the difficulty to process it in order to control or design the properties of the BNC [12].

Plant-based nanocellulose has many favorable properties which have been exploited by researchers including its barrier properties, high modulus, and environmental advantages such as being renewable, biodegradable, and biocompatible. Nanocellulos-based materials are available industrially and are thoroughly researched worldwide as shown by numerous books, reviews, conferences, articles (>1000

articles in 2016), and patents (4 per week in 2016). For this research project the significantly improved mechanical properties and chemical reactive surface of nanocellulose was considered to be advantageous to influence stem cell behavior in a systematic manner. The favorable mechanical properties of nanocellulose can be attributed to the hierarchical structure of plant fibers. This hierarchical structure of plant fibers starts from individual cellulose chains that are organized into cellulose fibers with highly reactive surfaces. These cellulose fibers consist of crystalline and amorphous regions, with the crystalline regions contributing to CNCs and the individual fibers consisting of CNFs. Bundled sets of cellulose fibers are present in the plant cell walls. Numerous plant cells then create plant fibers as seen in Figure 2. The characteristics of high mechanical properties and flexibility can be attributed to the crystalline, stiff regions and amorphous, elastic regions of the cellulose molecule. These properties are exploited in CNCs and CNFs. With CNCs being more rigid demonstrated by a theoretical Young's modulus being similar to Kevlar, and CNFs having more elastic properties and favoring entanglement in a nanoporous membrane [12].

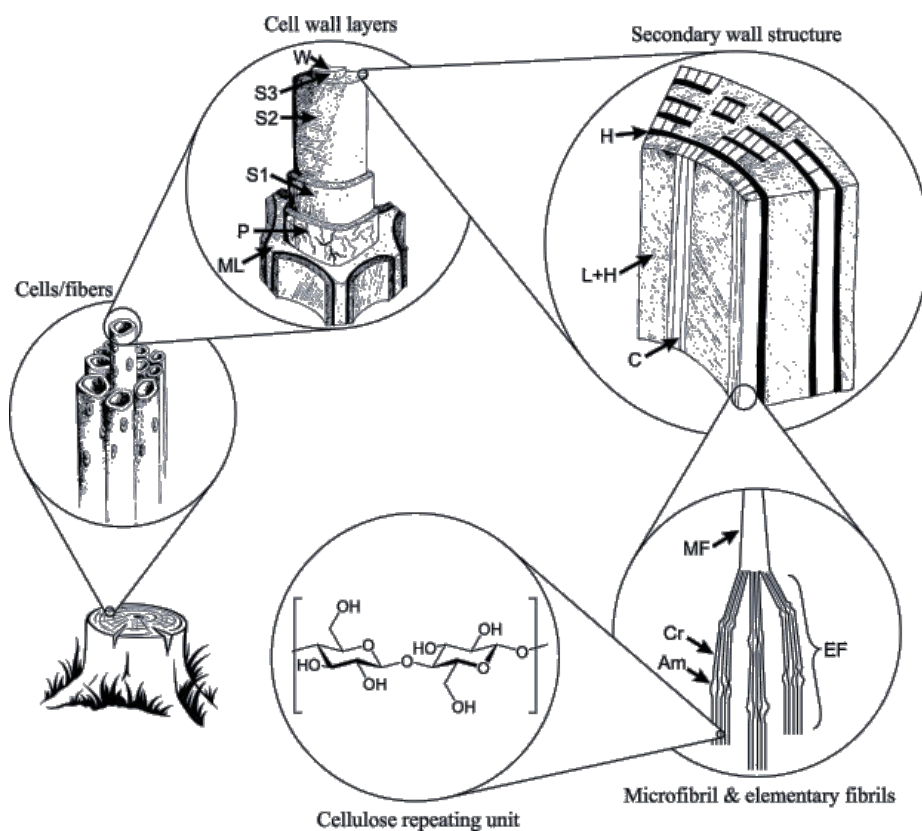


Figure 2. Hierarchical structure of plant fibers from cellulose chains [13]

Since nanocellulose is a well-known material for mechanical reinforcement, it was hypothesized that nanocellulose could be used to influence cell behavior necessary for stem cell differentiation, such as viability and attachment, without using extracellular factors such as growth factors, or non-renewable polymers. The use of nanocellulose for this specific biomedical application has not been thoroughly explored previously.

Because of mechanical and material properties of CNCs and CNFs, the present Ph.D. research entitled, *The use of Nanocellulose for Cell Culture*, was proposed as a collaboration between LGP2: Laboratory of Pulp and Paper Science and Graphic Arts in Grenoble, France and the Macromolecules and Interfaces Institute of the Department of Material Science and Engineering at Virginia Tech (USA) with collaboration with ERC Biomim at LMGP (Grenoble). Funding for this research was provided by the LabEx Tec 21 (Investissements d'Avenir - grant agreement n°ANR-11-LABX-0030). The main objective of this PhD was to provide a systematic way to carefully control the mechanics in a liquid state of a nanocellulose-based system for primary use in cell culture applications.

This objective was realized by employing the use of the two families of plant-based nanocellulose, CNCs and CNFs, and can be further characterized by the following:

1. Create a nanocomposite with CNCs and another renewable polymer with varying mechanical properties
2. Use green chemistry methods to produce a stimuli-responsive CNC-based nanocomposite in order to control the mechanical properties
3. Fabricate a CNF substrate with differing structural properties in order to control the release profile of a model protein for future growth factor release and/or to tailor the mechanical properties

In order to achieve these goals, the thesis has been divided into four chapters (Figure 3):

Chapter 1 is an extensive literature review focusing on the use of nanocellulose as a biocompatible material. The extraction of non-modified CNCs from agricultural waste, and CNF using enzymatic pre-treatment has been reviewed. As well as further functionalization and principles of the use of nanocellulose as nanocomposites, particle release carriers, and for use in stimuli-responsive materials. A special focus on the characteristics of stem cells and the use of nanocellulose for tissue engineering applications has been done.

Chapter 2 focuses on the production of high aspect ratio CNCs from a common agricultural waste product, maize husks which is based on a publication in Industrial Crops and Products.

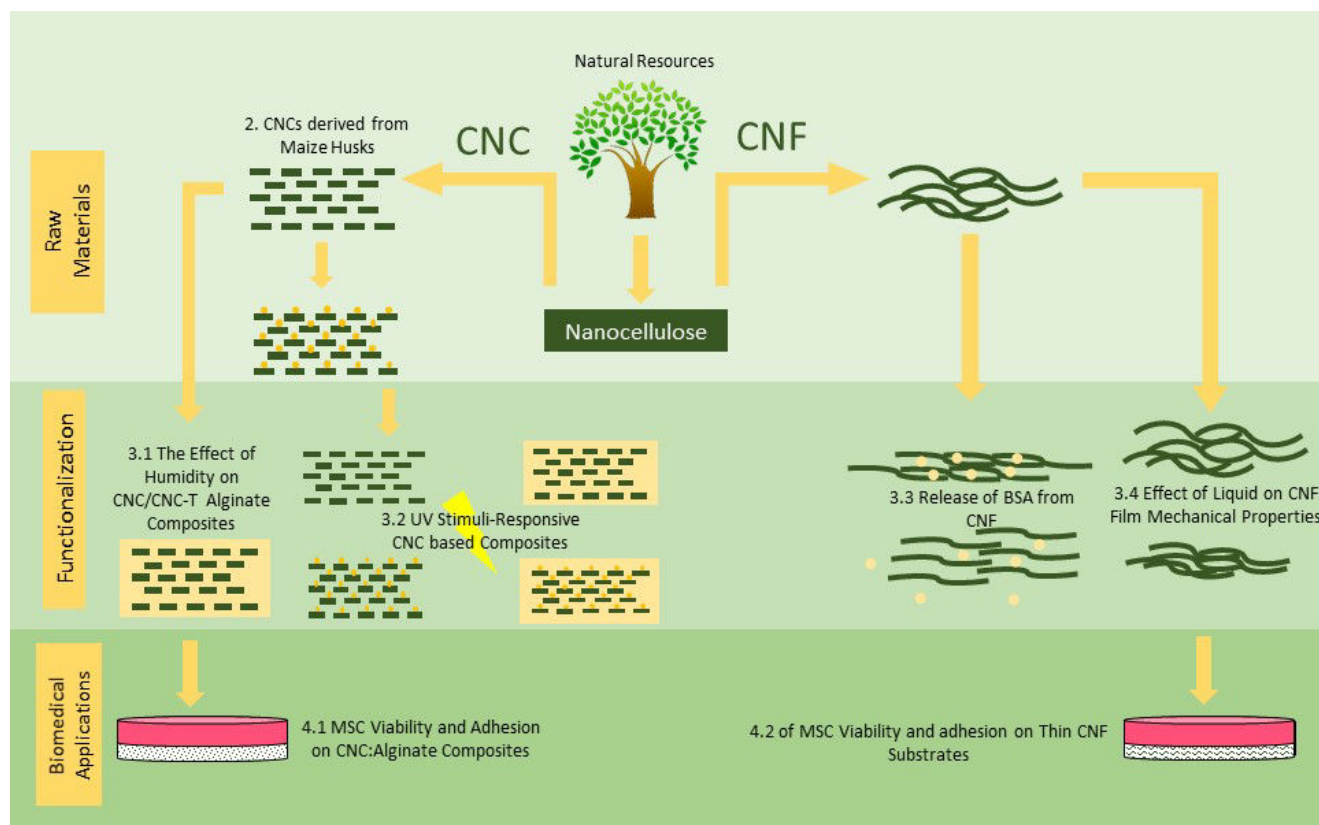


Figure 3. Schematic of chapter organization

Chapter 3 highlights the use of nanocellulose in functionalized materials. With **Chapter 3.1** detailing the creation and characterization of CNC-Alginate composites in physiological systems, the creation of a stimuli-responsive CNC-Alginate nanocomposite in **Chapter 3.2**, and the release of bovine serum albumin (BSA) from CNF in **Chapter 3.3**. **Chapter 3.4** is an introduction and proof of concept of the effect of liquid on the mechanical properties of CNF films.

The use of these nanocellulose systems and their influence on the behavior of stem cells is explored in detail in **Chapter 4**. The CNC-Alginate system developed and explained in Chapter 3.1 was used to determine if the addition of CNCs to alginate improved cell adhesion and viability of Mesenchymal stem cells (MSCs). A mechanically adaptive CNF-based substrate created through a simple curing process for use to modulate stem cell behavior will be presented as well.

This pluridisciplinary approach required research into specific topics which are presented and overviewed in **Chapter 1**. The research presented in this thesis illustrates many aspects of biomaterial design from the extraction of the raw material to creation of mechanically adaptive and functionalized materials and how they can possibly influence stem cell behavior in culture.

References

- [1] Vert M, Hellwich K-H, Hess M, Hodge P, Kubisa P, Rinaudo M, et al. Terminology for biorelated polymers and applications (IUPAC Recommendations 2012). *Pure and Applied Chemistry*. 2012;84:377-410.
- [2] Ma PX. Biomimetic materials for tissue engineering. *Advanced Drug Delivery Reviews*. 2008;60:184-98.
- [3] Shin H, Jo S, Mikos AG. Biomimetic materials for tissue engineering. *Biomaterials*. 2003;24:4353-64.
- [4] Lin N, Dufresne A. Nanocellulose in biomedicine: Current status and future prospect. *European Polymer Journal*. 2014;59:302-25.
- [5] Jorfi M, Foster EJ. Recent advances in nanocellulose for biomedical applications. *Journal of Applied Polymer Science*. 2015;132:41719.
- [6] Domingues RM, Gomes ME, Reis RL. The potential of cellulose nanocrystals in tissue engineering strategies. *Biomacromolecules*. 2014;15:2327-46.
- [7] Alberts B, Johnson A, Lewis J, Raff M, Roberts K, Walter P. *Molecular Biology of the Cell*. 4 ed. New York Garland Science; 2002.
- [8] Pålsson BØ, Bhatia SN. *Tissue Engineering*: Pearson Education; 2004.
- [9] Engler AJ, Sen S, Sweeney HL, Discher DE. Matrix elasticity directs stem cell lineage specification. *Cell*. 2006;126:677-89.
- [10] Siqueira G, Bras J, Dufresne A. Cellulose whiskers versus microfibrils: influence of the nature of the nanoparticle and its surface functionalization on the thermal and mechanical properties of nanocomposites. *Biomacromolecules*. 2008;10:425-32.
- [11] Klemm D, Heublein B, Fink HP, Bohn A. Cellulose: fascinating biopolymer and sustainable raw material. *Angewandte Chemie International Edition*. 2005;44:3358-93.
- [12] Dufresne A. *Nanocellulose: from nature to high performance tailored materials*: Walter de Gruyter; 2013.

[13] Nechyporchuk O, Belgacem MN, Bras J. Production of cellulose nanofibrils: A review of recent advances. *Industrial Crops and Products*. 2016.

Chapter 1. Literature Review

Chapter 1. Literature Review

1. Current Trends of Biomaterials	17
1.1 Ceramics	18
1.2 Metals	20
1.3 Polymers	20
1.4 Biosourced Materials	22
1.4.1 Collagen	22
1.4.2 Alginate	23
1.4.3 Chitin and Chitosan	23
1.4.4 Nanocellulose	25
2. Nanocellulose: Production, Characterization, and Applications	28
2.1 Production of Cellulose Nanocrystals and Cellulose Nanofibers	29
2.1.1 Cellulose Nanocrystal Production from Agrowaste	29
2.1.2 Production of Mechanically Homogenized and Enzymatically Pre-Treated Cellulose Nanofibers	31
2.2 Characterization of Nanocellulose	34
2.2.1 Morphological Characterization	34
2.2.2 Mechanical Properties of Nanocellulose	35
2.3 Nanocellulose Functionalization	38
2.3.1 TEMPO Mediated Oxidation of CNCs	40
2.3.2 Esterification of CNCs Using Green Chemistry	41
2.3.3 Functionalization for Nanocellulose-Based Composites	42
2.4 Nanocellulose-Based Composites	43
2.4.1 Nanocomposites with Biosourced Polymers	44
2.5 Applications of Functionalized Nanocellulose	47
2.5.1 CNCs in “Smart” or Stimuli-Responsive Materials	47
2.5.2 CNF Films as Controlled Release Systems	48
3. Tissue Engineering and Nanocellulose	50
3.1 Stem Cells: Types, Properties, and Differentiation	50
3.2 Cell Adhesion, Proliferation, and Differentiation with Biomaterials	54
3.3 Nanocellulose for Tissue Engineering	58
3.3.1 Cellulose Nanocrystals	58
3.3.2 Cellulose Nanofibers	64
4. Conclusions and Perspectives	73
5. Figures and Tables	74
6. References	76

1. Current Trends of Biomaterials

Biomaterials, also called biocompatible materials, are a relatively new field of study which is at the crossroads of chemistry, biology, material science, medicine, and engineering. Biomaterials are important factors in biomedical applications such as drug delivery, tissue engineering, and implantation [1]. While the definition of a biomaterial can differ among sources, it has been defined by Williams in 1987 as a material used in implants or devices, which interact with biological systems [2]. This definition has been updated by the International Union of Pure and Applied Chemistry (IUPAC) to: A biomaterial can be defined as any material that comes in contact with microorganisms, organisms, or living tissue in 2012 [3]. This definition encompasses a variety of materials ranging from polymers, ceramics, metals, and composites that come in contact with biological samples, as shown with some examples in Figure 1.1.

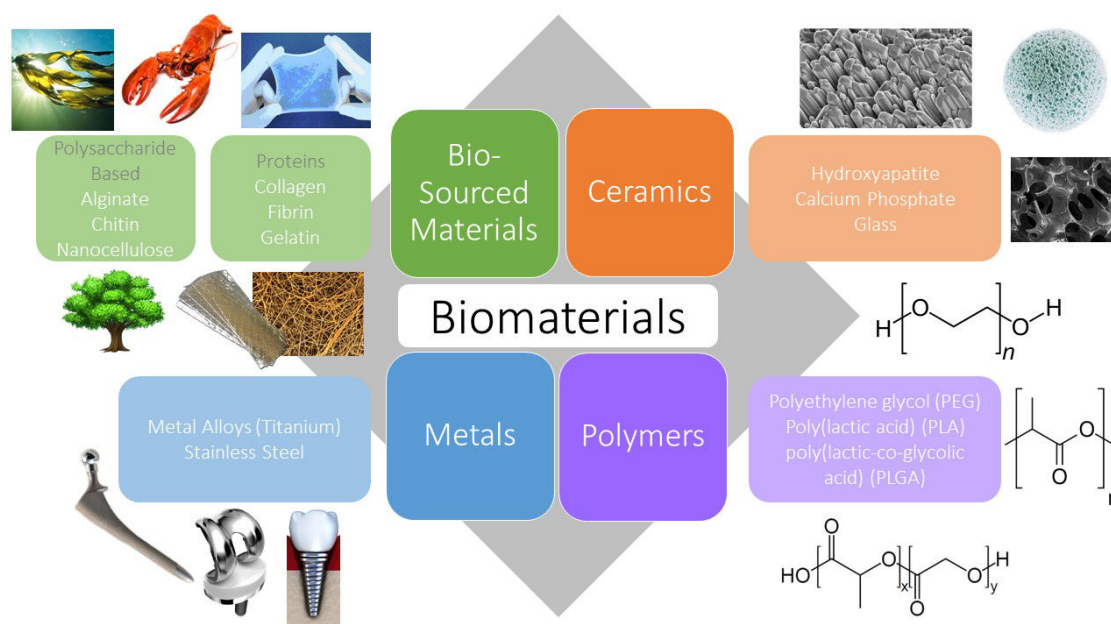


Figure 1.1 Scheme of different types of commonly used biomaterials

While the choice of biomaterial source depends on the final application, there are certain criteria that all biomaterials must have. One of the most important to be considered is biocompatibility. Biocompatibility can be defined as the ability of the material to perform within the host for a particular application as defined by Black and Hastings in 1998 [4]. Biocompatibility, or the standard of biocompatibility, can differ depending on the definition of biocompatibility; meaning that the surface biocompatibility can be acceptable for a biomaterial, but the mechanical or structural properties are

not biocompatible [5]. For a biomaterial to be completely biocompatible it must meet both of these standards. The performance of a device, or biomaterial, can depend greatly on the final application of the material. A device created for use in hip implantation will not have the same biocompatibility standards as a classic wound dressing. The biological response to a material can also be sometimes referred to as “bioreaction.” Common bioreactions include protein adsorption, bacterial adhesion, cell spreading, and apoptosis. These bioreactions can be correlated with the materials’ properties such as: surface chemistry, porosity, mechanical modulus, and swelling behavior [6].

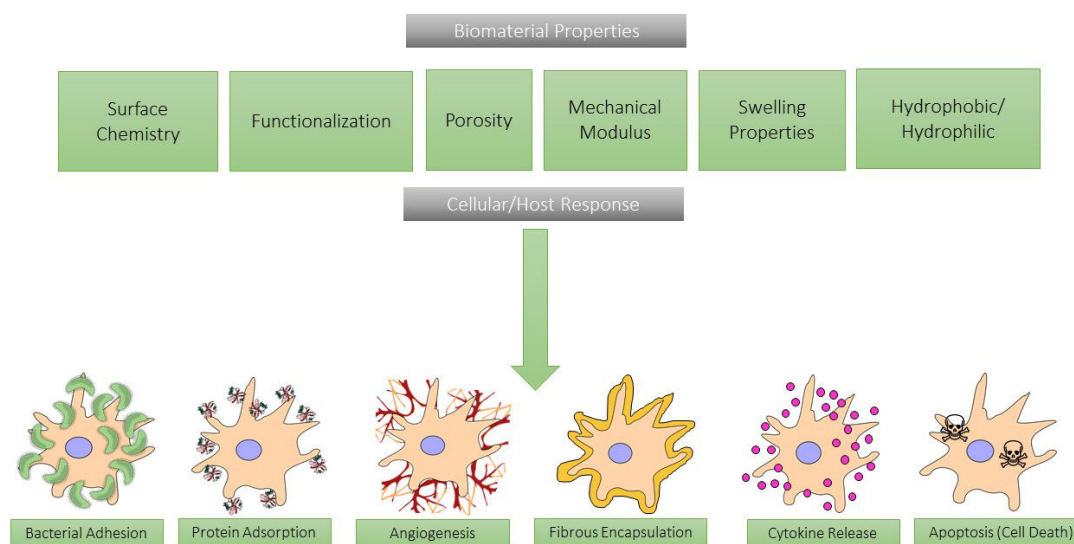


Figure 1.2. Cell or host response to physical biomaterial properties

A short overview of the different biomaterial properties and possible cell response are shown in Figure 1.2. Researchers must keep these properties in mind when developing a biomaterial.

1.1 Ceramics

The use of ceramics in biomedical applications is most widespread in orthopedics and dentistry as stated in the review by Thamaraiselvi et al. [7]. Ceramics as biomaterials can be classified into three distinct groups: bioinert, bioactive, or bioresorbable as defined by Dubok [8]. Bioinert ceramics are mainly used in implants that must withstand high mechanical pressure, while bioactive ceramics interact with the living tissue around and can induce bonds between the bone and the ceramic; bioresorbable are biodegraded by the metabolic system of the organism in which it is implanted [8]. The most commonly used ceramics in biomaterials are bioglasses and calcium based compounds which

include: calcium phosphates, calcium sulfate, and calcium carbonates. These materials are usually in the form of coatings, cement, granules, or powders. Calcium phosphates, such as hydroxyapatite, have been selected for use in biomedical applications in bone because of their presence in the natural process of bone remodeling and regeneration [9]. Bioglasses, in comparison, can either be silicate based, borate and borosilicate, or phosphate based and are usually in the form of a composite. Bioglass composites are an attractive tool for biomedical researchers for tissue engineering applications because they can be modified to fit the researchers need either chemically or via the manufacturing processes [10].

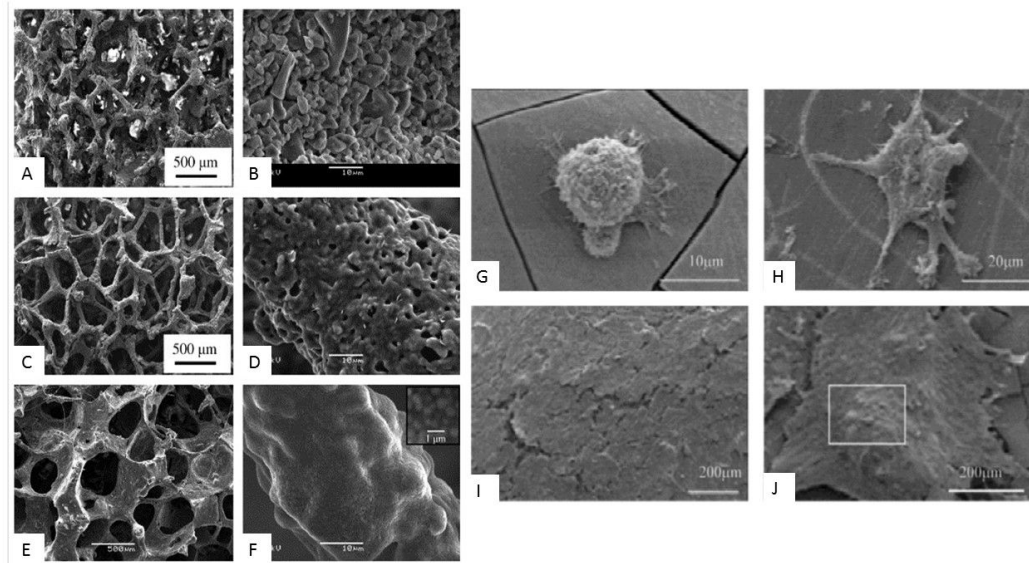


Figure 1.3. Pore structure and strut microstructure of 45S5 Bioglass®-derived foams from Chen et al. (A-F) [11] and SEM images of osteoblasts seeded on 45S5 Bioglass® at G) 2 , H) 6, and (I-J) 12 days with initial cell morphology being rounded at 2 days, extension of filopodia at 6 days, and cell sheet formation at 12 days [12]

For example, Chen et al. employed the use of 45S5 Bioglass® to create a biodegradable 3D scaffold for tissue engineering by sintering. This scaffold was highly crystalline, but became amorphous when exposed to simulated body fluid for 28 days. These results proved that bioglass can have tailorable mechanical properties by modulating the crystallinity of the sintered 45S5 Bioglass® [11]. Xynos and colleagues showed that *in vitro* seeded osteoblasts had a higher instance of maturation of osteoblasts and collagenous mineralization, which displays that bioglass can be used to stimulate growth and differentiation of human osteoblasts as indicated in Figure 1.3 [12].

1.2 Metals

Many implantable materials for orthopedic applications are composed of metals or metal alloys. The most commonly used are stainless steel, cobalt [6], titanium [13, 14], and magnesium [15] based alloys. Metals are usually chosen because of their high mechanical properties since they will be exposed to cyclic loading and cannot undergo biomechanical incompatibility. Biomechanical incompatibility can be defined as deficiencies in the mechanical properties of the material, and lack of integration between the implant and biological interface [13]. It has been shown that osteoblast response is dependent on the surface roughness of titanium based materials. Osteoblast differentiation was shown to increase on materials with higher surface roughness because of higher alkaline phosphate production and other indicators of differentiation such as lower proliferation and production of local growth factors like transforming growth factor-beta (TGF- β) as seen in Figure 1.4 [16].

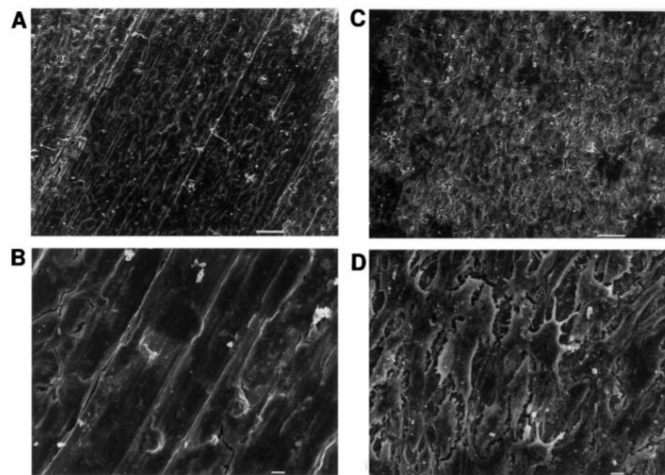


Figure 1.4. SEM images of osteoblasts cultured on A, B) rough titanium surface and C, D) smooth titanium after 24 hours. Rough titanium surfaces showed a continuous monolayer unlike on the smooth surface [16]

Although the main deterrent from using metallic based materials is the release of metallic particles or ions from corrosion, which can be toxic [17-19], it is worth noting that metal-based implants account for the largest biomaterials market, with 3.6 million orthopedic procedures taking place in the United States per year, 40% of these operations require implantation of metallic materials [6].

1.3 Polymers

Due to their tremendous availability and variety of physical properties, polymers can be tailored to researchers' needs ranging from hydrophobic, polar, to extremely hydrophilic [6]. Such flexibility allows them to be vastly utilized for biomaterial creation. While extensive research has taken place on

the use of polymers in biomedical applications the use of synthetic polymers is most common within the field of tissue engineering [20]. Synthetic polymers can be used in variety of applications ranging from scaffold fabrication for tissue engineering, hydrogels, drug delivery, and many more [21]. Commonly used polymers in tissue engineering and their applications are highlighted in Table 1.1.

Table 1.1. Synthetic polymers used in tissue engineering applications (adopted from [21])

Polymer	Fabrication	Applications
Polyvinyl Alcohol	Aerogels, Hydrogels	Nerve, Cartilage
Polyethylene Glycol	Hydrogels, Coatings	Cartilage, Angiogenesis
Poly(propylene fumarate)	Copolymer Hydrogels	Bone, Angiogenesis, Vascularization
Poly(anhydride)	Crosslinked Networks	Bone, Drug Delivery
Polyesters	Fibers, Aerogels, etc.	Drug Delivery, Muscle, Bone, Nerve, Angiogenesis, Cartilage

Previous trends focused on using polymers that did not illicit a biological response, but current research now focuses on synthetic polymers that are biodegradable or bioresorbable within the body [22]. In order for a synthetic polymer to be considered biodegradable it must have the following properties [23]:

- Degradation rate should match the host regeneration rate
- No sustained inflammatory response from the host
- Appropriate mechanical properties for the application
- Degraded products should be easily metabolized by the host

Numerous reviews since the 1990s have been written on the use of biodegradable polymers in tissue engineering [24] and the use of biodegradable polymers for biomedical applications [22, 25-27]. As stated before, the use of polymers within tissue engineering is widespread because of the numerous polymers available to researchers. One of the most commonly used is polyethylene glycol (PEG). While several research groups have been exploring the use of PEG in tissue engineering and are covered in reviews [28, 29], one advantage in the use of PEG is its capability to covalently bond. One example of this is the covalent bonding of heparin to the backbone of PEG to induce angiogenesis *in vivo*. It was shown that injectable heparin-PEG gels, which were then loaded with other growth factors (GF), increased tissue growth *in vivo* in porous polyurethane scaffolds in comparison to non-GF loaded scaffolds or non-heparin linked PEG with just GF loading. After 28 days *in vivo*, heparin-PEG gels were completely degraded and replaced by regenerated tissue [30]. These results suggest that

biodegradable heparin-PEG gels can be used for future studying involving tissue regeneration after myocardial infarctions.

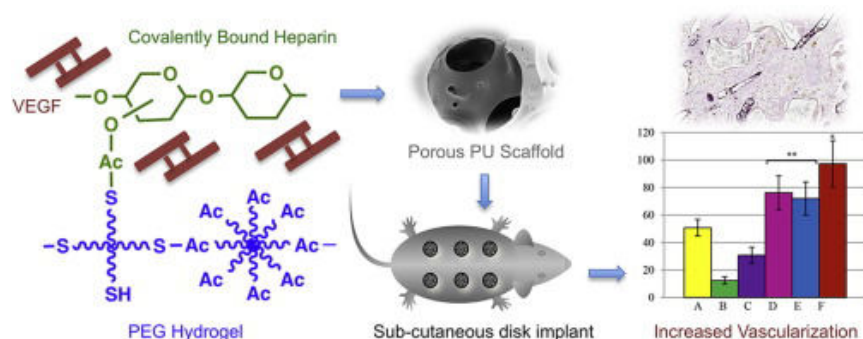


Figure 1.5. Schematic representation of increased angiogenesis *in vivo* after 28 days by covalently bonded heparin-PEG gels within polyurethane scaffolds [30]

1.4 Biosourced Materials

Biological components have long been of interest to researchers in the field of tissue engineering and in the development of biomaterials. Biosourced materials can include a variety biological components ranging from harvested extracellular matrix (ECM), proteins, polysaccharides such as collagen and alginate, and cellulose. While mammalian sourced materials have been of interest because of their biomimetic properties, plant or algae based materials are gaining attention because of their immunogenic properties in the case of alginate [20], and sustainability for nanocellulose and chitosan. The use of xenografts, or allograft sourced materials, could present an immunological response once implanted. Acellular grafts are commonly used in tissue engineering applications because of their inherent biomimetic properties that currently cannot be obtained by traditional biomedical engineering techniques [31].

1.4.1 Collagen

Biological polymers, such as collagen and fibrin, are of high interest to researchers because they are not highly immunogenic and the intrinsic mechanical properties of the collagen fibers already mimic what can be found in a biological system without any further modification. Collagen is one of the most important proteins found within the extracellular matrix of mammalian cells and is approximately 25-35% of the body protein content. Because of this large available supply commercially available collagen products have been industrially produced since the 1980s [32] Collagen has been used in a variety of applications ranging from hydrogels [33-35] and cell encapsulation [36] to scaffold creation of aerogels

[37]. One of the earliest examples of innovative collagen use in tissue engineering was conducted by Boland et al. in 2004. Collagen was electrospun into scaffolds for vascular tissue engineering because of its biomimetic properties in regards to mechanical properties. It was shown that collagen has the potential to create a distinct three layer vascular construct that could withstand shear forces and high pressure due to blood flow [38].

1.4.2 Alginate

Alginate is extracted from brown algae and contains 1,4-linked β -D-mannuronate (M) and α -L-guluronate (G) chains, in varying ratios depending on the source. These differences in ratios can create alginate gels with differing mechanical properties once crosslinked. Alginate is crosslinked by the interaction between a divalent cationic ion and the available G chains [39]. Crosslinked alginate gels are easily biodegradable [40-44] and have undesirable mechanical properties [45, 46], but are commonly used in a variety of biomedical fields such as drug delivery [47-49], wound healing [50, 51], and most important for this review, tissue engineering [52-54].

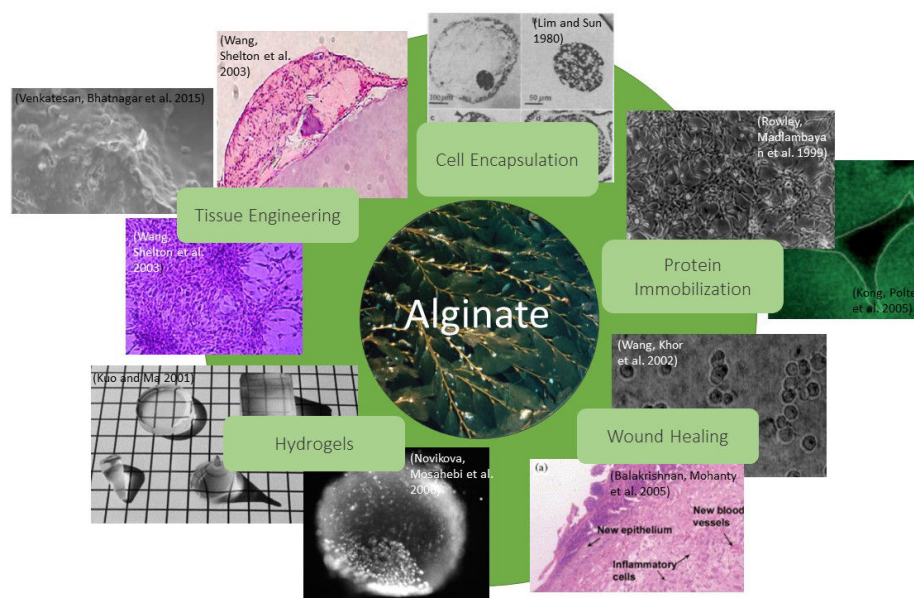


Figure 1.6. Uses of alginate in biomedical applications: tissue engineering [55, 56], hydrogels [54, 57], wound dressing [58, 59], protein immobilization [60, 61], and cell encapsulation [62]

1.4.3 Chitin and Chitosan

Chitin, or poly (β -(1-4)-N-acetyl-d-glucosamine), is the second most abundant polymer on earth after cellulose. Chitin can be obtained through a variety of sources from the exoskeleton of crustaceans to the cell walls of certain plant and fungi species. Chitosan is a derivative of chitin and is created by the

partial deacetylation of chitin by enzymatic hydrolysis or with concentrated sodium hydroxide [63]. Chitin and chitosan are considered to be biodegradable, biocompatible, and non-toxic [64, 65]. These qualities in combination with its abundance and renewability make it an attractive polysaccharide for researchers in the field of biomaterial development.

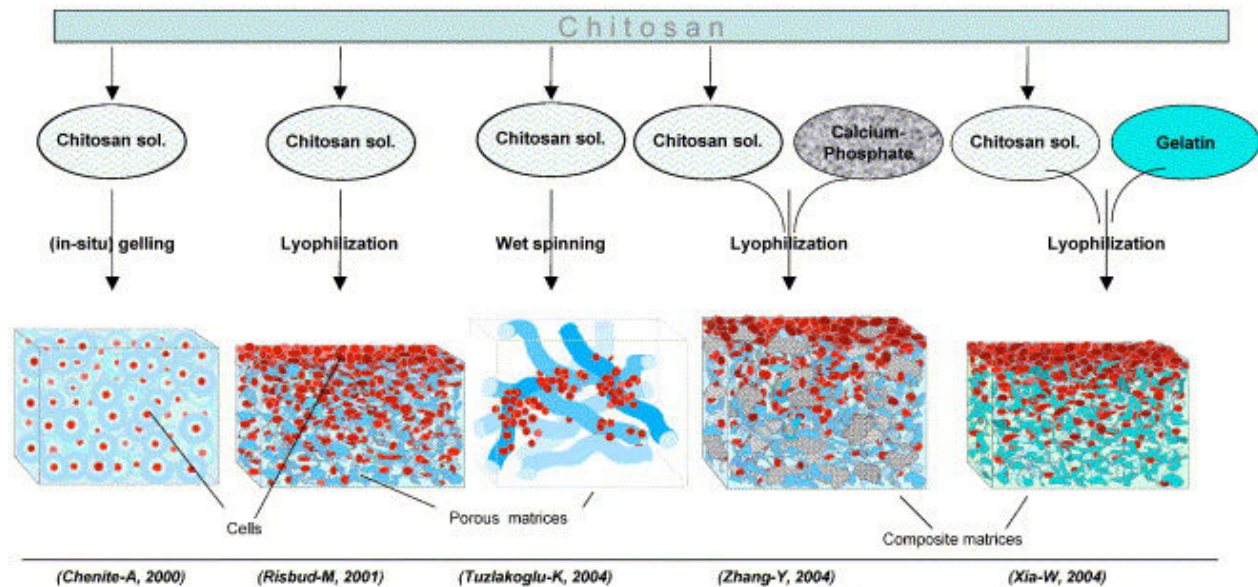


Figure 1.7. Fabrication techniques of chitosan-based materials for tissue engineering applications [66]

In regards to tissue engineering, chitosan or chitin inherently have low mechanical properties, which are not favorable for certain tissue engineering applications such as osteo-regeneration [63], but can be used in combination of other materials in order to create biomaterials with favorable mechanical properties. For example, chitosan has been used with calcium phosphate [67, 68], bioactive glass [69, 70], and hydroxyapatite [71] scaffolds for bone regeneration. Chitosan is a favorable material for bone growth because it has been shown to induce cell growth and mineralization of osteoblasts within culture [72]. Chitosan has been widely used for tissue engineering of articular cartilage [73, 74] because of the interactions between the cationic chitosan and glycoaminoglycans (GAGs) within the native cartilage tissue [75]. These GAGs are essential in the assistance of creating a favorable niche for chondrocytes. The uses of chitin and chitosan for biomedical applications can be further reviewed in multiple reviews of this topic [63, 66, 73, 76].

1.4.4 Nanocellulose

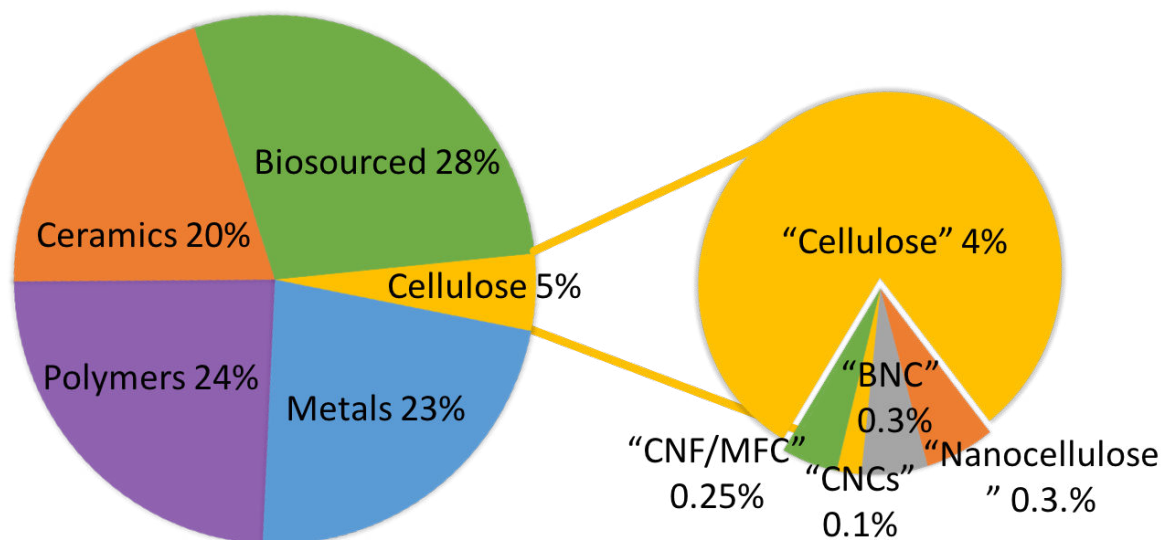


Figure 1.8. Number of publications from 2000-2017 with keywords “biomaterial” and cellulose= “cellulose,” “nanocellulose,” “bacterial nanocellulose” “cellulose nanocrystals,” “cellulose nanofibers,” “microfibrillated cellulose,” metal = “metal,” “titanium,” “magnesium,” “stainless steel,” “polymer,” ceramics = “ceramics,” “hydroxyapatite,” “bioglass,” biopolymer = “alginate,” “chitin,” “chitosan,” “collagen,” “fibrin,” and “fibronectin” on *SciFinder*

The use of nanocellulose in biomedical applications has advanced in recent years with some review articles focusing on this topic [77, 78]. However, as shown in Figure 1.8, nanocellulose is still a very innovative biomaterial with a low amount of publications since 2000. It is only about 0.3% of total scientific articles within the field of biomaterials. Nanocellulose can be obtained from vegetal biomass, bacteria, or tunicates, with the material properties depending greatly on the source [79]. Nanocellulose can be usually grouped into three categories: bacterial nanocellulose (BNC), cellulose nanocrystals (CNC), and cellulose nanofibrils (CNF). Nanocellulose in biomedical applications in the past only focused on bacterial nanocellulose because of the lack of possible lignin or hemicellulose contamination [80]. The use of cellulose nanocrystals and cellulose nanofibrils in cell culture and tissue engineering applications will be further explored in detail in future sections. BNC can be produced by many bacteria sources, but *Gluconacetobacter xylinus* is the most common and used in industrial applications [81, 82]. BNC is favored over CNF and CNCs not only because of possible contamination, but also because of its high crystallinity, oriented membrane formation, controllable water content,

and degree of polymerization [83]. While these are some advantages of BNC over CNF and CNCs, culture conditions, time required to obtain BNC, and high price are significant disadvantages of this form of nanocellulose [82].

Bacterial nanocellulose has long been used as a drug delivery system [84-86], wound healing construct [87-90], and even as a 3D printed scaffold for cartilage regeneration [91]. BNC was chosen as a scaffold for cartilage regeneration because of the mechanical properties of BNC matched closely with articular cartilage [91]. Other tissue engineering applications include loading of BNC hydrogels with bone morphogenetic protein-2 (BMP-2), which induced bone differentiation in C2C12 myoblasts [92], or collagen and human epidermal growth factor (hEGF), which increased fibroblast attachment to the BNC hydrogel [93]. BNC was used in conjunction with hydroxyapatite by Fang et al. and it was shown that hydroxyapatite improved the differentiation, proliferation, and attachment of human bone marrow stem cells in comparison to unmodified BNC [94].

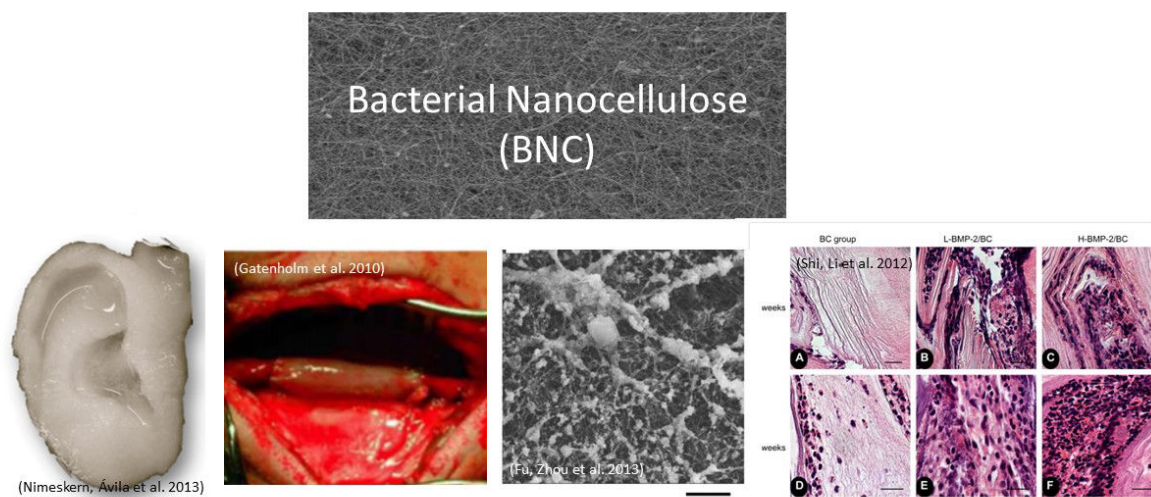


Figure 1.9. Examples of uses of BNC in biomedical applications such as scaffold construct [80, 91] and tissue engineering [87, 92]

Biomaterials encompasses a wide variety of materials available to researchers. The use of a material, whether biosourced or synthetic, is determined by many factors including: mechanical properties, immunological response, functionalization capabilities, and many more. The interest in plant based nanocellulose as a biomaterial has gained more interest in recent years, but still requires more

exploration by researchers. The biodegradability, sustainability, and numerous functionalization capabilities of nanocellulose makes it a promising biomaterial for the future.

2. Nanocellulose: Production, Characterization, and Applications

With approximately 250 megatons produced annually by biomass, cellulose is considered the most abundant polymer on earth [95]. While the source of cellulose can vary from plants, such as wood and cotton, to tunicates, and bacteria species, all cellulose consists of cellobiose (D-glucopyranosyl- α -1,4-D-glucopyranose) chains connected by intermolecular hydrogen bonds [96]. What differs from these sources is the amorphous and crystalline domains of the cellulose fibers, which are dependent on the cellulose source [97]. Cellulose molecules are arranged by biomass in order to create larger units, which Rowalnd et al. consider to be elementary fibrils [98]. These elementary fibers are then, via acid hydrolysis or mechanical treatment, capable of being reduced into two types of nanocellulose: cellulose nanocrystals (CNCs) or cellulose nanofibers (CNFs), respectively, as shown in Figure 2.1.

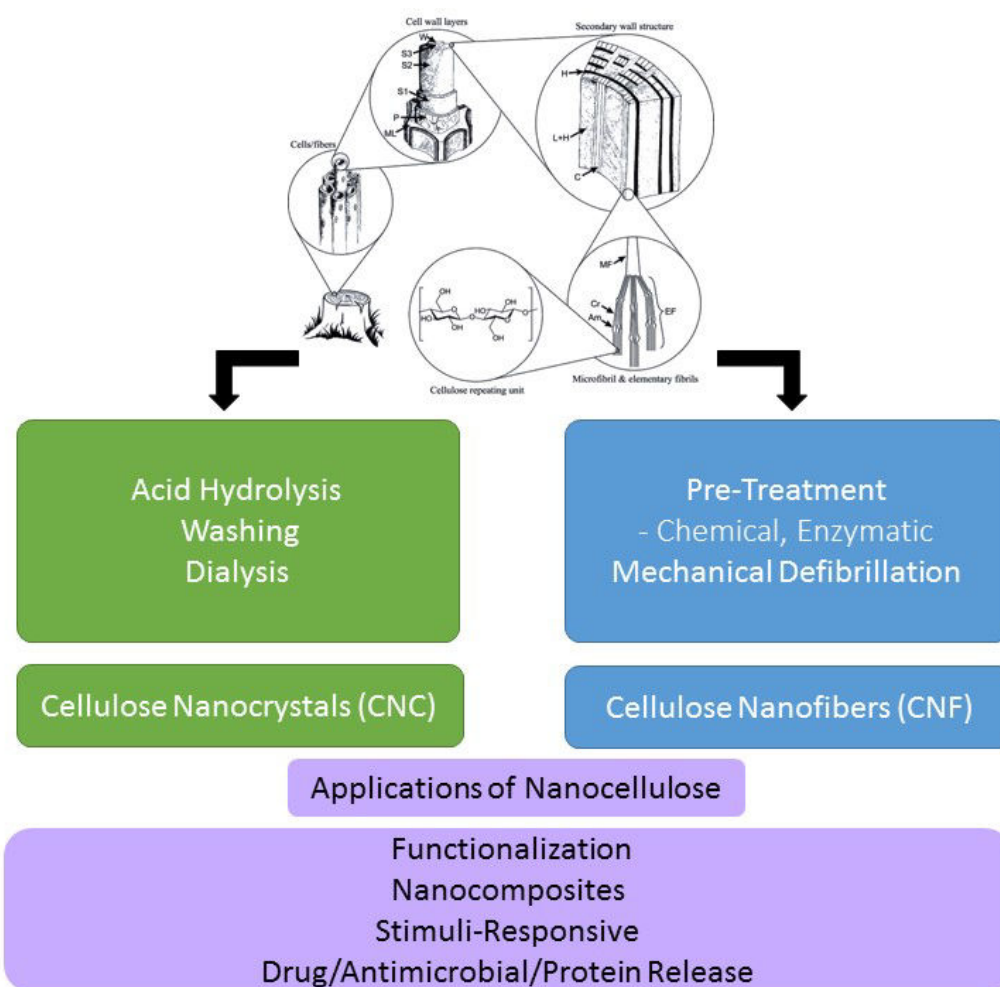


Figure 2.1. Hierarchical structure of plant fibers from cellulose chains [99] and steps to produce nanocellulose and some applications of nanocellulose use

CNCs typically have dimensions of approximately 150-500 nm in length and a diameter of 5-10 nm, and are derived from the destruction of the amorphous regions of cellulose fibers by acid hydrolysis. The first reported production of stable CNC suspension was conducted by Rånby et al. in the 1950s. In this study, CNCs were produced from wood and cotton by sulfuric acid hydrolysis, which is still the most common method used today [100]. Conversely, CNFs are commonly produced through mechanical disintegration of cellulose fiber. The first instance of this was done by Herrick et al. and Turbak et al. in 1983 through high-pressure homogenization of wood pulp. A shear thinning aqueous gel was produced with low solid content (2-7 wt%) [101] with fibrils having a diameter ranging from 20-60 nm and several microns in length [102, 103]. Industrialization of nanocellulose has made great advances since the 1980s with improvements in processing of CNCs during the washing steps (e.g. ultrafiltration) or CNF pretreatments (e.g. enzymatic or TEMPO oxidation). An exponential increase of interest of this subject within the past 5 years is evidenced by an increase in scientific publications (from 200 to 1000 annually) and patents (from 50 to 250 annually) [104]. These two types of nanocellulose have varying properties which can be harnessed by researchers for differing applications. The production techniques of CNCs and CNFs, with a focus on CNCs from agricultural waste will be further explored, as well as their main applications.

2.1 Production of Cellulose Nanocrystals and Cellulose Nanofibers

2.1.1 Cellulose Nanocrystal Production from Agrowaste

CNCs are traditionally derived from bleached wood fibers and cotton fibers, but the cost of these CNCs are still high. New research has explored the use of agricultural and industrial waste to create CNCs from renewable and low-cost materials. A recent review details such an approach [105].

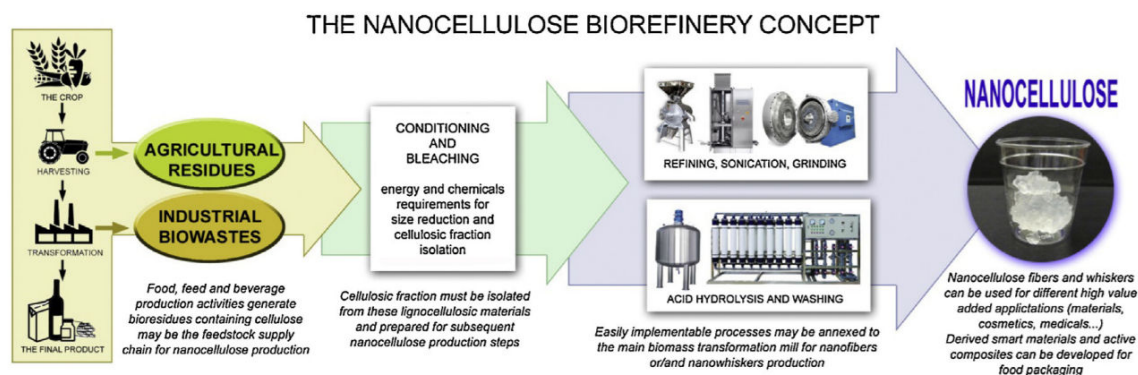


Figure 2.2 Nanocellulose biorefinery concept from agricultural and industrial waste [105]

This work has been a focus of various research publications comparing the properties of CNCs produced from agrowaste and wood [105, 106]. As the properties of the CNCs are influenced by the source [97], it can also be assumed that variety in sources will generate different chemical compositions, which will affect the final properties. The chemical content of the source material differs greatly, with wood based materials having higher lignin content compared to argowaste products [106]. The amount of lignin, hemicellulose, and cellulose content within a cellulose source will affect the “treatability” of the cellulose fibers, which in turn are related to the crystallinity, surface area, fiber porosity, and degree of polymerization of the cellulose.

Table 2.1. Properties of CNCs from Traditional Sources and Agrowastes

	CNC Source	Length (nm)	Width (nm)	Crystallinity (%)
Traditional CNCs	cotton [107]	135 ± 50	9 ± 10	77.0
	wood [108]	130 ± 67	5.9 ± 1.8	60.0
	tunicate [108]	1187 ± 1066	9.4 ± 5.0	80.0
Agrowaste CNCs	sugar cane bagasse [109]	255 ± 55	4 ± 2	87.5
	agave [110]	323 ± 113	11.4 ± 3.6	71.0
	banana pseudostems [111]	375 ± 100	17 ± 4	74.0
	barley [110]	329 ± 123	10.2 ± 3.5	66.0
	coconut husk [112]	179 ± 59	5.5 ± 1.4	62.2
	corn cob [113]	211 ± 44	53 ± 16	83.7
	soy husk [114]	123 ± 39	2.8 ± 0.7	73.5
	pineapple leaves [115]	249 ± 52	4.5 ± 1.4	73.0
	pea hulls [106]	584 ± 157	13 ± 5	71.0
	rice husk [116]	225 ± 45	18 ± 2	59.0
	rice straw [117]	116 ± 28	5 ± 2	90.7

Creation of CNCs from a cellulosic source follows four steps: chemical pre-treatment, bleaching, acid hydrolysis, and washing. CNCs produced using this method are outlined in Table 2.1. The most

commonly used pre-treatment consists of using a 2% solution of sodium hydroxide (NaOH) to swell the fiber to allow greater infiltration during the bleaching step in order to remove the lignin and hemicellulose [106]. A comparison of pre-treatments and the effect on the properties of CNCs from wood and vegetal sources was researched by García et al. The study concluded that pre-treatment greatly affects the crystallinity and surface charge of the ensuing CNCs [106]. Bleaching entails using a hypochlorite solution as outlined by Chaker et al. The removal of the lignin and hemicellulose is necessary to ensure maximum crystallinity of the produced CNCs [118]. For the third step, sulfuric acid hydrolysis is the most common method employed by researchers to create CNCs. Alternative techniques such as those involving subcritical water, for example, have been researched to create CNCs that do not require acid hydrolysis. The use of subcritical water was employed in order to bypass the numerous washing steps required following acid hydrolysis for future industrial applications and to reduce the environmental impact. CNCs with high crystallinity (79%) with high thermal stability were produced following treatment at 120°C at 20.3 MPa for 60 minutes [119], which is in correlation with sulfuric acid production of CNCs.

During CNC production, one of the most important factors is the yield. As there are multiple variables that can be modified during CNC production: acid choice, hydrolysis time, hydrolysis temperature, researchers have explored how changing these variables can affect the CNC properties. Reaction time of the acid hydrolysis using traditional methods (64 wt% sulfuric acid, 40–45°C) has been shown to have the greatest impact on the CNC yield. It has been noted that with increased reaction time the yield decreases due to the increased destruction of the CNCs [120]. This yield can differ depending on the source with the same reaction times as reported by dos Santos [115] and Silvério [113]. dos Santos reported a yield of 65% and 55% at 30 and 60 minutes for pineapple leaves [115]; while Silvério had a yield of 50% and 46% from corn cob [113] at the same time points. These results illustrate once again the importance of source material on CNC properties. CNCs, whether produced from more traditional sources (e.g. wood pulp) or agrowaste (e.g. corn cobs), have been employed in numerous research fields such as nanocomposites and the creation of “smart” materials. The uses of CNCs in these applications will be explored in future sections.

2.1.2 Production of Mechanically Homogenized and Enzymatically Pre-Treated Cellulose Nanofibers

Cellulose nanofibers (CNFs), otherwise known as cellulose nanofibrils or microfibrillated cellulose (MFC), are produced through the mechanical treatment of cellulose pulp. As with CNCs, the source

of cellulose can be wide ranging from wood to sisal fibers [121]. Production of CNF usually consists of five steps as outlined in Figure 2.3. As seen below, the characteristics of each step can vary depending on the desired properties of the CNF for the final application.

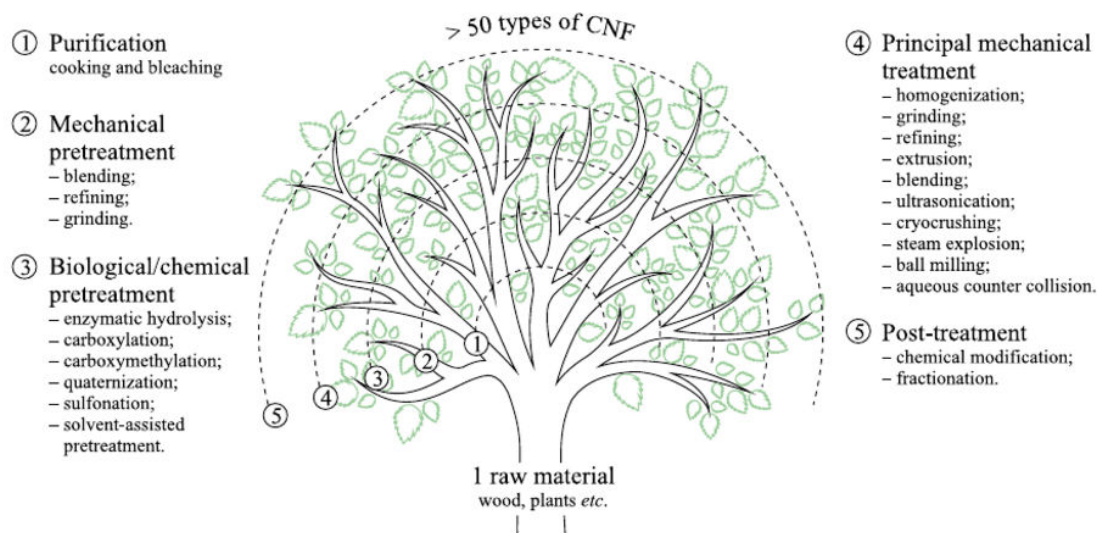


Figure 2.3. Schematic representation of CNF production steps from purification to post-treatment [99]

For the purposes of this overview a focus on mechanical homogenization and enzymatic pre-treatment and their implications for CNF properties will be explored. For a more intensive evaluation of CNF production and properties there are a number of review articles available by Lavoine et al. [122], Siró et al. [102], and Nechyporchuk et al. [99].

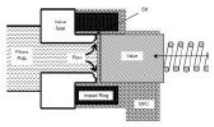
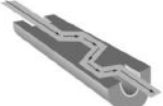
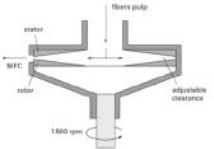
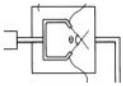
Homogenization of CNF, as first employed by Turbak et al. [103] and Herrick et al. [101], consists of pumping a suspension of cellulose fibers through a spring-loaded valve assembly at high pressure. The opening and closing of the valve at a rapid pace creates a pressure drop in the system, which in turn exerts high shearing forces onto the fibers. These high shearing forces allow high fibrillation of the cellulose fibers into CNF. It has been shown that with increased passes through the homogenizer the mechanical properties of CNF nanopaper can be improved with incremental increase between 16 and 30 passes [123].

Enzymes, or more specifically cellulases, can be employed to hydrolyze cellulose fiber by three distinct processes: 1. hydrolyze cellodextrin and cellobiose into glucose; 2. hydrolyze the amorphous regions of the cellulose fiber; or 3. act upon the ends of the cellulose chains to emancipate glucose or cellobiose. The most common processes employed by researchers are process 2 by endoglucanase and/or process 3 by exoglucanase [122]. In this work, endoglucanase was employed to enzymatically pre-treat

homogenized bleached sulfite softwood Domsjö pulp in order to increase swelling of the cellulose fibers for easier disintegration with low environmental impact [124].

The first reported use of enzymatic pre-treatment followed by homogenization was reported by Pääkkö et al. in 2007. Enzymatic pre-treatment and homogenization was employed to control the fibrillation of the cellulose fibers to the nanoscale and aid in the creation of cellulose I. They demonstrated that this method produced tailorable aqueous gels, with storage modulus dependent on the concentration of high aspect ratio CNF. It was suggested that this enzymatic pre-treatment is favorable to acid hydrolysis because of the creation of CNF with high aspect ratio and strong interconnectivity of the hydrogen bonds [125]. Recorded mechanical treatments used to produce CNF are shown in Table 2.2 adopted from Bardet [126].

Table 2.2. Mechanical Technologies Used for CNF Production [126]

	Scheme	Principle	Standard conditions	Indus. available	Energy MWh/ton	Supplier
Homogenization		Fiber suspension is subjected to a high pressure homogenizing action into a vessel through a very small nozzle. High velocity and pressure, as well as impact and shear forces on fluid generate shear rates in the stream and decrease the size of fibers to nanoscale particles	10-15 cycles 50 -150 MPa	Yes	9 -70	GEA Process Engineering Inc. Italy
Microfluidization		It includes intensifier pump to increase the pressure and interaction chamber to defibrillate the fibers using shear and impact forces against colliding streams and the channel walls	10-30 cycles 2000-3000 bars	Yes	3	Microfluidics Ind., USA
Ultra-fine friction grinding		The pulp slurry passes between a static and a rotating grind stone. The mechanism of fibrillation in grinder is to break down the hydrogen bond and the cell wall structure by shear forces and individualization of pulp to nanoscale fibers	5-60 cycles 1500-3000 rpm	Yes	1.3-3.1	Masuko Sangyo Co. Japan
Aqueous counter collision		Two water jets collide with each other at a high rate, inducing a wet and rapid pulverization of the samples into nanoscale objects dispersed in water.	40-60 cycles 200 MPa	No	-	-

Similar studies on the homogenization and enzymatically treated CNF from the source used in this study were conducted by Plackett et al. [127] and Minelli et al. [128] with diameters of approximately 15-40 nm. In two sequential studies by Sequeria et al. the impact of enzymatic pre-treatment conditions on the mechanical properties of CNF reinforced natural rubber composites was explored. The concentration of the enzymatic pre-treatment was shown to influence the Young's modulus of the 6 wt% CNF+ natural rubber composites, with endoglucanase pre-treated CNF imparting much lower mechanical properties (0.84 MPa) compared to exoglucanase pre-treated CNF (2.3 MPa). Interestingly,

pre-treated CNF and post-treated enzymatic CNF were also compared and produced composites with much higher Young's modulus (endoglucanase, 3.9 MPa, exoglucanase, 31.7 MPa)[121, 129]. CNF can be used in a variety of applications from antimicrobial release and drug delivery to tissue engineering and wound healing applications. The uses of CNF in these capacities will be detailed in future sections.

2.2 Characterization of Nanocellulose

2.2.1 Morphological Characterization

Characterization of the morphological properties of CNCs and CNFs is most commonly conducted through microscopy, but other techniques, such as dynamic light scattering (DLS) or 13-Carbon Nuclear Magnetic Resonance (^{13}C NMR) spectroscopy, can be employed. Depending on the nanocellulose type, certain microscopy techniques have advantages. Atomic force microscopy (AFM) is commonly used, but can produce results with inaccurate width measurements because of the overestimation due to the tip-broadening effect. Imaging with AFM is rapid, with quick preparation, but can produce images with low-resolution. Scanning electron microscopy (SEM) or field emission SEM (FEG-SEM) can also be used to improve the spatial resolution when compared to AFM. High resolution images obtained through a new technique by Chinga-Carrasco and Syverud that does not use a conductive metallic layer and has a short working distance (< 1 mm) and low acceleration voltage (< 1 kV) can improve image resolution with the aid of software [130, 131] when compared to AFM, but SEM is still known to overestimate the width as determined by Fuzuzumi et al. and Bondeson et al. [132, 133].

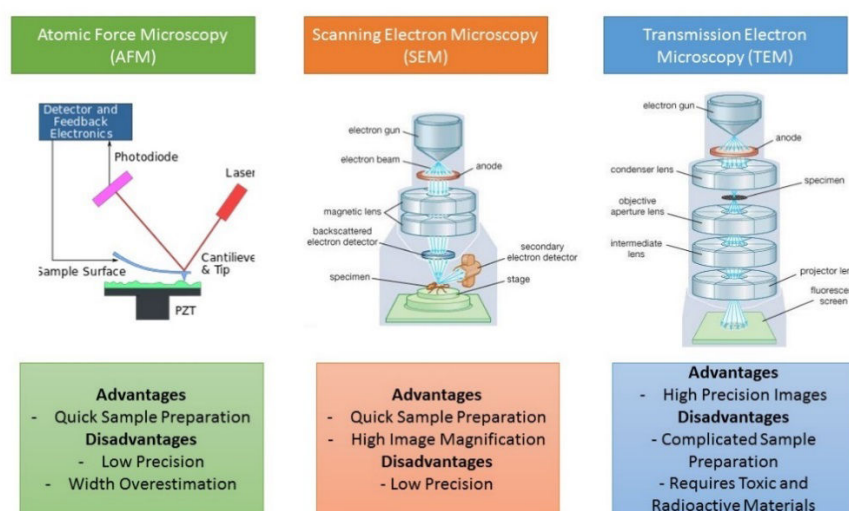


Figure 2.4. Common microscopy techniques used for nanocellulose characterization, AFM [134], SEM [135], and TEM

[136]

While Pääkkö et al. employed the use of ^{13}C NMR to determine CNF fiber width with accordance to AFM and transmission electron microscopy (TEM) [125], this technique is not commonly used. Researchers agree that TEM provides images with the highest degree of precision for both CNCs and CNFs, but sample preparation requires numerous steps and can be time consuming, or toxic, when compared to AFM and SEM. Preparation steps include deposition of a nanocellulose suspension on a UV-treated carbon-coated grid, staining by radioactive 2% uranyl acetate in water in order to improve the contrast, and drying of the suspension [82]. In comparison TEM provides higher resolution images than AFM or SEM, but requires higher attention to detail in the preparation of the samples.

2.2.2 Mechanical Properties of Nanocellulose

The mechanical properties of CNCs and CNFs can be attributed to the hierarchical structure of plant fibers. Plant fibers consist of smaller, organized components from individual cellulose chains and organized cellulose fibers to bundled, rigid plant cells as shown in Figure 2.1. This structure of lignocellulosic materials provides high mechanical properties to these materials, while also maintaining its capability of being flexible and resistant to environmental changes. The characteristics of high mechanical properties and flexibility can be attributed to the crystalline, stiff regions and amorphous, elastic regions of the cellulose molecule. These properties are exploited in CNCs and CNFs. With CNCs being more rigid demonstrated by a theoretical Young's modulus being similar to Kevlar, and CNFs having more elastic properties [82].

An important factor that can affect the mechanical properties of nanocellulose is the influence of hydrogen bonding. While increased hydrogen bonding can decrease the solubility of nanocellulose suspensions because of the increased interactions between particles [137], it can also improve the mechanical properties. In theoretical models of cellulose microfibril bundles that did not include hydrogen bonding, the Young's modulus of the fibers decreased 40% [138]. This decrease illustrates the importance of hydrogen bonding to maintain the mechanical properties of nanocellulose.

Mechanical Characterization of Cellulose Nanocrystals

The characterization of the mechanical properties of CNCs have been of interest to researchers since the 1930s, but with a heavier focus on determining the properties of the crystalline regions of cellulose I or cellulose II, not individual CNCs. Techniques employed to conduct these measurements include theoretical calculations and experimental techniques such as: AFM, Raman spectroscopy, x-ray diffraction (XRD), and wave propagation [82]. The specific Young's modulus of CNCs has been

calculated to approximately 85 J/g, which is much higher than steel (25 J/g) [139]. Measurements of the elastic modulus of CNCs from tunicates was conducted by Iwamoto et al. in 2009 by three-point bending test with AFM. They found that CNCs had a higher elastic modulus, 150 GPa, in crystals prepared from acid hydrolysis of cellulose fibers without any 2,2,6,6-tetramethylpiperidine-1-oxyl radical (TEMPO) oxidation pre-treatment [140]. The effect of humidity on the transverse modulus of CNCs from wood was measured by AFM tip indentation of CNCs by Lahijji et al. and was shown that relative humidity had a minimal effect on the stiffness of the CNCs (18-50 GPa at 0.1% relative humidity) which illustrates that CNCs are resistant to water penetration [141]. Table 2.3 from Dufresne outlines some mechanical properties of CNCs measured by various experimental procedures.

Table 2.3. Mechanical Properties of Crystalline Cellulose [82]

Material	Method	Longitudinal Modulus (GPa)	Transverse Modulus (GPa)
Cellulose I	Calculation	77-121 56 172.9*	
Cellulose I	Calculation	70.8** 76	51-57
Cellulose I	Calculation	167.5	11
Cellulose I	Calculation	134-135	
Cellulose I ₂	Calculation	127.8	
Cellulose I ₂	Calculation	136-155* 114-117**	
Cellulose I _β	Calculation	115.2	
Cellulose I _β	Calculation	124-155	
Cellulose I _β	Calculation	116-149* 124-127**	
Cellulose I _β	Calculation	156 at 300 K 117 at 500 K	
Cellulose I _β	Raman	143	
TEMPO-Oxidized Cellulose I _β	AFM	145	
Acid Hydrolyzed Cellulose I _β	ARM	150	
Disaccharide Cellulose I _β	Calculation	85.2* 37.6**	

Extended Cellulose I _β Chains (10-40 glucoses)	Calculation	126** 63.3**	
Bleached Ramie Fibers (Cellulose I)	XRD	134	
Ramie Fibers (Cellulose I)	XRD	122-135	
Ramie Fibers (Cellulose I)	Raman Inelastic Scattering	57-105 220	15
Purified Ramie Fibers (Cellulose I)	XRD	138	
Cellobiose (two hydrogen bonds – Cellulose I)	Calculation	136 ± 6	
Cellulose II	Calculation	162.1	50
Cellulose II	Calculation	83	
Cellulose II	Calculation	155	24-51
Cellulose II	Calculation	109-166* 101-106**	
Cellobiose (one hydrogen bond – Cellulose II)	Calculation	89 ± 4	
Fortisan H Fibers (Cellulose II)	XRD	70-90	
Mercerized Ramie Fibers (Cellulose II)	XRD	106-112	
Polynosics (Cellulose II)	XRD	88	
Cellulose III _I	XRD	87	
Cellulose III _{II}	XRD	58	
Cellulose IV _I	XRD	75	
Wood	AFM		18-50

* Intramolecular Hydrogen Bonds

** Without Intramolecular Hydrogen Bonds

Mechanical Characterization of Cellulose Nanofiber Films

Tensile testing is the most common technique used to determine the mechanical properties of CNF films. In this test, CNF films undergo constant uniaxial tension until samples are elongated until break. Properties such as Young's modulus, which are determined by the initial slope of the stress vs. strain curve, tensile strength, and elongation at break can be measured using this technique. In this research, tensile tests were employed to determine the mechanical properties of CNF films in dry and aqueous conditions since it is well-known that CNF films are susceptible to humidity. Interestingly, even with

the known hydrophilic nature of CNF, Svagan et al. and Henriksson et al. found that exposure to higher humidity did not have a negative effect on the Young's modulus of the CNF films when undergoing tensile testing [142, 143], but dynamic mechanical analysis (DMA) from 5 to 50% relative humidity decreases the storage modulus from 30 to 18.9 MPa as shown by Aulin et al. This is explained by the disturbance of the hydrogen bonding between the CNF fibers by the water vapor, which reduces the stiffness of the films [144]. Numerous studies have been conducted determining the mechanical properties of CNF films fabricated by solvent casting or filtration from different CNF sources. The differing values obtained for the Young's modulus, elongation at break, and strength vary greatly, as shown in Table 2.4 from Dufresne. This illustrates once again that cellulose source and CNF film preparation are important factors for determining material properties.

Table 2.4. Mechanical Properties of CNF Films in Ambient Conditions, Adapted from Dufresne [82]

Cellulose Source	Preparation	E (GPa)	ϵ (%)	σ (MPa)
Softwood	Filtration	16	1.7	250
		14	2.6	104
		10.4-13.7	3.3-10.1	129-214
		11	-	210
		6.9	7.6	233
		15.7-17.5	5.3-8.6	104-154
		13	-	223
		7.4-10.3	2.8-6.6	122-232
	Casting	-	-	80-100
		13	2.1	180
		2.5	6-11	80
		4.4-5.4	-	7-90
Hardwood	Filtration	6.2	7	222
		6.2-6.5	7-11.5	222-312
	Casting	1-3	2	10-60

2.3 Nanocellulose Functionalization

As stated previously, production of CNCs of CNFs can impart functional groups to the surface of the resulting nanocellulose whether through acid hydrolysis for CNCs or chemical pretreatments for CNF. It has been shown that the reactivity of nanocellulose is more pronounced at the primary hydroxyl group present at C6 compared to the secondary alcohols at C2 and C3 [145].

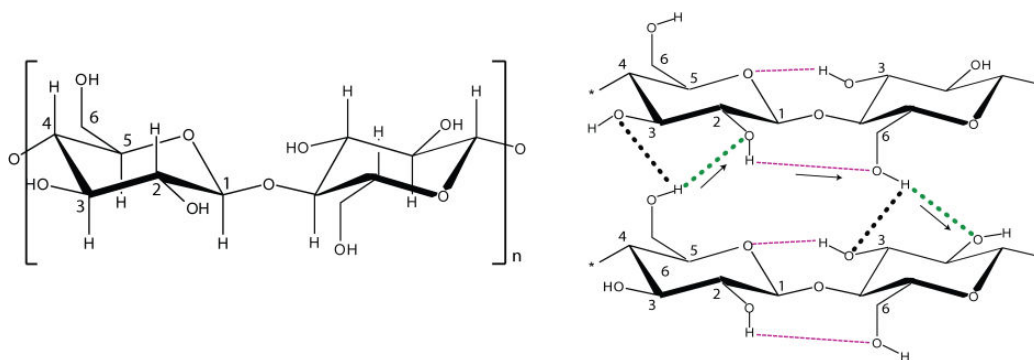


Figure 2.5. Chemical structure of cellulose [146]

This selective reactivity is taken advantage of during TEMPO mediated oxidation and esterification, which will be explored in detail, as well as other nanocellulose functionalization techniques. During CNC production through sulfuric acid hydrolysis, sulfate ester groups form on the surface of the CNCs. The amount of additional sulfate groups is dependent on the acid hydrolysis treatment conditions such as time, temperature, and concentration. Research has been conducted to compare the properties of CNCs produced from acid hydrolysis not sulfuric acid, such as hydrochloric acid [147] and phosphoric acid [148]. It has been shown that the use of an alternative to sulfuric acid imparts differing qualities to the CNCs such as higher capability for dispersion and thermal stability in the case of the addition of phosphate groups to the CNCs [148], and hydroxylated surfaces with higher thermal stability for hydrochloric acid [147]. Other instances of CNC production not using sulfuric acid with chemical surface modification involve the use of hydrochloric and acetic acid to create acetylated CNCs through Fischer-Speier esterification [149].

Pre-treatments of CNF can also produce surface groups onto the CNF. Common pre-treatments include: TEMPO mediated oxidation, carboxymethylation, and cationization. Carboxymethylation induces the creation of carboxyl groups on the surface of highly charged CNFs through a protocol developed by Wågberg et al. [150]. Cationization can be conducted through a variety of reagents such as: Girard's reagent T ((2-hydrazinyl-2-oxoethyl) trimethylazanium chloride, GT) [151], chlorocholine chloride (ClChCl) [152], and 2,3-epoxypropyltrimethylammonium chloride (EPTMAC) [153] to impart cationic groups onto the CNF. These pre-treatments are shown to help enhance the fibrillation of CNF, which is known to reduce energy consumption.

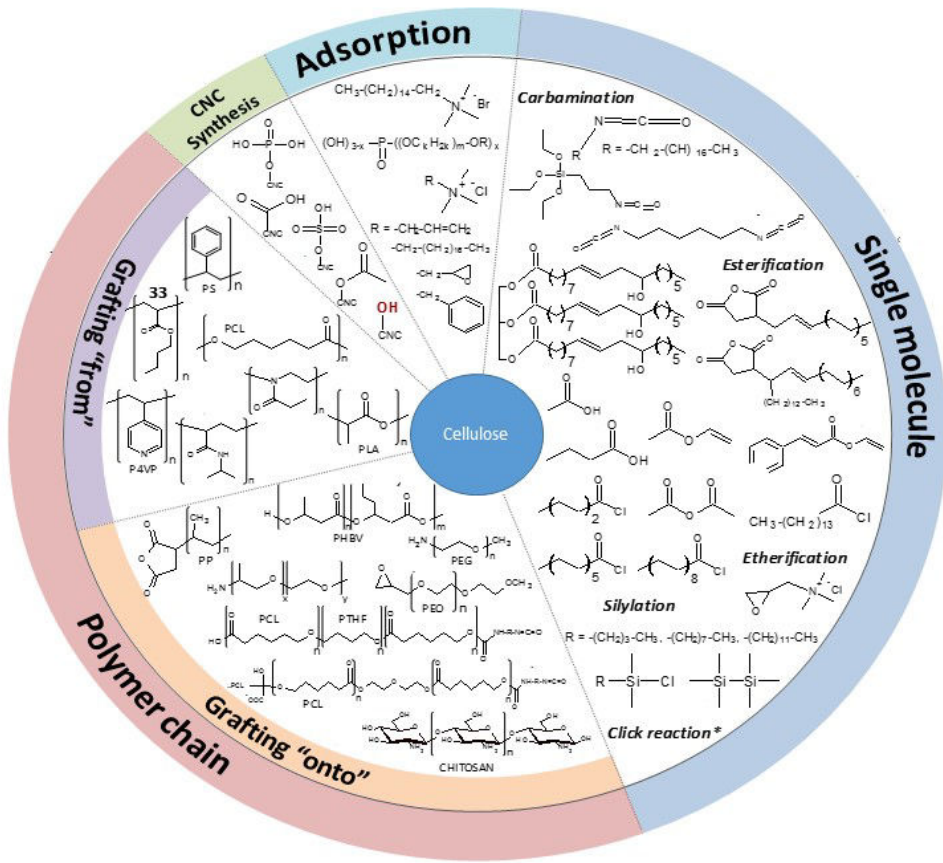


Figure 2.6. Functionalization agents used for physical and chemical functionalization of nanocellulose, adopted from Espino-Perez [154]

Other functionalization techniques used with nanocellulose, besides what can be produced during production include: adsorption, carbamination, etherification, silylation, click chemistry, grafting from, grafting to, and are thoroughly discussed in numerous reviews by Habibi et al., Tang et al., Eyley et al, and Missoum et al. [155-158] and are shown in Figure 2.6. For the purposes of this review, only TEMPO mediation oxidation and esterification will be covered in detail.

2.3.1 TEMPO Mediated Oxidation of CNCs

TEMPO mediated oxidation, which selectively converts primary alcohol groups to aldehyde and carboxyl groups, was introduced and further developed by the group of Isogai and Saito for CNFs [159-161] and Montanari and Hirota for CNCs [162, 163]. This reaction employs NaClO, NaBr and TEMPO as catalysts to oxidize cellulose as shown in Figure 2.7 at room temperature and pH 10-11.

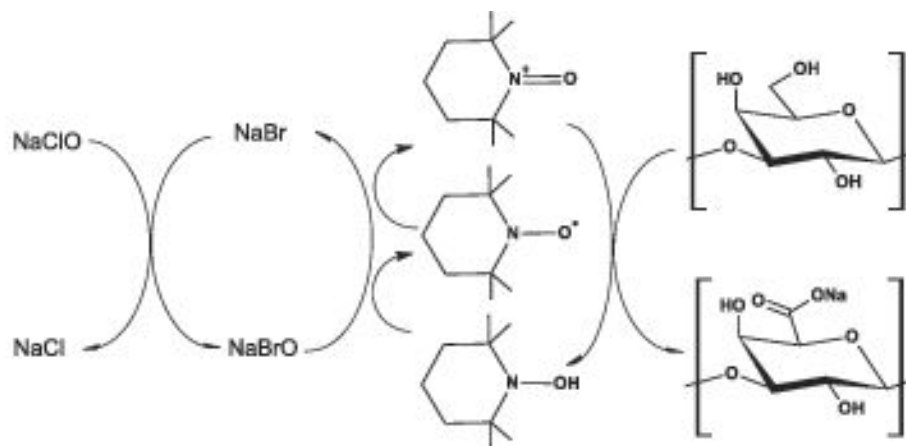


Figure 2.7. Chemical reaction of TEMPO mediated oxidation of cellulose

The efficacy of the oxidation is dependent on the reaction conditions. While more carboxylate groups can be added through the addition of more NaClO, the time required for oxidation increases. This additional time (+1.25 hours) only provides an additional 0.1 mmol/g of carboxylate groups to the surface [160]. Depolymerization or discoloration of the cellulose can occur through traditional TEMPO mediated oxidation methods. Other protocols have been proposed that replace NaBr with NaClO and NaClO is substituted with NaClO₂ at pH 7. This change in reaction oxidants prevents the formation of aldehyde groups while still maintaining the structure of CNCs [161].

The addition of carboxyl groups onto the surface of the nanocellulose allows for more dispersion within water because of the introduction of anions to the surface of the nanocellulose.

2.3.2 Esterification of CNCs Using Green Chemistry

The 12 principles of green chemistry as proposed by Anastas and Eghbali strive to use renewable processes and products, safer, environmentally-friendly chemicals and efficient protocols [164]. In this work, green chemistry principles were employed in CNC functionalization through esterification. Esterification employs the reactivity of the alcohol groups and their reaction with carboxyl groups. For use in CNCs, the first instance of CNC esterification was employed by Braun et al. through Fischer esterification of miscible acids: organic, butyric, and acetic acid. A single-step method was developed by the addition of these acids during the hydrochloric acid hydrolysis of cellulose fibers. It was shown that the dispersion of modified CNCs was improved through the esterification of approximately half of the hydroxyl groups to acetate and butyrate groups present on the CNCs [149]. This method was recently used by Boujemaoui et al. to create functionalized CNCs with available thiol groups, double

and triple bonds, and ATRP initiators for further functionalization [165]. Other examples employing green chemistry methods for CNC functionalization have been proposed. A solvent-free gas-phase esterification of freeze dried CNCs with polmitoyl chloride was performed by Berlioz et al., and a 1.17 degree of substitution was obtained [166]. Yuan et al. acetylated CNCs using an aqueous emulsion of iso-octadecenyl succinic anhydride and n-tetradecenyl succinic anhydride absorbed on the surface of CNCs, which were then freeze dried and heated to 150 °C to induce acetylation [167]. A new, green method for the solvent-free esterification of CNCs was proposed by Espino-Perez et al. called SolReact. In this protocol, the grafting agent, carboxylic acids, are the solvent as well. The evaporation of the water within the system encourages the esterification because of the *in situ* solvent exchange at a temperature above the melting point of the carboxylic acids. The carboxylic acid solvent is then recuperated through condensation and can be reused after purification through evaporation of any ethanol within the system, which is required to wash the functionalized CNCs. This method produced surface functionalized, hydrophobic CNCs without any changes in crystallinity or morphology [168]. This green, chemical modification of CNCs was used in this study and will be outlined in Chapter 3.2.

2.3.3 Functionalization for Nanocellulose-Based Composites

The use of CNCs within a polymer matrix can be limiting because of their hydrophilic nature. To overcome this, researchers can chemically modify the surface of the CNCs for improved interaction between the CNCs and a hydrophilic polymer. Common modification techniques for use in improved dispersion or hydrophobization of CNCs include carbamination, silylation, esterification, acetylation, and acylation as shown in Table 2.5. The differing protocols and results of esterification, which was employed in this work, was highlighted in section 2.3.2. Besides improving the dispersion of CNCs in apolar or low polar solvents, grafting of CNCs decreases the surface energy and provides greater compatibility between the matrix and CNCs upon heating, but problems can arise regarding the interaction between the CNCs through hydrogen bonding, which can limit and effect the mechanical properties of the nanocomposites [169].

Table 2.5. Surface Chemical Modifications of CNCs for use in Nanocomposites, from Mariano et al. [169]

	Grafting Agent	Purpose
Carbamination	n-Octadecylisocyanate	Dispersion in polycaprolactone
Silylation	Isocyanate propyl triethoxysilane	Hydrophobization
	Aminopropyltriethoxysilane,	n- Dispersion in polylactic acid (PLA)
	propyltrimethoxysilane,	

	methacryloxypropyltrimethoxysilane, acryloxypropyltrimethoxysilane	
	n-dodecyldimethyl-chlorosilane	Dispersion in chloroform, tetrahydrofuran (THF), Compatilization with PLA
	n-dodecyldimethyl-chlorosilane, isopropyl, n-butyl, n-octyl	Dispersion in (THF)
	Hexamethyldisilazane	Dispersion in acetate butyrate, acetone
Esterification, acetylation, acylation	Alkenyl succinic anhydride	Dispersion in polypropylene (PP), PLA Redispersion in water
	Acetic anhydride	Dispersion in chloroform
	Vinyl acetate	Dispersion in THF
	Acetic and butyric acids	Dispersion in toluene and ethyl acetate
	Palmitoyl acid	Hydrophobization
	Organic acid chloride aliphatic chain	Dispersion in polyethylene (PE)
	Iso-octadecenyl succinic anhydride, n-tetradecenyl succinic anhydride	Dispersion in low polarity solvents

2.4 Nanocellulose-Based Composites

Because of the inherent properties of nanocellulose, which include, renewability, high surface area, relative low cost, surface modification capabilities, and favorable mechanical response to stress, researchers have employed nanocellulose, specifically CNCs, as a filler in polymer nanocomposite systems [170]. One of the first instances of the use of CNCs as a nanofiller was conducted by Favier et al. in 1995. CNCs derived from tunicates, which have high crystallinity and aspect ratio, were dispersed in a matrix of poly(styrene-co-butyl acrylate) and shown to improve the storage modulus. This improvement was due to the creation of a percolation network between the CNCs [171, 172]. The effectiveness of the percolation network on the mechanical reinforcement is dependent on various properties of the CNCs such as: aspect ratio [173] and volume fraction [174] between the matrix and CNCs. Modelling of the percolation network of CNCs within composites was first detailed by Favier et al. [172]. Where the elastic tensile modulus, E_c is calculated by the following equation:

$$E_c = \frac{(1-2\psi+\psi V_R)E_S E_R + (1-V_R)\psi E_R^2}{(1-V_R)E_R + (V_R-\psi)E_S} \quad (\text{Eq. 1})$$

Where S refers to the soft polymer phase and R is the rigid CNC phase, ψ is the volume fraction and E is the modulus. If the stiffness of the reinforcing agent is much higher ($E_R \gg E_S$), the equation can

be simplified to $G = \psi E_R$, as stated by the series-parallel model of Takayanagi [175]. The volume fraction can be calculated as:

$$\psi = 0, \quad \text{for } V_R < V_{RC} \text{ (Eq. 2)}$$

$$\psi = V_R \left(\frac{V_R - V_{RC}}{1 - V_{RC}} \right)^b, \quad \text{for } V_R \geq V_{RC} \text{ (Eq. 3)}$$

Where the volume fraction of the filler and critical volume fraction at the percolation threshold is V_R and V_{RC} , respectively. The corresponding critical exponent, in this case 0.4 in a 3D network, is b [172]. For nanoparticles, which are rod-shaped like CNCs these equations can be re-written, where V_R is Φ_R , or the volume fraction of the CNCs, and V_{RC} is Φ_C , or the percolation threshold. For rod-like nanoparticles, Φ_C can be calculated as:

$$\Phi_C = \frac{0.7}{(L/D)} \text{ (Eq. 4)}$$

Where L/D is the aspect ratio of the CNCs as modified by Dufresne et al. in 2006 [176].

While the percolation network is an important component in nanocomposite design using CNCs, surface chemistry can also play a role. The hydrophilic nature of unmodified, acid hydrolysis derived CNCs makes them easy to incorporate into water-soluble polymer systems, but can be limiting [170]. The use of CNCs in water soluble polymers is quite high in regards to research articles. For example the reinforcement properties of CNCs have been employed in oxidized natural rubber [177], polyvinyl alcohol [178, 179], hydroxypropyl methylcellulose (HPMC) [180], and some thermoplastic polymers such as polycaprolactones [181, 182] and polylactic acid [183, 184]. For more extensive insight into the use of CNCs with other polymers there are numerous books and review articles covering this topic [169, 185-188].

2.4.1 Nanocomposites with Biosourced Polymers

Exploration of the use of CNCs within biosourced materials such as gelatin, collagen, and alginate is limited. While these materials have been extensively used in biomedical application, they do not always have favorable mechanical properties. However, the addition of CNCs to alginate, collagen, and gelatin could add additional mechanical reinforcement, or even tunable mechanical reinforcement that could be favorable for certain applications. Santos et al. added CNCs from cotton to fish gelatin plasticized with glycerol up to 15 wt% CNC addition. They also tested the effect of sonication of the CNCs within the gelatin on the properties of the solvent casted films. It was shown that the addition of CNCs above 5 wt% did not provide improvement in mechanical properties in film produced from non-sonicated CNCs, but did have improvement up to 15 wt% CNC in sonicated films. These results both illustrate

the importance of dispersion of CNCs within the nanocomposite, and that CNCs can be used with gelatin to improve the mechanical properties [189]. As with gelatin, there are minimal studies on the study of the effect of CNCs on the mechanical properties of collagen. Li et al. solvent casted collagen and added CNCs up to 10 wt%. The addition of CNCs provided improved mechanical properties up to 7 wt%, without any improvement at 10 wt% when undergoing tensile testing in ambient conditions. These results suggest that CNCs can once again improve the mechanical properties and be used for cell culture. The addition of CNCs at 7 wt% also had an improvement in cell adhesion and viability as suggested by the researchers because of the stiffness of the composites, but no statistical analysis was provided to suggest if this improved stiffness was significant [190].

Alginate Based Cellulose Nanocrystal Nanocomposites

Alginate, which was highlighted in section 1.5.1 for use as a biomaterial, is derived from brown algae and can be formed into a hydrogel by the interaction of divalent cationic ions with the 4-linked β -D-mannuronate (M) and α -L-guluronate (G) chains [39]. The addition of CNCs to alginate has been of interest to researchers in a variety of fields. The use of CNCs in the creation of alginate fibers has been extensively studied by Ureña-Benavides and Kitchens. CNCs were added to an alginate suspension and then created into fibers by wet spinning. The effect of differing ratios of CNCs on the orientation and mechanical properties of the resulting alginate CNC loaded fibers were analyzed in numerous publications. It was found that if the jet stretch remains constant CNC addition causes a negative effect on the alginate fiber tensile strength, but the jet stretch ratio is increased two-fold with the addition of 25 wt% CNCs which increases the tensile energy to break [191]. The orientation of the CNCs within the fibers was measured by wide-angle X-ray diffraction (WAXD) and it was shown that with increased load applied the CNCs spiraled along the longitudinal axis, which caused an increase in the elongation at break and decrease in the modulus. This orientation is quite similar to what occurs within native cellulose fibers, and shows that when CNCs are added to alginate they behave in a similar manner [192]. Similar fibers were constructed by Ma et al., but they also compared the effect of TEMPO-oxidized CNCs (CNC-Ts) on the mechanical and water adsorption properties of the fibers. It was shown that the addition of CNCs or CNC-Ts improved the mechanical properties at low weight percentage (0.5 wt%), but CNCs had better performance in regards to the mechanical properties and water absorbency when of the resulting fibers when compared to CNC-Ts [193].

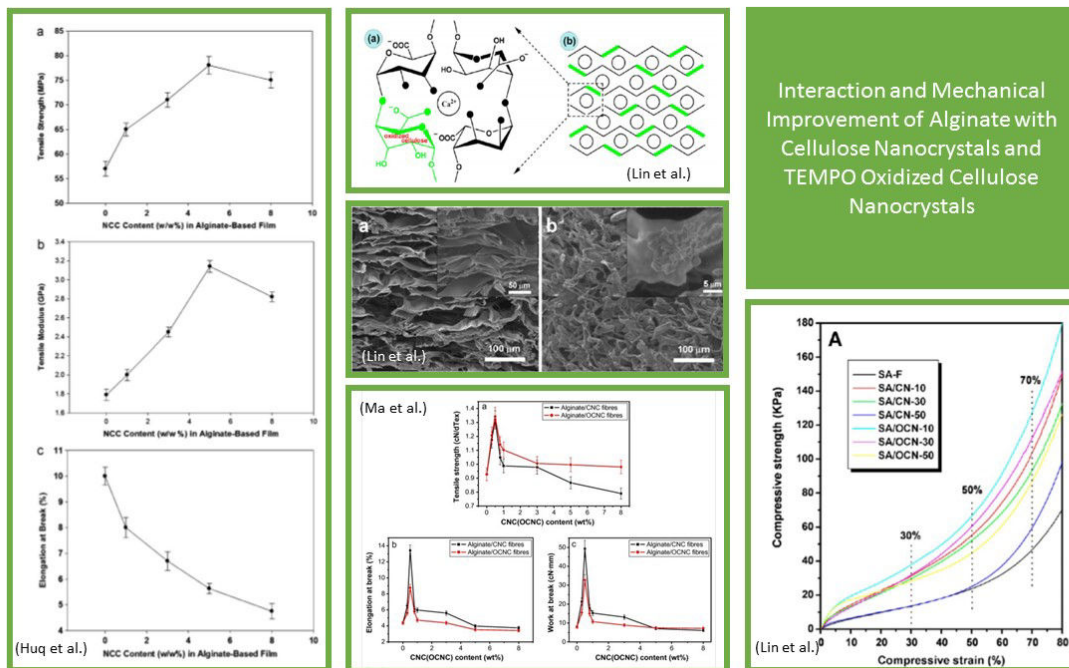


Figure 2.8. Examples of the use of CNCs to improve the mechanical properties of alginate, or increased interaction in crosslinking by CNC-Ts

The incorporation of CNCs or cellulose particles into nanocomposite films on the mechanical properties and effect of water has been explored by Abdollahi et al. and Huq et al. The addition of 5 wt% CNCs improved the water permeability by decreasing 31% compared to alginate, while also improving the tensile strength. Weight percentage above 5% (i.e. 6-8 wt%) did not show improved properties [194]. Similar results were obtained by Huq et al., Abdollahi et al. also had improved tensile strength, but only up to 5 wt% addition of cellulose nanoparticles (CPs). Additional CPs (10 wt%) actual caused a decrease in the tensile strength [195, 196].

CNCs have been incorporated into alginate to create nanocomposites, but also sponges. Lin et al. compared the effect of CNCs and CNC-Ts on the reinforcement of freeze dried alginate sponges. The addition of CNCs had a reinforcement effect up to 50 wt%, but CNC-Ts had a higher improvement because of the additional crosslinking provided by the CNC-Ts compared to the unmodified CNCs, as well as CNFs and CNT-Ts [197]. These results suggest that CNCs or CNC-Ts can improve the mechanical properties and even the water sensitivity of alginate, which can be favorable for applications ranging from food packaging to biomedicine.

2.5 Applications of Functionalized Nanocellulose

The reactivity of nanocellulose, as well as its ability to be a conduit for transport of active agents in the case of CNF, has long been of interest of researchers in nanocellulose-based materials for high-added value applications. The use of CNCs in “smart” or stimuli-responsive materials will be explored, as well as the use of CNF as an active agent carrier with a focus on biomedical applications.

2.5.1 CNCs in “Smart” or Stimuli-Responsive Materials

As outlined earlier, the reactivity of CNCs has long been of interest to researchers to create CNCs that can be functionalized for a variety of applications including improving the compatibility of CNCs with polymers for nanocomposites. While this is of importance for the use of CNCs in hydrophobic polymers, or for the use of CNCs in packaging applications, one field that CNCs are widely used is in the development of stimuli-responsive materials.

One of the first instances of the use of CNCs in a “smart” application was completed by Capadona et al. in 2008. In this pioneering work, tunicate CNCs derived from sulfuric acid hydrolysis were incorporated into 1:1 ethyleneoxide/epichlorohydrin copolymer (EO-EPI) nanocomposite that was responsive to water. The exposure of the composite to water disrupts the hydrogen bonding between the CNCs which causes a decrease in the stiffness of the composite, but upon drying the composite returns to its original stiffness. This suggests that the interaction between the CNCs is reversible, and can be tuned for specific applications depending on the amount of CNC filler [198].

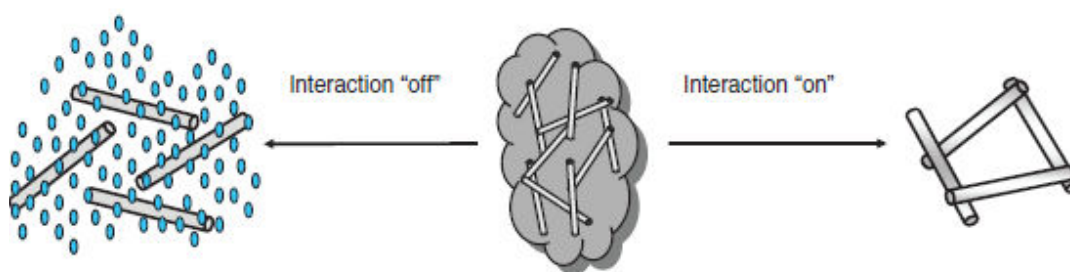


Figure 2.9. Schematic of switching of CNC interaction dependent on the hydrogen bonding [198]

Following the work of Capadona et al., others have extended this principle to create CNC-based systems that are responsive to a variety of stimulants such as water [104-106], pH [107, 108], temperature [109, 110], and most importantly for this research, light or ultraviolet (UV) radiation. The basic principle is to functionalize CNCs with groups that can either respond to the stimulus on their own, or have a secondary interaction with an initiator. Biyani et al. has explored the use of functionalized CNCs for use in light or UV stimuli responsive system through numerous publications.

Different functionalization motifs were used to create photoswitchable nanocomposites for either the enhancement of the mechanical properties, or to create photo-healable composites. CNCS functionalized with ureidopyrimidone (UPy) or UPy functionalized telechelic poly(ethylene-co-butylene) [199]. UV exposure also created a photo-healable system of a 2,6-bis(1'-methylbenzimidazolyl) pyridine (Mebip) ligand and $\text{Zn}(\text{NTf}_2)_2$ end functionalized telechelic poly(ethylene-co-butylene) matrix with 10 wt% CNCs. The introduction of UV light liquefies the system, which can then be used to fill any defects within the matrix. Once UV is removed, the system is restored to its original state [200].

In the case of mechanical properties, benzoderivatized CNCs were employed to facilitate a radical-mediated reaction between the functionalized CNCs and EO-EPI matrix to create shape-memory nanocomposites [201]. While the other case used coumarin-functionalized CNCs to utilize the dimerization of coumarin once exposed to UV. It was shown the storage modulus of the EO-EPI composite increased from 4 MPa of neat EO-EPI to 199 MPa with the addition of 10 wt% functionalized CNCs and further increased to 291 MPa upon UV exposure [202]. Other examples of the use of UV responsive functionalized CNCs for mechanical reinforcement was conducted by Fox et al. In this work thiol-ene click chemistry was employed with allyl functionalized CNCs in a poly(vinyl acetate) matrix to increase the mechanical properties in a wet state. It was shown that UV exposure increased the storage modulus by 500% (60 to 300 MPa), which is important because in non-functionalized systems CNC-based nanocomposites have a lessening of stiffness once exposed to water due to the lack of hydrogen bonding required for the formation of a the percolation network [203].

2.5.2 CNF Films as Controlled Release Systems

CNF films are commonly used as an active molecule carrier or drug delivery system because of the nanoporous structure that is created during fabrication. This nanoporous structure can be used to entrap particles or molecules that are then released. The most widespread application of this technique is for antibacterial or drug release. The use of CNF films incorporated with drugs such as paracetamol, caffeine, and more can be found in a review by Lin et al [77]. Antimicrobial components added to CNF by mixing include magnesium hydroxide and zinc oxide [204]

The release properties of CNF can be influenced by many factors such as: release medium, interactions between the CNF and release molecule, molecular size, and pH as defined by Kolakovic et al. [205]. Although the use of CNF for the release of growth factors, or model proteins like bovine serum

albumin (BSA) has not been previously studied, they can be advantageous for tissue engineering and other biomedical applications as later highlighted in this Ph.D. The only published instance of the incorporation of BSA with a purely nanocellulose system was conducted by Müller et al. in 2012 with bacterial nanocellulose (BNC). Müller and colleagues compared never-dried BNC to freeze-dried BNC and the efficacy of BSA release. It was determined that the release of BSA was dependent on the time, temperature, concentration of BSA, pre-swelling conditions, and BNC preparation. It was noted that freeze-dried BNC had a lower capacity for the uptake of BSA within solution because of the morphological changes that occur during freeze-drying. The release of BSA from BNC was found to follow the Ritger-Peppas model, and was a diffusion and swelling controlled process [84].

The use of nanocellulose in high-added value products such as nanocomposites, “smart” materials, and active particle release systems as well as its inherent properties make it an attractive material for researcher in variety of applications which include biomedical applications. The use of CNCs and CNFs within biomedical engineering has increased in recent years as illustrated by the recent review articles published by Lin et al. and Jorfi et al. [77, 78], but limited research has been conducted using nanocellulose in tissue engineering constructs. The potential of nanocellulose for use within tissue engineering will be explored in Section 3.

3. Tissue Engineering and Nanocellulose

The use of cells as therapeutic modalities is one of the most promising medical advancements of the future [20]. This effort, more easily referred to as tissue engineering, was first defined in 1988 by Skalak and Fox as:

The application of the principles and methods of engineering and life sciences toward the fundamental understanding of structure-function relationships in normal and pathological mammalian tissue and the development of biological substitutes to restore, maintain, or improve tissue function [206].

Tissue engineered constructs can consist of genetically modified cells, products that induce specific tissue response, or constructs that are a combination of cells with biomaterials, which are of importance to this work [20]. Cell and material choice are dictated by the future application of the tissue engineered product. Based on their properties and intended application, some materials are better suited for bone regeneration, while others may be better for revascularization. Other aspects such as cell biology must also be taken into consideration to better understand how material fabrication and characterization can influence cell behavior.

3.1 Stem Cells: Types, Properties, and Differentiation

When creating a tissue engineered construct it is important to decide what cell type will be used depending on the application. One of the most common types of cells to be used in regenerative medicine is stem cells. Stem cells can be defined as any cell that has the ability to self-renew, differentiate, and are immortal *in vivo* [207]. Depending on the stem cell type, stem cells can exhibit a variety of potencies or differentiation potential. Differentiation is how a cell changes its phenotype based on differential gene expression. Once a cell commits to a certain gene expression it is usually irreversible and causes a change in a particular function of the cell, or exhibited phenotype [20]. Stem cells can be generally grouped into three main categories: embryonic stem cells (ESCs), induced pluripotent stem cells (iPSCs), or adult stem cells. Each category of stem cell has specific properties that can be either advantageous or deterrents for researchers.

Table 3.1 Pros and Cons of Stem Cells

Type of Stem Cell	PROS	CONS
Embryonic Stem Cells (ESCs)[208]	<ul style="list-style-type: none"> -Pluripotent -Self-Renewing -Easily differentiate in vivo -Prolonged, undifferentiated proliferation in culture 	<ul style="list-style-type: none"> -Teratoma Formation -Immuno-rejection -Ethics -Need feeder layer of murine/human embryonic fibroblasts and leukemia inhibitory factor while culturing
Induced Pluripotent Stem Cells (iPSCs)[209]	<ul style="list-style-type: none"> -Pluripotent -Less ethical concern -Patient specific regenerative medicine 	<ul style="list-style-type: none"> -Teratoma Formation -Epigenetics
Adult Stem Cells[210]	<ul style="list-style-type: none"> -Patient specific regenerative medicine -Less likelihood of rejection 	<ul style="list-style-type: none"> -Multipotent -Rare in mature tissue

Embryonic and induced pluripotent stem cells have the capability to differentiate into a variety of type of cells because of their pluripotency, and are of interest to researchers because of their possible use in transplantation therapy [211]. In regards to embryonic stem cells some of the major concerns are the possible introduction of xenogenetic or allogenic material during culture because of the requirement to use murine/human embryonic fibroblasts in order to ensure that the cells remain potent [212]; also the use of embryonic stem cells has caused policy and ethics concerns in some countries [213]. Apprehensions for the use of iPSCs include possible changes within the epigenetics of the cell during induced differentiation [214]. Meaning, does the iPSC have the same genetic make-up as the patient's embryonic stem cells? A question that cannot be answered with today's technology. Adult stem cells are commonly used in the field of tissue engineering and regenerative medicine because of their ability to be patient specific. The function of adult stem cells *in vivo* is to either repair damaged tissue or to maintain homeostasis. Within their native environment adult stem cells can sustain their "stemness" for the life of the organism, but this stemness decreases once the cells are removed from their niche. To combat this lack of differentiation potential, researchers have turned to creating culture and tissue engineering environments that mimic the stem cell niche [215].

Adult stem cells can be pluripotent, but are most commonly multipotent or progenitor cells [216]. Progenitor cells can only differentiate along a certain cell germ line, or differentiation pathway [210].

Common adult stem cells are listed in Table 3.2. As illustrated below, adult stem cells can be found in a variety of tissue sources, and each differentiation pathway is dependent on the source [217].

Table 3.2 Adult Stem Cells: Sources and Differentiation Pathways [217]

Adult Stem Cell Type	Tissue Specific Location	Differentiation
Intestinal Epithelial Stem Cells	Epithelial cells at the base of intestinal crypts	Paneth's cells, brush-border enterocytes, mucus-secreting goblet cells, enteroendocrine cells of the villi
Lung Epithelial Stem Cells	Tracheal basal and mucus secreting cells, bronchiolar Clara cells, alveolar type II pneumocyte	Mucous and ciliated cells, type I and II pneumocytes
Keratinocytes	Basal layer of epidermis, hair follicles	Epidermis
Skeletal-Muscle Stem Cells	Muscle fiber	Skeletal muscle fibers
Pancreatic Stem Cells	Intrinslet, nestin positive cells, oval cells, duct cells	Beta cells
Hepatic Stem Cells	Terminal bile ductules	Oval cells
Neural Stem Cells	Ependymal cells, astrocytes	Neurons, astrocytes, oligodendrocytes
Hematopathic Stem Cells	Bone marrow, peripheral blood	Bone marrow, blood lymphohematopoietic cells
Mesenchymal Stem Cells	Bone marrow, peripheral blood	Bone, cartilage, tendon, adipose tissue, muscle, neural cells, marrow stroma

The focus of this review will now turn to one specific type of adult stem cell: mesenchymal stem cells (MSCs).

MSCs were first discovered by Friedenstein in the 1970s by isolating the cells from bone marrow [218], and observing that these cells have the capability to differentiate into chondrocytes, adipocytes, or osteoblasts [219]. Other sources of MSCs can include umbilical cord blood and adipose tissue. The properties of MSCs are dependent on the source as shown by Kern et al. They highlighted the differentiation potential, immune response, isolation success, and colony frequency of MSCs derived from these sources. It was noted that there were no significant differences between the cell morphology and presentation to the immune system, but there were lower isolation rates, colony frequency, and lack of adipogenic differentiation for MSCs from umbilical cord blood compared to MSCs from bone marrow and adipose tissue [220].

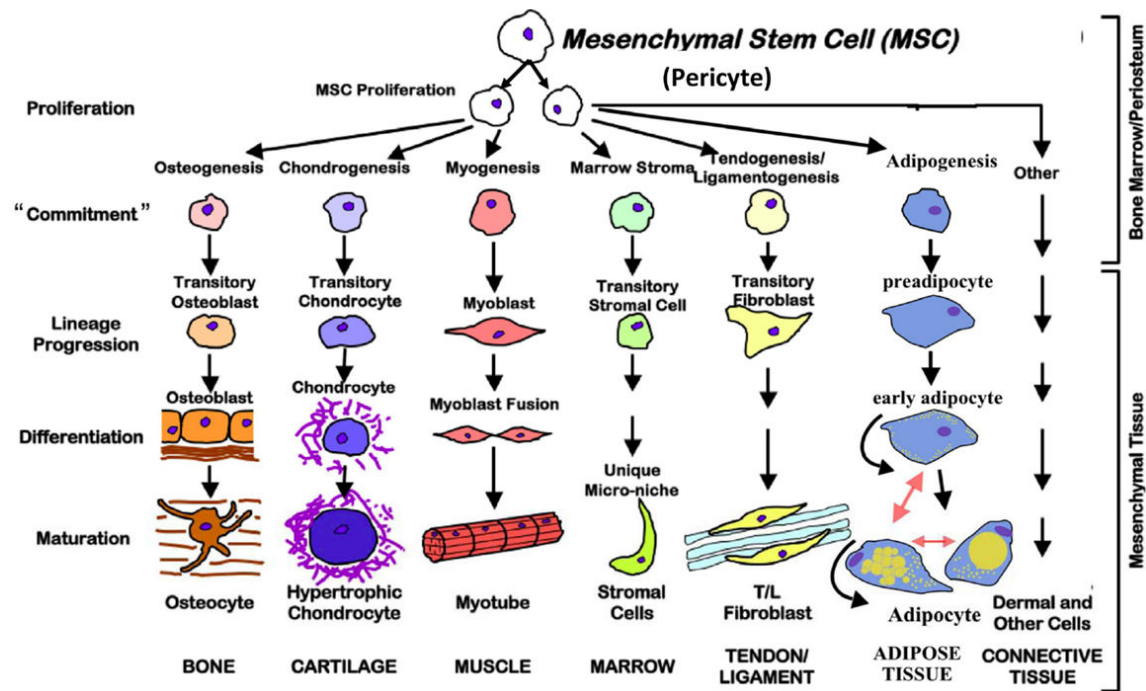


Figure 3.1. Possible differentiation pathways of mesenchymal stem cells, adopted from DiMarino et al. [221]

Advantages for using MSCs in tissue engineering applications include their differentiation potential, honing capabilities, retaining potency, and possible low immunological response. MSCs can migrate to injured sites within the body by chemokine-chemokine receptor interactions, and these interactions can be modulated by researchers to increase tissue repair *in vivo* [222]. While honing is an important feature for clinical applications of MSCs, the potential of MSCs to remain potent during expansion can be of great use of researchers in terms of having a supply of MSCs [223]. Other advantages of MSCs include their capability to not induce an immune response. MSCs, and differentiated MSCs are shown to not to express HLA Class II genes [224, 225]. HLA Class II are glycoproteins that are present on the surface of cells, which are required in the commencement of many immune responses [226]. While this lack of HLA Class II expression is an advantage, there are still some associated risks with donor rejection when MSCs are used as an allograph [227]. Recent research has shown the MSCs are not necessary immune privileged, but evade the immune response because HLA Class II expression can be activated *in vivo* by inflammatory response. This activation has lead researchers to question the belief that MSCs are “Universal Donors” deeming further research as necessary [228].

3.2 Cell Adhesion, Proliferation, and Differentiation with Biomaterials

To understand cell response when introduced to a biomaterial, it is important to note how cells attach and proliferate on a substrate's surface. The adhesion of the cells onto a substrate's surface is of importance because of the linkage between anchorage and cell viability and proliferation. Without adhesion cells undergo programmed cell death, or apoptosis, especially cells that are anchorage dependent, such as MSCs [229, 230]. Cells adhere to a substrate by probing their microenvironment and reorganizing their actin filaments within the cytoskeleton into filopodia to anchor themselves onto the substrate's surface [230, 231].

The adhesion of cells onto the surface is dependent on many factors such as material topography [229, 231, 232], mechanical properties [230, 233], surface chemistry [234], and many more. These possible modifications must be considered for many length scales. This means that modifications made on the cellular, or subcellular length scale will not have the same effect as modifications made on the supra-cellular scale. Typical tailoring techniques of biomaterials at the supra-cellular scale include insoluble factors, gradients, while at the cellular scale pore size and roughness have a larger impact [20].

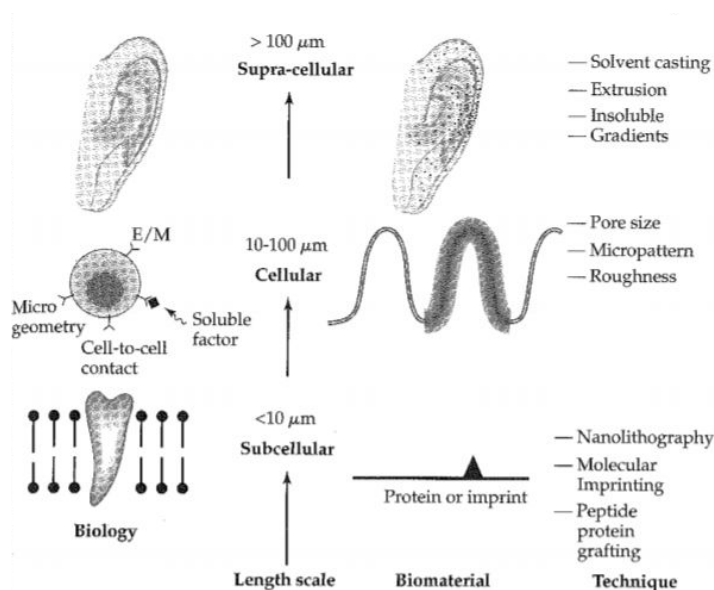


Figure 3.2. Length scales and modification techniques of biomaterials as adopted from Palsson et al. [20]

Surface roughening or patterning can be used by researchers to determine how these properties can influence cell adhesion, proliferation, and eventually differentiation. Work conducted by the research group of Dalby focuses on the cellular response to substrate topography. It has been proposed that patterning of polycaprolactone substrates on the nanoscale with an $\times y$ offset can cause MSCs to mineralize without any aid from osteogenic factors, and that this differentiation gene expression

differs compared to MSCs differentiated by biochemical factors [232], but MSCs can remain potent after 8 weeks in culture on substrates without any offset [235]. These results illustrate that surface patterning can be used to influence cells to differentiate, or to keep their differentiation potential. Micropatterning techniques are often used on biomaterials for orthopedic applications to induce MSC differentiation towards osteogenesis. Microstructured titanium has been shown to cause MSCs to express osteoblast markers via signaling of $\alpha 2\beta 1$ integrins of the osteoblasts, which then in turn causes the paracrine secretion of Dkk2. Dkk2 then can act upon distant MSCs, or MSCs co-cultured to differentiate into osteoblasts as well [236]. Cellular interactions between the host cells and implant can be enhanced by the patterning of surfaces that come in contact with bone tissue. Another example of how patterning of titanium can influence MSC fate was shown by Dumas et al. In this work titanium was patterned by a laser into three biomimetic textures. With each texture, there were significant differences in how the MSCs arranged their focal adhesions, which displays that MSCs can distinguish between topographical features. All MSCs cultured on patterned surfaces showed an increase in expression of osteogenic markers, while down-regulating adipogenic genes [237]. While one pattern has displayed the capacity to influence MSC adhesion, proliferation, and differentiation, the amount of roughness, or the creation of a gradient can influence MSC behavior. Faia-Torres et al. varied the surface roughness of polycaprolactone within a gradient MSC adhesion and degree differentiation differed depending on where on the gradient the cells were cultured in the presence of osteogenic media [238]. MSC differentiation potential and adhesion can be modulated by surface roughness or patterning of a substrate, but this is not the only technique available to researchers.

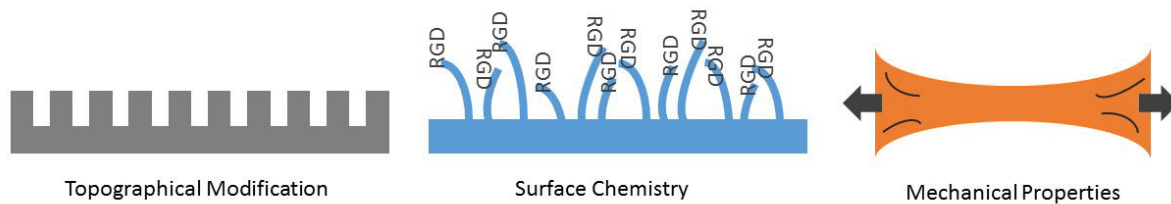


Figure 3.3. Pictorial representation of three common modification techniques to induce cell adhesion, proliferation, and differentiation

One of the most commonly used techniques to modulate the cellular adhesion or response to a biomaterial is to modify the surface chemistry. Surface chemistry modification usually consists of “attaching” or immobilizing ligands to the surface of the material that induce cell attachment, or using bulk chemistry modification to release growth factors. While ligand and growth factor choice are dependent on the application, a commonly used motif for MSC applications is RGD (arginine-lysine-

aspartic acid), ligand attachment. RGD can induce chondrogenic differentiation in early stages, or cartilage cell differentiation, of MSCs [239-241]. This occurs because RGD upregulates fibronectin production by the cells, which is necessary for cell adhesion [240, 242]. Work conducted by Salinas et al. created cleavable RGD sequences by thiol-acrylate photopolymerizing RGD into polyethylene glycol hydrogels [243] to induce chondrogenic differentiation. Other examples of using RGD include use of RGD modified alginate microbeads to encapsulate human MSCs [244], fabrication of a macroporous alginate scaffolds with RGD attached to alginate by aqueous carbodimide chemistry [245], others have coated hydroxyapatite disks with RGD to induce MSC attachment [246]. Surface chemistry can also be used to cause the release of growth factors from the substrate. Commonly used growth factors used with MSCs include transforming growth factor beta (TGF- β). TGF- β is important for the induction of chondrogenesis of MSCs [247]. TGF- β can be incorporated into biomaterials in a variety of ways including encapsulation by spontaneous emulsion in poly(lactic-co-glycolic acid) [248, 249], emulsion into crosslinked chitosan microspheres [250], incorporation into gelatin microspheres [251], equilibrium affinity binding of TGF- β to alginate-sulfate [252], and many more.

While surface chemistry, or release of growth factors can help with cell adhesion or differentiation, other techniques can be used to induce cell attachment and differentiation. It has been shown that the mechanical properties alone can influence cell behavior, which is of importance regarding this thesis. Seminal work by Engler in 2006 showed that by modulating the elasticity of collagen coated polyacrylamide gels, MSCs could differentiate into different cell types depending on the modulus. It was shown that MSCs cultured on substrates with lower elasticity displayed genetic markers for neurogenesis while cells cultured on higher elasticity substrates had markers for osteogenesis [233].

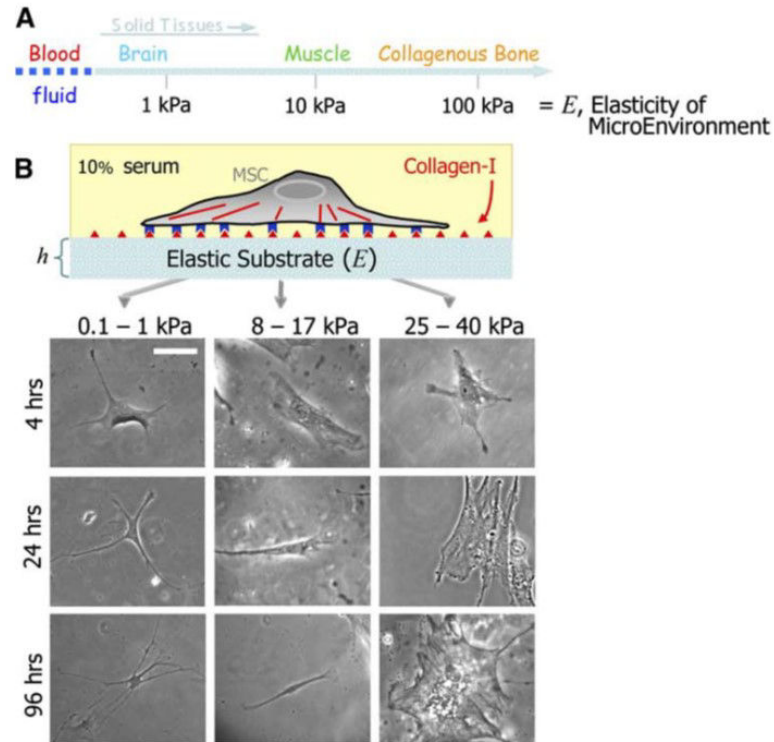


Figure 3.4. Schematic of how MSCs attach to collagen coated polyacrylamide gels with varying elasticity and images of MSCs with scale bar of 20 μm , from Engler et al.[233]

Following the work of Engler, other researchers have explored the use of polymers with tunable mechanical properties to induce changes in MSC behavior, including differentiation. Wang and colleagues created an injectable 3D hydrogel scaffold of gelatin-hydroxyphenylpropionic acid with varying mechanical properties; it was shown that with increased stiffness the proliferation rates of the MSCs decreased, while decreased stiffness induced neuronal differentiation [253]. It was shown by Park et al. that initial MSC attachment and spreading was dependent on the stiffness of the substrate. MSCs cultured on soft substrates had a lower proliferation rate and less spreading when compared to MSCs cultured on stiff polyacrylamide substrates. The modulus of the polyacrylamide gels was shown to range from 1-15 kPa. MSCs had a 30% less proliferation rate on 3-15 kPa substrates compared to 1 kPa substrates. In regards to differentiation it was determined that stiffness may not be specific to one particular differentiation pathway, but growth factors, and other biochemical factors can be used with substrate stiffness to ensure differentiation along a particular pathway [254]. Other strategies that have been employed by researchers to ensure or increase differentiation on mechanically tunable matrices for MSC differentiation include protein ligand attachment, such as RGD [255], and coating of tunable substrates with ECM proteins such as fibronectin, laminin, and collagen I,IV [256].

3.3 Nanocellulose for Tissue Engineering

The use of nanocellulose for tissue engineering and other biomedical application has gained interest in recent years with some review articles written on this topic [77, 78] . While nanocellulose in other biomedical applications such as drug delivery and wound healing have been explored extensively, the use of biomass based nanocellulose for tissue engineering applications with stem cells is a topic that has considerable research potential. Most research has focused on determining basic biocompatibility of nanocellulose based biomaterials, without much focus on cell differentiation potential. Common uses of nanocellulose include incorporating cellulose nanocrystals into polymer matrices to improve mechanical properties, or drug/antimicrobial release from cellulose nanofiber substrates. This section will explore the variety of techniques researchers have employed CNCs and CNFs for cell culture and tissue engineering.

3.3.1 Cellulose Nanocrystals

Limited studies have been conducted on the use of CNCs alone for possible tissue engineering applications. Previous studies focused on the inflammatory response of CNCs or cytotoxicity. Clift et al. conducted an *in vitro* triple cell co-culture of human blood monocyte derived macrophages, which are a type of white blood cell, human epithelial cells from the bronchial cell line, and human blood monocyte derived dendritic cells, which are messengers within the immune system. It was shown that cytotoxicity and inflammatory response to the cotton derived CNCs within culture media was dose dependent. The authors noted that their results should not be generalized because of the various preparation and characteristics of CNCs [257].

C2C12 myoblasts, or undifferentiated precursors of muscle cells, were cultured on tunicate cellulose nanocrystal spin-coated glass coverslips by Dugan et al. CNC deposition and orientation was controlled by varying the speed of the spin coater. It was shown that C2C12 attachment depended on the orientation of the CNCs, with increased attachment and orientation on higher oriented CNC surfaces. All CNC coated surfaces had significantly higher adhesion compared to the control. Regarding differentiation, CNC surfaces caused terminal differentiation of the C2C12 myoblasts into aligned myotubes as shown by morphological analysis [258].

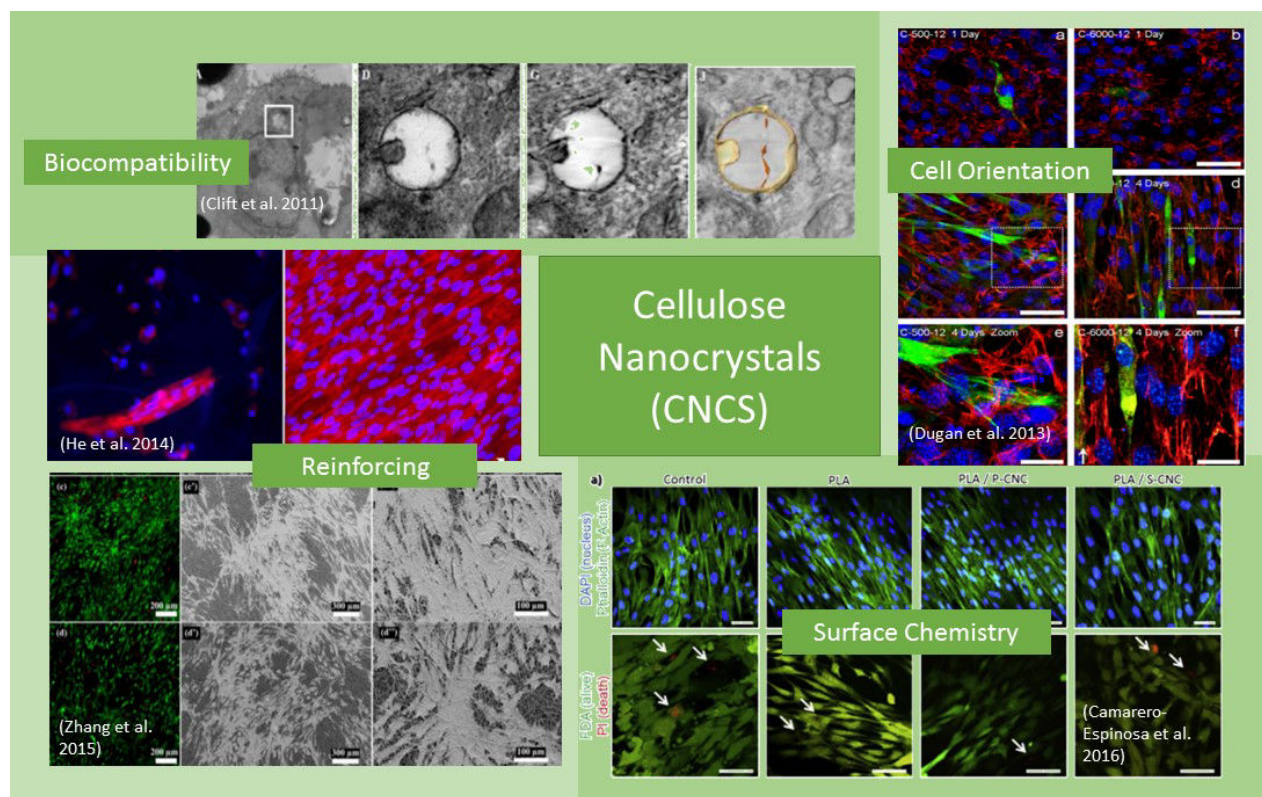


Figure 3.5. Properties and examples of uses of CNCs in cell culture and tissue engineering applications [257-261]

The use of CNCs for tissue engineering or for use in cell culture has mostly focused on incorporating CNCs into a polymer to improve the mechanical properties of the polymer. For example, Zhou and colleagues combined CNCs with poly(lactic acid) (PLA) that was grafted with maleic anhydride to create electrospun PLA and CNCs fiber scaffold. This scaffold was then tested with MSCs to determine biocompatibility. The addition of CNCs to the maleic anhydride poly(lactic acid) improved the mechanical properties of the fibers and were biocompatible, biodegradable, and supported cell proliferation [262]. Another use of CNCs within a scaffold for bone tissue engineering was conducted by Zhang et al. in 2015. In this study CNCs were grafted with polyethylene glycol (PEG) for incorporation into PLA to create an electrospun scaffold. This scaffold was then cultured with human MSCs for 14 days, and showed increased cell proliferation and adhesion compared to the control scaffold without any PEG-g-CNCs. The PEG-g-CNCs provided increased adhesion sites to the hMSCs due to the smaller diameter of the fibers and improved mechanical properties [260]. CNCs can be used as a filler within PLA electrospun fibers to not only improve the mechanical properties, but to increase cell adhesion and proliferation, which is promising for tissue engineering applications. Electrospinning of polymers is a common method used to create tissue engineering scaffolds. He et

al. wanted to employ this method to create a purely cellulose mat from regenerated cellulose that was reinforced with CNCs for use with human dental follicle cells (hDFCs). A cellulose-only electrospun biomaterial can support hDFCs adhesion and proliferation with increased extracellular matrix formation on the cellulose mats after 7 days in culture, while increasing mechanical properties with the addition of CNCs. It is suggested that an electrospun regenerated cellulose mat reinforced with CNCs can have great potential for use in applications requiring high shear forces such as artificial blood vessels [259].

Another instance of the use of mesenchymal stem cells for biomaterial evaluation is the evaluation of cellular uptake of poly(lactic-co-glycolic acid) (PLGA) microspheres loaded with fluorescein isothiocyanate conjugated bovine serum albumin (FITC-BSA) in polyvinyl alcohol (PVA)/CNC composite films by Rescignano et al. Human MSCs cultured on slowly dissolving PVA/CNC composites with PLGA microspheres had decreased cell viability after 14 days in culture compared to PVA films and the control, but no statistical analysis was reported in regards to significance. The uptake of the PLGA microspheres was controlled in the slowly degrading PVA/CNC composites with fluorescent exposure remaining within the MSCs up to 72 hours post seeding [263]. The uptake of the PLGA microspheres loaded with BSA suggests that this system can be employed for future use as a drug or growth factor delivery system in tissue engineered systems.

While the use of CNCs in tissue engineering applications is limited, there have been some research successes. Camarero-Espinosa and researchers used phosphoric acid (P-CNCs) and sulfuric acid-derived (S-CNCs) CNCs within poly(lactic acid) (PLA) to create a scaffold for cartilage regeneration, which mimicked the three distinct layers in native tissue.

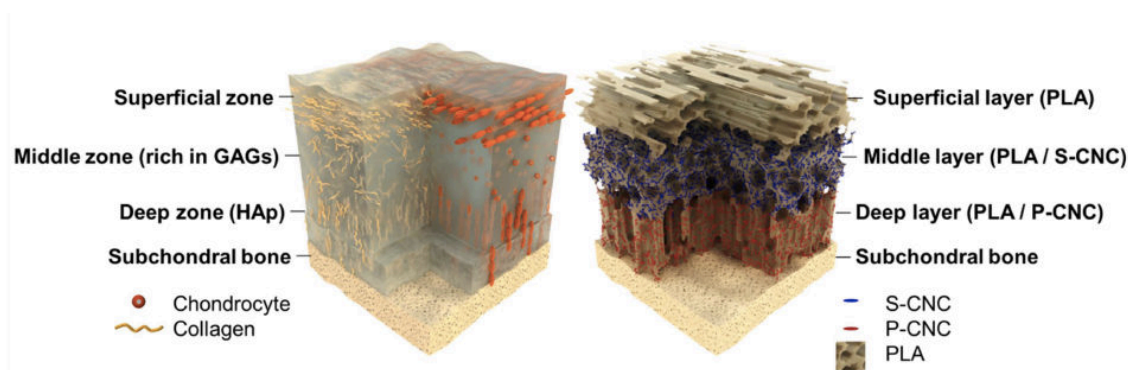


Figure 3.6. Comparison of native cartilage tissue versus the PLA/CNCs scaffold created by Camarero-Espinosa et al.

[261]

CNCs produced from different acid hydrolysis procedures were used to impart different properties within each layer. It was shown that P-CNCs induced the formation of a hydroxyapatite layer onto the PLA and a tubular morphology of chondrocytes, which is what is found in the native tissue deep zone. Cells within the middle layer presented a rounded morphology because of the ionic nature of the S-CNCs. After 2 and 4 weeks of culture with human fetal chondrocytes the multi-layer constructs displayed mechanical properties that were similar to native tissue. These results demonstrate that a multi-functional approach to cartilage tissue engineering can be achieved with cellulose nanocrystals [261]. Future exploration of the use of CNCs for tissue engineered constructs can be found in an extensive review by Domingues et al. [264].

Table 3.3. Uses of CNCs in Cell Culture/Tissue Engineering, Highlighted entries used cell lines similar to Ph.D. studies

Modification of CNCs	CNCs with Polymer	Use of Polymer	Cell Type	Cellular Characterization	Ref
no	no	no	BMEC, bEnd.3, RAW 264.7, MCF-10A, MDA-MB-231, MDA-MB-468, KB, PC-3 and C6	low cytotoxicity, low nonspecific cellular uptake	[265]
yes, folic acid conjugated	no	no	human (DBTRG-05MG, H4) rat (C6) brain tumor cells	low cytotoxicity, folate receptor-mediated cellular uptake	[266]
yes, folic acid conjugated	no	no	KB and MDA-MB-468 human cancer cells	low cytotoxicity, folate receptor-mediated cellular uptake	[267]
no	no	no	human bronchial epithelial BEAS 2B cells, Human Monocyte-Derived Macrophages (hMDMs)	neither genotoxic nor immunotoxic	[268]
no	no	no	human Bronchial Epithelial Lung 16HBE14o	low cytotoxicity, low inflammatory	[257]
yes	no	no	human embryonic kidney 293 (HEK 293) Spodoptera frugiperda (Sf9)	no noticeable cytotoxic effect effector cells were surrounded by CNC-FITC	[269]
yes, microspheres	no	no	human fibroblasts	fast cellular uptake, no transfection reagents or attachment of a receptor molecule	[270]
no	no	no	Chinese hamster lung fibroblast V79 Spodoptera frugiperda Sf9 insect cells	no significant cytotoxicity suggested correlation between the inhibitory effect and the carboxylic acid	[271]
no	no	no	murine myoblasts C2C12	myoblasts oriented along CNC patterns, terminal differentiation	[258]
no	yes	polylactic acid matrix for electrospinning	human adult adipose derived mesenchymal stem cells (hASCs)	basic cytocompatibility	[262]
yes, polyethylene glycol grafted CNC	yes	polylactic acid matrix for electrospinning	human mesenchymal stem cells (hMSCs)	increased cell adhesion, proliferation	[260]
no	yes	regenerated cellulose matrix for electrospinning	human dental follicle cells (hDFCs)	increased ECM formation	[259]
no	yes	polylactic acid coated with CNCs	human fetal chondrocytes	proliferating and hypertrophic chondrocytes as shown in collagen I/collagen II expression	[261]
no	yes	polylactid acid fibers coated with CNCs	NIH-3T3 mouse fibroblast cells	increased cell adhesion and spreading	[272]
no	yes	polyvinyl alcohol /starch sponge nanocomposite	monkey kidney fibroblast-like COS-7 cells	microscope images - no quantification of cell proliferation	[273]
yes, aldehyde modified CNC	yes	injectable carboxymethyl hydrogels cellulose and dextran	NIH 3T3 fibroblast cells	no decreased cell viability	[274]
no	yes	polyurethane	L929 murine fibroblasts	increased cell adhesion, proliferation	[275]

no	yes	Poly(3-hydroxybutyrate-co-3-hydroxyvalerate) (PHBV) matrix	human MG-63 osteosarcoma cells	low cytotoxicity, increased cell adhesion	[276]
no	yes	polyvinyl alcohol matrix with BSA-loaded poly(lactic-co-glycolic acid) microspheres	human bone marrow mesenchymal stem cells	low cytotoxicity, controlled uptake of BSA-loaded microparticles	[263]
no	yes	collagen matrix	NIH3T3 mouse fibroblast cells	low cytotoxicity, increased cell adhesion	[190]
no	yes	cellulose acetate for electrospinning	Wistar rat aortic vascular smooth muscle cells (VSMC)	increased cell adhesion, no decrease in cell viability	[277]

3.3.2 Cellulose Nanofibers

As with CNCs, there has been limited work regarding the use of CNFs for tissue engineering applications or with MSCs. Most research until this time has focused on determining if CNFs are biocompatible and suitable for use in cell culture. Preliminary studies used murine sourced cells such as NIH3T3 or L929 fibroblasts, to determine cell viability as outlined in Table 3.4

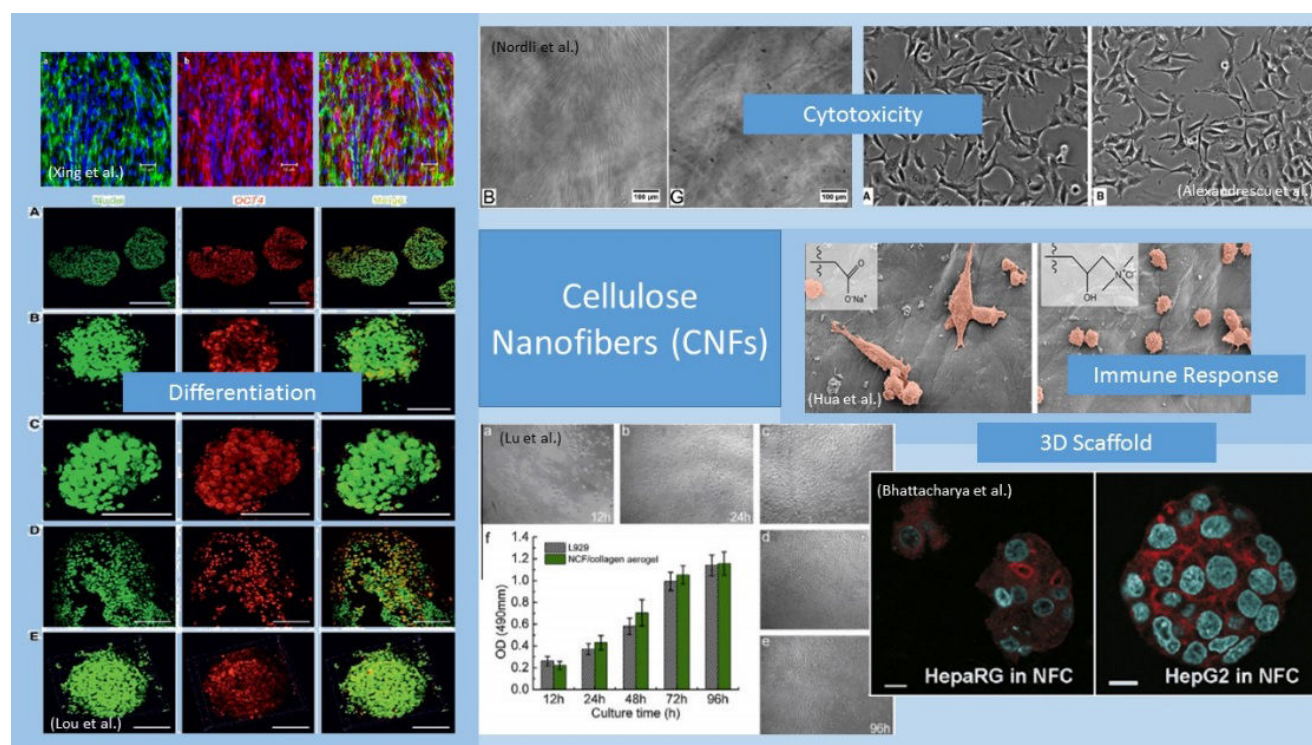


Figure 3.7. Cellular interactions, cytotoxicity, and tissue engineering potential of CNFs [278-283]

Studies employing human fibroblast or macrophages to determine the cytotoxicity or immunoregulatory response to CNFs have been conducted in recent years. Research conducted by Hua and colleagues modulated the surface chemistry of CNF films to observe cellular response. Human dermal fibroblasts were employed to determine indirect cytotoxicity, but also cellular adhesion on CNF films after 24 hours in culture. Lactate dehydrogenase (LDH) assay of culture media incubated with unmodified enzymatically derived, carboxymethylated (anionic), and trimethylammonium (cationic) 24 hours prior to cell seeding showed there was not a cytotoxic effect for any of the samples. This suggests that none of the CNF samples are leeching any material into the culture media that could be toxic. For direct cellular testing, cationic CNF had increased cellular adhesion compared to anionic and unmodified CNF films, with no significant differences reported between the anionic and

unmodified CNF films. It was hypothesized that the partial substitution of -OH favored cell adhesion, and that CNF films are suitable for future biomaterial development because of a lack of cytotoxic response [284].

Nordli et al. produced “ultrapure CNF” aerogels from sodium hydroxide treated cellulose fibers, which were then made into TEMPO-mediated oxidized CNF. This CNF was deemed to be “ultrapure” because of the continued decrease of lipopolysaccharide (LPS), or endotoxin, production by limulus amoebocyte lysate (LAL) assay when passing from 0.5% suspensions of NaOH bleached cellulose fiber to, TEMPO-oxidized CNF (CNF-T), or to CNF-T aerogels. Cytotoxicity of the CNF-T aerogels was tested using LDH assay, 3-(4,5-Dimethylthiazol-2-yl)-2,5-diphenyltetrazolium bromide (MTT) cell metabolic viability assay at 2 hours, 6 hours, and 24 hours post seeding and cytokine release following 24 hours in culture. It was shown for human dermal fibroblasts that cell viability for CNF-T aerogels and CNF-T suspension of 50 µg/mL decreased from 6 to 24 hours. This reduction in cell viability was not due to cell death, but a possible reduction in cell proliferation because of the lack of increase of LDH production at 24 hours. In regards to keratinocytes, there was a significant decrease in cell viability at 2 hours compared to the control for the CNF-T aerogel, but had similar metabolic response to the control at all time points for the CNF-T suspension. Cytokine release was determined using the supernatant of the cell culture 24 hours post-seeding to determine a possible inflammatory response. For fibroblasts there were no significant differences in cytokine production compared to the control for CNF-T aerogels, but the suspension of CNF-T reduced IL-8 production. CNF-T aerogels cultured with keratinocytes had significantly lower concentrations of VEGF, IL-10, IL-12, and IP-10. All cells cultured with CNF-T aerogels or CNF-T suspensions did not have elevated cytokine release compared to the control. These results display that “ultrapure” CNF-T can be produced and be suitable for future clinical wound healing applications [279].

The immune response to a biomaterial is an important factor to determine for future tissue engineering applications. Hua and researchers continued to explore the effect of surface chemistry of CNF films, but instead of using human dermal fibroblasts, human THP-1 monocytes were employed to measure myocyte or macrophage response. As with the study outlined earlier, unmodified enzymatically derived, carboxymethylated (anionic), and hydroxypropyltrimethylammonium (cationic) CNF films were tested to determine the concentration of cytokines released from human THP-1 monocytes after 24 hours in culture. Indirect cell viability and direct contact cell adhesion and cytokine response were tested. In indirect cytotoxicity testing all CNF materials did not illicit a toxic response. Human monocyte adhesion was significantly higher compared to the TMX (Thermanox® resistant plastic)

control. THP- α , a proinflammatory cytokine, secretion was not significantly different between cationic CNF and the control. Anionic CNF had the highest THP- α levels, but were not significant compared to cationic and unmodified CNF. Meaning that anionic and unmodified CNF films promote a proinflammatory state. IL-10 and IL-1ra secretion, or anti-inflammatory cytokines, were also determined in response to CNF exposure. IL-10 secretion was below the levels necessary for detection, but unmodified and anionic CNF produced IL-1ra levels that were significantly higher than the control. With anionic CNF having the highest response concentration. It was determined none of the CNF films produced an anti-inflammatory response, even with this reported significance, because of a feedback loop caused by just the presence of the materials and not a direct effect of the CNF. It was suggested that cationic CNF could be considered an inert material suitable to not illicit an immunoresponse [280].

The effect of CNF on the differentiation of stem cells has not been studied extensively, but there are some promising results using human mesenchymal stem cells (hMSCs), induced pluripotent stem cells (iPSCs), and embryonic stem cells (ESCs). Xing et al. created a gelatin/cellulose macrofiber (CMF) scaffold with 75% CMF content by solid–liquid phase separation of gelatin and CMF and sublimation of the solvent. Differentiation potential of hMSCs were determined by immunofluorescent staining, but differentiation was induced by osteogenic or adipogenic media. Therefore, these results cannot conclude that hMSC differentiation was induced by the gelatin/CMF scaffold alone. Following 35 days of culture in osteogenic or adipogenic media, hMSCs displayed phenotypes for both differentiation pathways. hMSCs cultured for 28 days in α -minimum essential medium, secreted fibronectin and collagen IV, which is essential for ECM formation and cell interaction and signaling. While actin staining indicated that there was substantial adhesion to the scaffold [278]. But these results were not compared to a control or other scaffold formulations. Therefore, no considerable conclusions can be made besides that gelatin/CMF scaffolds can be used for hMSCs cell culture.

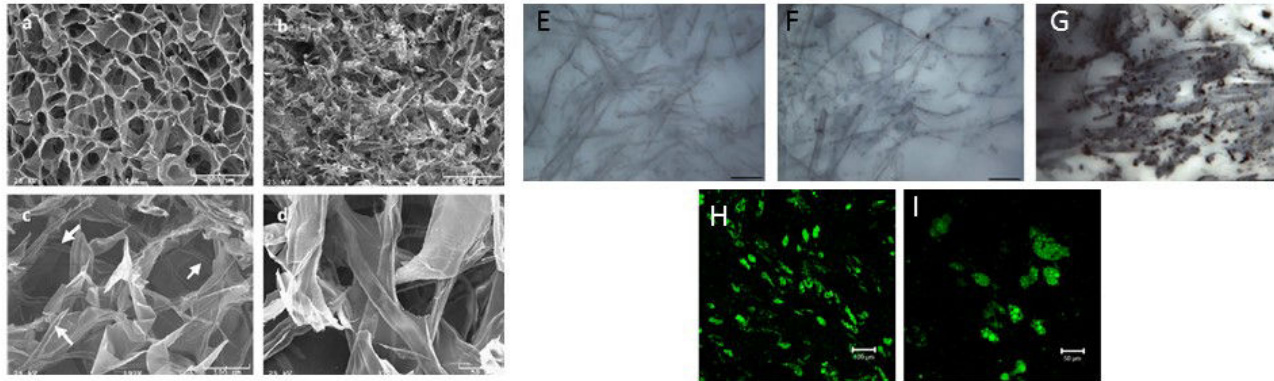


Figure 3.8. SEM images of a) gelatin scaffold, and b-d) 75% CMF/gelatin scaffold, Von Kossa staining of osteo-induced hMSCs in e) 75% cellulose fiber/gelatin scaffold and without induction after 8 weeks in culture for f) gelatin scaffold and g) 75% CMF/gelatin scaffold, Nile Red staining of h, i) 75% cellulose fiber/gelatin scaffold with adipogenic induction after 35 days in culture [278].

The only reported use of iPSCs and ESCs with CNFs was conducted by Lou et al. in 2014. CNF hydrogels with varying CNF amounts were fabricated to determine the effect of CNF concentration on iPSC behavior. Hydrogels with 1 wt% CNF did not induce spherical formation of the iPSCs, but iPSCs and ESCs spheroids formed on 0.5 wt% hydrogel with size increasing over time. This spheroid formation is essential to maintain pluripotency. An important step for directed stem cell differentiation is to maintain this 3D cell structure while transferring cells to a new system that would induce differentiation. In order to determine if the CNF hydrogel could be destroyed, but the spheroids remain intact, cellulase enzyme was used to remove the hydrogel. It was determined that the viability of the cells was significantly decreased at cellulase concentrations at and below 300 $\mu\text{g}/\text{mg}$ of cellulose. All spheroids remained unbroken and maintained pluripotency at cellulase concentrations of 50, 200, and 500 $\mu\text{g}/\text{mg}$ of cellulose. But cellulase concentrations below 200 $\mu\text{g}/\text{mg}$ did not sufficiently remove all the CNF.

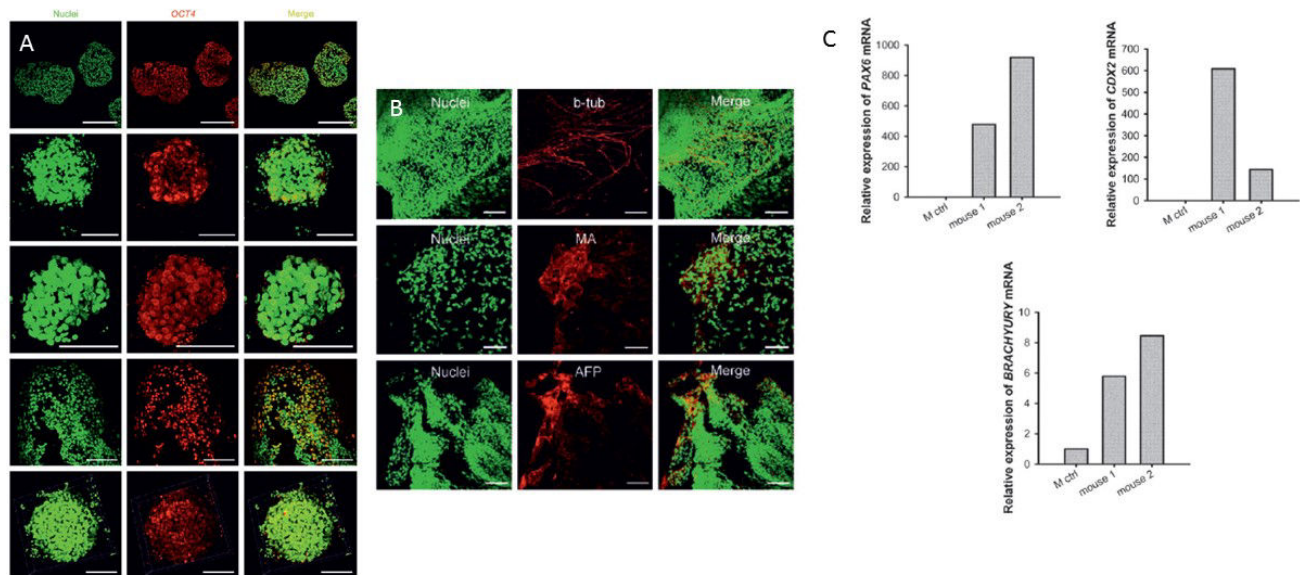


Figure 3.9. A) pluripotency marker OCT4 of hESCs following 7 days in culture in 0.5 wt% CNF hydrogel, B) induced *in vitro* differentiation of iPSCs following transfer after 26 days of culture in CNF hydrogel with three germ layer markers b-tubulin type III (b-tub), muscle actin (MA), and a fetoprotein (AFP). C) CDX2, and BRACHYURY mRNA expression in 6-week-old teratoma formed from hESCs that had previously been cultured in 0.5 wt.% CNF hydrogel for 26 days [283].

Following 26 days in culture in 0.5 wt% CNF hydrogel all cells retained their pluripotency as determined by pluripotency marker OCT4 staining and RT-PCR. As stated earlier, it was important to determine if the spheroids could retain their pluripotency following culture with 3D CNF hydrogel, removal of cellulose, and transfer to a 2D system. After 9 days of culture, hESCs maintained pluripotency following removal of CNF and when transferred to a 2D matrigel system, and iPSCs maintained pluripotency after 12 days of culture and transfer. To assess the directed differentiation potential of iPSCs following 3D culture, iPSCs spheroids were cultured in CNF hydrogels as well as matrigel control and then transferred to gelatin coated dishes. It was shown that iPSCs did not express the same levels of genetic markers for all three germ layers when compared to the control, which suggests that they are not equipped for directed differentiation on a 2D system. Teratoma formation was evaluated to assess the pluripotency of hESCs. *In vivo* evaluation of hESCs was conducted after 26 days of culture in 0.5 wt% CNF hydrogel. hESC spheroids were transferred to two nude NMRI mice and assessed after 6 weeks *in vivo*. Teratoma formation occurred for hESCs cultured in CNF hydrogels, but not the Matrigel system as evidenced by histology and also gene expression of PAX6, CDX2, and BRACHYURY. This indicates that hESCs cultured in CNF maintain their pluripotency. CNF

hydrogels can be employed to create a sustainable, xeno-free system without crosslinking to maintain iPSC and hESC pluripotency [283].

Table 3.4 Uses of CNFs in Cell Culture/Tissue Engineering, Highlighted entries used cell lines similar to Ph.D. studies

Modification of CNFs	of CNFs	with	Use of Polymer	Cell Type	Cellular Characterization	Ref
no	no	no		Human macrophage-like THP-1 cells	showed no significant changes in the Cell Index no significant expression of TNF- α	[285]
no	no	no		L929 murine fibroblasts	low cytotoxicity	[286]
no	no	no		RAW 264.7 murine macrophages, human peripheral blood derived monocytes (PBMCs)	low cytotoxicity, no immune response	[287]
no	no	no		bovine fibroblasts	cytotoxicity dependent on dose	[288]
no, CNF hydrogel	no	no		hPSCs: H9-GFP, WA07, iPS(IMR90)-4	cell differentiation, maintained pluripotency	[283]
no, 3D CNF hydrogel	no	no		Human HepaRG cells	increased cell viability, induced formation of 3D multicellular spheroids, hepatic differentiation	[289]
no	no	no		human hepatic cell lines (HepG2 and HepaRG)	spheroid formation of cells	[281]
no	yes		Pectin/carboxymethyl cellulose/CNF composite	NIH3T3 murine fibroblasts	increased cell viability	[290]
no	yes		CNF, calcium peroxide layered nanocomposites	L929 murine fibroblasts	decreased cell attachment and proliferation	[291]

No, CMF	yes	CNF/gelatin scaffold	Human Mesenchymal Stem Cells (hMSCs), CRL-2020 glioblastoma	CRL-2020 cells did not form colonies with cellulose fibers, hMSCs excreted ECM and maintained differentiation potential	[278]
Yes, carboxymethylated-CNF, trimethylammonium-CNF	no	no	human dermal fibroblasts (hDF)	decreased cytotoxicity for carboxymethylated compared to unmodified and trimethylammonium-CNF promotion of cell differentiation, migration and adhesion for carboxymethylated-CNF	[284]
yes, anionic/catioic	no	no	human THP-1 monocytes	anionic CNF - proinflammatory phenotype cationic CNF - no inflammatory activation CNF - mild activation	[280]
yes, crosslinked polyamide-epichlorohydrin resin CNF areogels	no	no	NIH3T3 murine fibroblasts	low cytotoxicity	[292]
yes, TEMPO-oxidized CNF	no	no	normal human dermal fibroblasts, human epidermal keratinocytes	reduced of metabolic activity, no significant cell death, no inflammatory response	[279]

yes, TEMPO-oxidized, crosslinking agent polyethyleneimine (PEI) or the surfactant cetyl trimethylammonium (CTAB)	no	no	NIH3T3 murine fibroblasts	low cytotoxicity for TEMPO-oxidized CNF, high cytotoxicity with CTAB, reduced cell viability with PEI crosslinked samples	[293]
yes, dialdehyde CNFs	yes	CNF/collagen areogel	L929 murine fibroblasts	low cytotoxicity	[282]

4. Conclusion and Perspectives

Nanocellulose is a new, exciting biomaterial that has tremendous potential a new biomaterial. The functionalization capabilities of nanocellulose, its use as mechanical reinforcement, as well as active agent carrier properties make it attractive to researchers for a variety of biomedical applications ranging from wound healing to drug delivery. While research using nanocellulose as a biomaterial is limited, it is gaining more interest year after year not only because of its versatility, but also its environmental properties.

A systematic study of the use of nanocellulose as a biomaterial will be presented: from the production of CNCs from agricultural waste, to the use of CNF to induce cell differentiation.

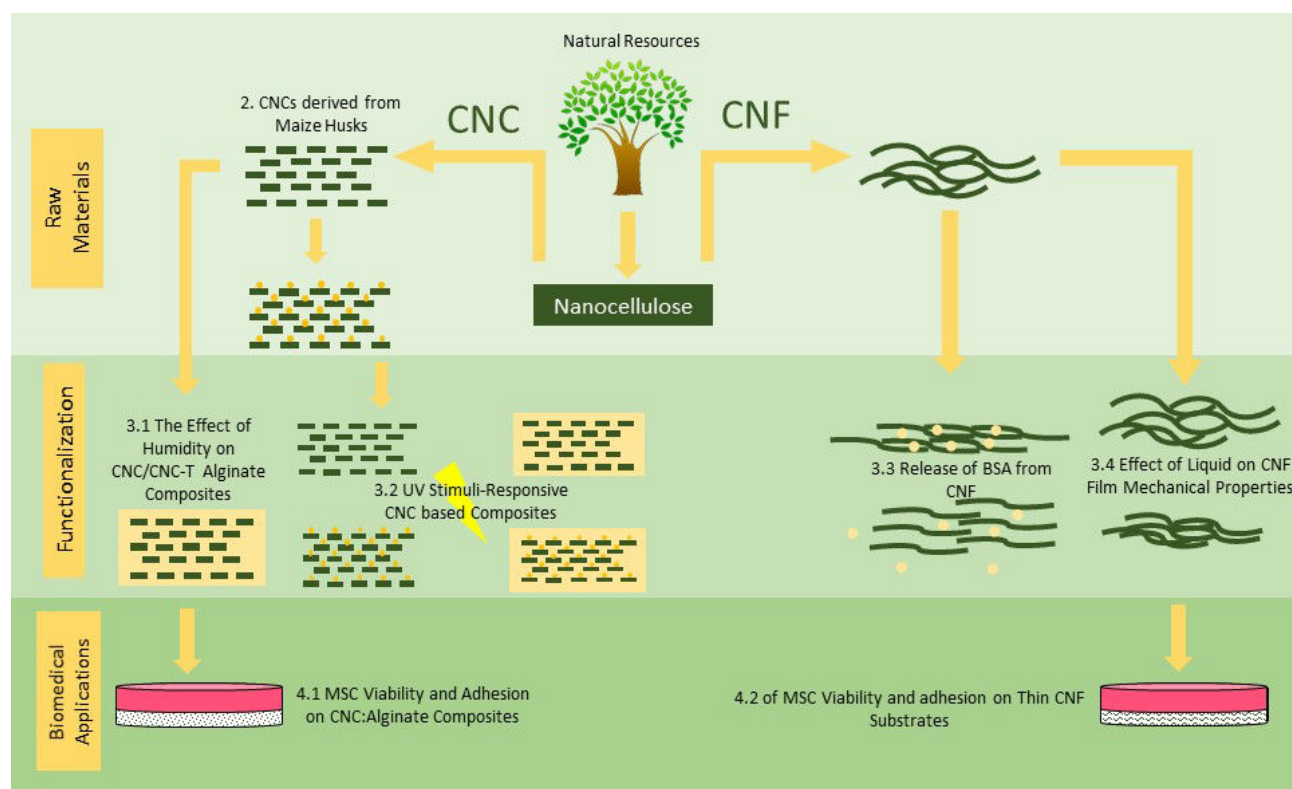


Figure 4.1. Schematic representation of thesis

Through this work it has been demonstrated that nanocellulose can be used in a variety of applications for biomedical applications, and that the modification potential of nanocellulose can impart favorable characteristics to biomedical constructs that can be harnessed by researchers in the future.

5. Figures and Tables

Figures

Figure 1.1. Scheme of different types of commonly used biomaterials

Figure 1.2. Cell or host response to physical biomaterial properties

Figure 1.3. Pore structure and strut microstructure of 45S5 Bioglass®-derived foams from Chen et al. [11]

Figure 1.4. SEM images of osteoblasts cultured on titanium surfaces [16].

Figure 1.5. Schematic representation of increased angiogenesis by covalently bonded heparin-PEG gels within polyurethane scaffolds [30]

Figure 1.6. Uses of alginate in biomedical applications: tissue engineering [55, 56], hydrogels [54, 57], wound dressing [58, 59], protein immobilization [60, 61], and cell encapsulation [62]

Figure 1.7. Fabrication techniques of chitosan-based materials for tissue engineering applications [66]

Figure 1.8. Number of publications from 2000-2017 using different types of biomaterials

Figure 1.9. Examples of uses of BNC in biomedical applications such as scaffold construct [91], wound healing [87, 89], and tissue engineering [92]

Figure 2.1. Hierarchical structure of plant fibers from cellulose chains [98] and steps to produce nanocellulose and some applications of nanocellulose use

Figure 2.2 Nanocellulose biorefinery concept from agricultural and industrial waste [104]

Figure 2.3. Schematic representation of CNF production steps from purification to post-treatment [98]

Figure 2.4. Common microscopy techniques used for nanocellulose characterization, AFM [134], SEM [135], and TEM [136]

Figure 2.5. Chemical structure of cellulose [146]

Figure 2.6. Functionalization agents used for physical and chemical functionalization of nanocellulose, adopted from Espino-Perez [154]

Figure 2.7. Chemical reaction of TEMPO mediated oxidation of cellulose

Figure 2.8. Examples of the use of CNCs to improve the mechanical properties of alginate, or increased interaction in crosslinking by CNC-Ts

Figure 2.9. Schematic of switching of CNC interaction dependent on the hydrogen bonding [198]

Figure 3.1. Possible differentiation pathways of mesenchymal stem cells, adopted from DiMarino et al. [216]

Figure 3.2. Length scales and modification techniques of biomaterials as adopted from Palsson et al. [20]

Figure 3.3. Pictorial representation of three common modification techniques to induce cell adhesion, proliferation, and differentiation

Figure 3.4. Schematic of how MSCs attach to collagen coated polyacrylamide gels with varying elasticity and images of MSCs with scale bar of 20 μm , from Engler et al.[233]

Figure 3.5. Properties and examples of uses of CNCs in cell culture and tissue engineering applications [257-261]

Figure 3.6. Comparison of native cartilage tissue versus the PLA/CNCs scaffold created by Camarero-Espinosa et al. [261]

Figure 3.7. Cellular interactions, cytotoxicity, and tissue engineering potential of CNFs [278-283]

Figure 3.8. SEM images of gelatin/CMF scaffold with hMSCs [278].

Figure 3.9. Pluripotency of hESCs and iPSCs cultured within 3D CNF [283].

Figure 4.1. Schematic representation of thesis

Tables

Table 1.1. Synthetic polymers used in tissue engineering applications adopted from [21]

Table 2.1. Properties of CNCs from Traditional Sources and Agrowastes

Table 2.2. Mechanical Technologies Used for CNF Production [126]

Table 2.3. Mechanical Properties of Crystalline Cellulose [82]

Table 2.4. Mechanical Properties of CNF Films in Ambient Conditions, Adapted from Dufresne [82]

Table 2.5. Surface Chemical Modifications of CNCs for use in Nanocomposites, from Mariano et al. [169]

Table 3.1 Pros and Cons of Stem Cells

Table 3.2 Adult Stem Cells: Sources and Differentiation Pathways [212]

Table 3.3. Uses of CNCs in Cell Culture/Tissue Engineering

Table 3.4 Uses of CNFs in Cell Culture/Tissue Engineering

6. References

- [1] Ratner BD, Hoffman AS, Schoen FJ, Lemons JE. Biomaterials science: a multidisciplinary endeavor. *Biomaterials science: an introduction to materials in medicine*. 2004;1-9.
- [2] Williams DF. Definitions in Biomaterials: Proceedings of a Consensus Conference of the European Society for Biomaterials, Chester, Engl., March 3-5, 1986: Elsevier; 1987.
- [3] Vert M, Hellwich K-H, Hess M, Hodge P, Kubisa P, Rinaudo M, et al. Terminology for biorelated polymers and applications (IUPAC Recommendations 2012). *Pure and Applied Chemistry*. 2012;84:377-410.
- [4] Black J, Hastings G. *Handbook of biomaterial properties*: Springer Science & Business Media; 2013.
- [5] Ramakrishna S, Huang Z-M, Kumar GV, Batchelor AW, Mayer J. *An Introduction to Biocomposites* Imperial College Press; 2004.
- [6] Ratner BD, Hoffman AS, Schoen FJ, Lemons JE. *Biomaterials science: an introduction to materials in medicine*: Academic press; 2004.
- [7] Thamaraiselvi T, Rajeswari S. Biological evaluation of bioceramic materials-a review. *Carbon*. 2004;24:172.
- [8] Dubok VA. Bioceramics—Yesterday, Today, Tomorrow. *Powder Metallurgy and Metal Ceramics*. 2000;39:381-94.
- [9] Verron E, Khairoun I, Guicheux J, Bouler JM. Calcium phosphate biomaterials as bone drug delivery systems: a review. *Drug Discov Today*. 2010;15:547-52.
- [10] Dziadek M, Stodolak-Zych E, Cholewa-Kowalska K. Biodegradable ceramic-polymer composites for biomedical applications: A review. *Materials Science and Engineering: C*. 2017;71:1175-91.
- [11] Chen QZ, Thompson ID, Boccaccini AR. 45S5 Bioglass®-derived glass—ceramic scaffolds for bone tissue engineering. *Biomaterials*. 2006;27:2414-25.
- [12] Xynos I, Hukkanen M, Batten J, Buttery L, Hench L, Polak J. Bioglass® 45S5 stimulates osteoblast turnover and enhances bone formation in vitro: implications and applications for bone tissue engineering. *Calcified Tissue International*. 2000;67:321-9.
- [13] Geetha M, Singh AK, Asokamani R, Gogia AK. Ti based biomaterials, the ultimate choice for orthopaedic implants – A review. *Progress in Materials Science*. 2009;54:397-425.
- [14] Long M, Rack H. Titanium alloys in total joint replacement—a materials science perspective. *Biomaterials*. 1998;19:1621-39.

- [15] Staiger MP, Pietak AM, Huadmai J, Dias G. Magnesium and its alloys as orthopedic biomaterials: a review. *Biomaterials*. 2006;27:1728-34.
- [16] Lincks J, Boyan B, Blanchard C, Lohmann C, Liu Y, Cochran D, et al. Response of MG63 osteoblast-like cells to titanium and titanium alloy is dependent on surface roughness and composition. *Biomaterials*. 1998;19:2219-32.
- [17] Puleo DA, Huh WW. Acute toxicity of metal ions in cultures of osteogenic cells derived from bone marrow stromal cells. *Journal of Applied Biomaterials*. 1995;6:109-16.
- [18] Jacobs JJ, Gilbert JL, Urban RM. Current concepts review-corrosion of metal orthopaedic implants. *J Bone Joint Surg Am*. 1998;80:268-82.
- [19] Lhotka C, Szekeres T, Steffan I, Zhuber K, Zweymüller K. Four-year study of cobalt and chromium blood levels in patients managed with two different metal-on-metal total hip replacements. *Journal of Orthopaedic Research*. 2003;21:189-95.
- [20] Pålsson BØ, Bhatia SN. *Tissue Engineering*: Pearson Education; 2004.
- [21] Elisseeff JH, Yamada Y, Langer R. Biomaterials for tissue engineering. *Tissue Engineering and Biodegradable Equivalents: Scientific and Clinical Applications*. 2002:1-23.
- [22] Nair LS, Laurencin CT. Biodegradable polymers as biomaterials. *Progress in Polymer Science*. 2007;32:762-98.
- [23] Lloyd AW. Interfacial bioengineering to enhance surface biocompatibility. *Medical device technology*. 2001;13:18-21.
- [24] Gunatillake PA, Adhikari R. Biodegradable synthetic polymers for tissue engineering. *Eur Cell Mater*. 2003;5:1-16.
- [25] Tian H, Tang Z, Zhuang X, Chen X, Jing X. Biodegradable synthetic polymers: Preparation, functionalization and biomedical application. *Progress in Polymer Science*. 2012;37:237-80.
- [26] Ulfery BD, Nair LS, Laurencin CT. Biomedical applications of biodegradable polymers. *Journal of Polymer Science Part B: Polymer Physics*. 2011;49:832-64.
- [27] Hayashi T. Biodegradable polymers for biomedical uses. *Progress in Polymer Science*. 1994;19:663-702.
- [28] Veronese FM. Peptide and protein PEGylation: a review of problems and solutions. *Biomaterials*. 2001;22:405-17.
- [29] Ifkovits JL, Burdick JA. Review: photopolymerizable and degradable biomaterials for tissue engineering applications. *Tissue Engineering*. 2007;13:2369-85.

- [30] van Rensburg AJ, Davies NH, Oosthuysen A, Chokoza C, Zilla P, Bezuidenhout D. Improved vascularization of porous scaffolds through growth factor delivery from heparinized polyethylene glycol hydrogels. *Acta biomaterialia*. 2016.
- [31] Badylak SF, Lantz GC, Coffey A, Geddes LA. Small intestinal submucosa as a large diameter vascular graft in the dog. *Journal of Surgical Research*. 1989;47:74-80.
- [32] Friess W. Collagen–biomaterial for drug delivery. *European Journal of Pharmaceutics and Biopharmaceutics*. 1998;45:113-36.
- [33] Bosnakovski D, Mizuno M, Kim G, Takagi S, Okumura M, Fujinaga T. Chondrogenic differentiation of bovine bone marrow mesenchymal stem cells (MSCs) in different hydrogels: influence of collagen type II extracellular matrix on MSC chondrogenesis. *Biotechnology and Bioengineering*. 2006;93:1152-63.
- [34] Tabata Y, Miyao M, Ozeki M, Ikada Y. Controlled release of vascular endothelial growth factor by use of collagen hydrogels. *Journal of Biomaterials Science, Polymer Edition*. 2000;11:915-30.
- [35] Helary C, Bataille I, Abed A, Illoul C, Anglo A, Louedec L, et al. Concentrated collagen hydrogels as dermal substitutes. *Biomaterials*. 2010;31:481-90.
- [36] Hunt NC, Grover LM. Cell encapsulation using biopolymer gels for regenerative medicine. *Biotechnology Letters*. 2010;32:733-42.
- [37] Yannas IV. Models of organ regeneration processes induced by templates. *Annals of the New York Academy of Sciences*. 1997;831:280-93.
- [38] Boland ED, Matthews JA, Pawlowski KJ, Simpson DG, Wnek GE, Bowlin GL. Electrospinning collagen and elastin: preliminary vascular tissue engineering. *Front Biosci*. 2004;9:e32.
- [39] George M, Abraham TE. Polyionic hydrocolloids for the intestinal delivery of protein drugs: alginate and chitosan—a review. *Journal of Controlled Release*. 2006;114:1-14.
- [40] Simmons CA, Alsberg E, Hsiong S, Kim WJ, Mooney DJ. Dual growth factor delivery and controlled scaffold degradation enhance in vivo bone formation by transplanted bone marrow stromal cells. *Bone*. 2004;35:562-9.
- [41] Alsberg E, Kong H, Hirano Y, Smith M, Albeiruti A, Mooney D. Regulating bone formation via controlled scaffold degradation. *Journal of dental research*. 2003;82:903-8.
- [42] Bouhadir KH, Lee KY, Alsberg E, Damm KL, Anderson KW, Mooney DJ. Degradation of partially oxidized alginate and its potential application for tissue engineering. *Biotechnology Progress*. 2001;17:945-50.

- [43] Bajpai SK, Sharma S. Investigation of swelling/degradation behaviour of alginate beads crosslinked with Ca^{2+} and Ba^{2+} ions. *Reactive and Functional Polymers*. 2004;59:129-40.
- [44] Shoichet MS, Li RH, White ML, Winn SR. Stability of hydrogels used in cell encapsulation: An in vitro comparison of alginate and agarose. *Biotechnology and Bioengineering*. 1996;50:374-81.
- [45] Drury JL, Dennis RG, Mooney DJ. The tensile properties of alginate hydrogels. *Biomaterials*. 2004;25:3187-99.
- [46] Lee KY, Mooney DJ. Alginate: properties and biomedical applications. *Progress in Polymer Science*. 2012;37:106-26.
- [47] Tønnesen HH, Karlsen J. Alginate in drug delivery systems. *Drug Development and Industrial Pharmacy*. 2002;28:621-30.
- [48] Choi B, Park HJ, Hwang S, Park J. Preparation of alginate beads for floating drug delivery system: effects of CO_2 gas-forming agents. *International Journal of Pharmaceutics*. 2002;239:81-91.
- [49] Stockwell A, Davis S, Walker S. In vitro evaluation of alginate gel systems as sustained release drug delivery systems. *Journal of Controlled Release*. 1986;3:167-75.
- [50] Barnett S, Varley S. The effects of calcium alginate on wound healing. *Annals of the Royal College of Surgeons of England*. 1987;69:153.
- [51] Boateng JS, Matthews KH, Stevens HN, Eccleston GM. Wound healing dressings and drug delivery systems: a review. *Journal of Pharmaceutical Sciences*. 2008;97:2892-923.
- [52] Lee KY, Mooney DJ. Hydrogels for tissue engineering. *Chemical Reviews*. 2001;101:1869-80.
- [53] Drury JL, Mooney DJ. Hydrogels for tissue engineering: scaffold design variables and applications. *Biomaterials*. 2003;24:4337-51.
- [54] Kuo CK, Ma PX. Ionically crosslinked alginate hydrogels as scaffolds for tissue engineering: Part 1. Structure, gelation rate and mechanical properties. *Biomaterials*. 2001;22:511-21.
- [55] Venkatesan J, Bhatnagar I, Manivasagan P, Kang K-H, Kim S-K. Alginate composites for bone tissue engineering: a review. *International Journal of Biological Macromolecules*. 2015;72:269-81.
- [56] Wang L, Shelton RM, Cooper PR, Lawson M, Triffitt JT, Barralet JE. Evaluation of sodium alginate for bone marrow cell tissue engineering. *Biomaterials*. 2003;24:3475-81.
- [57] Novikova LN, Mosahebi A, Wiberg M, Terenghi G, Kellerth JO, Novikov LN. Alginate hydrogel and matrigel as potential cell carriers for neurotransplantation. *J Biomed Mater Res A*. 2006;77:242-52.
- [58] Balakrishnan B, Mohanty M, Umashankar P, Jayakrishnan A. Evaluation of an in situ forming hydrogel wound dressing based on oxidized alginate and gelatin. *Biomaterials*. 2005;26:6335-42.

- [59] Wang L, Khor E, Wee A, Lim LY. Chitosan-alginate PEC membrane as a wound dressing: Assessment of incisional wound healing. *Journal of biomedical materials research*. 2002;63:610-8.
- [60] Rowley JA, Madlambayan G, Mooney DJ. Alginate hydrogels as synthetic extracellular matrix materials. *Biomaterials*. 1999;20:45-53.
- [61] Kong HJ, Polte TR, Alsberg E, Mooney DJ. FRET measurements of cell-traction forces and nano-scale clustering of adhesion ligands varied by substrate stiffness. *Proceedings of the National Academy of Sciences of the United States of America*. 2005;102:4300-5.
- [62] Lim F, Sun AM. Microencapsulated islets as bioartificial endocrine pancreas. *Science*. 1980;210:908-10.
- [63] Jayakumar R, Menon D, Manzoor K, Nair SV, Tamura H. Biomedical applications of chitin and chitosan based nanomaterials—A short review. *Carbohydrate Polymers*. 2010;82:227-32.
- [64] VandeVord PJ, Matthew HW, DeSilva SP, Mayton L, Wu B, Wooley PH. Evaluation of the biocompatibility of a chitosan scaffold in mice. *Journal of Biomedical Materials Research Part A*. 2002;59:585-90.
- [65] Seeherman H, Li R, Wozney J. A review of preclinical program development for evaluating injectable carriers for osteogenic factors. *J Bone Joint Surg Am*. 2003;85:96-108.
- [66] Di Martino A, Sittinger M, Risbud MV. Chitosan: a versatile biopolymer for orthopaedic tissue-engineering. *Biomaterials*. 2005;26:5983-90.
- [67] Zhang Y, Zhang M. Synthesis and characterization of macroporous chitosan/calcium phosphate composite scaffolds for tissue engineering. *Journal of biomedical materials research*. 2001;55:304-12.
- [68] Zhang Y, Zhang M. Calcium phosphate/chitosan composite scaffolds for controlled in vitro antibiotic drug release. *Journal of biomedical materials research*. 2002;62:378-86.
- [69] Peter M, Binulal N, Soumya S, Nair S, Furuike T, Tamura H, et al. Nanocomposite scaffolds of bioactive glass ceramic nanoparticles disseminated chitosan matrix for tissue engineering applications. *Carbohydrate Polymers*. 2010;79:284-9.
- [70] Peter M, Kumar PTS, Binulal NS, Nair SV, Tamura H, Jayakumar R. Development of novel α -chitin/nanobioactive glass ceramic composite scaffolds for tissue engineering applications. *Carbohydrate Polymers*. 2009;78:926-31.
- [71] Peter M, Ganesh N, Selvamurugan N, Nair S, Furuike T, Tamura H, et al. Preparation and characterization of chitosan–gelatin/nanohydroxyapatite composite scaffolds for tissue engineering applications. *Carbohydrate Polymers*. 2010;80:687-94.

- [72] Seol Y-J, Lee J-Y, Park Y-J, Lee Y-M, Rhyu I-C, Lee S-J, et al. Chitosan sponges as tissue engineering scaffolds for bone formation. *Biotechnology Letters*. 2004;26:1037-41.
- [73] Suh J-KF, Matthew HW. Application of chitosan-based polysaccharide biomaterials in cartilage tissue engineering: a review. *Biomaterials*. 2000;21:2589-98.
- [74] Hsu Sh, Whu SW, Hsieh SC, Tsai CL, Chen DC, Tan TS. Evaluation of Chitosan-alginate-hyaluronate Complexes Modified by an RGD-containing Protein as Tissue-engineering Scaffolds for Cartilage Regeneration. *Artificial organs*. 2004;28:693-703.
- [75] Madhally SV, Matthew HW. Porous chitosan scaffolds for tissue engineering. *Biomaterials*. 1999;20:1133-42.
- [76] Sionkowska A. Current research on the blends of natural and synthetic polymers as new biomaterials: Review. *Progress in Polymer Science*. 2011;36:1254-76.
- [77] Lin N, Dufresne A. Nanocellulose in biomedicine: Current status and future prospect. *European Polymer Journal*. 2014;59:302-25.
- [78] Jorfi M, Foster EJ. Recent advances in nanocellulose for biomedical applications. *Journal of Applied Polymer Science*. 2015;132:41719.
- [79] Klemm D, Schumann D, Kramer F, Heßler N, Koth D, Sultanova B. Nanocellulose materials—Different cellulose, different functionality. *Macromolecular symposia: Wiley Online Library*; 2009. p. 60-71.
- [80] Gatenholm P, Klemm D. Bacterial nanocellulose as a renewable material for biomedical applications. *MRS Bulletin*. 2010;35:208-13.
- [81] Klemm D, Schumann D, Kramer F, Heßler N, Hornung M, Schmauder H-P, et al. Nanocelluloses as innovative polymers in research and application. *Polysaccharides II: Springer*; 2006. p. 49-96.
- [82] Dufresne A. *Nanocellulose: from nature to high performance tailored materials*: Walter de Gruyter; 2013.
- [83] Klemm D, Heublein B, Fink HP, Bohn A. Cellulose: fascinating biopolymer and sustainable raw material. *Angewandte Chemie International Edition*. 2005;44:3358-93.
- [84] Müller A, Ni Z, Hessler N, Wesarg F, Müller FA, Kralisch D, et al. The biopolymer bacterial nanocellulose as drug delivery system: investigation of drug loading and release using the model protein albumin. *Journal of Pharmaceutical Sciences*. 2013;102:579-92.

- [85] Moritz S, Wiegand C, Wesarg F, Hessler N, Müller FA, Kralisch D, et al. Active wound dressings based on bacterial nanocellulose as drug delivery system for octenidine. *International Journal of Pharmaceutics*. 2014;471:45-55.
- [86] Abeer MM, Amin M, Iqbal MC, Martin C. A review of bacterial cellulose-based drug delivery systems: their biochemistry, current approaches and future prospects. *Journal of Pharmacy and Pharmacology*. 2014;66:1047-61.
- [87] Fu L, Zhou P, Zhang S, Yang G. Evaluation of bacterial nanocellulose-based uniform wound dressing for large area skin transplantation. *Materials Science and Engineering: C*. 2013;33:2995-3000.
- [88] Berndt S, Wesarg F, Wiegand C, Kralisch D, Müller FA. Antimicrobial porous hybrids consisting of bacterial nanocellulose and silver nanoparticles. *Cellulose*. 2013;20:771-83.
- [89] Czaja W, Krystynowicz A, Bielecki S, Brown RM. Microbial cellulose—the natural power to heal wounds. *Biomaterials*. 2006;27:145-51.
- [90] Czaja WK, Young DJ, Kawecki M, Brown RM. The future prospects of microbial cellulose in biomedical applications. *Biomacromolecules*. 2007;8:1-12.
- [91] Nimeskern L, Ávila HM, Sundberg J, Gatenholm P, Müller R, Stok KS. Mechanical evaluation of bacterial nanocellulose as an implant material for ear cartilage replacement. *Journal of the mechanical behavior of biomedical materials*. 2013;22:12-21.
- [92] Shi Q, Li Y, Sun J, Zhang H, Chen L, Chen B, et al. The osteogenesis of bacterial cellulose scaffold loaded with bone morphogenetic protein-2. *Biomaterials*. 2012;33:6644-9.
- [93] Lin YK, Chen KH, Ou KL, Min L. Effects of different extracellular matrices and growth factor immobilization on biodegradability and biocompatibility of macroporous bacterial cellulose. *Journal of Bioactive and Compatible Polymers*. 2011;26:508-18.
- [94] Fang B, Wan Y-Z, Tang T-T, Gao C, Dai K-R. Proliferation and osteoblastic differentiation of human bone marrow stromal cells on hydroxyapatite/bacterial cellulose nanocomposite scaffolds. *Tissue Engineering Part A*. 2009;15:1091-8.
- [95] Urruzola I, Robles E, Serrano L, Labidi J. Nanopaper from almond (*Prunus dulcis*) shell. *Cellulose*. 2014;21:1619-29.
- [96] Habibi Y, Lucia LA, Rojas OJ. Cellulose nanocrystals: chemistry, self-assembly, and applications. *Chemical Reviews*. 2010;110:3479-500.
- [97] Bras J, Viet D, Bruzzese C, Dufresne A. Correlation between stiffness of sheets prepared from cellulose whiskers and nanoparticles dimensions. *Carbohydrate Polymers*. 2011;84:211-5.

- [98] Rowland SP, Roberts EJ. The nature of accessible surfaces in the microstructure of cotton cellulose. *Journal of Polymer Science Part A: Polymer Chemistry*. 1972;10:2447-61.
- [99] Nechyporchuk O, Belgacem MN, Bras J. Production of cellulose nanofibrils: A review of recent advances. *Industrial Crops and Products*. 2016.
- [100] Rånby B, Ribí E. Über den feinaufbau der zellulose. *Experientia*. 1950;6:12-4.
- [101] Herrick FW, Casebier RL, Hamilton JK, Sandberg KR. Microfibrillated cellulose: morphology and accessibility. *J Appl Polym Sci: Appl Polym Symp*;(United States): ITT Rayonier Inc., Shelton, WA; 1983.
- [102] Siró I, Plackett D. Microfibrillated cellulose and new nanocomposite materials: a review. *Cellulose*. 2010;17:459-94.
- [103] Turbak AF, Snyder FW, Sandberg KR. Microfibrillated cellulose, a new cellulose product: properties, uses, and commercial potential. *J Appl Polym Sci: Appl Polym Symp*;(United States): ITT Rayonier Inc., Shelton, WA; 1983.
- [104] Hoeng F, Denneulin A, Bras J. Use of nanocellulose in printed electronics: a review. *Nanoscale*. 2016;8:13131-54.
- [105] García A, Gandini A, Labidi J, Belgacem N, Bras J. Industrial and crop wastes: A new source for nanocellulose biorefinery. *Industrial Crops and Products*. 2016;93:26-38.
- [106] García A, Labidi J, Belgacem MN, Bras J. The nanocellulose biorefinery: woody versus herbaceous agricultural wastes for NCC production. *Cellulose*. 2016:1-12.
- [107] de Moraes Teixeira E, Corrêa A, Manzoli A, de Lima Leite F, de Oliveira C, Mattoso L. Cellulose nanofibers from white and naturally colored cotton fibers. *Cellulose*. 2010;17:595-606.
- [108] Sacui IA, Nieuwendaal RC, Burnett DJ, Stranick SJ, Jorfi M, Weder C, et al. Comparison of the properties of cellulose nanocrystals and cellulose nanofibrils isolated from bacteria, tunicate, and wood processed using acid, enzymatic, mechanical, and oxidative methods. *ACS Applied Materials & Interfaces*. 2014;6:6127-38.
- [109] de Moraes Teixeira E, Bondancia TJ, Teodoro KBR, Corrêa AC, Marconcini JM, Mattoso LHC. Sugarcane bagasse whiskers: extraction and characterizations. *Industrial Crops and Products*. 2011;33:63-6.
- [110] Espino E, Cakir M, Domenek S, Román-Gutiérrez AD, Belgacem N, Bras J. Isolation and characterization of cellulose nanocrystals from industrial by-products of Agave tequilana and barley. *Industrial Crops and Products*. 2014;62:552-9.

- [111] Mueller S, Weder C, Foster EJ. Isolation of cellulose nanocrystals from pseudostems of banana plants. *RSC Adv.* 2014;4:907-15.
- [112] Rosa M, Medeiros E, Malmonge J, Gregorski K, Wood D, Mattoso L, et al. Cellulose nanowhiskers from coconut husk fibers: Effect of preparation conditions on their thermal and morphological behavior. *Carbohydrate Polymers.* 2010;81:83-92.
- [113] Silvério HA, Flauzino Neto WP, Dantas NO, Pasquini D. Extraction and characterization of cellulose nanocrystals from corn cob for application as reinforcing agent in nanocomposites. *Industrial Crops and Products.* 2013;44:427-36.
- [114] Neto WPF, Silvério HA, Dantas NO, Pasquini D. Extraction and characterization of cellulose nanocrystals from agro-industrial residue—Soy hulls. *Industrial Crops and Products.* 2013;42:480-8.
- [115] dos Santos RM, Neto WPF, Silvério HA, Martins DF, Dantas NO, Pasquini D. Cellulose nanocrystals from pineapple leaf, a new approach for the reuse of this agro-waste. *Industrial Crops and Products.* 2013;50:707-14.
- [116] Johar N, Ahmad I, Dufresne A. Extraction, preparation and characterization of cellulose fibres and nanocrystals from rice husk. *Industrial Crops and Products.* 2012;37:93-9.
- [117] Jiang F, Hsieh Y-L. Chemically and mechanically isolated nanocellulose and their self-assembled structures. *Carbohydrate Polymers.* 2013;95:32-40.
- [118] Chaker A, Alila S, Mutjé P, Vilar MR, Boufi S. Key role of the hemicellulose content and the cell morphology on the nanofibrillation effectiveness of cellulose pulps. *Cellulose.* 2013;20:2863-75.
- [119] Novo LP, Bras J, García A, Belgacem N, Curvelo AA. Subcritical water: A method for green production of cellulose nanocrystals. *ACS Sustainable Chemistry & Engineering.* 2015;3:2839-46.
- [120] Kargarzadeh H, Ahmad I, Abdullah I, Dufresne A, Zainudin SY, Sheltami RM. Effects of hydrolysis conditions on the morphology, crystallinity, and thermal stability of cellulose nanocrystals extracted from kenaf bast fibers. *Cellulose.* 2012;19:855-66.
- [121] Siqueira G, Tapin-Lingua S, Bras J, da Silva Perez D, Dufresne A. Mechanical properties of natural rubber nanocomposites reinforced with cellulosic nanoparticles obtained from combined mechanical shearing, and enzymatic and acid hydrolysis of sisal fibers. *Cellulose.* 2011;18:57-65.
- [122] Lavoine N, Desloges I, Dufresne A, Bras J. Microfibrillated cellulose - its barrier properties and applications in cellulosic materials: a review. *Carbohydrate Polymers.* 2012;90:735-64.
- [123] Nakagaito AN, Yano H. The effect of morphological changes from pulp fiber towards nano-scale fibrillated cellulose on the mechanical properties of high-strength plant fiber based composites. *Applied Physics A.* 2004;78:547-52.

- [124] Henriksson M, Henriksson G, Berglund L, Lindström T. An environmentally friendly method for enzyme-assisted preparation of microfibrillated cellulose (MFC) nanofibers. *European Polymer Journal*. 2007;43:3434-41.
- [125] Pääkkö M, Ankerfors M, Kosonen H, Nykänen A, Ahola S, Österberg M, et al. Enzymatic hydrolysis combined with mechanical shearing and high-pressure homogenization for nanoscale cellulose fibrils and strong gels. *Biomacromolecules*. 2007;8:1934-41.
- [126] Bardet R. Nanocelluloses as Potential Materials for Specialty Papers. Grenoble, France Université Grenoble Alpes 2014.
- [127] Plackett D, Anturi H, Hedenqvist M, Ankerfors M, Gällstedt M, Lindström T, et al. Physical properties and morphology of films prepared from microfibrillated cellulose and microfibrillated cellulose in combination with amylopectin. *Journal of Applied Polymer Science*. 2010;117:3601-9.
- [128] Minelli M, Baschetti MG, Doghieri F, Ankerfors M, Lindström T, Siró I, et al. Investigation of mass transport properties of microfibrillated cellulose (MFC) films. *Journal of Membrane Science*. 2010;358:67-75.
- [129] Siqueira G, Tapin-Lingua S, Bras J, da Silva Perez D, Dufresne A. Morphological investigation of nanoparticles obtained from combined mechanical shearing, and enzymatic and acid hydrolysis of sisal fibers. *Cellulose*. 2010;17:1147-58.
- [130] Syverud K, Xhanari K, Chinga-Carrasco G, Yu Y, Stenius P. Films made of cellulose nanofibrils: surface modification by adsorption of a cationic surfactant and characterization by computer-assisted electron microscopy. *Journal of Nanoparticle Research*. 2011;13:773-82.
- [131] Chinga-Carrasco G, Syverud K. Computer-assisted quantification of the multi-scale structure of films made of nanofibrillated cellulose. *Journal of Nanoparticle Research*. 2010;12:841-51.
- [132] Fukuzumi S, et al. . Transparent and High Gas Barrier Films of Cellulose Nanofibers Prepared by TEMPO-Mediated Oxidation. *Biomacromolecules*. 2008;10:162-5.
- [133] Bondeson D, Mathew A, Oksman K. Optimization of the isolation of nanocrystals from microcrystalline cellulose by acid hydrolysis. *Cellulose*. 2006;13:171-80.
- [134] Atomic Force Microscopy (AFM) Project. In: Advanced Projects Laboratory UoO, editor.
- [135] Ford BJ, Bradbury S, Joy DC. Scanning electron microscope (SEM). *Encyclopedia Britannica* 2016.
- [136] Ford BJ, Bradbury S, Joy DC. Transmission electron microscope (TEM). *Encyclopedia Britannica* 2011.

- [137] Notley SM. Stretching and solvency of charged cellulose chains. *ACS Applied Materials & Interfaces*. 2009;1:1218-23.
- [138] Favier V, Cavaille J, Canova G. Etude de nouveaux matériaux composites obtenus à partir de latex filmogènes et de whiskers de cellulose: effets de percolation mécanique. *Journées nationales sur les composites* 1996. p. 47-58.
- [139] Dufresne A. Nanocellulose: a new ageless bionanomaterial. *Materials Today*. 2013;16:220-7.
- [140] Iwamoto S, Kai W, Isogai A, Iwata T. Elastic modulus of single cellulose microfibrils from tunicate measured by atomic force microscopy. *Biomacromolecules*. 2009;10:2571-6.
- [141] Lahiji RR, Xu X, Reifengerger R, Raman A, Rudie A, Moon RJ. Atomic force microscopy characterization of cellulose nanocrystals. *Langmuir*. 2010;26:4480-8.
- [142] Svagan AJ, Azizi Samir MA, Berglund LA. Biomimetic polysaccharide nanocomposites of high cellulose content and high toughness. *Biomacromolecules*. 2007;8:2556-63.
- [143] Henriksson M, Berglund LA, Isaksson P, Lindstrom T, Nishino T. Cellulose nanopaper structures of high toughness. *Biomacromolecules*. 2008;9:1579-85.
- [144] Aulin C, Gällstedt M, Lindström T. Oxygen and oil barrier properties of microfibrillated cellulose films and coatings. *Cellulose*. 2010;17:559-74.
- [145] Hebeish A, Guthrie J. *The chemistry and technology of cellulosic copolymers*: Springer Science & Business Media; 2012.
- [146] Hon DN-S. Cellulose: a random walk along its historical path. *Cellulose*. 1994;1:1-25.
- [147] Yu H, Qin Z, Liang B, Liu N, Zhou Z, Chen L. Facile extraction of thermally stable cellulose nanocrystals with a high yield of 93% through hydrochloric acid hydrolysis under hydrothermal conditions. *Journal of Materials Chemistry A*. 2013;1:3938-44.
- [148] Camarero Espinosa S, Kuhnt T, Foster EJ, Weder C. Isolation of thermally stable cellulose nanocrystals by phosphoric acid hydrolysis. *Biomacromolecules*. 2013;14:1223-30.
- [149] Braun B, Dorgan JR. Single-step method for the isolation and surface functionalization of cellulosic nanowhiskers. *Biomacromolecules*. 2008;10:334-41.
- [150] Wågberg L, Decher G, Norgren M, Lindström T, Ankerfors M, Axnäs K. The build-up of polyelectrolyte multilayers of microfibrillated cellulose and cationic polyelectrolytes. *Langmuir*. 2008;24:784-95.
- [151] Lämätäinen H, Suopajarvi T, Sirviö J, Hormi O, Niinimäki J. Fabrication of cationic cellulosic nanofibrils through aqueous quaternization pretreatment and their use in colloid aggregation. *Carbohydrate Polymers*. 2014;103:187-92.

- [152] Ho T, Zimmermann T, Hauert R, Caseri W. Preparation and characterization of cationic nanofibrillated cellulose from etherification and high-shear disintegration processes. *Cellulose*. 2011;18:1391-406.
- [153] Olszewska A, Eronen P, Johansson L-S, Malho J-M, Ankerfors M, Lindström T, et al. The behaviour of cationic nanofibrillar cellulose in aqueous media. *Cellulose*. 2011;18:1213.
- [154] Espino-Perez E. Development of renewable nanocomposites for packaging by the functionalization of polysaccharide nanocrystals Massy, France L'Institut des Sciences et Industries du Vivant et de l'Environnement (AgroParis Tech); 2014.
- [155] Habibi Y. Key advances in the chemical modification of nanocelluloses. *Chemical Society Reviews*. 2014;43:1519-42.
- [156] Tang J, Sisler J, Grishkewich N, Tam KC. Functionalization of cellulose nanocrystals for advanced applications. *Journal of Colloid and Interface Science*. 2017.
- [157] Eyley S, Thielemans W. Surface modification of cellulose nanocrystals. *Nanoscale*. 2014;6:7764-79.
- [158] Missoum K, Belgacem MN, Bras J. Nanofibrillated cellulose surface modification: a review. *Materials*. 2013;6:1745-66.
- [159] Saito T, Nishiyama Y, Putaux J-L, Vignon M, Isogai A. Homogeneous suspensions of individualized microfibrils from TEMPO-catalyzed oxidation of native cellulose. *Biomacromolecules*. 2006;7:1687-91.
- [160] Saito T, Kimura S, Nishiyama Y, Isogai A. Cellulose nanofibers prepared by TEMPO-mediated oxidation of native cellulose. *Biomacromolecules*. 2007;8:2485-91.
- [161] Isogai A, Saito T, Fukuzumi H. TEMPO-oxidized cellulose nanofibers. *Nanoscale*. 2011;3:71-85.
- [162] Montanari S, Roumani M, Heux L, Vignon MR. Topochemistry of carboxylated cellulose nanocrystals resulting from TEMPO-mediated oxidation. *Macromolecules*. 2005;38:1665-71.
- [163] Hirota M, Tamura N, Saito T, Isogai A. Water dispersion of cellulose II nanocrystals prepared by TEMPO-mediated oxidation of mercerized cellulose at pH 4.8. *Cellulose*. 2010;17:279-88.
- [164] Anastas P, Eghbali N. Green chemistry: principles and practice. *Chemical Society Reviews*. 2010;39:301-12.
- [165] Boujemaoui A, Mongkhontreerat S, Malmström E, Carlmark A. Preparation and characterization of functionalized cellulose nanocrystals. *Carbohydrate Polymers*. 2015;115:457-64.

- [166] Berlio S, Molina-Boisseau S, Nishiyama Y, Heux L. Gas-phase surface esterification of cellulose microfibrils and whiskers. *Biomacromolecules*. 2009;10:2144-51.
- [167] Yuan H, Nishiyama Y, Wada M, Kuga S. Surface acylation of cellulose whiskers by drying aqueous emulsion. *Biomacromolecules*. 2006;7:696-700.
- [168] Espino-Perez E, Domenek S, Belgacem N, Sillard C, Bras J. Green process for chemical functionalization of nanocellulose with carboxylic acids. *Biomacromolecules*. 2014;15:4551-60.
- [169] Mariano M, El Kissi N, Dufresne A. Cellulose nanocrystals and related nanocomposites: review of some properties and challenges. *Journal of Polymer Science Part B: Polymer Physics*. 2014;52:791-806.
- [170] Simonsen J, Habibi Y. Cellulose nanocrystals in polymer matrices. *The Nanoscience and Technology of Renewable Biomaterials: John Wiley & Sons, Ltd; 2009. p. 273-92.*
- [171] Favier V, Canova G, Cavallé J, Chanzy H, Dufresne A, Gauthier C. Nanocomposite materials from latex and cellulose whiskers. *Polymers for Advanced Technologies*. 1995;6:351-5.
- [172] Favier V, Dendievel R, Canova G, Cavaille J, Gilormini P. Simulation and modeling of three-dimensional percolating structures: case of a latex matrix reinforced by a network of cellulose fibers. *Acta Materialia*. 1997;45:1557-65.
- [173] Surve M, Pryamitsyn V, Ganesan V. Universality in structure and elasticity of polymer-nanoparticle gels. *Physical Review Letters*. 2006;96:177805.
- [174] Surve M, Pryamitsyn V, Ganesan V. Polymer-bridged gels of nanoparticles in solutions of adsorbing polymers. *The Journal of chemical physics*. 2006;125:064903.
- [175] Takayanagi M, Uemura S, Minami S. Application of equivalent model method to dynamic rheo-optical properties of crystalline polymer. *Journal of Polymer Science Part C: Polymer Symposia: Wiley Online Library; 1964. p. 113-22.*
- [176] Dufresne A. Comparing the mechanical properties of high performances polymer nanocomposites from biological sources. *Journal of Nanoscience and Nanotechnology*. 2006;6:322-30.
- [177] Mariano M, El Kissi N, Dufresne A. Cellulose nanocrystal reinforced oxidized natural rubber nanocomposites. *Carbohydrate Polymers*. 2016;137:174-83.
- [178] Peresin MS, Habibi Y, Zoppe JO, Pawlak JJ, Rojas OJ. Nanofiber composites of polyvinyl alcohol and cellulose nanocrystals: manufacture and characterization. *Biomacromolecules*. 2010;11:674-81.

- [179] Roohani M, Habibi Y, Belgacem NM, Ebrahim G, Karimi AN, Dufresne A. Cellulose whiskers reinforced polyvinyl alcohol copolymers nanocomposites. *European Polymer Journal*. 2008;44:2489-98.
- [180] Bilbao-Sainz C, Bras J, Williams T, Sénechal T, Orts W. HPMC reinforced with different cellulose nano-particles. *Carbohydrate Polymers*. 2011;86:1549-57.
- [181] Siqueira G, Abdillahi H, Bras J, Dufresne A. High reinforcing capability cellulose nanocrystals extracted from *Syngonanthus nitens* (Capim Dourado). *Cellulose*. 2010;17:289-98.
- [182] Siqueira G, Fraschini C, Bras J, Dufresne A, Prud'homme R, Laborie M-P. Impact of the nature and shape of cellulosic nanoparticles on the isothermal crystallization kinetics of poly (ϵ -caprolactone). *European Polymer Journal*. 2011;47:2216-27.
- [183] Oksman K, Mathew A, Bondeson D, Kvien I. Manufacturing process of cellulose whiskers/poly(lactic acid) nanocomposites. *Composites Science and Technology*. 2006;66:2776-84.
- [184] Mathew AP, Oksman K, Sain M. The effect of morphology and chemical characteristics of cellulose reinforcements on the crystallinity of poly(lactic acid). *Journal of Applied Polymer Science*. 2006;101:300-10.
- [185] Azizi Samir MAS, Alloin F, Dufresne A. Review of recent research into cellulosic whiskers, their properties and their application in nanocomposite field. *Biomacromolecules*. 2005;6:612-26.
- [186] Moon RJ, Martini A, Nairn J, Simonsen J, Youngblood J. Cellulose nanomaterials review: structure, properties and nanocomposites. *Chemical Society Reviews*. 2011;40:3941-94.
- [187] Hubbe MA, Rojas OJ, Lucia LA, Sain M. Cellulosic nanocomposites: a review. *BioResources*. 2008;3:929-80.
- [188] Siqueira G, Bras J, Dufresne A. Cellulosic bionanocomposites: a review of preparation, properties and applications. *Polymers*. 2010;2:728-65.
- [189] Santos TM, Men de Sá Filho MS, Caceres CA, Rosa MF, Morais JPS, Pinto AM, et al. Fish gelatin films as affected by cellulose whiskers and sonication. *Food Hydrocolloids*. 2014;41:113-8.
- [190] Li W, Guo R, Lan Y, Zhang Y, Xue W, Zhang Y. Preparation and properties of cellulose nanocrystals reinforced collagen composite films. *Journal of Biomedical Materials Research Part A*. 2014;102:1131-9.
- [191] Ureña-Benavides EE, Brown PJ, Kitchens CL. Effect of jet stretch and particle load on cellulose nanocrystal– alginate nanocomposite fibers. *Langmuir*. 2010;26:14263-70.
- [192] Ureña-Benavides EE, Kitchens CL. Wide-Angle X-ray Diffraction of Cellulose Nanocrystal– Alginate Nanocomposite Fibers. *Macromolecules*. 2011;44:3478-84.

- [193] Ma X, Li R, Zhao X, Ji Q, Xing Y, Sunarso J, et al. Biopolymer composite fibres composed of calcium alginate reinforced with nanocrystalline cellulose. *Composites Part A: Applied Science and Manufacturing*. 2017;96:155-63.
- [194] Huq T, Salmieri S, Khan A, Khan RA, Le Tien C, Riedl B, et al. Nanocrystalline cellulose (NCC) reinforced alginate based biodegradable nanocomposite film. *Carbohydrate Polymers*. 2012;90:1757-63.
- [195] Abdollahi M, Alboofetileh M, Rezaei M, Behrooz R. Comparing physico-mechanical and thermal properties of alginate nanocomposite films reinforced with organic and/or inorganic nanofillers. *Food Hydrocolloids*. 2013;32:416-24.
- [196] Abdollahi M, Alboofetileh M, Behrooz R, Rezaei M, Miraki R. Reducing water sensitivity of alginate bio-nanocomposite film using cellulose nanoparticles. *International Journal of Biological Macromolecules*. 2013;54:166-73.
- [197] Lin N, Bruzzese C, Dufresne A. TEMPO-oxidized nanocellulose participating as crosslinking aid for alginate-based sponges. *ACS Appl Mater Interfaces*. 2012;4:4948-59.
- [198] Capadona JR, Shanmuganathan K, Tyler DJ, Rowan SJ, Weder C. Stimuli-responsive polymer nanocomposites inspired by the sea cucumber dermis. *Science*. 2008;319:1370-4.
- [199] Biyani MV, Foster EJ, Weder C. Light-healable supramolecular nanocomposites based on modified cellulose nanocrystals. *ACS Macro Letters*. 2013;2:236-40.
- [200] Coulibaly S, Roulin A, Balog S, Biyani MV, Foster EJ, Rowan SJ, et al. Reinforcement of optically healable supramolecular polymers with cellulose nanocrystals. *Macromolecules*. 2013;47:152-60.
- [201] Biyani MV, Jorfi M, Weder C, Foster EJ. Light-stimulated mechanically switchable, photopatternable cellulose nanocomposites. *Polymer Chemistry*. 2014;5:5716-24.
- [202] Biyani MV, Weder C, Foster EJ. Photoswitchable nanocomposites made from coumarin-functionalized cellulose nanocrystals. *Polymer Chemistry*. 2014;5:5501-8.
- [203] Fox JD, Capadona JR, Marasco PD, Rowan SJ. Bioinspired water-enhanced mechanical gradient nanocomposite films that mimic the architecture and properties of the squid beak. *Journal of the American Chemical Society*. 2013;135:5167-74.
- [204] Saini S. Surface Modication of Cellulose Nanofiber to Impart Active Properties for Packaging. Grenoble, France Université Grenoble Alpes 2016.

- [205] Kolakovic R, Peltonen L, Laukkanen A, Hellman M, Laaksonen P, Linder MB, et al. Evaluation of drug interactions with nanofibrillar cellulose. *European Journal of Pharmaceutics and Biopharmaceutics*. 2013;85:1238-44.
- [206] Skalak R, Fox CF. Tissue engineering: proceedings of a workshop, held at Granlibakken, Lake Tahoe, California, February 26-29, 1988: Alan R. Liss; 1988.
- [207] Alberts B, Johnson A, Lewis J, Raff M, Roberts K, Walter P. *Molecular Biology of the Cell*. 4 ed. New York Garland Science; 2002.
- [208] National Institutes of Health USDoHaHS. What are embryonic stem cells? In: National Institutes of Health USDoHaHS, editor. NIH Stem Cell Information Home Page Stem Cell Information. Bethesda, MD: National Institutes of Health, U.S. Department of Health and Human Services; 2016.
- [209] National Institutes of Health USDoHaHS. What are induced pluripotent stem cells? In: National Institutes of Health USDoHaHS, editor. In Stem Cell Information. Bethesda, MD: National Institutes of Health, U.S. Department of Health and Human Services 2016.
- [210] National Institutes of Health USDoHaHS. What are the similarities and differences between embryonic and adult stem cells? In: National Institutes of Health USDoHaHS, editor. NIH Stem Cell Information Home Page In Stem Cell Information. Bethesda, MD: National Institutes of Health, U.S. Department of Health and Human Services; 2016.
- [211] Gearhart J. New potential for human embryonic stem cells. *Science*. 1998;282:1061-2.
- [212] Richards M, Fong C-Y, Chan W-K, Wong P-C, Bongso A. Human feeders support prolonged undifferentiated growth of human inner cell masses and embryonic stem cells. *Nature Biotechnology*. 2002;20.
- [213] De Wert G, Mummery C. Human embryonic stem cells: research, ethics and policy. *Human reproduction*. 2003;18:672-82.
- [214] Kim K, Doi A, Wen B, Ng K, Zhao R, Cahan P, et al. Epigenetic memory in induced pluripotent stem cells. *Nature*. 2010;467:285-90.
- [215] Barrilleaux B, Phinney DG, Prockop DJ, O'connor KC. Review: ex vivo engineering of living tissues with adult stem cells. *Tissue Engineering*. 2006;12:3007-19.
- [216] Young HE, Black AC. Adult stem cells. *The Anatomical Record Part A: Discoveries in Molecular, Cellular, and Evolutionary Biology*. 2004;276:75-102.
- [217] Körbling M, Estrov Z. Adult stem cells for tissue repair—a new therapeutic concept? *New England Journal of Medicine*. 2003;349:570-82.

- [218] Friedenstein AJ, Gorskaja J, Kulagina N. Fibroblast precursors in normal and irradiated mouse hematopoietic organs. *Experimental hematology*. 1976;4:267-74.
- [219] Prockop DJ. Marrow stromal cells as stem cells for nonhematopoietic tissues. *Science*. 1997;276:71-4.
- [220] Kern S, Eichler H, Stoeve J, Klüter H, Bieback K. Comparative analysis of mesenchymal stem cells from bone marrow, umbilical cord blood, or adipose tissue. *Stem Cells*. 2006;24:1294-301.
- [221] DiMarino AM, Caplan AI, Bonfield TL. Mesenchymal stem cells in tissue repair. *Frontiers in immunology*. 2013;4:201.
- [222] Chamberlain G, Fox J, Ashton B, Middleton J. Concise review: mesenchymal stem cells: their phenotype, differentiation capacity, immunological features, and potential for homing. *Stem Cells*. 2007;25:2739-49.
- [223] Pittenger MF, Mackay AM, Beck SC, Jaiswal RK, Douglas R, Mosca JD, et al. Multilineage potential of adult human mesenchymal stem cells. *Science*. 1999;284:143-7.
- [224] Le Blanc K. Immunomodulatory effects of fetal and adult mesenchymal stem cells. *Cytotherapy*. 2003;5:485-9.
- [225] Majumdar MK, Keane-Moore M, Buyaner D, Hardy WB, Moorman MA, McIntosh KR, et al. Characterization and functionality of cell surface molecules on human mesenchymal stem cells. *Journal of biomedical science*. 2003;10:228-41.
- [226] Pujol-Borrell R, Todd I, Doshi M, Bottazzo GF, Sutton R, Gary D, et al. HLA class II induction in human islet cells by interferon- γ plus tumour necrosis factor or lymphotoxin. *Nature*. 1987;326:304-6.
- [227] Barry FP, Murphy JM. Mesenchymal stem cells: clinical applications and biological characterization. *The international journal of biochemistry & cell biology*. 2004;36:568-84.
- [228] Ankrum JA, Ong JF, Karp JM. Mesenchymal stem cells: immune evasive, not immune privileged. *Nature Biotechnology*. 2014;32:252-60.
- [229] Dalby MJ, Gadegaard N, Oreffo RO. Harnessing nanotopography and integrin-matrix interactions to influence stem cell fate. *Nature materials*. 2014;13:558-69.
- [230] Discher DE, Janmey P, Wang YL. Tissue cells feel and respond to the stiffness of their substrate. *Science*. 2005;310:1139-43.
- [231] Dalby MJ, Gadegaard N, Riehle MO, Wilkinson CD, Curtis AS. Investigating filopodia sensing using arrays of defined nano-pits down to 35 nm diameter in size. *The international journal of biochemistry & cell biology*. 2004;36:2005-15.

- [232] Dalby MJ, Gadegaard N, Tare R, Andar A, Richle MO, Herzyk P, et al. The control of human mesenchymal cell differentiation using nanoscale symmetry and disorder. *Nature materials*. 2007;6:997-1003.
- [233] Engler AJ, Sen S, Sweeney HL, Discher DE. Matrix elasticity directs stem cell lineage specification. *Cell*. 2006;126:677-89.
- [234] Anderson HJ, Dalby MJ, Sahoo JK, Ulijn RV. Mesenchymal Stem Cell Fate: Applying Biomaterials for Control of Stem Cell Behavior. *Frontiers in Bioengineering and Biotechnology*. 2016;4:38.
- [235] McMurray RJ, Gadegaard N, Tsimbouri PM, Burgess KV, McNamara LE, Tare R, et al. Nanoscale surfaces for the long-term maintenance of mesenchymal stem cell phenotype and multipotency. *Nature materials*. 2011;10:637-44.
- [236] Olivares-Navarrete R, Hyzy SL, Hutton DL, Erdman CP, Wieland M, Boyan BD, et al. Direct and indirect effects of microstructured titanium substrates on the induction of mesenchymal stem cell differentiation towards the osteoblast lineage. *Biomaterials*. 2010;31:2728-35.
- [237] Dumas V, Guignandon A, Vico L, Mauclair C, Zapata X, Linossier MT, et al. Femtosecond laser nano/micro patterning of titanium influences mesenchymal stem cell adhesion and commitment. *Biomedical Materials*. 2015;10:055002.
- [238] Faia-Torres AB, Guimond-Lischer S, Rottmar M, Charnley M, Goren T, Maniura-Weber K, et al. Differential regulation of osteogenic differentiation of stem cells on surface roughness gradients. *Biomaterials*. 2014;35:9023-32.
- [239] Salinas CN, Cole BB, Kasko AM, Anseth KS. Chondrogenic differentiation potential of human mesenchymal stem cells photoencapsulated within poly (ethylene glycol)–arginine-glycine-aspartic acid-serine thiol-methacrylate mixed-mode networks. *Tissue Engineering*. 2007;13:1025-34.
- [240] Tavella S, Bellese G, Castagnola P, Martin I, Piccini D, Doliana R, et al. Regulated expression of fibronectin, laminin and related integrin receptors during the early chondrocyte differentiation. *Journal of Cell Science*. 1997;110:2261-70.
- [241] DeLise A, Fischer L, Tuan R. Cellular interactions and signaling in cartilage development. *Osteoarthritis and cartilage*. 2000;8:309-34.
- [242] Yamada KM. Integrin signaling. *Matrix Biology*. 1997;16:137-41.
- [243] Salinas CN, Anseth KS. The enhancement of chondrogenic differentiation of human mesenchymal stem cells by enzymatically regulated RGD functionalities. *Biomaterials*. 2008;29:2370-7.

- [244] Yu J, Du KT, Fang Q, Gu Y, Mihardja SS, Sievers RE, et al. The use of human mesenchymal stem cells encapsulated in RGD modified alginate microspheres in the repair of myocardial infarction in the rat. *Biomaterials*. 2010;31:7012-20.
- [245] Re'em T, Tsur-Gang O, Cohen S. The effect of immobilized RGD peptide in macroporous alginate scaffolds on TGF β 1-induced chondrogenesis of human mesenchymal stem cells. *Biomaterials*. 2010;31:6746-55.
- [246] Sawyer A, Hennessy K, Bellis S. Regulation of mesenchymal stem cell attachment and spreading on hydroxyapatite by RGD peptides and adsorbed serum proteins. *Biomaterials*. 2005;26:1467-75.
- [247] Barry F, Boynton RE, Liu B, Murphy JM. Chondrogenic differentiation of mesenchymal stem cells from bone marrow: differentiation-dependent gene expression of matrix components. *Experimental cell research*. 2001;268:189-200.
- [248] Jaklenec A, Hinckfuss A, Bilgen B, Ciombor DM, Aaron R, Mathiowitz E. Sequential release of bioactive IGF-I and TGF- β 1 from PLGA microsphere-based scaffolds. *Biomaterials*. 2008;29:1518-25.
- [249] DeFail AJ, Chu CR, Izzo N, Marra KG. Controlled release of bioactive TGF- β 1 from microspheres embedded within biodegradable hydrogels. *Biomaterials*. 2006;27:1579-85.
- [250] Lee JE, Kim KE, Kwon IC, Ahn HJ, Lee S-H, Cho H, et al. Effects of the controlled-released TGF- β 1 from chitosan microspheres on chondrocytes cultured in a collagen/chitosan/glycosaminoglycan scaffold. *Biomaterials*. 2004;25:4163-73.
- [251] Park H, Temenoff JS, Holland TA, Tabata Y, Mikos AG. Delivery of TGF- β 1 and chondrocytes via injectable, biodegradable hydrogels for cartilage tissue engineering applications. *Biomaterials*. 2005;26:7095-103.
- [252] Re'em T, Kaminer-Israeli Y, Ruvinov E, Cohen S. Chondrogenesis of hMSC in affinity-bound TGF-beta scaffolds. *Biomaterials*. 2012;33:751-61.
- [253] Wang L-S, Chung JE, Chan PP-Y, Kurisawa M. Injectable biodegradable hydrogels with tunable mechanical properties for the stimulation of neurogenic differentiation of human mesenchymal stem cells in 3D culture. *Biomaterials*. 2010;31:1148-57.
- [254] Park JS, Chu JS, Tsou AD, Diop R, Tang Z, Wang A, et al. The effect of matrix stiffness on the differentiation of mesenchymal stem cells in response to TGF- β . *Biomaterials*. 2011;32:3921-30.
- [255] Pek YS, Wan AC, Ying JY. The effect of matrix stiffness on mesenchymal stem cell differentiation in a 3D thixotropic gel. *Biomaterials*. 2010;31:385-91.

- [256] Rowlands AS, George PA, Cooper-White JJ. Directing osteogenic and myogenic differentiation of MSCs: interplay of stiffness and adhesive ligand presentation. *Am J Physiol Cell Physiol*. 2008;295:C1037-44.
- [257] Clift MJ, Foster EJ, Vanhecke D, Studer D, Wick P, Gehr P, et al. Investigating the interaction of cellulose nanofibers derived from cotton with a sophisticated 3D human lung cell coculture. *Biomacromolecules*. 2011;12:3666-73.
- [258] Dugan JM, Collins RF, Gough JE, Eichhorn SJ. Oriented surfaces of adsorbed cellulose nanowhiskers promote skeletal muscle myogenesis. *Acta biomaterialia*. 2013;9:4707-15.
- [259] He X, Xiao Q, Lu C, Wang Y, Zhang X, Zhao J, et al. Uniaxially aligned electrospun all-cellulose nanocomposite nanofibers reinforced with cellulose nanocrystals: scaffold for tissue engineering. *Biomacromolecules*. 2014;15:618-27.
- [260] Zhang C, Salick MR, Cordie TM, Ellingham T, Dan Y, Turng L-S. Incorporation of poly (ethylene glycol) grafted cellulose nanocrystals in poly (lactic acid) electrospun nanocomposite fibers as potential scaffolds for bone tissue engineering. *Materials Science and Engineering: C*. 2015;49:463-71.
- [261] Camarero-Espinosa S, Rothen-Rutishauser B, Weder C, Foster EJ. Directed cell growth in multi-zonal scaffolds for cartilage tissue engineering. *Biomaterials*. 2016;74:42-52.
- [262] Zhou C, Shi Q, Guo W, Terrell L, Qureshi AT, Hayes DJ, et al. Electrospun Bio-Nanocomposite Scaffolds for Bone Tissue Engineering by Cellulose Nanocrystals Reinforcing Maleic Anhydride Grafted PLA. *ACS Applied Materials & Interfaces*. 2013;5:3847-54.
- [263] Rescignano N, Fortunati E, Montesano S, Emiliani C, Kenny JM, Martino S, et al. PVA bio-nanocomposites: a new take-off using cellulose nanocrystals and PLGA nanoparticles. *Carbohydrate Polymers*. 2014;99:47-58.
- [264] Domingues RM, Gomes ME, Reis RL. The potential of cellulose nanocrystals in tissue engineering strategies. *Biomacromolecules*. 2014;15:2327-46.
- [265] Dong S, Hirani AA, Colacino KR, Lee YW, Roman M. Cytotoxicity and cellular uptake of cellulose nanocrystals. *Nano Life*. 2012;2:1241006.
- [266] Dong S, Cho HJ, Lee YW, Roman M. Synthesis and cellular uptake of folic acid-conjugated cellulose nanocrystals for cancer targeting. *Biomacromolecules*. 2014;15:1560-7.
- [267] Colacino KR, Arena CB, Dong S, Roman M, Davalos RV, Lee YW. Folate conjugated cellulose nanocrystals potentiate irreversible electroporation-induced cytotoxicity for the selective treatment of cancer cells. *Technology in cancer research & treatment*. 2014;tcrt. 2012.500428.

- [268] Catalán J, Ilves M, Järventaus H, Hannukainen KS, Kontturi E, Vanhala E, et al. Genotoxic and immunotoxic effects of cellulose nanocrystals in vitro. *Environmental and molecular mutagenesis*. 2015;56:171-82.
- [269] Mahmoud KA, Mena JA, Male KB, Hrapovic S, Kamen A, Luong JH. Effect of surface charge on the cellular uptake and cytotoxicity of fluorescent labeled cellulose nanocrystals. *ACS Applied Materials & Interfaces*. 2010;2:2924-32.
- [270] Liebert T, Kostag M, Wotschadlo J, Heinze T. Stable cellulose nanospheres for cellular uptake. *Macromolecular bioscience*. 2011;11:1387-92.
- [271] Male KB, Leung AC, Montes J, Kamen A, Luong JH. Probing inhibitory effects of nanocrystalline cellulose: inhibition versus surface charge. *Nanoscale*. 2012;4:1373-9.
- [272] Hossain KMZ, Hasan MS, Boyd D, Rudd CD, Ahmed I, Thielemans W. Effect of cellulose nanowhiskers on surface morphology, mechanical properties, and cell adhesion of melt-drawn polylactic acid fibers. *Biomacromolecules*. 2014;15:1498-506.
- [273] Wang Y, Chang C, Zhang L. Effects of freezing/thawing cycles and cellulose nanowhiskers on structure and properties of biocompatible starch/PVA sponges. *Macromolecular Materials and Engineering*. 2010;295:137-45.
- [274] Yang X, Bakaic E, Hoare T, Cranston ED. Injectable polysaccharide hydrogels reinforced with cellulose nanocrystals: morphology, rheology, degradation, and cytotoxicity. *Biomacromolecules*. 2013;14:4447-55.
- [275] Rueda L, Saralegi A, Fernández-d'Arlas B, Zhou Q, Alonso-Varona A, Berglund LA, et al. In situ polymerization and characterization of elastomeric polyurethane-cellulose nanocrystal nanocomposites. Cell response evaluation. *Cellulose*. 2013;20:1819-28.
- [276] Yu H-Y, Qin Z-Y, Yan C-F, Yao J-M. Green nanocomposites based on functionalized cellulose nanocrystals: A study on the relationship between interfacial interaction and property enhancement. *ACS Sustainable Chemistry & Engineering*. 2014;2:875-86.
- [277] Jia B, Li Y, Yang B, Xiao D, Zhang S, Rajulu AV, et al. Effect of microcrystal cellulose and cellulose whisker on biocompatibility of cellulose-based electrospun scaffolds. *Cellulose*. 2013;20:1911-23.
- [278] Xing Q, Zhao F, Chen S, McNamara J, DeCoster MA, Lvov YM. Porous biocompatible three-dimensional scaffolds of cellulose microfiber/gelatin composites for cell culture. *Acta biomaterialia*. 2010;6:2132-9.

- [279] Nordli HR, Chinga-Carrasco G, Rokstad AM, Pukstad B. Producing ultrapure wood cellulose nanofibrils and evaluating the cytotoxicity using human skin cells. *Carbohydrate Polymers*. 2016;150:65-73.
- [280] Hua K, Ålander E, Lindström T, Mihranyan A, Strømme M, Ferraz N. Surface chemistry of nanocellulose fibers directs monocyte/macrophage response. *Biomacromolecules*. 2015;16:2787-95.
- [281] Bhattacharya M, Malinen MM, Lauren P, Lou YR, Kuisma SW, Kanninen L, et al. Nanofibrillar cellulose hydrogel promotes three-dimensional liver cell culture. *J Control Release*. 2012;164:291-8.
- [282] Lu T, Li Q, Chen W, Yu H. Composite aerogels based on dialdehyde nanocellulose and collagen for potential applications as wound dressing and tissue engineering scaffold. *Composites Science and Technology*. 2014;94:132-8.
- [283] Lou YR, Kanninen L, Kuisma T, Niklander J, Noon LA, Burks D, et al. The use of nanofibrillar cellulose hydrogel as a flexible three-dimensional model to culture human pluripotent stem cells. *Stem Cells Dev*. 2014;23:380-92.
- [284] Hua K, Carlsson DO, Ålander E, Lindström T, Strømme M, Mihranyan A, et al. Translational study between structure and biological response of nanocellulose from wood and green algae. *Rsc Advances*. 2014;4:2892-903.
- [285] Kollar P, Závalová V, Hošek J, Havelka P, Sopuch T, Karpíšek M, et al. Cytotoxicity and effects on inflammatory response of modified types of cellulose in macrophage-like THP-1 cells. *International immunopharmacology*. 2011;11:997-1001.
- [286] Čolić M, Mihajlović D, Mathew A, Naseri N, Kokol V. Cytocompatibility and immunomodulatory properties of wood based nanofibrillated cellulose. *Cellulose*. 2015;22:763-78.
- [287] Vartiainen J, Pöhler T, Sirola K, Pylkkänen L, Alenius H, Hokkinen J, et al. Health and environmental safety aspects of friction grinding and spray drying of microfibrillated cellulose. *Cellulose*. 2011;18:775-86.
- [288] Pereira M, Raposo N, Brayner R, Teixeira E, Oliveira V, Quintão C, et al. Cytotoxicity and expression of genes involved in the cellular stress response and apoptosis in mammalian fibroblast exposed to cotton cellulose nanofibers. *Nanotechnology*. 2013;24:075103.
- [289] Malinen MM, Kanninen LK, Corlu A, Isoniemi HM, Lou Y-R, Yliperttula ML, et al. Differentiation of liver progenitor cell line to functional organotypic cultures in 3D nanofibrillar cellulose and hyaluronan-gelatin hydrogels. *Biomaterials*. 2014;35:5110-21.

- [290] Ninan N, Muthiah M, Park I-K, Elain A, Thomas S, Grohens Y. Pectin/carboxymethyl cellulose/microfibrillated cellulose composite scaffolds for tissue engineering. *Carbohydrate Polymers*. 2013;98:877-85.
- [291] Chang C-W, Wang M-J. Preparation of Microfibrillated Cellulose Composites for Sustained Release of H₂O₂ or O₂ for Biomedical Applications. *ACS Sustainable Chemistry & Engineering*. 2013;1:1129-34.
- [292] Cai H, Sharma S, Liu W, Mu W, Liu W, Zhang X, et al. Aerogel microspheres from natural cellulose nanofibrils and their application as cell culture scaffold. *Biomacromolecules*. 2014;15:2540-7.
- [293] Alexandrescu L, Syverud K, Gatti A, Chinga-Carrasco G. Cytotoxicity tests of cellulose nanofibril-based structures. *Cellulose*. 2013;20:1765-75.

Chapter 2 Extraction and Process Analysis of High Aspect Ratio Cellulose Nanocrystals from Corn (*Zea mays*) Agricultural Residue

This chapter is based on *Extraction and characterization of cellulose nanocrystals from corn (*Zea mays*) agricultural residue*. **Industrial Crops and Products**. (2017)

Abstract	102
1. Introduction	103
2. Materials and Methods	104
2.1 Materials	104
2.2 Methods	104
2.2.1 Bleaching of Maize Husks	104
2.2.2 Acid Hydrolysis for Maize Cellulose Nanocrystal (m-CNC) Production	104
2.2.3 Determination of Extractives, Acid Insoluble Lignin, Holocellulose, Hemicellulose, and Cellulose Content	105
2.2.4 Preparation of Nanocomposite Films	106
2.3 Characterization of CNCs	106
2.3.1 Conductometric Titration	106
2.3.2 Yield of CNCs.....	107
2.3.3 Fourier Transform Infrared Spectroscopy (FTIR)	107
2.3.4 Atomic Force Microscopy (AFM)	107
2.3.5 Dynamic Light Scattering (DLS).....	107
2.3.6 Crystallinity	108
2.3.7 Thermal Stability	108
2.3.8 Zeta Potential	108
2.3.9 Optical Properties	109
2.3.10 Tensile Testing	109
2.3.11 Dynamic Mechanical Analysis (DMA).....	109
2.3.12 Economic Evaluation	109
3.. Results and Discussion.....	110
3.1 Characterization of Raw Material	110
3.1.1 Determination of Extractives, Holocellulose, Hemicellulose, Cellulose, Lignin, and Ash	110
3.2. Characterization of Cellulose Nanocrystals	111
3.2.1 Conductometric Titration	111
3.2.2 Composition of Maize CNCs	112
3.2.2 Dimensional Analysis	113

3.2.3 Crystallinity	114
3.2.4 Thermal Stability	115
3.2.5 Zeta Potential	116
3.2.6 Optical Properties	116
3.2.7 Mechanical Properties	116
3.2.8 Economic Evaluation	122
4. Conclusion	123
5. Acknowledgements.....	124
6. References	124
7. Figures and Tables	128

Extraction and Process Analysis of High Aspect Ratio Cellulose Nanocrystals from Corn (*Zea mays*) Agricultural Residue

Megan Smyth^{a,b}, Araceli García^{a,b,c}, Chris Rader^d, E. Johan Foster^d and Julien Bras^{a,b,e*}

a. CNRS, LGP2, 461 Rue de la Papeterie, 38402, Saint-Martin-d'Hères, France

b. Université Grenoble Alpes, LGP2, 38000 Grenoble, France

c. University of Cordoba, Organic Chemistry Department, Campus Rabanales, Edificio Marie Curie (C-3), Crta Nnal IV, km 396, 14014 Cordoba, Spain

d. Virginia Polytechnic Institute and State University (Virginia Tech), Macromolecules Innovation Institute (MII), Department of Materials Science and Engineering, Blacksburg, Virginia 24061, USA

e. Institut Universitaire de France, 75005 Paris, France

Abstract

Cellulose nanocrystals (CNCs) have long been an interest of researchers because of their exceptional mechanical properties as well as being sourced from natural, inexpensive, and renewable materials. In this work, maize CNCs (m-CNC) were obtained from maize (*Zea mays*) husk. This material is a common waste product from agricultural production in different parts of the world, and of potential value if CNCs with advantageous properties are extracted from them. Maize husk is a major agricultural waste in the United States and is used for erosion prevention or to produce insulating materials, paper, and other chemicals. Dried materials were alkali treated, bleached, and hydrolyzed to create CNCs using sulfuric acid. The extracted CNCs were found to have a length of 940 ± 70 nm and width of 6 ± 2 nm, high aspect ratio of approximately 157, and increase the Young's modulus of natural rubber composites from 0.89 ± 0.15 MPa to 1.98 ± 0.73 MPa with the addition of 2 wt% m-CNCs. Other characterization techniques employed in this study are dynamic light scattering (DLS), conductometry, thermal gravimetric analysis (TGA), x-ray diffraction (XRD), and optical transmittance. Maize husks provided high aspect ratio cellulose I β CNCs, similar to tunicate CNCs, but with much lower processing required. Therefore, m-CNCs are more cost effective as shown by an economic evaluation. This study could provide assistance for producing CNC from one of the world's largest supplies of agricultural waste.

1. Introduction

In 2013, the worldwide output of maize (*Zea mays*) was approximately 1 trillion tons as reported by the Food and Agricultural Organization of the United Nations, with the United States producing 350 million tons of that in 2013 [1]. The maize plant is comprised of the stalk, leaf, cob, and husk. The cob, which is the edible part of the plant, is 20% of the plant's mass and the remaining parts are agricultural waste. The husk of the maize plant is 10% of the plant's mass [2]. For the 640 million tons of corn produced, a significant 45 million tons are maize husks [3].

The husk of the maize is commonly thought of as a residue of maize harvesting, and is commonly used to prevent erosion [4] or to produce insulating materials, paper, and other chemicals [5]. Work has been done to obtain fibers from maize husk for textile applications [6]. The use of maize husk as a source for nanocellulose crystals would provide a natural resource that is renewable, low cost, and can be a large source worldwide for cellulosic material, not just in the United States. By using an agricultural residue the environmental impact would be lessened, and would conserve land by extracting cellulose from a common food source.

The composition of the maize husk has been extensively characterized [7-9] as well as the crystallinity, chemical composition, and some mechanical properties [6, 9]. Prado-Martinez, reported the following percentages of hemicellulose, α -cellulose, lignin, and ash in maize husk, respectively, 78.86, 43.14, 23, and 0.761[7]. For the chemical composition, Duguid and colleagues have stated that the maize husk contains 44.71% carbon, 0.35% nitrogen, and other trace amounts of phosphorous, potassium, calcium, magnesium, zinc, copper, manganese, and iron using National Renewable Energy Laboratory (NREL) protocols [8].

Arroyo Rosas has studied the crystallinity, chemical composition, and the mechanical properties of maize husk nanofibers as a nanofiller in thermoplastic starch based composites. The crystallinity was reported to be 55.1% for nonhomogenized nanofibers and 60.4% for homogenized samples using XRD, with I_{α} =33.54% and I_{β} =66.54%, I_{α} =19.96% and I_{β} =80.04%, for nonhomogenized and homogenized, respectively, as measured by FTIR. The Young's Modulus of nanofibers based thermoplastic starch composites increased as the percentage of nanofibers increased from 15 GPa with 0% fiber to 40, 60, 100, 120 GPa for 3, 5, 10, 20% addition of nanofibers, respectively [9]. While Reddy has reported that the crystallinity was approximately 48-50%, and had a crystal size of 3.2 nm [6].

There have been previous studies conducted extracting nanocellulose crystals from other parts of the maize plant, such as the straw, which includes the husk [6, 10], and the cob [11]. The maize straw

includes any agricultural products that remain in the field following harvest including leaves, stalks, and husks [12].

The purpose of this study was to present a protocol to extract cellulose nanocrystals (m-CNCs) from a common agricultural waste, maize husk. CNCs were produced by acid hydrolysis following an alkali and bleaching treatment to isolate the cellulose from the other chemical compounds such as hemicelluloses and lignin. Acid hydrolysis degraded the amorphous component of the cellulose, while retaining the crystalline part, which conforms the CNCs. The composition, morphology, thermal stability, crystallinity, and mechanical properties were measured to see if there is potential to use CNCs derived from maize husk for applications in material science.

2. Methods and Materials

2.1 Materials

Dried maize (*Zea mays*) husk was purchased from Industria Agrícola Carredana S.A. de C.V. (Ciudad de Mexico, Mexico). Sodium chlorite (NaClO_2) and hydrochloric acid (HCl) were purchased from Sigma-Aldrich France Ltd. (Lyon, France). Sodium hydroxide (NaOH) was purchased from Carl Roth GmbH + Co. KG (Rheinhäfen Karlsruhe, Germany). Ethanol ($\text{C}_2\text{H}_6\text{O}$) and sulfuric acid (H_2SO_4) were purchased from Chimie Plus (Denicé, France). Reagent grade for analysis Toulene was purchased from Panreac Química (Barcelona, Spain). Cellulose nanocrystals (w-CNCs) were purchased from University of Maine Process Development Center (Orono, Maine, USA). The w-CNCs were extracted from wood pulp using sulfuric acid hydrolysis. All materials were used without any modification. Natural rubber (NR) latex was provided by Centrotrade Deutschland GmbH (Eschborn, Germany) with a solid content of ≈ 60 wt% with spherical particles with an average diameter of 300 nm.

2.2 Methods

2.2.1 Bleaching of Maize Husks

Dried maize husk was milled following TAPPI standard T257 cm-85 [13] using a Retsch 2000 mill (Haan, Germany) with a 4 mm sieve. The dried, milled maize husk was placed in 2% NaOH solution, with a 1:20 solid to liquid ratio, overnight at ambient conditions to remove hemicelluloses and ash. The husk particles were removed by filtration and washed with deionized H_2O (DI- H_2O) until the affluent was clear and had a $\text{pH} \approx 7$. The washed fibers were placed in a three-neck flask, and per 10 g of dry mass of fiber, 110 mL of DI- H_2O , 110 mL of acetic buffer solution, 110 mL of 1.7% NaClO_2

solution were added to create a suspension of liquid and fibers and heated at 80°C for 2 hours under continuous stirring. The pulp was filtered and washed with DI-H₂O until a neutral pH was achieved.

2.2.2 Acid Hydrolysis for Maize Cellulose Nanocrystal (m-CNC) Production

The bleached maize husk fibers were suspended in 34.4 mL of DI-H₂O and 72.1 g of concentrated sulfuric acid per 10 g of dried fiber mass was added dropwise to the suspension under stirring at 15°C. The suspension was heated to 45°C once the sulfuric acid was added and stirred for 45 minutes. The hydrolysis was stopped with the addition of DI-H₂O ice cubes. The suspension was centrifuged and washed until a pH of 4.5 was obtained. A neutral pH was achieved by dialysis in DI-H₂O with the water changed daily. The suspension was sonicated for 5 minutes (50% discontinuous, 50% power) and filtered through 1 µm nylon mesh following dialysis. The filtrate was stored in the refrigerator and 3 drops of chloroform was added to prevent denaturation.

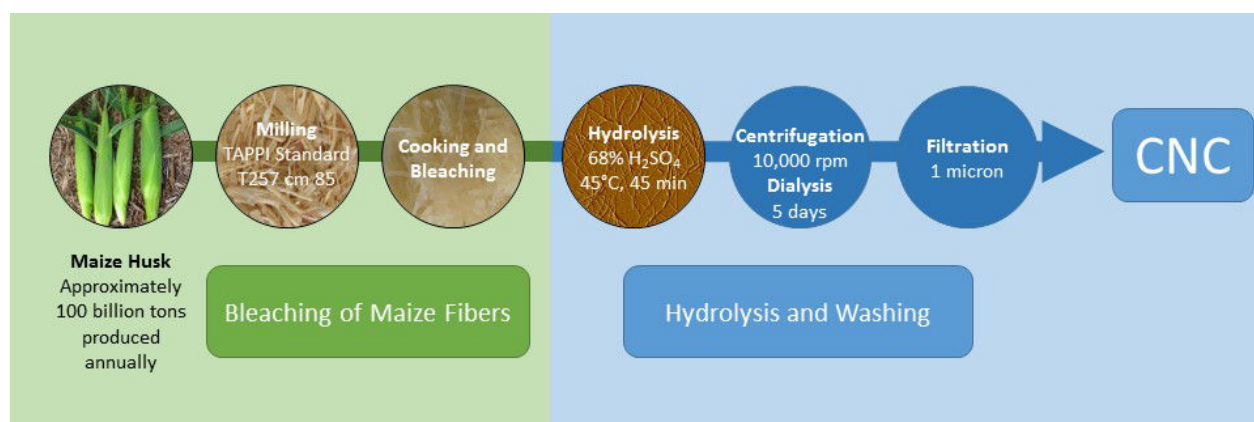


Figure 1. Schematic of m-CNC production from maize husk

2.2.3 Determination of Extractives, Acid Insoluble Lignin, Holocellulose, Hemicellulose, and Cellulose Content

Extractives were determined according to TAPPI standard T207 cm-97 [14], using ethanol-toluene as the extraction media. The extractives removed from lignocellulosic matter mainly consist of low molecular weight carbohydrates, salts, waxes, fats, resins, and non-volatile hydrocarbons. To determine this, 4.0 ± 0.1 g of milled maize husk was placed in a previously tarred extraction thimble and placed in a Soxhlet system. 150 mL of 2:1 ethanol-toulene was used to extract for 6-8 hours under reflux. The extraction thimble was then dried at 105 ± 3 °C for 24 hours. Following cooling, the thimble was weighed. The now extractives-free sample was placed in a desiccator for further analysis.

Acid insoluble lignin content was determined using TAPPI standard T222 om-98 [15]. 1.0 ± 0.1 g of moisture and extractive free sample was mixed with 15 mL 72% sulfuric acid and kept at 20 °C for 1 hr. Followed by the addition of 575 mL of DI-H₂O was added and kept under reflux for 4 hours. The insoluble fraction was filtered and washed until pH \approx 7. The sample was dried for 24 hours at 105 °C and was weighed.

Holocellulose content was determined using a protocol established by Wise et al. [16]. 2.5 g of extractive free sample was mixed with 80 mL hot water and kept at 70°C. 0.5 mL glacial acetic acid and 2.6 mL of 25% NaClO₂ were added each hour for 6-8 hours.

Cellulose and hemicellulose determination was determined by adding 2 g of a moisture free holocellulose sample to 10 mL of 17.5% NaOH. 5 mL of 17.5% NaOH were added every 5 minutes until a final volume of 25 mL was achieved. Following 30 minutes, 33 mL of DI-H₂O was added and stirred for 1 hr. The recovered fraction as washed and filtered with 100 mL 8.3% NaOH and then twice with DI-H₂O. 15 mL of 10% acetic acid was added and washed until pH \approx 7. The dried sample was weighed [17].

Ash content was determined following TAPPI T211 om-93, which is based on the mass of the material following combustion at 525 °C for 3 hours [18].

2.2.4 Preparation of Nanocomposite Films

Nanocomposite films were prepared following the protocol of Mariano and colleagues [19]. Suspensions of m-CNC and w-CNC were sonicated for 5 minutes. CNCs were added to a suspension of 5 g of natural rubber latex (NR) with varying amounts (0.1, 0.5, 1, 2 wt%). These amounts correspond to below the percolation threshold of the m-CNCs (0.1 wt %), at the percolation threshold (0.5 wt%), and above (1, 2 wt%) [20]. The suspensions of NR latex and CNCs were agitated for 6 hours to increase homogeneity, followed by casting on aluminum plates at 30 °C for 24 hours. The dried nanocomposites were conditioned for 4 days at 25 °C, 50% relative humidity before mechanical testing.

2.3 Characterization of CNCs

2.3.1 Conductometric Titration

The sulfate content of hydrolyzed m-CNCs was determined by conductometric titration. Samples of m-CNC (10 mg) were added to 15 mL of 0.01 M hydrochloric acid solution and stirred for 10 minutes. The stability of the suspension was obtained and verified using an Easy Five conductivity meter

(Mettler Toledo SAS, Greifensee, Switzerland). Once the suspension was stable, it was titrated with 0.01 M Sodium Hydroxide. The amount of sulfate groups was calculated by using the equivalence point, which equals the volume of NaOH needed to titrate the HCl. All conductometric measurements were done in triplicate and averaged.

2.3.2 Yield of CNCs

The yield of CNCs produced was calculated using the following equation:

$$\text{yield (\%)} = \frac{M_{\text{bleached}}}{M_{\text{dry CNC}}} \times 100 \quad (\text{Eq. 1})$$

Where M_{bleached} is the mass of the dry, bleached fiber in g, and $M_{\text{dry CNC}}$ is the dry mass of CNCs in grams.

2.3.3 Fourier Transform Infrared Spectroscopy (FTIR)

Fourier Transform Infrared Spectroscopy (FTIR) was done on raw maize husk fiber, bleached maize husk fiber, and m-CNCs using a Perkin Elmer Spectrum One spectrometer (Waltham, Massachusetts, USA). 32 scans from 6000-400 cm^{-1} with a resolution of 1 cm^{-1} were carried out and analyzed using Spectrum software (Perkin Elmer, Waltham, Massachusetts, USA).

2.3.4 Atomic Force Microscopy (AFM)

Suspensions of approximately 0.2 mL 0.0001 wt% of m-CNC and w-CNC were prepared, and placed on the surface of a cleaved mica plate. The CNC coated mica plates were dried overnight at ambient conditions, and then analyzed using atomic force microscopy. Images were acquired using tapping mode with a Nanoscope IIA microscope from Veeco Instruments (Plainview, New York, USA) at a frequency of 265-340 Hz. Silicon cantilevers with a curvature of 10-15 nm were used (OTESPA®, Bruker, Billerica, Massachusetts, USA). AFM images were analyzed using Nanoscope Analysis (Plainview, New York, USA) and ImageJ (U. S. National Institutes of Health, Bethesda, Maryland, USA).

2.3.5 Dynamic Light Scattering (DLS)

To determine the size of the nanoparticles, dynamic light scattering was carried out using a Vasco Particle Size Meter (Cordouan Technologies, Pessac, France). Ten measurements with 60 second time

step and a noise ratio of 1.06 were carried out for each sample in triplicate. The polydispersion index of the DLS measurements was under 0.2 to determine if the measurements are precise. The measurements were collected and analyzed using nanoQ software (Cordouan Technologies, Pessac, France). The cumulative method was used at the hydrodynamic diameter (z^*) was measured. DLS analysis does not measure the actual dimensions of the particle, only the change in intensity of the scattered light to calculate the hydrodynamic diameter, which could not be precise because CNCs have a rod-like shape, and not a sphere used in traditional DLS.

2.3.6 Crystallinity

The crystallinity of lyophilized CNC samples was measured using X-ray diffraction (XRD). XRD diffractogram patterns were measured using a PW 1720 X-ray generator (Phillips, Eindhoven, Netherlands) at 45 kV and 40mA with Cu K α radiation with a wavelength of 0.154 nm in a range of $2\theta=6-56^\circ$ with a fixed step interval. The samples were lyophilized and ground into a powder using a mortar and pestle. The crystallinity index was calculated according to the following equation,

$$C_I^{XRD} = \frac{I_{002} - I_{am}}{I_{002}} \times 100 \quad (\text{Eq. 2})$$

and corresponds to the ratio of the interference of the [002] crystal planes, which was subtracted by the amorphous regions, and the total peak height [002] of the crystal planes. (I_{002}) was observed at 22° .

2.3.7 Thermal Stability

Thermogravimetric measurements were performed with a Perkin Elmer STA 6000 (Waltham, Massachusetts, USA). The temperature ranged from 25 °C to 900 °C with a heating rate of 10 °C/min. The tests were carried out under air (20 mL/min) and under atmospheric conditions for comparison of thermoxidative degradation. The samples ranged in mass between 10 to 20 mg. All results were analyzed with Pyris Series software (Perkin Elmer, Waltham, Massachusetts, USA).

2.3.8 Zeta Potential

Zeta potential of CNC suspensions were measured by a Malvern Zetasizer 3000 (Malvern, United Kingdom). 10 mL of approximately 0.001% suspensions of m-CNC and w-CNC was measured in triplicate. Results are reported in mean \pm standard deviation. The zeta potential is calculated by applying

the Henry equation to the electrophoretic mobility of the CNCs within the aqueous suspension with Smoluchowski approximation with a Henry's function value of 1.5 [21, 22]. Electrophoretic mobility is determined by measuring the velocity of the CNCs by laser doppler velocimetry. Zeta potential is calculated by the following equation:

$$U_E = \frac{2\varepsilon z f(ka)}{3\eta} \quad (\text{Eq. 3})$$

Where U_E is the electrophoretic mobility, ε is dielectric constant, z is zeta potential, Henry's function is $f(ka)$, and η is viscosity.

2.3.9 Optical Properties

m-CNC and w-CNC films were analyzed with UV spectroscopy. The films were loaded into the spectroscopy with a film holder. The absorbance from 300-800 nm was measured with ten scans in spectrum mode with a UV Spectrometer (Shimadzu, Kyoto, Japan) with a normal incidence and repeated in triplicate.

2.3.10 Tensile Testing

Mechanical properties of the samples were measured using a TA Instruments RSA 3 (New Castle, Delaware, USA). CNC based films produced from solvent casting underwent rectangular tension measurements at a rate of 0.001 mm/s. Storage modulus was measured using a single point analysis at 25 °C, 1 Hz, and 0.001 mm of constant strain. CNC composites of natural rubber were tested at an extension rate of 0.05 mm/s and the Young's Modulus was calculated from the stress vs. strain curve. The stress vs. strain curves were measured and analyzed using TA Orchestrator (New Castle, Delaware, USA). Three measurements were taken for each film, and then averaged.

2.3.11 Dynamic Mechanical Analysis (DMA)

Dynamic Mechanical Analysis of the CNC composites were measured using a TA Instruments RSA 3 (New Castle, Delaware, USA). Rectangular samples with a length ≈ 10 mm and width of ≈ 5 mm were measured in isochronal conditions at 1 Hz from -80 to 10 °C with a heating rate of 2 °C/min.

2.3.12 Economic Evaluation

An economic evaluation was proposed for the industrial CNC production from maize husk, using the same methodology described in a previous work [23]. For this purpose, the process conditions used during the experimental part (section 2.2 Methods) were considered as the basis of the study: 100 kg of bleached cellulose, treated with 68% H₂SO₄ solution at a solid to liquid ratio of 1:10, for 1 h at 45 °C (hydrolysis step with around 33% yield) followed by a washing step, which requires 4000 kg of water. The result of the evaluation showed that the industrial production of cellulose nanocrystals from this agrowaste would require around 2.1 kg of acid, 138.8 kg of water and 295.8 kcal of energy per kg of CNC produced.

3. Results and Discussion

3.1 Characterization of Raw Material

3.1.1 Determination of Extractives, Holocellulose, Hemicellulose, Cellulose, Lignin, and Ash

In lignocellulosic materials extractives mostly consist of low molecular weight salts, fats, waxes, resins, carbohydrates, and non-volatile hydrocarbons. The extractives in the maize husk, following Soxhlet extraction under reflux of 2:1 ethanol-toulene are reported to be 6.64% of the dry mass of dried maize husk.

Holocellulose is the sum of cellulose and hemicelluloses, or otherwise known as the water insoluble carbohydrate fraction of lignocellulosic materials. The amount of holocellulose in maize husk following bleaching is reported to be 80.18%. The value for the percentage of cellulose within Maize husk is in accordance with literature values reported by Kurakake et al. in 2001, with a cellulose percentage of 21.8% in corn husk [24].

Table 1. Summary of composition of maize husk following extractive protocols

Extractives (%) ¹	Holocellulose (%) ² (Hemicellulose + Cellulose)	Hemicellulose(%) ³	Cellulose (%) ³	Acid Insoluble Lignin (%) ⁴	Ash (%) ⁵
6.6	80.2	48.9	31.3	10.9	2.7

¹ TAPPI standard T207 cm-97, ² Wise et al. 1946, ³ Rowell, 1983, ⁴ TAPPI standard T222 om-98,

⁵ TAPPI T211 om-93

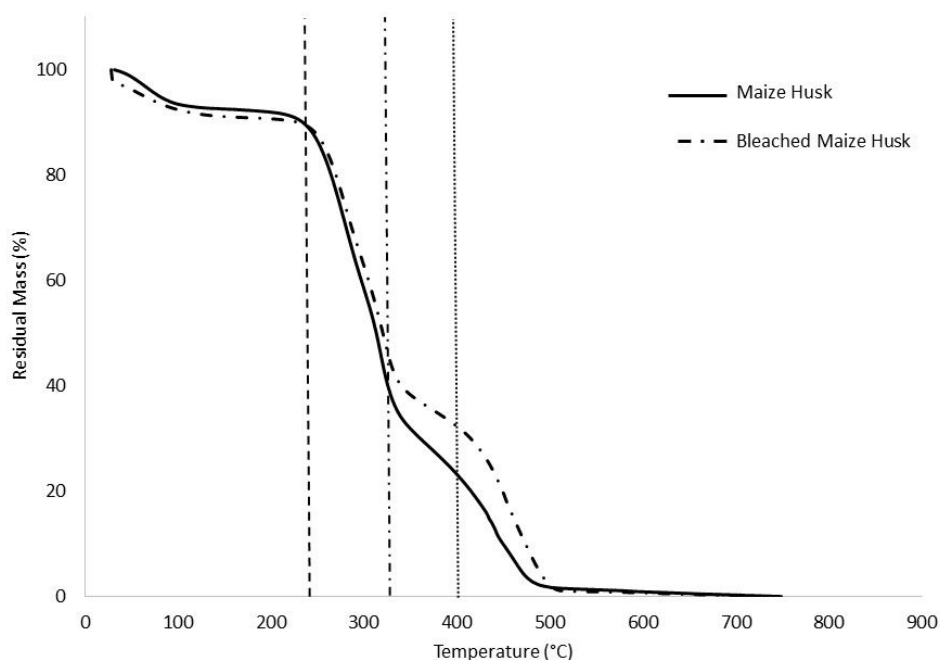


Figure 2. Thermograms of raw maize husk and bleached maize husk measured from 30-900 °C with a temperature rate increase of 10 °C per minute under air

The thermal decomposition of a biomass can be divided into four distinct stages: removal of moisture and decomposition of hemicellulose, cellulose, and lignin [25, 26]. It has been determined in studies by Yang et al. that hemicellulose and cellulose has a maximum degradation temperature, or temperature at the maximum of the derivative of the weight percent, of 268 °C and 355 °C, respectively, and a range of 220-315 °C for hemicellulose and 315-400 °C for cellulose. The decomposition of lignin is more difficult to characterize using TGA because degradation of lignin degrades slowly in the temperature range of 30-900°C [27]. The raw and bleached maize husk underwent thermogravimetric analysis from 25-900 °C with a temperature increase of 10 °C/min under air.

3.2. Characterization of Cellulose Nanocrystals

3.2.1 Conductometric Titration

Sulfuric acid based hydrolysis introduces sulfate ester moieties onto the surface of the extracted CNCs and changes the charge density of m-CNCs. This negative charge density was determined using

conductometric titration. After 45 minutes of hydrolysis, m-CNCs had a charge density of 1.01×10^{-6} mol/g

3.2.2 Composition of Maize CNCs

The composition and percent yield of m-CNCs was carried out to determine if there was any possible hemicellulose or lignin remaining within the m-CNCs. The percent yield of m-CNCs from bleached maize husk fiber of 15.61%, which is in accordance to literature of other waste agricultural CNCs produced by sulfuric acid hydrolysis [11, 28].

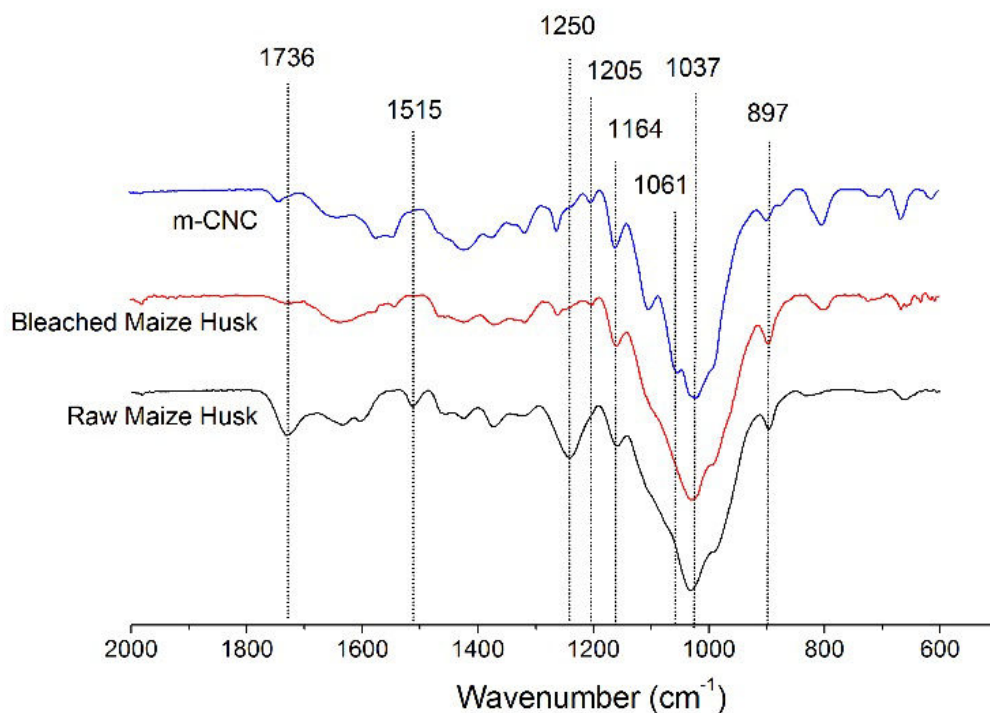


Figure 3. FTIR spectra for raw Maize fiber, bleached Maize fiber, and m-CNCs obtained by sulfuric acid hydrolysis.

FTIR was performed on raw maize husk fiber, bleached maize husk fiber, and m-CNCs to determine if any residual hemicelluloses or lignin remained following bleaching of the fiber or acid hydrolysis of the CNCs. Hemicellulose and lignin have characteristic vibrations within the FTIR spectra at 1736 cm^{-1} because of the C=O stretching, and at 1250 cm^{-1} or the asymmetric =C-O-C present in ether, phenol, and ester groups. As shown in Figure 3 these peaks have lessened from the raw maize fiber to the m-CNC spectra, with complete disappearance in the bleached fiber spectra. This complete removal from the raw maize fiber to the bleached fiber shows that hemicellulose and lignin were successfully removed through the bleaching process using sodium hydroxide. The appearance of a peak at 1205 cm^{-1}

cm^{-1} only occurs in the spectra for m-CNC. This is because this peak corresponds to the vibration of $\text{S}=\text{O}$, which is because of the presence of the sulfate groups added to the m-CNCs following sulfuric acid hydrolysis[11].

A peak at 1515 cm^{-1} appears in the raw maize fiber spectrum, this is indicative of the presence of lignin because of the aromatic structure of lignin and this wavenumber corresponds to the $\text{C}=\text{C}$ of an aromatic ring. In regards to the characteristics of cellulose, peaks at 1061 cm^{-1} and 897 cm^{-1} refer to the $\text{C}-\text{O}$ stretching and $\text{C}-\text{H}$ rocking, respectively. All spectra have a peak at these wavenumbers, but are clearly more intense for the m-CNC sample as it contains a larger amount of pure cellulose.

3.2.2 Dimensional Analysis

The dimensions of the m-CNCs and w-CNCs were determined using dynamic light scattering and AFM. Dimensional analysis of m-CNCs using AFM showed very promising results for using m-CNCs in applications which require CNCs with a high aspect ratio, similar to tunicate derived CNCs. The AFM images in Figure 4 show long, thin crystals with average dimensions of $940 \pm 70\text{ nm}$ in length and $6 \pm 2\text{ nm}$ in width for m-CNC, and smaller crystals with dimensions of $170 \pm 16\text{ nm}$ in length and $24 \pm 22\text{ nm}$ in width for w-CNCs.

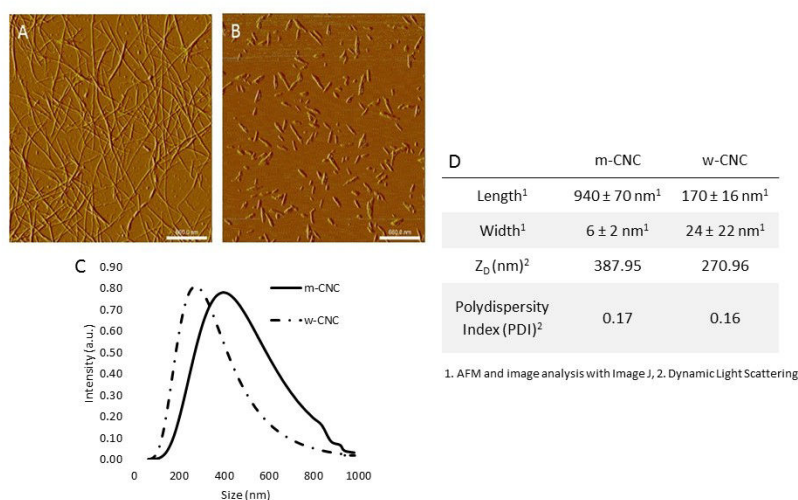


Figure 4. CNC AFM images from suspensions of 0.0001 wt% of A) m-CNC, B) w-CNC acquired by tapping mode in air. C) Size distribution of m-CNC and w-CNC nanoparticles from 0.001 wt% suspensions in DI- H_2O as determined by DLS. D) Length and width measurements of maize derived CNCs and commercial CNCs suspensions of approximately 0.001 wt% as determined by AFM, and Hydrodynamic diameter (Z_D), polydispersity index (PDI) determined by dynamic light scattering.

The DLS results, which include the Z_D , or hydrodynamic diameter and polydispersity index (PDI), are shown in Figure 4. The PDI measurement for the suspension shows the degree of homogeneity within the size distribution of the sample. The closer the PDI value is to 0 the more homogeneous the sample, while values closer to 1 indicate that the sample has a wide size distribution. The low PDI reported of the m-CNCs and w-CNCs signifies that the samples are mono-dispersed. The m-CNCs and w-CNCs size distribution, as shown in Figure 4, have a wide range and follow a Gaussian distribution. In regards to the average size of the particles, m-CNCs have a larger average Z_D compared to w-CNCs, which indicate a larger diameter. These results cannot be assumed to be conclusive, because DLS measurements require that the particles have a spherical shape, and both m-CNCs and w-CNCs are known to be rod-like materials. DLS is used in our results to confirm that the isolated CNCs are in fact nanoparticles, and follow a Gaussian size distribution.

3.2.3 Crystallinity

Crystallinity of the CNC samples were measured using x-ray diffraction, with the results being shown in Figure 5. Cellulose I has typical peaks located at 15.7° and 22.6° [29]. The crystallinity index for commercial and maize CNCs are reported in Figure 5, B. The crystallinity spectra was normalized with the respect to the maximum. The CNCs derived from maize husk have a much lower crystallinity compared to the commercially derived CNCs. This can be attributed to possible residual sugars, lignin, hemicelluloses, etc., or that the hydrolysis procedure for m-CNCs has not been optimized. The crystallinity index observed in our study are comparable to previous studies of nanofibers from maize husk as reported by Arroyo Rosas of 55.1% [9]. This low crystallinity can also be related to the function of the maize husk. The maize husk must be flexible in order to cover and protect the cob.

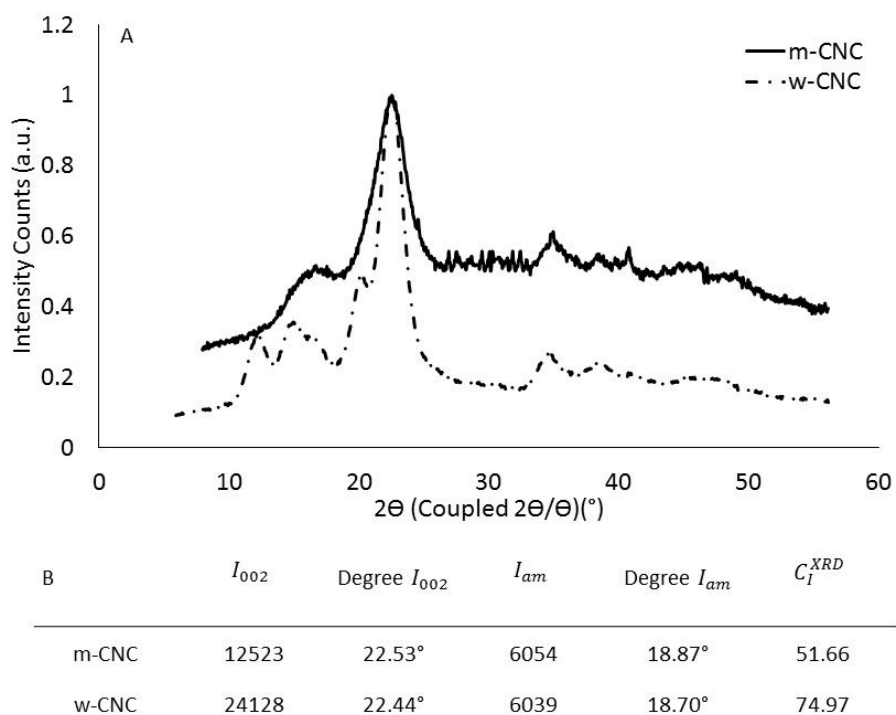


Figure 5. A) X-ray diffraction patterns w-CNC obtained from powder of m-CNC and w-CNC. B) Crystallinity intensities of m-CNC and w-CNC

3.2.4 Thermal Stability

CNCs can be used in a variety of applications with one of those applications being reinforcement in materials. In material processing, thermal stability is a must in order to have materials which can withstand typical processing conditions, which can include melt processing of polymers [30]. Thermogravimetric analysis curves of m-CNC and w-CNC are shown in Figure 6. The loss of weight under 100 °C can be attributed to the evaporation of residual water within the samples, which is approximately 5-6 % of the sample mass [28]. Thermogravimetric analysis of CNC also corroborates the absence of hemicelluloses in the produced whiskers. As observed in Figure 2, raw material (Maize husk) showed two maximum degradation rates at 282 °C and 321 °C, attributed to hemicelluloses and cellulose, respectively. The thermogram of the produced CNC sample presents a single sharp peak at 300 °C, characteristic for cellulose, indicating that hemicelluloses were removed during CNC production process.

Samples of pure cellulose exhibit a single weight loss event, while samples with surface groups, such as sulfate groups, typically have two weight loss events. The first weight loss event can be attributed

to the sulfate groups attached to the surface of CNC, while the second event is attributed to the -OH groups [31].

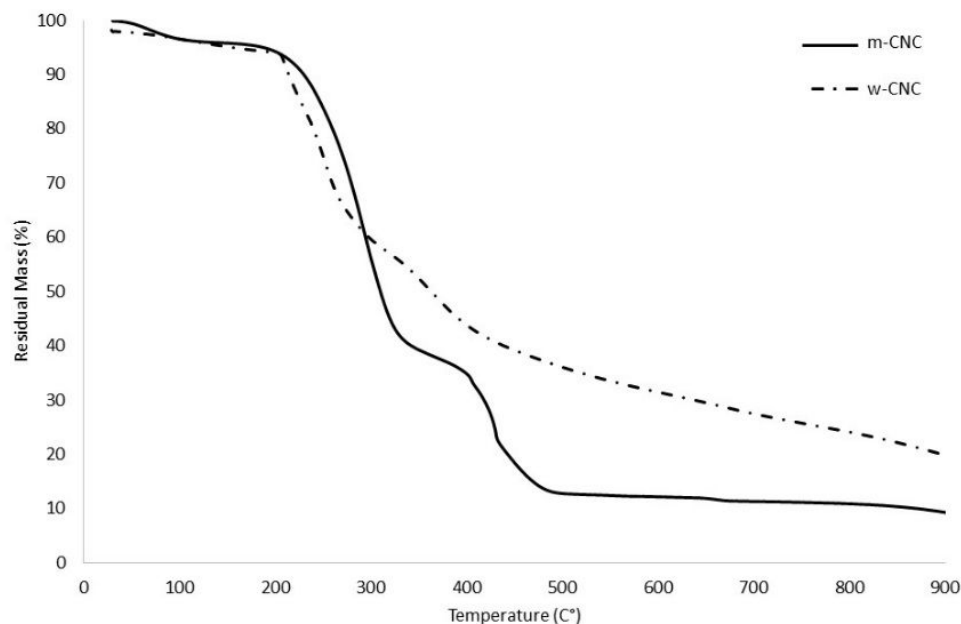


Figure 6. TGA thermograms of m-CNC and w-CNC measured from 30-900 °C with a temperature rate increase of 10 °C per minute under air

3.2.5 Zeta Potential

Zeta potential of m-CNCs and w-CNCs is reported to be -28.3 ± 1.1 mV and -43.0 ± 0.6 mV, respectively. m-CNCs display a lower zeta potential when compared the w-CNCs. Zeta potential relates to the dispersity of the CNCs because of the imparted surface charge due to the acid hydrolysis. This suggests that there are less anionic sulfate groups on the surface of the m-CNCs. These sulfate surface charges are believed to cause an increase in the surface charge of the particle and increase the dispersion stability of the CNCs [21]. Kargarzadeh et al. explored how acid hydrolysis conditions could affect zeta potential, with increased acid hydrolysis time relating to an increase in zeta potential and a decrease in agglomeration. Our results are in accordance with their findings, and suggest that m-CNCs have less dispersive capabilities in suspension when compared to commercially available wood CNCs.

3.2.6 Optical Properties

The optical properties of CNC are of interest in a variety of applications including specialty paper, counterfeit prevention, and packaging. This is because CNCs self-assemble and impart coloration because of the interaction between light and the surrounding microstructure. This phenomena is called structural coloration [32]. Commercial CNCs exhibit much higher transmittance compared to maize derived CNCs. This indicates that m-CNCs would not be preferable for applications where transparent CNC films are needed. Informational data on transmittance and images of m-CNC and w-CNC films are in shown in Figure 7.

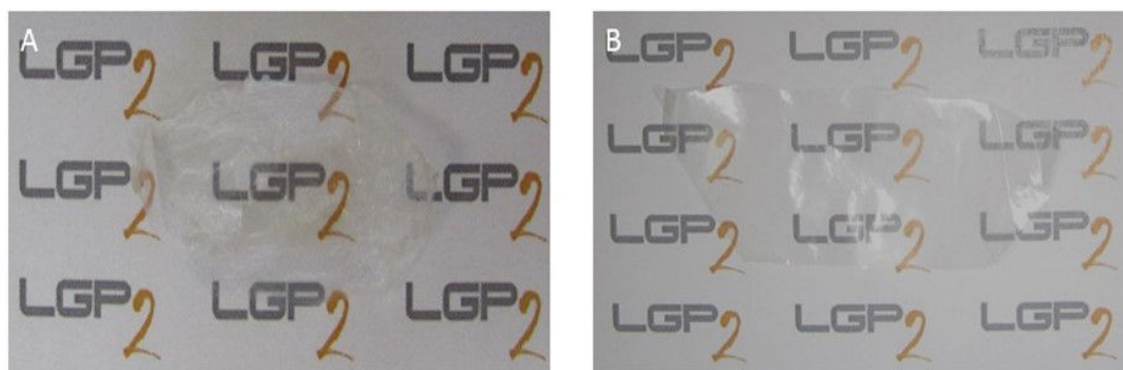


Figure 7. Images of A) 0.079 wt% suspension solvent casted film of m-CNC, B) 1 wt% w-CNC

3.2.7 Mechanical Properties

Tensile tests were conducted on solvent casted films of m-CNC and w-CNC. The results at ambient conditions reveal that m-CNC have a higher elongation at break compared to w-CNC, but w-CNC have both a larger Young's and storage modulus. The differences in moduli can be attributed to differences in crystallinity. Higher crystallinity is associated with higher strength and lower extensibility [33]. The low E values for maize nanocellulose casted films can be attributed to the thickness of each of the samples, as well as the lower crystallinity.

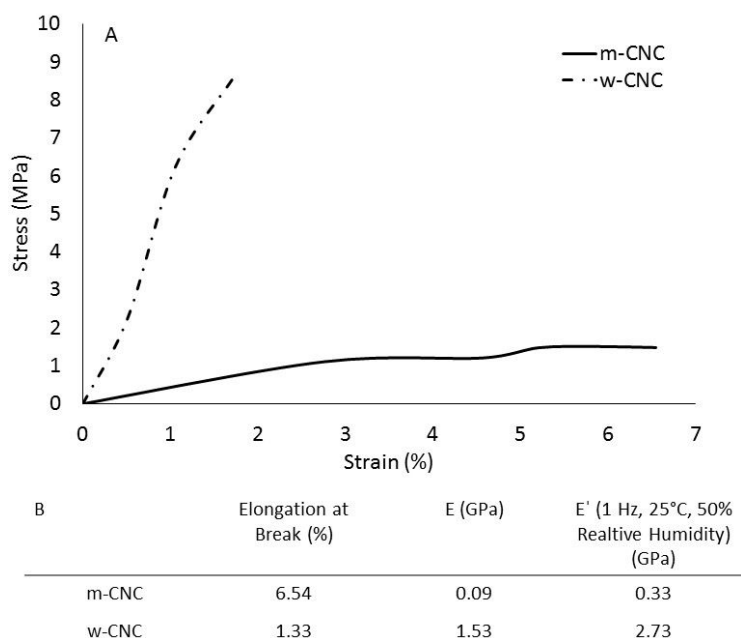


Figure 8. A) Stress vs. Strain curves of m-CNC and w-CNC films prepared by casting, which are 0.01 mm thick for CNCs and cut into rectangular shapes with a length of 5 mm and width of 5 mm for CNC. Tested on a TA Instruments RSA 3 with an extension rate of 0.001 mm/s. B) Elongation at break, Young's Modulus, and Storage Modulus of m-CNC and w-CNC films as measured by tensile tests of solvent casted films of m-CNC and w-CNC.

The lowering of mechanical properties compared to other sources of CNCs can be favorable in applications where transparent, flexible films are desired. Previous studies have been conducted CNC and polyethylene glycol (PEG) composites, and with the addition of PEG, previously brittle CNC films became flexible [34]. This flexibility was only achieved because of the addition of PEG, but with m-CNCs it is possible to have flexibility without the addition of a plasticizer as shown in Figure 9.

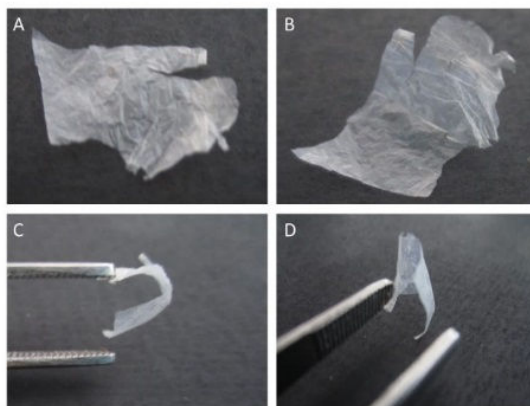


Figure 9. Images of 0.079 wt% solvent casted film of m-CNC

Composites of natural rubber (NR) and CNCs were produced to determine the usefulness of m-CNCs for polymer reinforcement. Natural rubber was chosen as a polymer matrix because of its extensive use in studies [19, 35-37]. Composites at and below the percolation network weight percentage for m-CNC (0.5%) were fabricated as reported in the methods and materials section. The mechanical properties of these composites were determined with tensile test and dynamic mechanical analysis. The results from the tensile test are reported in Figure 10A. As reported in Table 2 the elongation at breaks for the NR/m-CNC for the same mass percentage of NR/w-CNC are lower, while the Young's moduli are higher, with an exception for 1.0% m-CNC. These differences in elongation at break and Young's moduli suggest that the m-CNCs create a more brittle and stiff composite compared to w-CNCs and increase the mechanical properties in regards to tensile testing.

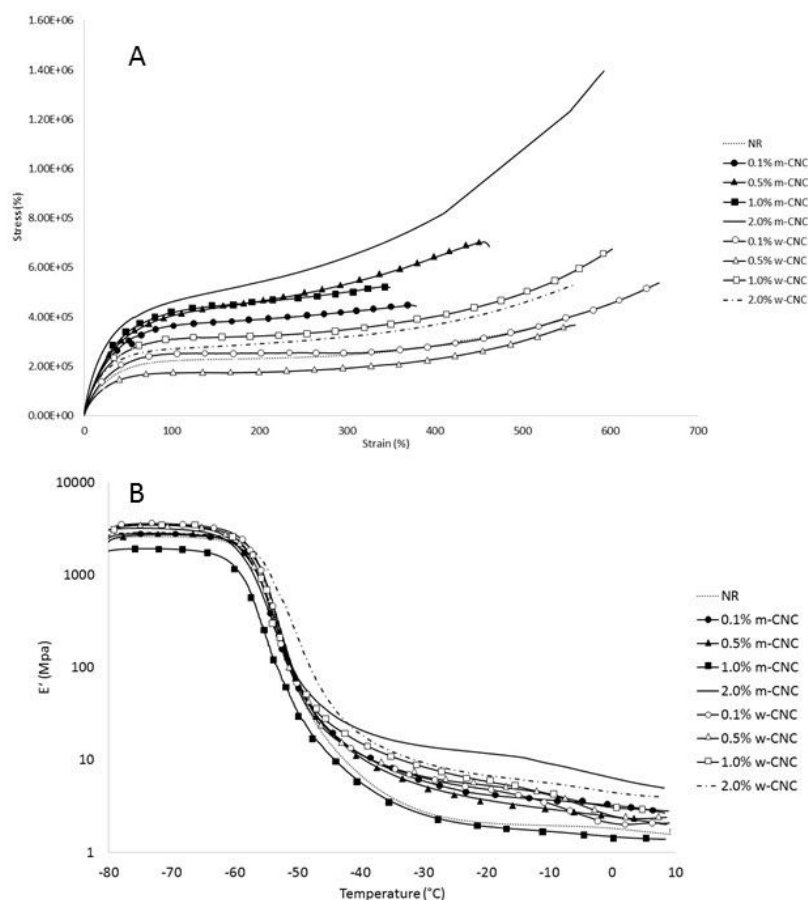


Figure 10. A) Stress vs. Strain curves of m-CNC/NR and w-CNC/NR composites prepared by mixing of suspensions of CNCs and natural rubber by casting, which are approximately 0.5 mm thick and cut into rectangular shape with a width of 5 mm and length of 10mm. Tested with a TA Instruments RSA 3 with an extension rate of 0.05 mm/s. B) Temperature dependent dynamic mechanical analysis of m-CNC/NR and w-CNC/NR composites prepared by mixing

of suspensions of CNCs and natural rubber by casting, which are approximately 0.5 mm thick and cut into rectangular shape with a width of 5 mm and length of 10mm. Tested with a TA Instruments RSA 3 from -80 °C-10 °C with a heating rate of 2 °C/min and a constant frequency of 1 Hz.

Table 2. Elongation at break, Young's modulus, and storage modulus of m-CNC and w-CNC composites with natural rubber. ¹. Measured by tensile testing and ² measured by temperature dependent dynamic mechanical analysis.

	NR	0.1% m-CNC	0.5% m-CNC	1.0% m-CNC	2.0% m-CNC	0.1% w-CNC	0.5% w-CNC	1.0% w-CNC	2.0% w-CNC
Elongation at Break (%) ¹	552±87.8	379±32.8	461±126	349±13.0	593±90.6	655±148	579±156	602±255	557±39.6
E (MPa) ¹	0.89±0.15	1.27±0.78	1.33±0.09	1.21±0.46	1.98±0.73	0.97±0.04	0.83±0.03	1.35±0.12	1.40±0.18
E' -70°C (Mpa) ²	2588±185	2808±122	2734±131	1903±134	3131±216	3563±208	3453±189	3446±1142	2862±198
E' -15°C (Mpa) ²	2.00±0.47	3.89±1.77	3.26±0.35	1.79±0.17	10.8±1.01	4.13±1.08	4.87±0.18	5.07±0.81	6.20±1.59

Dynamic mechanical analysis of the composites was conducted, which varied the temperature below and above the glass transition temperature of natural rubber, which is approximately -48 °C. Figure 10B shows that the storage modulus at -70 °C and -15 °C for all the composites, with exception of 1.0% m-CNC are higher than natural rubber, and with maximum storage modulus at both temperatures for 2.0% m-CNCs (3131 MPa @ -70 °C, 10.8 MPa @ -15 °C). These results suggest that m-CNCs reinforce natural rubber and with a higher capacity compared to w-CNCs, which have a lower aspect ratio when compared to m-CNCs. This phenomenon of higher reinforcement with higher aspect ratio is well reported in literature by many researchers including the work of Weder and colleagues and Bras et al. [38-40].

Table 3. Summary of CNC characteristics from maize (m-CNC), cotton (co-CNC), wood (wood-CNC), tunicate (t-CNC), sugarcane bagasse (s-CNC), agave (a-CNC), banana psuedostems (b-CNC), and barley (br-CNC)

	Length (nm)	Width (nm)	Crystallinity (%)	Predominate Polymorph	Fabrication Technique (Characterization)	Elongation at break (%)	E, E', Tensile Strength (Pa)
m-CNC	940 ± 66.38	5.84 ± 0.22	50.7	Iβ	Solvent casted film NR Composites (Traction/DMA)	6.54	E: 9.25E+07 E': 3.29E+08 Composite Results in Table #
co-CNC [41]* [39]†	135 ± 50*	19 ± 10*	77.0*	I*	PVA + 16.5 wt% CNC composite (DMA) †	---	E' at 85°C: 4.00E+09†
wood-CNC [42]* [43] †	130 ± 67*	5.9 ± 1.8*	60.*	Iα*	Segmented polyurethanes + 1 wt% CNC composite (Traction) †	142 ± 28†	E: 6.56 ± 1.06E+06†
t-CNC[42]* [39]†	1187 ± 1066*	9.4 ± 5.0*	80.0*	Iβ*	PVA + 16.5 wt% CNC composite† (DMA)	---	E' at 85°C: 5.00E+09†

s-CNC [44]* [45]†	255 ± 55*	4 ± 2*	87.5*	I & II*	Linear PVA + 10 wt% CNC composite† (Traction)	≈50†	Tensile Strength: ≈5.5E+04†
a-CNC [46]	323 ± 113	11.4 ± 3.6	71.0	I	---	---	--
b-CNC [38]	375 ± 100	17 ± 4	74.0	I	EO-EPI + 12 wt% b-CNC composite (DMA)	---	E' at -60°C: 5.20E+09 at 25°C:2.17E+06
br-CNC [46]	329 ± 123	10.2 ± 3.5	66.0	I	---	---	---

Even with the low reported crystallinity of the CNCs (~50%) derived from maize husks, these CNCs exhibit favorable mechanical properties in natural rubber composites as well as aspect ratio. This increase in aspect ratio in comparison to other agricultural residue derived CNCs and traditional CNC sources such as wood, cotton, and tunicate show that maize CNCs can be favorable in certain applications. Especially if a flexible CNC with a high aspect ratio is needed, while still imparting reinforcement to a polymer matrix.

3.2.8 Economic Evaluation

As demonstrated in the present work, the morphologic and crystallinity features of CNC from maize husk resulted analogous to those reported for tunicates [42, 47].

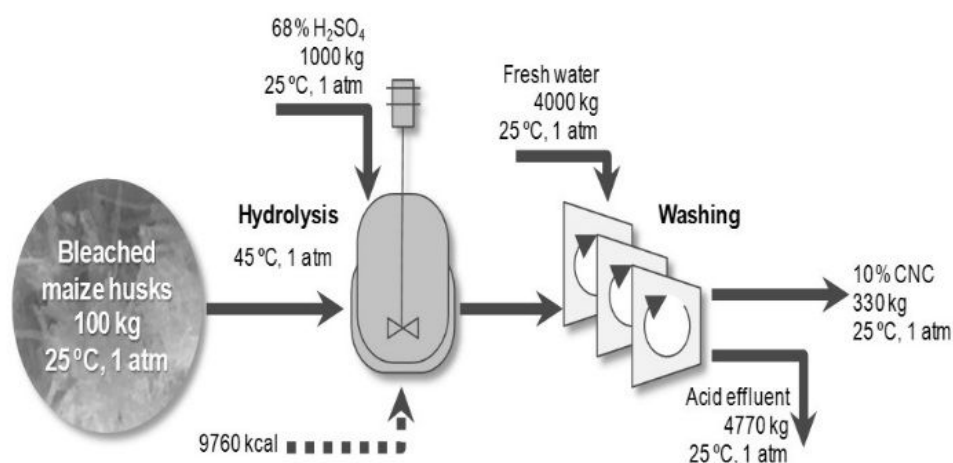


Figure 11. Schematic of m-CNC production from maize husk for mass-energy consumption

As described by Jorfi et al. [47], the production of CNC from tunicate cellulose is carried out in the same way for other lignocellulosic sources, entailing a similar hydrolysis step (around 45% H_2SO_4 solution at a solid to liquid ratio of 1:183) and washing/purification process with a 55% yield of CNC. In this sense, considering only the hydrolysis step, the production of CNC from tunicates would consume more than 75 times more of acid, 10 times more water, and almost 25 times more energy than from maize husks (152.7 kg H_2SO_4 , 182.0 kg H_2O and 7175.6 kcal per kg of CNC produced). It is well known that tunicates require arduous and sometimes expensive purification and extraction steps for the obtaining of tunic cellulose pulp, that the cellulose yielded from these sea animals normally is never higher than 16% of their total weight [48]. Another deterrent of using tunicates is the high price and small supply [49]. For all these reasons, the present work demonstrated an easier and less cost-

associated method for the obtaining of high aspect ratio CNC, using conventional methods but from a more available, cheap, renewable, and sustainable source of cellulose.

4. Conclusion

Unused agricultural residues from *Zea mays* has the potential to be one of the largest supplies of cellulose in the world because of the high levels of maize production, especially within the United States. Approximately 100 billion tons of maize husk are produced annually. Isolation of CNCs from maize husk would not cause a disruption in the current feed production because it is a waste product. This fact, as well as being environmentally friendly makes nanocellulose from maize husk to be a very attractive material for future research. The “green” aspect of maize CNCs makes them suitable for future research applications because of their high aspect ratio, lack of disturbance in the food supply chain, and the economic advantages because maize husk is a waste product, and is much cheaper to produce compared to tunicate CNCs, which have a similar aspect ratio.

It was shown that successful isolation of CNCs was achieved by sulfuric acid hydrolysis with a yield percentage of 15.61% and removal of hemicellulose and lignin as shown by FTIR and TGA of the raw fiber and chemically bleached cellulose fiber. Negatively charged CNCs (-28.3 mV) were produced due to the sulfuric acid with high aspect ratio (L/D) of 157. CNCs from maize had favorable thermal stability ($\sim 300^{\circ}\text{C}$) and crystallinity of 51.7%, which can be favorable for use in nanocomposites. Commercially derived CNCs from wood, w-CNCs, were compared to the m-CNCs. The addition of m-CNCs to natural rubber composites at 2 wt% showed an improvement in the Young's modulus of natural rubber higher with m-CNCs (1.98 ± 0.73 MPa) compared to w-CNCs (1.40 ± 0.18). This improvement with a low filler content can be attributed to the high aspect ratio of the m-CNCs. The CNCs were of high quality with similar properties to tunicate derived CNCs. Tunicate CNCs are difficult to obtain because they can only be resourced from tunicate populations in certain areas of the world, and have to be highly processed to remove residual proteins and other naturally occurring products within the tunicate CNCs. It was shown the m-CNCs require less solvent compared to tunicate CNCs, which makes them more economic. Future studies will need to be conducted to optimize hemicellulose and lignin removal, and to increase the yield of CNC production. These cellulose nanomaterials could be of interest in a variety of applications in the manufacturing of nanocomposites, while being “eco, green, or environmentally” friendly.

5. Acknowledgements

The authors would like to thank Lísias Pereira Nova for his assistance in producing the CNC, and Spanish Ministry of Economy, Industry and Competitiveness (Juan de la Cierva Incorporacion IJCI-2015-23168) for providing scholarships to the researchers involved. XRD measurements were conducted by Thierry Encinas at Grenoble INP – CMTC. LGP2 is part of the LabEx Tec 21 (Investissements d’Avenir - grant agreement n°ANR-11-LABX-0030) and of the Énergies du Futur and PolyNat Carnot Institutes (Investissements d’Avenir - grant agreements n°ANR-11-CARN-007-01 and ANR-11-CARN-030-01). This work been partially supported by the LabEx Tec 21 (Investissements d’Avenir - grant agreement n°ANR-11-LABX-0030).

6. References

- [1] Faostat. Food and Agricultural Organization of the United Nations Statistics Division; 2015.
- [2] Myers DK. Harvesting Corn Residue. In: Underwood JF, editor.: Ohio State University Extension Department of Horticulture and Crop Science.
- [3] Pordesimo LO, Hames BR, Sokhansanj S, Edens WC. Variation in corn stover composition and energy content with crop maturity. *Biomass and Bioenergy*. 2005;28:366-74.
- [4] Padgitt M, et al. . Production practices for major crops in US agriculture, 1990-97. Growth. 2000.
- [5] Gogerty R. Crop leftovers: More uses, more value. *Resource: Engineering & Technology for Sustainable World*. 1996;3:6-9.
- [6] Reddy N, Yang Y. Structure and properties of high quality natural cellulose fibers from cornstalks. *Polymer*. 2005;46:5494-500.
- [7] Prado-Martinez Mea. Caracterización de hojas de mazorca de maíz y de bagazo de caña para la elaboración de una pulpa celulósica mixta Madera y Bosques. 2012;18.
- [8] Duguid KB, Montross MD, Radtke CW, Crofcheck CL, Wendt LM, Shearer SA. Effect of anatomical fractionation on the enzymatic hydrolysis of acid and alkaline pretreated corn stover. *Bioresource Technology*. 2009;100:5189-95.
- [9] Arroya Rosas K. Biocompuestos de almidón termoplástico con microfibras de celulosa Altamira, Tamaulipas, México Instituto Politecnico Nacional 2008.
- [10] Rehman N, de Miranda MIG, Rosa SML, Pimentel DM, Nachtigall SMB, Bica CID. Cellulose and Nanocellulose from Maize Straw: An Insight on the Crystal Properties. *Journal of Polymers and the Environment*. 2013.

- [11] Silvério HA, Flauzino Neto WP, Dantas NO, Pasquini D. Extraction and characterization of cellulose nanocrystals from corncob for application as reinforcing agent in nanocomposites. *Industrial Crops and Products*. 2013;44:427-36.
- [12] Hall T. Corn Stover as an Emergency Feed Source and the Potential for a Supplemental PAN Allowance For Small Grain Sown After Stover Removal. North Carolina Department of Agriculture and Consumer Services ; 2007.
- [13] TAPPI. Sampling and preparing wood for analysis 1985.
- [14] TAPPI. Water solubility of wood and pulp 1993.
- [15] TAPPI. Acid-insoluble lignin in wood and pulp. 1998.
- [16] Wise LE, Murphy M, D ADIECO A. A chlorite holocellulose, its fractionation and bearing on summative wood analysis and studies on the hemicelluloses. 1946.
- [17] Rowell R. The Chemistry of Solid Wood 185th Meeting of the American Chemical Society. Seattle, Washington 1983.
- [18] TAPPI. Ash in wood, pulp, paper and paperboard: combustion at 525°C. 1993.
- [19] Mariano M, El Kissi N, Dufresne A. Cellulose nanocrystal reinforced oxidized natural rubber nanocomposites. *Carbohydrate Polymers*. 2016;137:174-83.
- [20] Mariano M, El Kissi N, Dufresne A. Cellulose nanocrystals and related nanocomposites: review of some properties and challenges. *Journal of Polymer Science Part B: Polymer Physics*. 2014;52:791-806.
- [21] Kargarzadeh H, Ahmad I, Abdullah I, Dufresne A, Zainudin SY, Sheltami RM. Effects of hydrolysis conditions on the morphology, crystallinity, and thermal stability of cellulose nanocrystals extracted from kenaf bast fibers. *Cellulose*. 2012;19:855-66.
- [22] Hunter R. Zeta Potential in Colloid Science Academic Press. New York. 1981.
- [23] Novo LP, Bras J, García A, Belgacem N, Curvelo AA. Subcritical water: A method for green production of cellulose nanocrystals. *ACS Sustainable Chemistry & Engineering*. 2015;3:2839-46.
- [24] Kurakake M, Kisaka W, Ouchi K, Komaki T. Pretreatment with ammonia water for enzymatic hydrolysis of corn husk, bagasse, and switchgrass. *Applied Biochemistry and Biotechnology*. 2001;90:251-9.
- [25] Yang H, Yan R, Chen H, Lee DH, Liang DT, Zheng C. Pyrolysis of palm oil wastes for enhanced production of hydrogen rich gases. *Fuel Processing Technology*. 2006;87:935-42.

- [26] Raveendran K, Ganesh A, Khilar KC. Pyrolysis characteristics of biomass and biomass components. *Fuel*. 1996;75:987-98.
- [27] Yang H, Yan R, Chen H, Lee DH, Zheng C. Characteristics of hemicellulose, cellulose and lignin pyrolysis. *Fuel*. 2007;86:1781-8.
- [28] Neto WPF, Silvério HA, Dantas NO, Pasquini D. Extraction and characterization of cellulose nanocrystals from agro-industrial residue–Soy hulls. *Industrial Crops and Products*. 2013;42:480-8.
- [29] Sèbe G, Ham-Pichavant Fdr, Ibarboure E, Koffi ALC, Tingaut P. Supramolecular structure characterization of cellulose II nanowhiskers produced by acid hydrolysis of cellulose I substrates. *Biomacromolecules*. 2012;13:570-8.
- [30] Lin N, Dufresne A. Surface chemistry, morphological analysis and properties of cellulose nanocrystals with gradiented sulfation degrees. *Nanoscale*. 2014;6:5384-93.
- [31] Roman M, Winter WT. Effect of sulfate groups from sulfuric acid hydrolysis on the thermal degradation behavior of bacterial cellulose. *Biomacromolecules*. 2004;5:1671-7.
- [32] Kinoshita S, Yoshioka S, Miyazaki J. Physics of structural colors. *Reports on Progress in Physics*. 2008;71:076401.
- [33] Ward K. Crystallinity of cellulose and its significance for the fiber properties. *Textile Research Journal*. 1950;20:363-72.
- [34] Bardet R, Belgacem N, Bras J. Flexibility and color monitoring of cellulose nanocrystal iridescent solid films using anionic or neutral polymers. *ACS Appl Mater Interfaces*. 2015;7:4010-8.
- [35] Bras J, Hassan ML, Bruzesse C, Hassan EA, El-Wakil NA, Dufresne A. Mechanical, barrier, and biodegradability properties of bagasse cellulose whiskers reinforced natural rubber nanocomposites. *Industrial Crops and Products*. 2010;32:627-33.
- [36] Pasquini D, de Moraes Teixeira E, da Silva Curvelo AA, Belgacem MN, Dufresne A. Extraction of cellulose whiskers from cassava bagasse and their applications as reinforcing agent in natural rubber. *Industrial Crops and Products*. 2010;32:486-90.
- [37] Nagalakshmaiah M, Mortha G, Dufresne A. Structural investigation of cellulose nanocrystals extracted from chili leftover and their reinforcement in cariflex-IR rubber latex. *Carbohydrate Polymers*. 2016;136:945-54.
- [38] Mueller S, Weder C, Foster EJ. Isolation of cellulose nanocrystals from pseudostems of banana plants. *RSC Adv*. 2014;4:907-15.

- [39] Shanmuganathan K, Capadona JR, Rowan SJ, Weder C. Bio-inspired mechanically-adaptive nanocomposites derived from cotton cellulose whiskers. *Journal of Materials Chemistry*. 2010;20:180-6.
- [40] Bras J, Viet D, Bruzzese C, Dufresne A. Correlation between stiffness of sheets prepared from cellulose whiskers and nanoparticles dimensions. *Carbohydrate Polymers*. 2011;84:211-5.
- [41] de Moraes Teixeira E, Corrêa A, Manzoli A, de Lima Leite F, de Oliveira C, Mattoso L. Cellulose nanofibers from white and naturally colored cotton fibers. *Cellulose*. 2010;17:595-606.
- [42] Sacui IA, Nieuwendaal RC, Burnett DJ, Stranick SJ, Jorfi M, Weder C, et al. Comparison of the Properties of Cellulose Nanocrystals and Cellulose Nanofibrils Isolated from Bacteria, Tunicate, and Wood Processed Using Acid, Enzymatic, Mechanical, and Oxidative Methods. *ACS applied materials & interfaces*. 2014;6:6127-38.
- [43] Eichhorn SJ, Dufresne A, Aranguren M, Marcovich NE, Capadona JR, Rowan SJ, et al. Review: current international research into cellulose nanofibres and nanocomposites. *Journal of Materials Science*. 2010;45:1-33.
- [44] de Moraes Teixeira E, Bondancia TJ, Teodoro KBR, Corrêa AC, Marconcini JM, Mattoso LHC. Sugarcane bagasse whiskers: extraction and characterizations. *Industrial Crops and Products*. 2011;33:63-6.
- [45] Mandal A, Chakrabarty D. Studies on the mechanical, thermal, morphological and barrier properties of nanocomposites based on poly(vinyl alcohol) and nanocellulose from sugarcane bagasse. *Journal of Industrial and Engineering Chemistry*. 2014;20:462-73.
- [46] Espino E, Cakir M, Domenek S, Román-Gutiérrez AD, Belgacem N, Bras J. Isolation and characterization of cellulose nanocrystals from industrial by-products of Agave tequilana and barley. *Industrial Crops and Products*. 2014;62:552-9.
- [47] Jorfi M, Roberts MN, Foster EJ, Weder C. Physiologically responsive, mechanically adaptive bio-nanocomposites for biomedical applications. *ACS Applied Materials & Interfaces*. 2013;5:1517-26.
- [48] Zhao Y, Li J. Excellent chemical and material cellulose from tunicates: diversity in cellulose production yield and chemical and morphological structures from different tunicate species. *Cellulose*. 2014;21:3427-41.
- [49] Lollipop Tunicate - *Nephtheis fascicularis*. That Pet Place 2015.

Figures and Tables

Figures

Figure 1. Schematic of m-CNC production from maize husk

Figure 2. Thermograms of raw maize husk and bleached maize husk measured from 30-900 °C with a temperature rate increase of 10 °C per minute under air

Figure 3. FTIR spectra for raw Maize fiber, bleached Maize fiber, and m-CNCs obtained by sulfuric acid hydrolysis.

Figure 4. CNC AFM images from suspensions of 0.0001 wt% of A) m-CNC, B) w-CNC, C) Size distribution of m-CNC and w-CNC nanoparticles in DI-H₂O as determined by DLS. D) Length and width measurements determined by AFM, and Hydrodynamic diameter (Z_D), polydispersity index (PDI) determined by dynamic light scattering.

Figure 5. A) X-ray diffraction patterns w-CNC obtained from powder of m-CNC and w-CNC. B) Crystallinity intensities of m-CNC and w-CNC

Figure 6. TGA thermograms of m-CNC and w-CNC measured from 30-900 °C with a temperature rate increase of 10 °C per minute under air

Figure 7. Images of A) 0.079 wt% suspension solvent casted film of m-CNC, B) 1 wt% w-CNC

Figure 8. A) Stress vs. Strain curves of m-CNC and w-CNC films B) Elongation at break, Young's Modulus, and Storage Modulus of m-CNC and w-CNC films

Figure 9. Images of 0.079 wt% solvent casted film of m-CNC

Figure 10. A) Stress vs. Strain curves of m-CNC/NR and w-CNC/NR B) Temperature dependent dynamic mechanical analysis of m-CNC/NR and w-CNC/NR composites

Figure 11. Schematic of m-CNC production from maize husk for mass-energy consumption

Tables

Table 1. Summary of composition of maize husk following extractive protocols

Table 2. Elongation at break, Young's modulus, and storage modulus of m-CNC and w-CNC composites with natural rubber. ¹ Measured by tensile testing and ² measured by temperature dependent dynamic mechanical analysis.

Table 3. Summary of CNC characteristics from maize (m-CNC), cotton (co-CNC), wood (wood-CNC), tunicate (t-CNC), sugarcane bagasse (s-CNC), agave (a-CNC), banana psuedostems (b-CNC), and barley (br-CNC)

Chapter 3. Nanocellulose-Based Materials in Physiological Conditions

Chapter 3. Nanocellulose-Based Materials in Physiological Conditions

3.1. Effect of Hydration on the Material and Mechanical Properties of Cellulose Nanocrystal-Alginate Composites	133
3.2. Characterization and Mechanical Properties of Ultraviolet Stimuli-Responsive Functionalized Cellulose Nanocrystal -Alginate Composites	165
3.3. Incorporation and Release of Bovine Serum Albumin from Cellulose Nanofiber Films for Growth Factor Release Applications	191
3.4 Mechanical Properties of Thin Cellulose Nanofiber Films in Liquid.....	211
Figures and Tables	225

Chapter 3.1 Effect of Hydration on the Material and Mechanical Properties of Cellulose Nanocrystal-Alginate Composites

This subchapter is based on *The effect of hydration on the material and mechanical properties of cellulose nanocrystal-alginate composites*. **Carbohydrate Polymers**. Under Revision

Abstract	135
1. Introduction	135
2. Materials and Methods	137
2.1 Materials	138
2.2 Methods	138
2.2.1 TEMPO Oxidation of Cellulose Nanocrystals	138
2.2.2 Determination of Carboxyl Group Addition Following TEMPO Oxidation	138
2.2.3 Preparation of CNC-Alginate, CNCT-Alginate Thin Films	139
2.3 Characterization and Analysis	139
2.3.1 Atomic Force Microscopy (AFM)	139
2.3.2 X-Ray Diffraction (XRD).....	140
2.3.3 Thermal Stability	140
2.3.4 Optical Properties	140
2.3.5 Water and D-PBS Uptake	141
2.3.6 Leaching of Ca^{2+} from CNC:Alginate, CNC-T:Alginate Crosslinked Films	141
2.3.7 Mechanical Properties	141
2.3.8 Statistical Analysis.....	142
3. Results and Discussion.....	142
3.1 Characterization of TEMPO Oxidized Cellulose Nanocrystals	142
3.2 Material Properties of CNC:Alginate vs CNC-T:Alginate Composites in Dry Conditions	144
3.2.1 Thermal Stability.....	144
3.2.2 Optical Properties	146
3.3 Effect of Liquid Immersion on CNC/CNC-T:Alginate Composites	147
3.3.1 DI-H ₂ O and D-PBS Uptake	147
3.3.2 Complexometric Titration to Determine Ca^{2+} Leaching in DI-H ₂ O and D-PBS.....	149
3.4 Mechanical Testing of CNC/CNC-T:Alginate Composites	151
3.4.1 Mechanical Testing in Humid Conditions.....	151
3.4.2 Tensile Testing in Dry and Wet Conditions	154
4. Conclusion	159
5. Acknowledgements.....	160
6. References	160

Effect of Hydration on the Material and Mechanical Properties of Cellulose Nanocrystal-Alginate Composites

Megan Smyth^{a,b}, Marie-Stella M'Bengue^{a,b}, Maxime Terrien^a, Julien Bras^{a,b}, E. Johan Foster^d

a. CNRS, LGP2, 461 Rue de la Papeterie, 38402, Saint-Martin-d'Hères, France

b. Université Grenoble Alpes, LGP2, 38000 Grenoble, France

c. Institut Universitaire de France, 75005 Paris, France

d. Macromolecules and Interfaces Institute, Virginia Tech, Department of Materials Science & Engineering, 445 Old Turner Street, 203 Holden Hall, Blacksburg, VA 24061, USA

Abstract

Alginate is commonly used in the form of hydrogels in biomedical applications. It is known to be highly sensitive to liquid exposure and can degrade or solubilize easily. This study attempts to improve the mechanical and material properties in various humidity conditions and in liquid immersion of thin alginate films with the addition of unmodified and oxidized cellulose nanocrystals (CNCs, CNC-Ts). CNCs and CNC-Ts were added to alginate composites in varying amounts, and the material and mechanical properties were measured in dry, humid, and liquid conditions. It was shown that the properties can be enhanced with the addition of nanocellulose as tested by liquid uptake and mechanical testing. These results suggest that the addition of TEMPO-oxidized nanocellulose crystals improves the performance and longevity of alginate when exposed to phosphate buffer solution (PBS) compared to deionized water.

1. Introduction

Alginate has long been of interest to researchers within the field of biomedical engineering, especially within the fields of tissue engineering [1-3], wound healing [4, 5], and drug delivery[6-8]. It has been widely shown that alginate is biocompatible, can have controlled gelation, is relatively non-toxic, and is cost effective [9]. Alginate is extracted from biomass and derived from a family of brown algae. It contains 1,4-linked β -D-mannuronate (M) and α -L-guluronate (G) chains in variable ratios. The G chains of alginate can interact with multivalent cationic ions to induce gelation and form a hydrogel, which can be tailored depending on the amount of cationic ions available to the G chains to form ionic interactions [10].

When considered pure, crosslinked alginate materials are known to easily degrade or solubilize when used in biomedical applications [11-15] and have very low mechanical properties [16, 17]. Because of these properties composites with an alginate matrix have been studied with various reinforcement or blend polymers such as, chitosan [18], cellulose [19-21], and more recently cellulose nanocrystals [21-24].

Ionic crosslinking of alginate with nanocellulose is very promising and has already been used to produced capsules [25] or sponges [23]. In such a 3D material strategy, the addition of nanocrystals [23] or nanofibers [26] has also been utilized, for specific purpose like drug release or extruded biocomposite preparation.

Cellulose nanocrystals can be extracted by a variety of methods, but the most common method used is acid hydrolysis in order to remove the amorphous regions of the cellulose [27]. Nanosized crystals are obtained from biomass which has environmental advantages (biobased, biodegradable, biocompatible) but also have tremendously favorable properties, e.g. extremely high modulus, liquid crystal organization, pickering emulsions, barrier, nucleating agent, and much more. Since the mid of 1990's [28, 29], a special interest in nanocellulose as a reinforcing agent in nanocomposites has been thoroughly researched. CNCs have been used as fillers in a variety of matrixes such as water soluble polymers (e.g. HPMC [30], polyvinyl alcohol [31-33]), latex (natural rubber, oxidized natural rubber [34, 35]) or even thermoplastic biopolymers (polylactic acid [36, 37], Polycaprolactones [38, 39] and many more [40, 41]. With many reviews written on this topic of reinforcement by CNCs [40, 42-46], it is now commonly accepted that such CNCs are promising and their industrialization has progressed since start of 2010's.

Alginate is commonly used in the form of a hydrogel in biomedical applications, but has some significant drawbacks. These three-dimensional networks of cross-linked alginate retain significant amounts of water. This high water content is suitable for physiological applications because of the similarities in structure [47], but the level of humidity, or water content, can change depending on the application. For example, materials used in wound healing applications could be exposed to less humidity compared to a material that would need to be implanted [48]. This exposure to water not only changes the mechanical properties of alginate but also encourages degradation, which is difficult to control in alginate systems [49]. Other research focusing on the use of alginate in humid or wet conditions showed that with increased relative humidity the mechanical properties decreased because of the hydrophilic nature of alginate [50], and that in a wet state the crosslink film had lower tensile strength compared to dry films and a higher elongation at break [51]. The puncture strength of alginate

and chitosan films decreased in physiological conditions when compared to ambient conditions. It was also shown that puncture strength could be modulated with amount of CaCl_2 used in the crosslinking step [52]. These studies illustrate that the mechanical properties of alginate based films are effected by the introduction of aqueous media within the system.

Interest in nanocellulose and alginate materials has increased in recent years with the rise of research pertaining to the use of nanocellulose in biomedical applications. Composites and films of different types of cellulose and alginate have been previously studied, but without an emphasis on the effect of humidity and hydration on the mechanical properties of these materials. Previous work conducted by Phisalaphong et al. and Kanjanamosit et al. explored the use of bacterial cellulose as a reinforcement for alginate films [19, 20]. Through their work, they determined that with increased alginate content the tensile strength of the films decreased when tested in ambient, or dry conditions. Research focused on alginate and microfibrillated cellulose (MFC), also called cellulose nanofibers (CNF), was done by Sirviö and colleagues in 2014 to determine the effectiveness of CNF-alginate films as barrier films in packaging. They displayed that with the addition of CNF, the tensile strength of the film increased, similar to results obtained with alginate and bacterial nanocellulose [53]. The mechanical properties of CNC-alginate hydrogels or sponges has been previously reported by Huq et al. and Lin et al. Huq tested the effect of the addition of CNCs to alginate hydrogels. It was shown that with increased CNCs content the tensile strength increased with a maximum achieved with the addition of 5% of CNCs [22]. Compressive strength of TEMPO oxidized CNC-alginate 3D sponges was analyzed by Lin and colleagues, and was shown that the addition of CNCs had a reinforcement effect, and that oxidized CNCs had a higher improvement compared to neat CNCs due to possible enhanced crosslinking with the additional carboxyl groups added to the nanocellulose and the alginate [23].

While previous work with nanocellulose and alginate focused on the mechanical properties of 3D systems (sponge or hydrogel) or of thin films in dry conditions (or classified as ‘ambient’), there has been no research on how the material and mechanical properties of alginate thin films change in humid or even in aqueous liquid immersion. This study attempts to illustrate how CNCs and TEMPO-oxidized CNCs can be used to modulate the material response of these composites in DI- H_2O compared to phosphate buffer solution (PBS) by measuring swelling and if (or how much) Ca^{2+} is leached from the system. A comparison of the effect of type of liquid on the mechanical properties of CNC and alginate composites has not been studied previously. In this work, the effect of varying levels of humidity, and water versus PBS submersion at physiological temperature on the mechanical properties of CNC/CNC-T and alginate nanocomposites were investigated in detail to determine that

these nanocomposites can be used under physiological conditions because of the improvement of properties compared to water.

2. Materials and Methods

2.1 Materials

Sodium alginate from brown algae, calcium chloride (CaCl_2), Dubecco's Phosphate Buffer Solution (D-PBS), (2,2,6,6-tetramethylpiperidin-1-yl)oxyl (TEMPO), sodium bromide, sodium hypochlorite, ethylenediaminetetraacetic acid (EDTA), ammonium chloride, magnesium chloride hexahydrate, ammonia, and Eriochrome® Black T indicator were purchased from Sigma-Aldrich France Ltd. (Lyon, France). Sodium hydroxide (NaOH) was purchased from Carl Roth (Germany). Ethanol was purchased from Chimie Plus (Saint-Paul-de-Varax, France). Cellulose nanocrystals (CNCs) were purchased from University of Maine Process Development Center (Orono, Maine, USA). The CNCs were extracted from softwood pulp using sulfuric acid hydrolysis. All materials were used without any modification.

2.2 Methods

2.2.1 TEMPO Oxidation of Cellulose Nanocrystals

TEMPO oxidation of CNC followed a protocol already established in literature by Fukuzumi et al with some modification [54]. CNC (3 g dry weight) was suspended in 200 mL of deionized water by sonication and magnetic stirring. TEMPO and sodium bromide (0.886 g and 0.972 g) were dissolved in 100 mL of deionized water by stirring for 1.5 hours. Once the TEMPO and sodium bromide solution was completely dissolved it was added dropwise to the CNC suspension. Sodium hypochlorite (18 g) was added to the suspension and the pH was maintained at 10 by the addition of 0.25 M sodium hydroxide. The suspension was stirred for 3 hours to obtain oxidized nanocrystals. The reaction was quenched by the addition of ethanol (15 mL), and centrifuged to recover the insoluble fraction. Following centrifugation, the oxidized nanocrystals are suspended in deionized water ($\text{DI-H}_2\text{O}$) and dialyzed for one week until a neutral pH was obtained.

2.2.2 Determination of Carboxyl Group Addition Following TEMPO Oxidation

The density of carboxyl groups added to the oxidized CNCs was determined using conductimetric titration. Approximately 15 mg of the TEMPO-oxidized CNCs (CNC-Ts) were added to 50 mL $\text{DI-H}_2\text{O}$ and ultrasonicated for 5 minutes. The pH of the suspension was adjusted to 2 by the addition of

0.1M HCl to protonate the carboxylate groups. The solution was titrated against 0.1M NaOH in 0.1mL increments. The degree of oxidation was determined by the following equation as developed by da Silva Perez et al.[55].

$$\text{Degree of Oxidation } \left(\frac{\mu\text{mol}}{\text{g}} \right) = \frac{162 - c \cdot (V_2 - V_1)}{m - 36 \cdot ([V_2] - [V_1])} \text{ (Equation 1.)}$$

Where c is the concentration of NaOH (mol/L), V_1 and V_2 are the first and second equivalent volumes of the plateau (L) and m is the mass of the CNC-T (g). All results were done in triplicate with the mean and standard deviation reported.

2.2.3 Preparation of CNC-Alginate, CNCT-Alginate Thin Films

CNC-Alginate composites were made by soaking 0.6 g of sodium alginate in 20 mL DI-H₂O overnight and stirring mildly for 2 hours to form a homogeneous suspension. Suspensions of varying ratios of CNC or CNC-T to sodium alginate were made with the amounts highlighted in Table 1. CNC and alginate suspensions were stirred for 30 minutes. CNC-alginate suspensions were solvent casted and allowed to dry at ambient conditions for 48 hours and then at 45°C for 24 hours. Dried films were then soaked overnight in CaCl₂ solution with concentration from 0.1 to 1 M CaCl₂ and rinsed. The crosslinked films were dried again at ambient conditions for 24 hours under fume hood evaporation.

Table 1. Amounts of CNC, CNC-T, and sodium alginate for fabrication of composites

Ratio CNC (or CNC-T):Alginate	3 wt% Sodium Alginate Solution(mL)	1 wt% CNC (or CNC-T) Suspension(mL)
Alginate	20	0
10:90	18	6
30:70	14	18
50:50	10	30
70:30	6	42

2.3 Characterization and Analysis

2.3.1 Atomic Force Microscopy (AFM)

Suspensions of approximately 0.2 mL 0.0001 wt% CNC and CNC-T were prepared, and placed on the surface of a cleaved mica plate. The coated mica plates were dried overnight at ambient conditions, and then analyzed using atomic force microscopy. Images were acquired using tapping mode with a Nanoscope IIA microscope from Veeco Instruments (Plainview, New York, USA) at a frequency of ~265-340 Hz. Silicon cantilevers with a curvature of 10-15 nm were used (OTESPA®, Bruker, Billerica, Massachusetts, USA). AFM images were analyzed using Nanoscope Analysis (Plainview, New York, USA) and ImageJ (U. S. National Institutes of Health, Bethesda, Maryland, USA) from 50 samples with dimensions reported at mean \pm standard deviation.

2.3.2 X-Ray Diffraction (XRD)

The crystallinity of lyophilized CNC samples was measured using X-ray diffraction (XRD). XRD diffractogram patterns were measured using a PW 1720 X-ray generator (Phillips, Eindhoven, Netherlands) at 45 kV and 40mA with Cu K α radiation with a wavelength of 0.154 nm in a range of $2\theta=6-56^\circ$ with a fixed step interval. The samples were lyophilized and ground into a powder using a mortar and pestle. The crystallinity index was calculated according to the following equation,

$$C_I^{XRD} = \frac{I_{002} - I_{am}}{I_{002}} \times 100 \quad (\text{Equation 2})$$

and corresponds to the ratio of the interference of the [002] crystal planes, which was subtracted by the amorphous regions, and the total peak height [002] of the crystal planes. I_{002} was observed at 22.5° and I_{am} at 18° [56].

2.3.3 Thermal Stability

Thermogravimetric measurements were performed with a Perkin Elmer STA 6000 (Waltham, Massachusetts, USA). The temperature ranged from 25 °C to 900 °C with a heating rate of 10 °C/min. The tests were carried out under air (20 mL/min) and under atmospheric conditions for comparison of thermoxidative degradation. The samples ranged in mass between 10 to 20 mg. All results were analyzed with Pyris Series software (Perkin Elmer, Waltham, Massachusetts, USA). At least duplicates were prepared to check reproducibility and most representative spectra were selected.

2.3.4 Optical Properties

Films were analyzed with UV spectroscopy. The films were loaded into the spectrometer with a film holder. The absorbance from 300-800 nm was measured with ten scans in spectrum mode with a UV Spectrometer (Shimadzu, Kyoto, Japan) with a normal incidence and repeated in triplicate.

2.3.5 Water and D-PBS Uptake

Samples were placed in DI-H₂O or D-PBS for varying time points, removed, and weighed following excess water removal between two sheets of absorbent paper. The liquid uptake was calculated using the following formula:

$$\text{Water and D - PBS Uptake } (W_D) = \frac{M_t - M_0}{M_0} * 100 \quad (\text{Equation 3})$$

An average of at least three measurements have been calculated.

2.3.6 Leaching of Ca²⁺ from CNC:Alginate, CNC-T:Alginate Crosslinked Films

A complexometric EDTA based titration was carried out following the soaking of CNC:Alginate and CNC-T:Alginate samples in 50 mL of DI-H₂O or D-PBS for 24 hours. The DI-H₂O or D-PBS that the composite films were soaked in, was titrated to determine the amount of Ca²⁺ that was released from the film following crosslinking. 10 mL of DI-H₂O or D-PBS was added to 20 mL 0.05 M EDTA. An ammonia buffer solution of pH = 10.5 of ammonia and ammonium chloride was prepared; 10 mL of this buffer was added to the solution of DI-H₂O or D-PBS and EDTA. 1 mL of Eriochrome Black T indicator was added to the solution. The sample was titrated with 0.025 M magnesium chloride solution until the indicator changed from blue to a permanent pink color. All titrations have been done at least in triplicate.

2.3.7 Mechanical Properties

Films were dried and conditioned at least 24 hours before analysis in a temperature and humidity controlled room at 23 °C and 50% humidity. Mechanical properties of the samples were measured using a TA Instruments RSA 3 (New Castle, Delaware, USA). The distance between the clamps was 10 mm with a width of approximately 5 mm. For varying the level of humidity, a humidity generator specially designed for such purpose was used (TecPap, Grenoble, France). Water vapor is sent into a chamber around the clamps and humidity level is controlled by a monitor. After calibration, samples

were measured at 10%, 30%, 50%, and 70% relative humidity for 15 hours. Measurements were performed for 15 hours at a frequency of 1 Hz with a constant strain of 3%. Samples underwent rectangular tension measurements at a rate of 0.01 mm/s for dried films and 0.001 mm/s for submerged films conditioned for 24 hours prior to testing. The stress vs strain curves were measured and analyzed using TA Orchestrator (New Castle, Delaware, USA). Three measurements were taken for each film and then averaged.

2.3.8 Statistical Analysis

Statistical analysis was done using OriginLab for surface roughness of films, colorimetric titration, and storage modulus of 30:70 CNC:Alginate films vs. relative humidity. A linear-regression test was done for storage modulus vs. humidity, and an ANOVA one-way test with Bonferoni post-hoc testing was done to test the significance of surface roughness and complexometric titration results. All results are reported in average \pm standard deviation from three independent experiments unless otherwise noted.

3. Results and Discussion

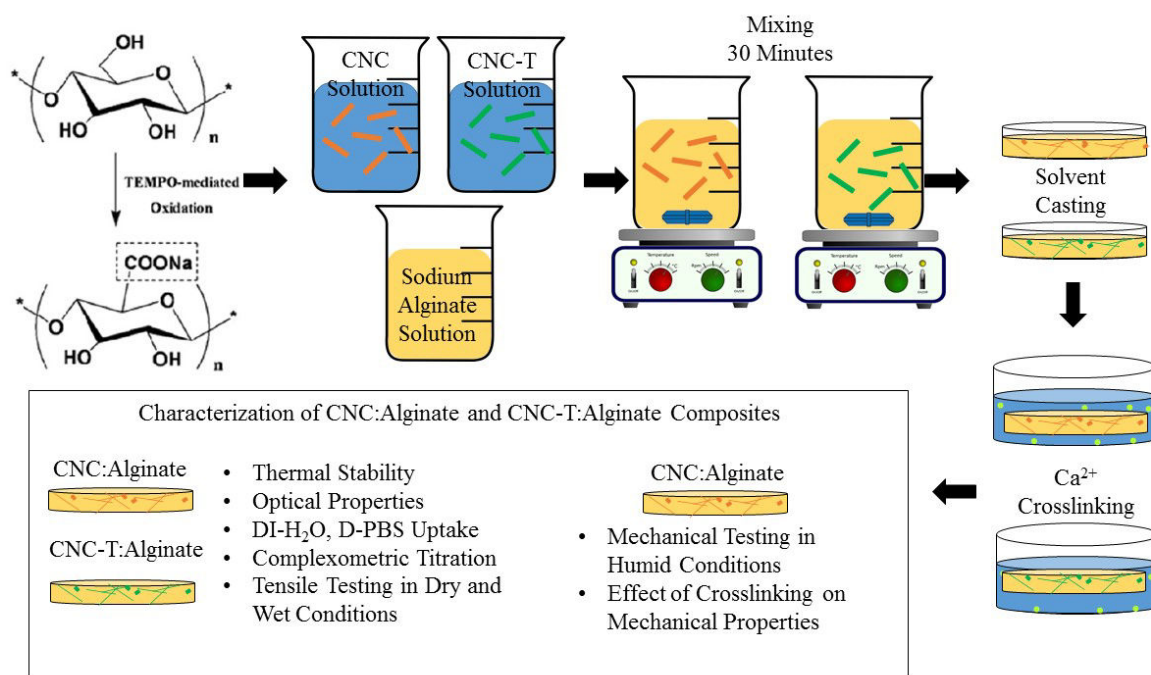


Figure 1. Schematic representation of preparation of CNC:Alginate and CNC-T:Alginate nanocomposites and characterization

3.1 Characterization of TEMPO Oxidized Cellulose Nanocrystals

The amount of carboxyl groups added to the CNCs following TEMPO-based oxidation was determined using conductometric titration. The titration curve is shown in Figure 2. An average amount of carboxyl groups in CNCT is $895 \pm 288 \mu\text{mol/g}$. These results are consistent with previously reported protocols [57].

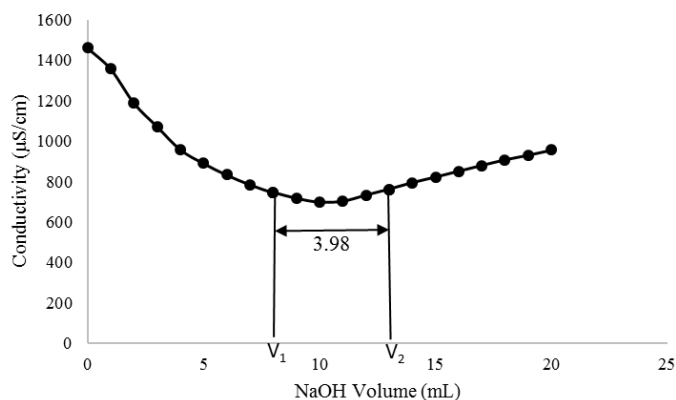
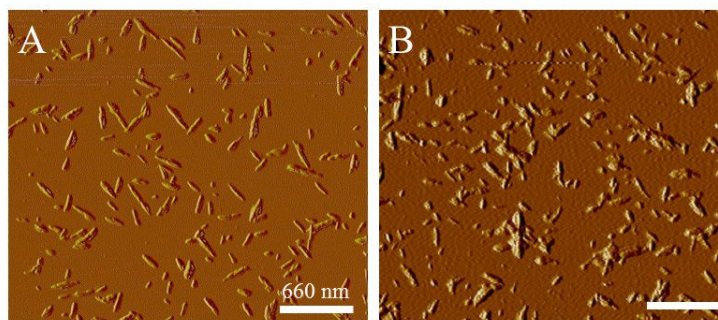


Figure 2. Conductimetric titration of CNC-T to determine amount of hydroxyl groups added to CNC after TEMPO-mediated oxidation.

Figure 3 shows AFM spectrograms of CNC and CNC-T. Their dimensions calculated by image J analysis are $145 \times 19 \text{ nm}$ and 134×32 respectively, which is in accordance with literature.



	CNC	CNC-T
Length (nm)	145 ± 43	132 ± 32
Width (nm)	19 ± 5	32 ± 9

Figure 3. CNC AFM images from suspensions of 0.0001 wt% of A) CNC B) CNC-T acquired by tapping mode in air. C) Length and width measurements of CNCs and CNC-Ts suspensions of approximately 0.001 wt% as determined by ImageJ analysis of AFM images from N=25

It is also worth noting that TEMPO oxidation slightly decreased the crystallinity of the CNCs as shown by XRD measurement which provides a crystallinity index of 77% and 71% for CNC and CNC-T respectively. XRD spectrographs are shown in Figure 4.

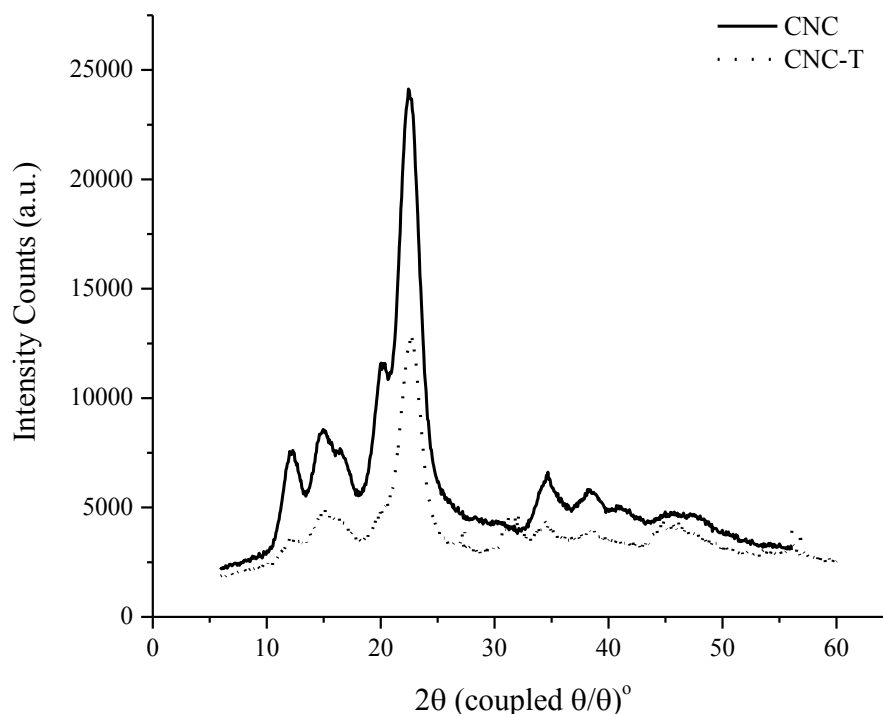


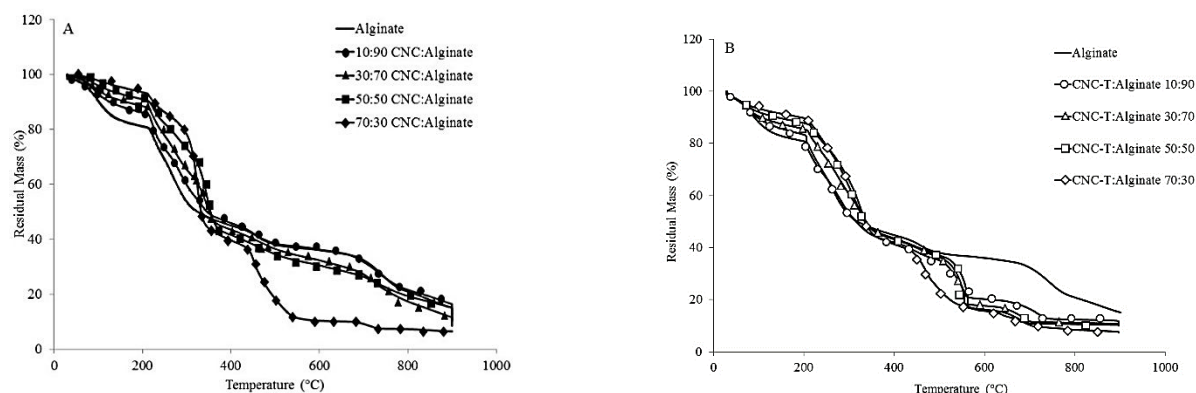
Figure 4. XRD spectra of CNC and CNC-T obtained from powder

3.2 Material Properties of CNC:Alginate vs CNC-T:Alginate Composites in Dry Conditions

3.2.1 Thermal Stability

CNC:Alginate and CNC-T:Alginate thin films composites were crosslinked with 0.45 M CaCl_2 . The thermal stability of the alginate composites is an important measure in order to determine if the addition of nanocellulose can improve or deteriorate the thermal resistance. This can be of interest for fabrication techniques that may require a high temperature and to determine the initial amount of water within the composites since alginate is very hydrophilic. Thermograms were performed from 30-900°C with a rate of 10°C/min after conditioning dried thin films in 50%, 25°C. As seen in Figure 5, the addition of CNC or CNC-T causes a decrease in the amount of weight loss from 30-100°C. This temperature region is known to correlate with the evaporation of water within the composite. It shows

that addition of CNC or CNC-T decrease the humidity of thin films from 20% to even less than 10% when 30% of nanocrystals is introduced. That means the dried films are more “structured” and adsorbed less humidity as already shown with 3D sponges [23].



Weight Loss Percent at Temperature (%)

Sample	Temperature (°C)					
	100°C	200°C	300°C	400°C	500°C	600°C
Alginate	12.05	19.31	47.63	55.26	62.06	64.02
10:90 CNC:Alginate	6.98	13.86	40.1	54.04	61.43	63.68
30:70 CNC:Alginate	5.78	11.48	34.55	56.46	63.45	67.64
50:50 CNC:Alginate	3.98	8.98	26.96	58.38	65.47	69.48
70:30 CNC:Alginate	2.18	6.41	21.7	60.31	81.62	89.63
10:90 CNC-T:Alginate	10.4	16.59	46.65	57.93	64.78	79.7
30:70 CNC-T:Alginate	9.49	14.5	39.34	56.8	63.68	82.35
50:50 CNC-T:Alginate	7.93	12.2	34.27	56.34	62.87	83.68
70:30 CNC-T:Alginate	6.66	10.3	36.75	58.68	75.97	84.29

Figure 5. Thermograms of A) CNC:Alginate composites and B) CNC-T:Alginate composites measured by TGA from 30-900°C at a rate of 10°C/min. With indicative curves of cellulose degradation with composites with CNCs. C) Weight loss in percent for samples at 100, 200, 300, 400, 500, and 600°C.

Cellulose nanocrystals that are derived from acid hydrolysis using sulfuric acid are known to have

$-\text{SO}_4^{-2}$ groups on their surface [58]. This additional sulfuric group is known to exhibit a degradation temperature at approximately 250-290°C [59]. While TEMPO oxidized CNCs have an additional carboxylic groups with a degradation temperature around 300-360°C [58]. It can be important to note from Figure 5 that the weight loss percentage at 300°C is greater for composites with CNC-T compared to CNC. This is most likely related to the presence of -OH groups on the oxidized CNC as well as the residual $-\text{SO}_4^{-2}$ that are not oxidized since TEMPO oxidation is selective. Even with this increase in degradation at 300°C for CNC-T composites are still more stable compared to alginate. At elevated temperatures, above 500°C CNC-T composites are less stable than CNC composites and alginate with a higher amount of degradation occurring at 600°C.

3.2.2 Optical Properties

Transmittance of the composites was measured using UV-Vis spectroscopy and is reported in Figure 6. As seen in Figure 6, the transparency of the composite films decreases with increased CNC or CNC-T amount, as related. It can also be noted that for composites of 70:30 CNC-T:Alginate some aggregations are formed, especially Figure 6 F-I. Composites composed of CNC-T the transmittance decreases with increased CNC-T, while CNC composites do not show a clear trend with increasing CNC amount, but all composites have a reported transmittance from 300-800 nm lower than pure alginate.

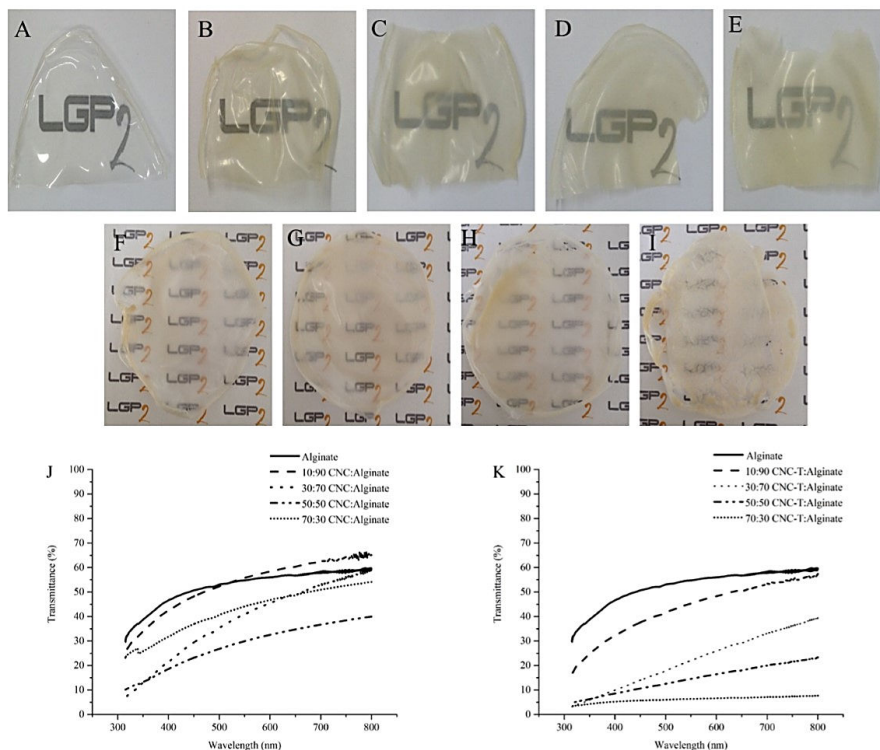


Figure 6. Optical images of A) Alginate, B) 10:90 CNC:Alginate, C) 30:70 CNC:Alginate, D) 50:50 CNC:Alginate, E) 70:30 CNC:Alginate, F) 10:90 CNC-T:Alginate, G) 30:70 CNC-T:Alginate, H) 50:50 CNC-T:Alginate, and I) 70:30 CNC-T:Alginate with noticeable increase of opaqueness with increased CNC and CNC-T amounts in the composites.

Transmittance versus wavelength as measured by UV-Vis spectroscopy for J) CNC:Alginate and K) CNC-T:Alginate composites.

3.3 Effect of Liquid Immersion on CNC/CNC-T:Alginate Composites

3.3.1 DI-H₂O and D-PBS Uptake

The swelling or liquid uptake properties of the composites was studied to determine if the samples remain stable within liquid for prolonged periods of time. Dulbecco's Phosphate-Buffered Saline (D-PBS) was chosen in addition to deionized water (DI-H₂O) to determine if these composites would be suitable for biomedical applications like cell culture. D-PBS is commonly used in cell culture and does not contain any additional calcium or magnesium ions, which could influence crosslinking within the composites. The composites were prepared with 0.45M of CaCl₂, dried, stabilized, and then suspended in deionized water or D-PBS for 24 hours with weight measurements taken at various time points to monitor the uptake of liquid.

As seen in Figure 7, the swelling percentage differs with submersion liquid (DI-H₂O vs. D-PBS). Water adsorption behavior of the composites differed greatly when compared to D-PBS. In spite of high standard deviation, the overall trend notes that with the addition of nanocellulose, either CNCs or

CNC-Ts, the adsorption of water decreases. There are some instances where the overall swelling percentage at 24 hours increases for CNC based composites compared to alginate (i.e. 10:90, 50:50, and 70:30), while the trend for previous time points show a decrease (i.e. from 0-0.33 hr). This high heterogeneity and variation is a limiting parameter to make any definitive conclusions. After 24 hours, swelling could be considered as similar. On the contrary, Alginate:CNC-T composites show less variability with the samples showing less water adsorption at 24 hours compared to alginate. It passes from about 50% of swelling to 30% when more than 50% CNC-T is added.

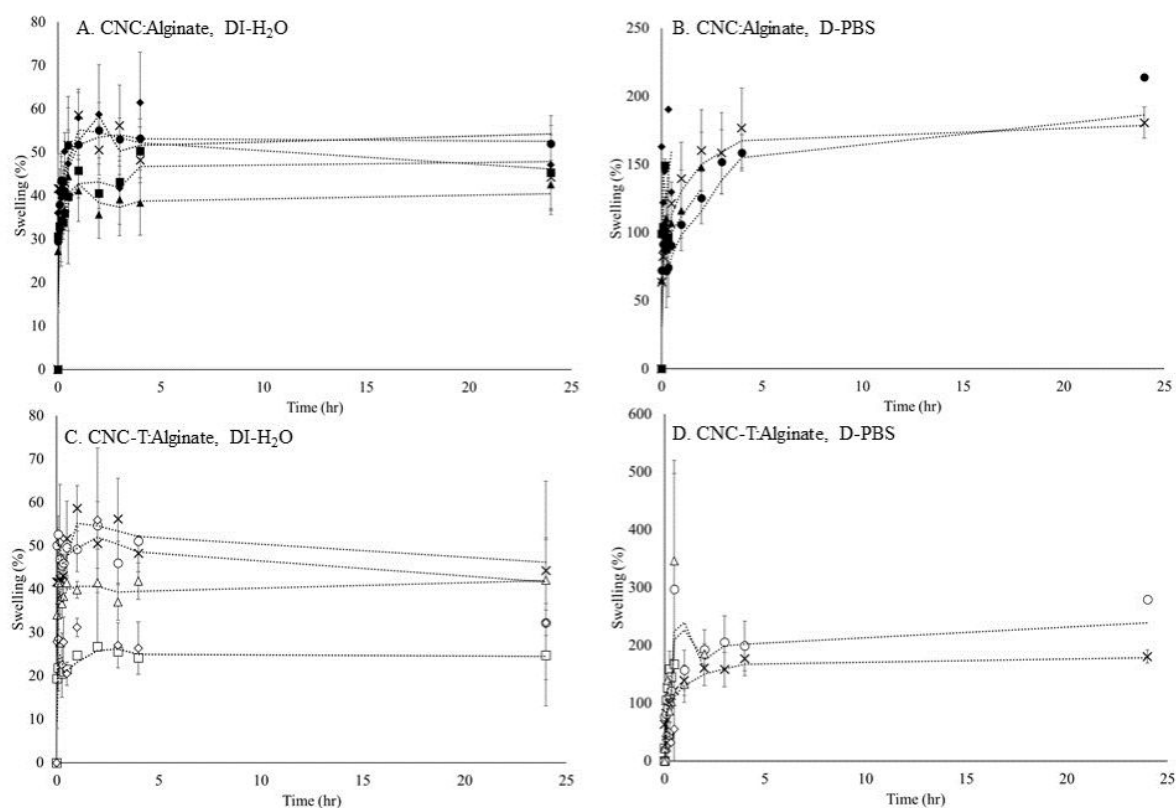


Figure 7. The percentage of swelling due to A,) water and B,D) D-PBS uptake in CNC:Alginate (A,B) CNC-T:Alginate (C,D) for various time points until 24 hours as calculated using Equation 3.

It can be noted that for all the composites D-PBS causes a higher increase in swelling percentage and even degradation within the CNC-T containing samples, especially at higher ratios of CNC-T. This can possibly be explained by the intrusion of ions from the D-PBS into the “egg-box” structure of the crosslinked alginate and disturbing the bonds [14, 60]. For CNC:Alginate composites there is an

increase from approximately 30-60% swelling in deionized water to 50-200% swelling depending on the amount of CNCs added to the alginate. With increased CNC amount the swelling slightly increased with degradation occurring in 70:30 CNC:Alginate composites.

CNC-T based composites showed an increase in swelling from 20-60% to 50-300% in DI-H₂O vs. D-PBS with higher variability compared to CNC based composites in D-PBS. Degradation of the samples occurred for composites with the following ratios of CNC-T:Alginate in D-PBS above 4 hr in D-PBS: 30:70, 50:50, 70:30, which explains why no values at 24h were measured. This increased degradation shows that with increased CNC-T amount the composites no longer remain stable in D-PBS and may not be suitable for biomedical applications. The effect of swelling of alginate based gels was studied previously by Drury and colleagues in 2004. It was shown that alginate gels exposed to PBS (containing Ca²⁺ and Mg²⁺) had a higher degree of swelling, and that this increase can be explained by a decrease in crosslinking and a loss of calcium from within the alginate [16]. It was also shown by Bajpai et al. that with increased ion exchange the loosening of the “egg-box” structure occurred because ions were binding to the carboxylate groups [14]. This can explain why degradation and swelling increased for CNC-T based composites since there are more available carboxyl groups to disrupt, and therefore easier for water to enter the composite and less Ca²⁺ available for the egg box crosslinking; Lin et al. have shown similar behavior with 3D sponges [23]. Once the composite reaches equilibrium the “egg-box” structure collapses, the CNC-Ts leave the composite, and the composites dissolve. Therefore, in applications where structural integrity is necessary in liquid conditions, the addition of CNCs would be favorable to CNC-Ts based on these results.

3.3.2 Complexometric Titration to Determine Ca²⁺ Leaching in DI-H₂O and D-PBS

As shown in the previous section, the swelling and eventual degradation of the composites in D-PBS can be attributed to the increased swelling caused by ion exchange within the composites. The amount of Ca²⁺ leaching, or being released from the composites, was then measured in DI-H₂O and D-PBS by complexometric titration using EDTA. Samples were soaked in either deionized water or D-PBS for 24 hours and the soaking liquid was titrated. As shown in Table 2, the percent of Ca²⁺ remaining within the composites differed once again for CNC vs. CNC-T containing composites and soaking liquid DI-H₂O vs. D-PBS.

Table 2. Determination of amount of Ca^{+2} remaining within CNC:Alginate or CNC-T:Alginate composites following 24 hours in DI- H_2O or D-PBS by complexometric titration using EDTA. All results were done in triplicate and reported with average and standard deviation.

Sample	mmol Ca^{2+} Leached in DI H_2O /10 mL	% Ca^{2+} in Composite after soaking in DI H_2O	mmol Ca^{2+} Leached in DI D-PBS/10 mL	% Ca^{2+} in Composite after soaking in D-PBS
Alginate	1.39±0.0010	69.12±0.02	1.79±0.0007	60.17±0.01
CNC:Alginate				
10:90	1.39±0.0030	69.22±0.07	1.71±0.0019	60.17±0.04
30:70	1.39±0.0006	69.07±0.01	1.71±0.0006	61.91±0.01
50:50	1.38±0.0003	69.24±0.01	1.71±0.0783	61.90±1.74
70:30	1.39±0.0003	69.22±0.01	1.71±0.0033	61.95±0.07
CNC-T:Alginate				
10:90	1.27±0.0743	73.36±1.65	1.22±0.0639	72.90±1.42
30:70	1.20±0.0048	73.36±0.11	1.20±0.0171	73.25±0.38
50:50	1.20±0.0014	73.32±0.03	1.20±0.0730	73.23±1.62
70:30	1.20±0.0724	73.23±1.61	1.20±0.0099	73.39±0.22

What is interesting to note is that in comparison to the study on the effect of liquid choice on swelling behavior, the CNC-T based composites retained more Ca^{2+} ions compared to CNC:Alginate composites in both DI- H_2O and D-PBS. Significance ($p < 0.05$) between the same composite (i.e. alginate in deionized water vs. D-PBS) and between different composites with same ratio in same liquid

(i.e. 10:90 CNC:Alginate vs. 10:90 CNC-T:Alginate in D-PBS) were tested using a two-way ANOVA test. For the same composite in different liquid (DI-H₂O vs. D-PBS) only alginate and CNC based composites showed significant differences between amount of Ca²⁺ remaining in the composite. In deionized water only 10:90 CNC:Alginate vs. 10:90 CNC-T:Alginate did not show any significant difference, while all composites had significant difference in D-PBS. This significance displays that with composites of same ratio but with different nanocellulose composition, the amount of Ca²⁺ remaining in the sample is dependent on whether the CNCs have been oxidized or not, while composites with same type of nanocellulose are dependent on liquid (DI-H₂O vs. D-PBS). This suggests that oxidized CNCs retain the Ca²⁺ ions better than CNCs, but does not explain why CNC-Ts have higher swelling properties and degradation compared to CNC composites. There was a larger amount of precipitate present in soaked CNC-T based composites compared to CNC based composites. It is hypothesized that this precipitate may contain other salts present within the D-PBS that do not complex with the EDTA through the titration or leaching of CNC-Ts from the composite. This would explain why CNC-T:Alginate composites have less release of Ca²⁺, but have increased swelling.

3.4 Mechanical Testing of CNC/CNC-T:Alginate Composites

3.4.1 Mechanical Testing in Humid Conditions

In order to see how the concentration of the crosslinking agent, calcium chloride (CaCl₂), effects the mechanical properties in humid conditions 30:70 CNC:Alginate composites were crosslinked with varying molarity of CaCl₂ (0.15, 0.25, 0.45, 0.55, 0.60, 0.65, 0.75, and 1 M). These molarities were chosen in order to have composites crosslinked with solutions above and below a molarity of 0.45 M. The 30:70 CNC:Alginate composites were tested for 15 hours at 50% relative humidity and room temperature at a constant frequency of 1 Hz and strain of 3%. Figure 8 displays that with increased molarity until 0.55 M there is an increase in the storage modulus. Following the peak storage modulus at 5.2 GPa there is a decrease in the storage modulus with a maximum decrease at 0.02 GPa for composites crosslinked with 1 M CaCl₂. This decrease in storage modulus has a correlation, but shows that an increase in the amount of available Ca²⁺ ions does not cause an increase in the mechanical properties of the composites.

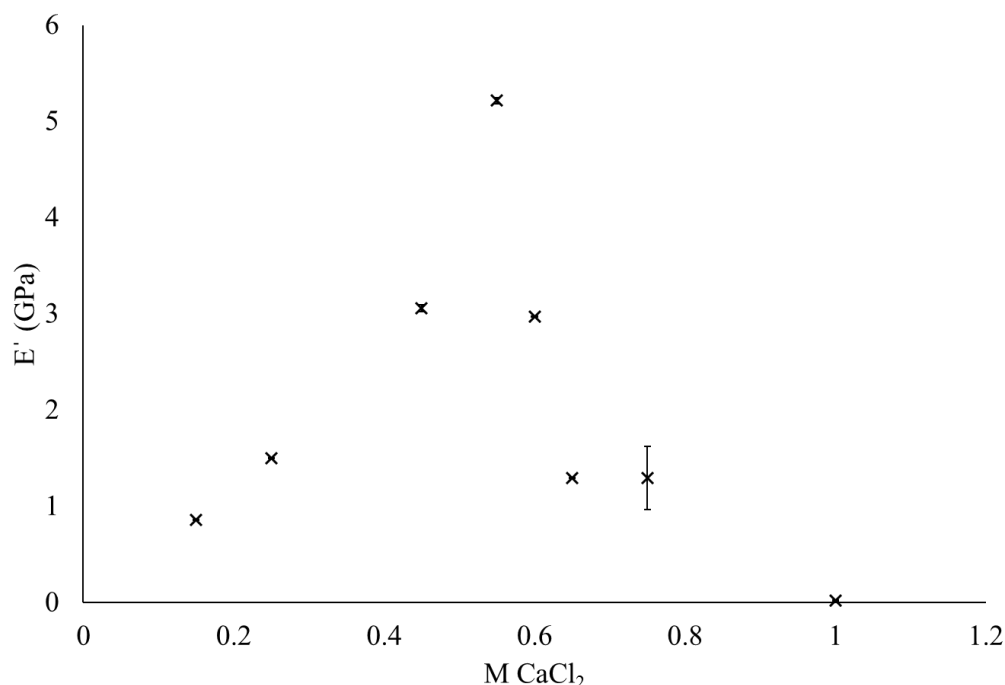


Figure 8. Storage modulus of 30:70 CNC:Alginate composites crosslinked with varying molarity of calcium chloride measured at 50% relative humidity for 15 hours at constant frequency of 1Hz and constant strain of 3%. Results are reported for N=6 with an average and standard deviation. All points have a standard deviation, but are quite small. E' for composite crosslinked with 1M CaCl₂ is reported to be 0.02 GPa.

It would be expected that with an increase in the amount of Ca²⁺ ions within the crosslinking solution there would be a continued increase in the storage modulus of the composite, while our results show that this is not the case. While there is an increase to a certain molarity of CaCl₂, there is a sharp decrease afterwards. It is suggested that with increased Ca²⁺ a saturation point occurs within the composite in the formation of the “egg-box” structure. Once the amount of “egg-box” formation reaches a maximum the introduction of additional Ca²⁺ causes a disturbance the already formed “egg-box” structures. The increased Ca²⁺ concentration outside the “egg-box” possibly causes a shift in the ionic equilibrium within the composite and the Ca²⁺ holding the “egg-box” together is dislocated by the infiltration of additional ions causes a decrease in the mechanical properties. This optimum will be key if high strength films at dried state are expected.

It has been well documented that alginate is very hydrophilic and sensitive to changes in humidity. In order to test how humidity effects the mechanical properties of alginate composites 30:70 CNC:Alginate composites with 0.45M of CaCl₂ were tested in various relative humidity. 30:70 CNC:Alginate was chosen to test based on previous traction tests in dried state, as it showed the most

favorable results. The results from this traction test will be further expanded upon in the following section. 30:70 CNC:Alginate composite was tested at room temperature for 15 hours at 10%, 30%, 50%, and 70% with dynamical mechanical analysis at a constant frequency of 1 Hz and 3% strain. As shown in Figure 9 with increased humidity the tensile storage modulus (E') of the composite decreases ($R^2 = 0.99$). The changes in the mechanical properties can be related back to the results and explanation of the water uptake results. With increased humidity, the higher presence of water vapor. This increased water vapor causes can infiltrate in the “egg-box” structure of the crosslinked alginate and cause a disturbance that can reduce the strength of the structure. This reduction in strength can explain why the composite would show a decrease in the storage modulus with increase humidity.

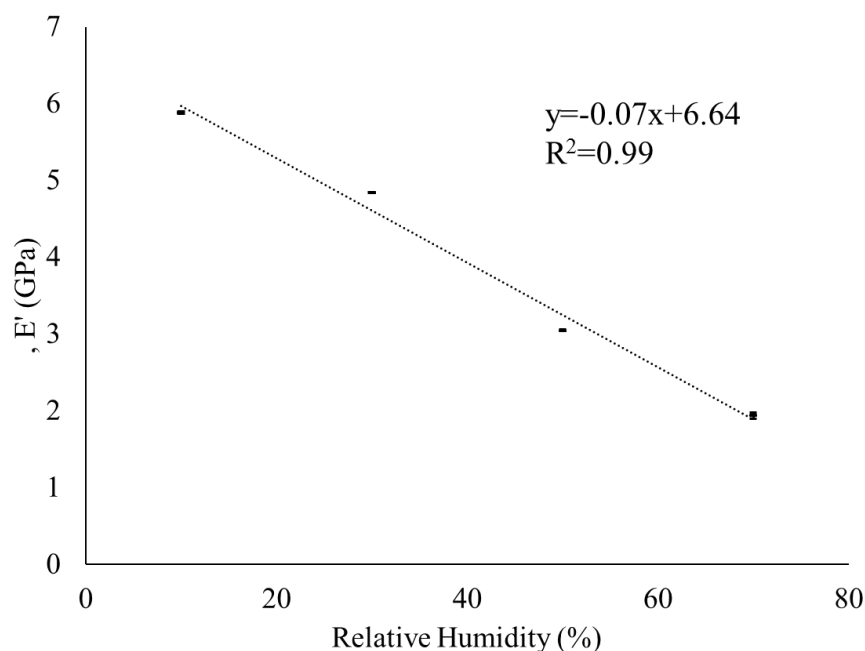


Figure 9. Storage modulus of 30:70 CNC:Alginate composites measured at 10%, 30%, 50%, and 70% relative humidity for 15 hours at constant frequency of 1 Hz and constant strain of 3%. Note that error bars are present, but standard deviation was very low.

3.4.2 Tensile Testing in Dry and Wet Conditions

In order to see the effects of hydration on the mechanical properties of the composites, tensile tests were done after soaking the composites in either DI- H_2O or D-PBS 24 hours prior to testing. The tensile tests of hydrated samples were done in comparison to dry, never hydrated composites. Figure 10 shows the results of these tests for CNC:Alginate and CNC-T:Alginate composites. Figure 10 A, B displays the results in ambient conditions of dry and it can be noted that for both composites with

CNC and CNC-T there is a decrease in the elongation at break. This shows that the composites become stiffer with increased nanocellulose content when compared to alginate. Overall there is an increase in the Young's modulus with increased nanocellulose content, but with a few exceptions. For CNC:Alginate composites there is a decrease in the Young's modulus for composites composed of 50:50 CNC:Alginate, and for CNC-T composites at ratios of 50:50 and 70:30. CNC and CNC-T based composites show similar properties in ambient conditions, but this will change once the composites are exposed to liquid.

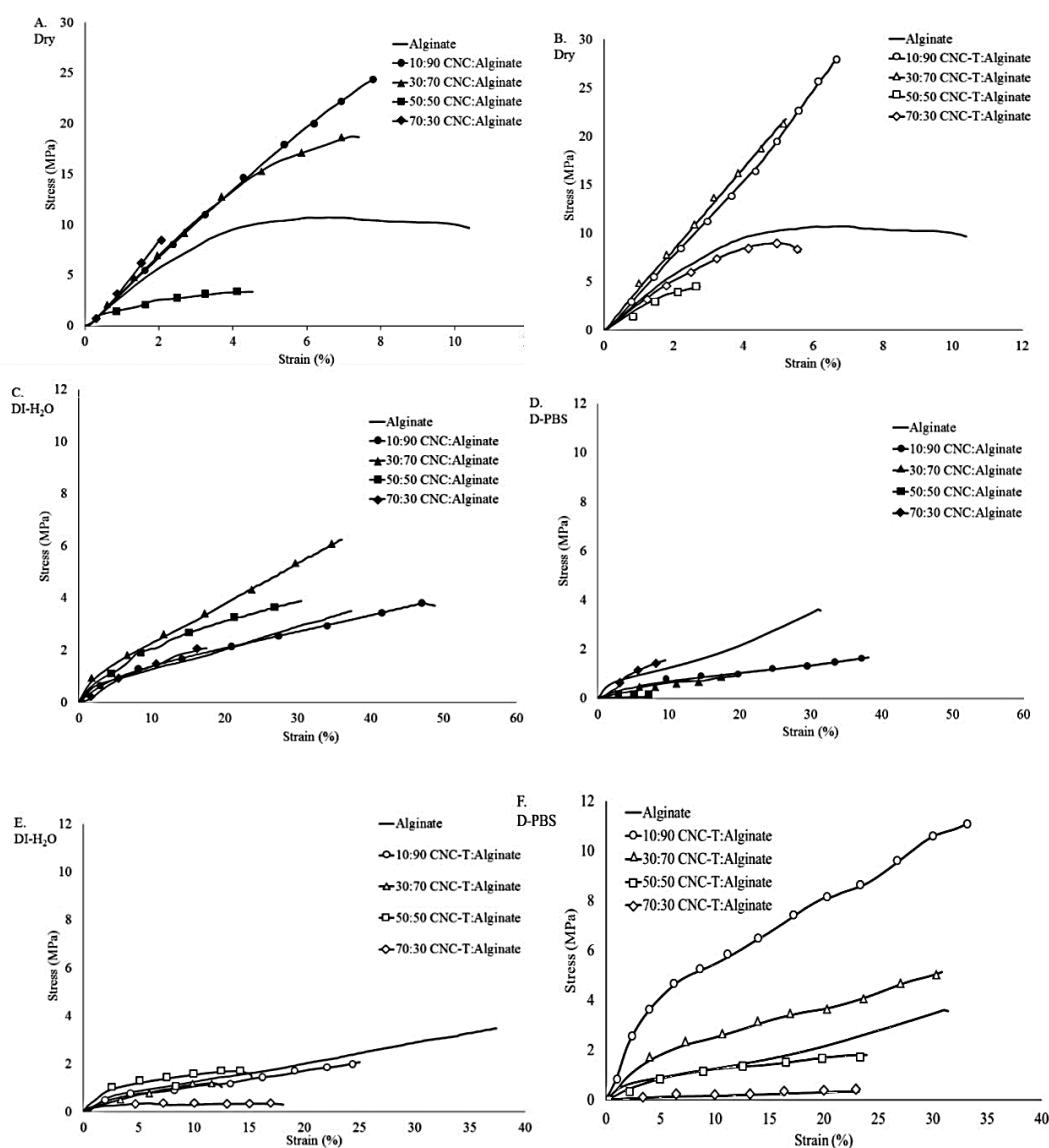


Figure 10. Stress-strain curves of in ambient conditions (A, B), in aqueous conditions in DI-H₂O (C, E) and D-PBS (D, F) at 37°C for CNC:Alginate composites (A, C, D) and CNC-T:Alginate composites (B, E, F).

Since alginate is sensitive to water, it was interesting to see how the mechanical properties would change when submerged in either deionized water or D-PBS at physiological temperature. Composites tested in DI-H₂O showed differing results when compared to dry conditions. For instance, the elongation at break increased, strain at break and Young's modulus decreased for all CNC:Alginate and CNC-T:Alginate composites in DI-H₂O and D-PBS compared to the same composites in dry conditions. When compared to alginate in DI-H₂O, elongation at break increased only for 10:90 and 30:70 CNC:Alginate composites, while strain at break and Young's modulus only increased for 30:70 CNC:Alginate composites. In D-PBS, 10:90 CNC:Alginate had an increase in elongation at break compared to alginate, but 10:90 CNC-T:Alginate had an increase in elongation at break, strain at break, and Young's modulus when compared to alginate.

Table 3. Mechanical properties of Alginate, CNC:Alginate composites, and CNC-T:Alginate composites in dry conditions, DI-H₂O, and D-PBS

	Dry Conditions			DI-H ₂ O @ 37°C			D-PBS @ 37°C		
Sample	Elongation at Break (%)	Strain at Break (MPa)	Young's Modulus (MPa)	Elongation at Break (%)	Strain at Break (MPa)	Young's Modulus (MPa)	Elongation at Break (%)	Strain at Break (MPa)	Young's Modulus (MPa)
Alginate	10.39	9.66	292	37.4	3.41	49.7	31.38	3.57	20.2
CNC:Alginate									
10:90	7.80	24.39	349	51.53	3.15	23.2	38.58	1.68	10.4
30:70	7.41	18.70	361	40.98	6.34	53.3	19.82	0.91	6.22
50:50	4.52	3.36	133	31.08	3.88	38.9	12.02	0.05	15.8
70:30	2.16	8.52	425	17.55	2.08	8.17	9.52	1.54	16.6
CNC-T:Alginate									
10:90	6.70	33.0	397	33.63	2.02	25.3	32.98	11.05	76.0
30:70	5.21	21.8	437	22.57	1.03	30.2	30.83	5.13	35.0
50:50	2.75	4.51	233	21.43	1.46	41.6	23.92	1.81	16.0
70:30	5.82	7.33	277	26.70	0.30	16.8	23.19	0.33	2.10

For tensile testing, it can be said that in dry conditions both CNC and CNC-T based composites showed similar properties, but differed when submerged and tested in liquid. For CNC:Alginate composites when tested in D-PBS compared to DI-H₂O, the mechanical properties in all measures decreased. This difference in performance can be once again related to the results obtained for the leaching of calcium ions as measured by complexometric titration (see Section 3.3). It was shown that CNC:Alginate composites retain a larger amount of Ca²⁺ within DI-H₂O than D-PBS. This leaching of Ca²⁺, or disruption of the “egg-box” structure of the composites is more pronounced in D-PBS because of the shift in ionic equilibrium. It is hypothesized that these results differ from what occurred during the swelling tests because of the mechanical stress the composites were under during tensile testing. The applied tension to the composites allows the ions present in D-PBS to easily infiltrate and disrupt the “egg box” structure more quickly compared to a static system.

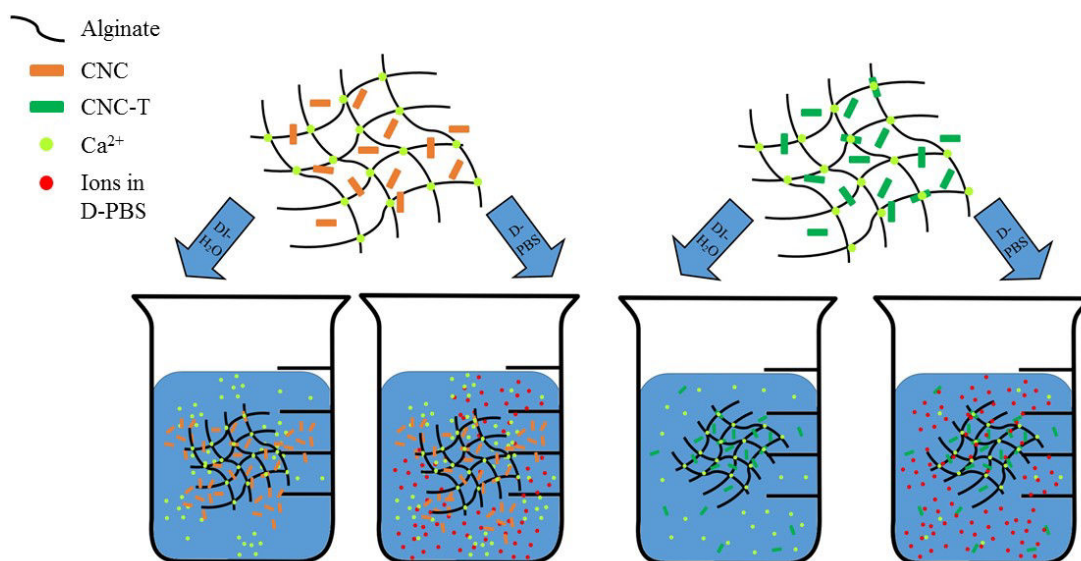


Figure 11. Schematic representation of improved crosslinking with CNC-T versus CNC in D-PBS. For CNC-T:Alginate composites there is improved interaction between the Ca²⁺ ions, the ions present in D-PBS and CNC-Ts which causes less Ca²⁺ ions to be leached from the composites compared to CNC-based systems in D-PBS and also DI-H₂O.

For CNC-T:Alginate composites the differences in mechanical performance was not as pronounced compared to CNC:Alginate. While there were some interesting results, such as an increase in Young's modulus, elongation at break, and strain at break for the 10:90 CNC-T:Alginate composite in D-PBS versus DI-H₂O, overall there was not much change in properties from deionized water to D-PBS as illustrated in Table 3, except for the large increase for the 10:90 CNC-T:Alginate composite. This lack

of change between the properties of the composite can be caused by the lack of leaching of calcium ions within the composite in D-PBS with the percent of Ca^{2+} ions remaining within the composites to be similar and without a significant decrease like the CNC based composites. The ionic nature of the D-PBS does not have such a pronounced effect on the mechanical properties of the oxidized CNC composites because the oxidized CNCs have greater interaction between the crosslinked Ca^{2+} ions within the “egg box” structure compared to CNC:Alginate composites.

4. Conclusion

To the best of the authors’ knowledge this work is the first to show that the addition of cellulose nanocrystals or oxidized cellulose nanocrystals can modulate the material properties of alginate composites under biologically relevant conditions (humid conditions or immersed in different liquids). The main focus of this work was to see how hydration would affect the properties of CNC and CNC-T based alginate composites since it is envisioned that these composites would be used in applications which would expose them to liquid. The effect of humidity on the mechanical properties of CNC:Alginate composites was shown to decrease the storage modulus with increased humidity, which was an expected result because of the hydrophilic nature of alginate. Also the molarity of the crosslinking agent (CaCl_2) was shown to have positive correlation with increased molarity until 0.55 M, with a sharp change to negative correlation for values crosslinked with 0.55-1M CaCl_2 .

The effect of deionized water on CNC and CNC-T based alginate composites showed that for both types of CNCs the water uptake decreased when compared to alginate, but had decreased mechanical properties when compared to tensile testing in dry conditions. Interestingly, the exposure of these composites to D-PBS had differing reactions depending on the use of the type of CNCs. CNC-T based alginate composites showed some improvement in mechanical properties compared to DI- H_2O when tested in D-PBS, which is supported by the lessening of leaching of Ca^{2+} ions as shown by complexometric titration. The ionic nature of D-PBS allows for greater disruption of the “egg box” structure within alginate and CNC/Alginate composites compared to CNC-T/Alginate composites. It is suggested that CNC-Ts are more resistant to this disruption. This is important because of the future applications within the biomedical field. Most of which are in aqueous conditions in D-PBS, and that CNC-T based composites may be favorable.

This extensive study on the use of CNCs and CNC-Ts in conjunction with alginate displays that composites can be easily fabricated and show improvement in the material properties of alginate, and that the properties can be tuned depending on the amount of nanocellulose added to the composites.

These results can be of use especially in applications of alginate in a humid or hydrated setting with ionic liquids such as D-PBS.

5. Acknowledgements

LGP2 is part of the LabEx Tec 21 (Investissements d'Avenir - grant agreement n°ANR-11-LABX-0030) and of the PolyNat Carnot Institutes (Investissements d'Avenir - grant agreements n° ANR-11-CARN-030-01). This work been partially supported by the LabEx Tec 21 (Investissements d'Avenir - grant agreement n°ANR-11-LABX-0030).

6. References

- [1] Lee KY, Mooney DJ. Hydrogels for tissue engineering. *Chemical Reviews*. 2001;101:1869-80.
- [2] Drury JL, Mooney DJ. Hydrogels for tissue engineering: scaffold design variables and applications. *Biomaterials*. 2003;24:4337-51.
- [3] Kuo CK, Ma PX. Ionically crosslinked alginate hydrogels as scaffolds for tissue engineering: Part 1. Structure, gelation rate and mechanical properties. *Biomaterials*. 2001;22:511-21.
- [4] Barnett S, Varley S. The effects of calcium alginate on wound healing. *Annals of the Royal College of Surgeons of England*. 1987;69:153.
- [5] Boateng JS, Matthews KH, Stevens HN, Eccleston GM. Wound healing dressings and drug delivery systems: a review. *Journal of Pharmaceutical Sciences*. 2008;97:2892-923.
- [6] Tønnesen HH, Karlsen J. Alginate in drug delivery systems. *Drug Development and Industrial Pharmacy*. 2002;28:621-30.
- [7] Choi B, Park HJ, Hwang S, Park J. Preparation of alginate beads for floating drug delivery system: effects of CO₂ gas-forming agents. *International Journal of Pharmaceutics*. 2002;239:81-91.
- [8] Stockwell A, Davis S, Walker S. In vitro evaluation of alginate gel systems as sustained release drug delivery systems. *Journal of Controlled Release*. 1986;3:167-75.
- [9] Gombotz WR, Wee SF. Protein release from alginate matrices. *Advanced Drug Delivery Reviews*. 2012;64:194-205.
- [10] George M, Abraham TE. Polyionic hydrocolloids for the intestinal delivery of protein drugs: alginate and chitosan—a review. *Journal of Controlled Release*. 2006;114:1-14.
- [11] Simmons CA, Alsberg E, Hsiong S, Kim WJ, Mooney DJ. Dual growth factor delivery and controlled scaffold degradation enhance in vivo bone formation by transplanted bone marrow stromal cells. *Bone*. 2004;35:562-9.

- [12] Alsberg E, Kong H, Hirano Y, Smith M, Albeiruti A, Mooney D. Regulating bone formation via controlled scaffold degradation. *Journal of dental research*. 2003;82:903-8.
- [13] Bouhadir KH, Lee KY, Alsberg E, Damm KL, Anderson KW, Mooney DJ. Degradation of partially oxidized alginate and its potential application for tissue engineering. *Biotechnology Progress*. 2001;17:945-50.
- [14] Bajpai SK, Sharma S. Investigation of swelling/degradation behaviour of alginate beads crosslinked with Ca²⁺ and Ba²⁺ ions. *Reactive and Functional Polymers*. 2004;59:129-40.
- [15] Shoichet MS, Li RH, White ML, Winn SR. Stability of hydrogels used in cell encapsulation: An in vitro comparison of alginate and agarose. *Biotechnology and Bioengineering*. 1996;50:374-81.
- [16] Drury JL, Dennis RG, Mooney DJ. The tensile properties of alginate hydrogels. *Biomaterials*. 2004;25:3187-99.
- [17] Lee KY, Rowley JA, Eiselt P, Moy EM, Bouhadir KH, Mooney DJ. Controlling mechanical and swelling properties of alginate hydrogels independently by cross-linker type and cross-linking density. *Macromolecules*. 2000;33:4291-4.
- [18] Li Z, Ramay HR, Hauch KD, Xiao D, Zhang M. Chitosan–alginate hybrid scaffolds for bone tissue engineering. *Biomaterials*. 2005;26:3919-28.
- [19] Phisalaphong M, Suwanmajo T, Tammarate P. Synthesis and characterization of bacterial cellulose/alginate blend membranes. *Journal of Applied Polymer Science*. 2008;107:3419-24.
- [20] Kanjanamosit N, Muangnapoh C, Phisalaphong M. Biosynthesis and characterization of bacteria cellulose–alginate film. *Journal of Applied Polymer Science*. 2010;115:1581-8.
- [21] Abdollahi M, Alboofetileh M, Rezaei M, Behrooz R. Comparing physico-mechanical and thermal properties of alginate nanocomposite films reinforced with organic and/or inorganic nanofillers. *Food Hydrocolloids*. 2013;32:416-24.
- [22] Huq T, Salmieri S, Khan A, Khan RA, Le Tien C, Riedl B, et al. Nanocrystalline cellulose (NCC) reinforced alginate based biodegradable nanocomposite film. *Carbohydrate Polymers*. 2012;90:1757-63.
- [23] Lin N, Bruzzese C, Dufresne A. TEMPO-oxidized nanocellulose participating as crosslinking aid for alginate-based sponges. *ACS Appl Mater Interfaces*. 2012;4:4948-59.
- [24] Ureña-Benavides EE, Brown PJ, Kitchens CL. Effect of jet stretch and particle load on cellulose nanocrystal–alginate nanocomposite fibers. *Langmuir*. 2010;26:14263-70.

- [25] Tiquet P. Gelled, freeze-dried capsules or agglomerates of nanoobjects or nanostructures, nanocomposite materials with polymer matrix comprising them, and methods for preparation thereof. Google Patents; 2009.
- [26] Lemahieu L, Bras J, Tiquet P, Augier S, Dufresne A. Extrusion of Nanocellulose-Reinforced Nanocomposites Using the Dispersed Nano-Objects Protective Encapsulation (DOPE) Process. *Macromolecular Materials and Engineering*. 2011;296:984-91.
- [27] Rånby B, Ribi E. Über den feibau der zellulose. *Experientia*. 1950;6:12-4.
- [28] Favier V, Dendievel R, Canova G, Cavaillé J, Gilormini P. Simulation and modeling of three-dimensional percolating structures: case of a latex matrix reinforced by a network of cellulose fibers. *Acta Materialia*. 1997;45:1557-65.
- [29] Favier V, Canova G, Cavaillé J, Chanzy H, Dufresne A, Gauthier C. Nanocomposite materials from latex and cellulose whiskers. *Polymers for Advanced Technologies*. 1995;6:351-5.
- [30] Bilbao-Sainz C, Bras J, Williams T, Sénechal T, Orts W. HPMC reinforced with different cellulose nano-particles. *Carbohydrate Polymers*. 2011;86:1549-57.
- [31] Peresin MS, Habibi Y, Zoppe JO, Pawlak JJ, Rojas OJ. Nanofiber composites of polyvinyl alcohol and cellulose nanocrystals: manufacture and characterization. *Biomacromolecules*. 2010;11:674-81.
- [32] Roohani M, Habibi Y, Belgacem NM, Ebrahim G, Karimi AN, Dufresne A. Cellulose whiskers reinforced polyvinyl alcohol copolymers nanocomposites. *European Polymer Journal*. 2008;44:2489-98.
- [33] Jorfi M, Roberts MN, Foster EJ, Weder C. Physiologically responsive, mechanically adaptive bio-nanocomposites for biomedical applications. *ACS Applied Materials & Interfaces*. 2013;5:1517-26.
- [34] Mariano M, El Kissi N, Dufresne A. Cellulose nanocrystal reinforced oxidized natural rubber nanocomposites. *Carbohydrate Polymers*. 2016;137:174-83.
- [35] Annamalai PK, Dagnon KL, Monemian S, Foster EJ, Rowan SJ, Weder C. Water-Responsive Mechanically Adaptive Nanocomposites Based on Styrene-Butadiene Rubber and Cellulose Nanocrystals Processing Matters. *ACS Applied Materials & Interfaces*. 2014;6:967-76.
- [36] Oksman K, Mathew A, Bondeson D, Kvien I. Manufacturing process of cellulose whiskers/poly(lactic acid) nanocomposites. *Composites Science and Technology*. 2006;66:2776-84.
- [37] Mathew AP, Oksman K, Sain M. The effect of morphology and chemical characteristics of cellulose reinforcements on the crystallinity of poly(lactic acid). *Journal of Applied Polymer Science*. 2006;101:300-10.

- [38] Siqueira G, Abdillahi H, Bras J, Dufresne A. High reinforcing capability cellulose nanocrystals extracted from *Syngonanthus nitens* (Capim Dourado). *Cellulose*. 2010;17:289-98.
- [39] Siqueira G, Fraschini C, Bras J, Dufresne A, Prud'homme R, Laborie M-P. Impact of the nature and shape of cellulosic nanoparticles on the isothermal crystallization kinetics of poly (ϵ -caprolactone). *European Polymer Journal*. 2011;47:2216-27.
- [40] Jorfi M, Foster EJ. Recent advances in nanocellulose for biomedical applications. *Journal of Applied Polymer Science*. 2015;132:41719.
- [41] Camarero-Espinosa S, Boday DJ, Weder C, Foster EJ. Cellulose nanocrystal driven crystallization of poly (d, l-lactide) and improvement of the thermomechanical properties. *Journal of Applied Polymer Science*. 2015;132.
- [42] Mariano M, El Kissi N, Dufresne A. Cellulose nanocrystals and related nanocomposites: review of some properties and challenges. *Journal of Polymer Science Part B: Polymer Physics*. 2014;52:791-806.
- [43] Azizi Samir MAS, Alloin F, Dufresne A. Review of recent research into cellulosic whiskers, their properties and their application in nanocomposite field. *Biomacromolecules*. 2005;6:612-26.
- [44] Moon RJ, Martini A, Nairn J, Simonsen J, Youngblood J. Cellulose nanomaterials review: structure, properties and nanocomposites. *Chemical Society Reviews*. 2011;40:3941-94.
- [45] Hubbe MA, Rojas OJ, Lucia LA, Sain M. Cellulosic nanocomposites: a review. *BioResources*. 2008;3:929-80.
- [46] Siqueira G, Bras J, Dufresne A. Cellulosic bionanocomposites: a review of preparation, properties and applications. *Polymers*. 2010;2:728-65.
- [47] Sakiyama-Elbert S, Hubbell J. Functional biomaterials: design of novel biomaterials. *Annual Review of Materials Research*. 2001;31:183-201.
- [48] Mano JF. Viscoelastic properties of chitosan with different hydration degrees as studied by dynamic mechanical analysis. *Macromolecular bioscience*. 2008;8:69-76.
- [49] Lee KY, Mooney DJ. Alginate: properties and biomedical applications. *Progress in Polymer Science*. 2012;37:106-26.
- [50] Olivas GI, Barbosa-Cánovas GV. Alginate–calcium films: water vapor permeability and mechanical properties as affected by plasticizer and relative humidity. *LWT-Food science and technology*. 2008;41:359-66.

- [51] Pereira R, Carvalho A, Vaz DC, Gil M, Mendes A, Bártolo P. Development of novel alginate based hydrogel films for wound healing applications. *International Journal of Biological Macromolecules*. 2013;52:221-30.
- [52] Remunan-Lopez C, Bodmeier R. Mechanical, water uptake and permeability properties of crosslinked chitosan glutamate and alginate films. *Journal of Controlled Release*. 1997;44:215-25.
- [53] Sirviö JA, Kolehmainen A, Lämätäinen H, Niinimäki J, Hormi OE. Biocomposite cellulose-alginate films: promising packaging materials. *Food Chemistry*. 2014;151:343-51.
- [54] Fukuzumi S, et al. . Transparent and High Gas Barrier Films of Cellulose Nanofibers Prepared by TEMPO-Mediated Oxidation. *Biomacromolecules*. 2008;10:162-5.
- [55] da Silva Perez D, Montanari S, Vignon MR. TEMPO-mediated oxidation of cellulose III. *Biomacromolecules*. 2003;4:1417-25.
- [56] Segal L, Creely J, Martin Jr A, Conrad C. An empirical method for estimating the degree of crystallinity of native cellulose using the X-ray diffractometer. *Textile Research Journal*. 1959;29:786-94.
- [57] Hoeng F, Denneulin A, Neuman C, Bras J. Charge density modification of carboxylated cellulose nanocrystals for stable silver nanoparticles suspension preparation. *Journal of Nanoparticle Research*. 2015;17:244.
- [58] Roman M, Winter WT. Effect of Sulfate Groups from Sulfuric Acid Hydrolysis on the Thermal Degradation Behavior of Bacterial Cellulose. *Biomacromolecules*. 2004;5:1671-7.
- [59] Lin N, Dufresne A. Surface chemistry, morphological analysis and properties of cellulose nanocrystals with gradiented sulfation degrees. *Nanoscale*. 2014;6:5384-93.
- [60] Grant GT, Morris ER, Rees DA, Smith PJ, Thom D. Biological interactions between polysaccharides and divalent cations: the egg-box model. *FEBS Letters*. 1973;32:195-8.

Chapter 3.2 Characterization and Mechanical Properties of Ultraviolet Stimuli-Responsive Functionalized Cellulose Nanocrystal Alginate Composites

This subchapter is based on *Characterization and Mechanical Properties of Ultraviolet Stimuli-Responsive Functionalized Cellulose Nanocrystal Alginate Composites*. **Journal of Polymer Science**. Submitted

Abstract	167
1. Introduction	168
2. Materials and Methods	169
2.1 Materials	169
2.2 Methods	170
2.2.1 Chemical Grafting of 4-pentenoic acid to Cellulose Nanocrystals	170
2.2.2 Fabrication of 4-pentenoic acid-g-CNC/Alginate/ACVA Composites	170
2.3 Characterization of Grafted CNCs	171
2.3.1 Atomic Force Microscopy (AFM)	171
2.3.2 Dynamic Light Scattering (DLS)	171
2.3.3 X-Ray Diffraction (XRD)	171
2.3.4 Thermogravimetric Analysis (TGA)	172
2.3.5 Fourier Transform Infrared Spectroscopy (FTIR)	172
2.3.6 Solid state carbon-13 nuclear magnetic resonance (^{13}C NMR)	172
2.4 Characterization of PA-g-CNC/alginate/ACVA composites	173
2.4.1 Water Uptake.....	173
2.4.2 Mechanical Testing	173
3. Results and Discussion.....	173
3.1 Dimensional Analysis of CNCs	173
3.2 Characterization of Functionalized CNCs	175
3.3. Characterization of PA-g-CNC/alginate/ACVA Composites	178
3.3.1 Indirect Confirmation of Crosslinking	178
3.3.2 Mechanical Analysis: Tensile Testing	180
4. Conclusion	184
5. Acknowledgements.....	184
6. References	184

Characterization and Mechanical Properties of Ultraviolet Stimuli-Responsive Functionalized Cellulose Nanocrystal Alginate Composites

Megan Smyth^{a,b}, Chris Rader^c, Julien Bras^{a,b,c}, E. Johan Foster^c

a. 1. CNRS, LGP2, 461 Rue de la Papeterie, 38402, Saint-Martin-d'Hères, France

b. Université Grenoble Alpes, LGP2, 38000 Grenoble, France

c. Macromolecules Innovation Institute, Virginia Tech, Department of Materials Science & Engineering, 445 Old Turner Street, 203 Holden Hall, Blacksburg, VA 24061, USA

d. Institut Universitaire de France, 75005 Paris, France

Abstract

The poor mechanical properties of alginate when exposed to aqueous solutions has been a problem which has plagued researchers within the biomedical field. In order to be able to improve the mechanical properties in a systematic manner, functionalized cellulose nanocrystals (CNCs) were added to alginate and UV-induced crosslinked following an azo-initiated free radical polymerization. CNCs were functionalized with 4-pentenoic acid (PA-g-CNCs) using a simple, environmentally friendly solvent-free esterification. The dimensional and crystallinity properties of PA-g-CNCs remained unchanged following esterification as shown by atomic force microscopy (AFM), dynamic light scattering (DLS), and x-ray diffraction (XRD). Thermogravimetric analysis (TGA), Fourier transform infrared spectroscopy (FTIR), and ¹³C nuclear magnetic resonance (NMR) indicated that 4-pentenoic acid was present on the surface of CNCs through bulk analysis. These PA-g-CNCs were then used in the creation of PA-g-CNC:Alginate composites with an azo-initiator to induce UV-dependent crosslinking for the improvement of the mechanical properties of alginate. It was shown that the properties of alginate can be enhanced with the addition of functionalized CNCs as tested by swelling of the nanocomposites in water and mechanical testing in wet and dry conditions. These

results suggest that the addition of PA-g-CNCs and crosslinking by UV-dependent free radical polymerization improves the performance of alginate when tested in dry conditions, but without any apparent dependence to azo-initiated crosslinking when exposed to water in regards to mechanical properties.

1. Introduction

Cellulose nanocrystals, or CNCs, have been used by researchers as a means to improve the mechanical properties of polymer matrices since the mid-1990s [1]. CNCs are commonly derived from biomass cellulose through acid hydrolysis, either sulfuric [2], hydrochloric [3], or phosphoric[4] acid or even subcritical water [5]. Since the 2010's, these innovative materials are industrially available, in majority of cases, by sulfuric acid hydrolysis. The properties of CNCs can vary greatly depending on the method of isolation and the source [6-9]. CNCs are used as a reinforcement nanoscale filler as shown by many review articles focusing on composites of CNCs [10-14]. To highlight, CNC based composites of thermoplastic biopolymers [15-17] and water soluble polymers [18-20] were the first to be developed, but the focus of CNC composites has recently turned to the use of bio-sourced matrices such as natural rubber [21-26] or alginate [27-30]. Alginate is derived from algae and contains 1,4-linked β -D-mannuronate (M) and α -L-guluronate (G) chains in variable ratios. Gelation of alginate occurs when the G chains interact with divalent cationic ions, and can be tuned by varying the amount of cationic ions accessible to the G chains [31]. Since alginate is commonly used in biomedical applications [32-39] the mechanical properties have been extensively studied and are reported to be not favorable in aqueous conditions [40, 41].

Chemical functionalization of CNCs has been used to improve the interface between the polymer matrix and CNCs since the mid 2000's. Commonly used functionalization motifs include TEMPO-mediated oxidation [42, 43], non-covalent surface modification via adsorption as first reported by Heux et al. in 2000 [44], amidation through peptidic-linkage with 1-ethyl-3-(3-dimethylaminopropyl)carbodiimide (EDC) and N-hydroxysuccinimide (NHS) as first shown by Araki [45], esterification, carbamatation as first shown by Siqueira [46], graft polymerization and many more, which are shown in the many review papers on this topic [47-49]. Esterification occurs through the hydroxyl groups present at the surface of the CNCs. Many different esterification reactions have been

studied such as Fischer esterification of acetylated CNCs [50, 51], transesterification [52], and the most common, acetylation [53]. Environmentally friendly methods of esterification include protocols developed by Yuan et al. which uses alkenyl succinic anhydride aqueous emulsions mixed with CNC suspensions, freeze-dried, and further melted to graft CNCs [54], and a solvent-free gas-phase esterification of dried CNCs under reduced pressure created by Berlioz et al. [55].

In this work we employed a new esterification technique developed by Espino-Pérez and colleagues, which is environmentally friendly, solvent free, and does not require any additional processing of the CNCs [56]. Similar work has been done recently by Boujemaoui by directly grafting certain organic acids to CNCs during hydrolysis of cellulose fiber with hydrochloric acid and adding organic acid [57]. However, to the best of our knowledge, this is the first reported use of 4-pentenoic acid grafted to CNCs, in this case for use in stimuli-responsive materials.

CNCs have long been used to create stimuli-responsive or “smart” materials. Pioneering work done by Capadona et al. used the biological model of a sea cucumber to develop a CNC, 1:1 ethyleneoxide/epichlorohydrin copolymer (EO-EPI) composite that was mechanically responsive to water [58]. CNCs have been employed to create smart materials that are responsive to water [59-61], pH [62, 63], temperature [64, 65], and light [66-68]. Biyani et al. used two different functionalized CNCs in an EO-EPI matrix to develop photoswitchable nanocomposites. One work employed the use of a radical-mediated reaction with benzo-derivatized CNCs [66], while the other used coumarin-derivatized CNCs to exploit the dimerization reaction coumarin derivatives undergo when exposed to UV [67]. Another example of the use functionalized CNCs in the development of a light-sensitive mechanically adaptive material is by Fox et al., which used thiol-ene click chemistry with allyl functionalized CNCs in a poly(vinyl acetate) matrix [68].

In this study, we created mechanically adaptive grafted CNC, alginate composites through photoinitiated crosslinking. 4-Pentenoic acid functionalized CNCs (PA-g-CNCs) were mixed with alginate and 4,4-azobis(4-cyanovaleric acid) (ACVA), an azo-initiator, solvent casted, and exposed to ultraviolet (UV) radiation. It is proposed that ACVA will induce free-radical polymerization and favor “crosslinking” of the PA-g-CNCs through the available allyl group when exposed to UV light. It is hypothesized that these crosslinked PA-g-CNCs will impart higher mechanical properties to the alginate in aqueous condition compared to unmodified CNCs because of the increased interaction between the PA-g-CNCs than what occurs because of the percolation network properties of CNCs. The mechanical properties of the composites were studied in relation UV exposure time, composition, and water exposure at physiological temperature.

2. Materials and Methods

2.1 Materials

Cellulose nanocrystals (CNCs) were purchased from the University of Maine Process Development Center (USA). The CNCs were extracted from softwood pulp using sulfuric acid hydrolysis. Ethanol and acetone were purchased from Chimie Plus (Denicé, France). 4-Pentenoic acid (PA), hydrochloric acid (HCl), sodium alginate, 4,4'-azobis(4-cyanovaleric acid) (ACVA) was purchased from Sigma-Aldrich (USA). All materials were used without any modification.

2.2 Methods

2.2.1 Chemical Grafting of 4-pentenoic acid to Cellulose Nanocrystals

For the grafting of 4-pentenoic acid to CNCs, a modified protocol proposed by Espino-Perez et al. [56] was performed. A solution of 10 %wt CNCs in deionized water was solvent exchanged from DI-H₂O to ethanol to acetone and finally 4-pentenoic acid. The CNC solution of 4-pentenoic acid was dispersed using a 200W sonication probe (Sonifier® S-250A, Branson, Danbury, Connecticut, USA), for 5 minutes. The pH of the solution was adjusted to 4.3 using 0.1M HCl. The round bottom flask of the CNC solution was added to a closed-distillation system with a condenser held at 5°C. The solution was put in an oil bath at 110°C to ensure the evaporation of any residual water in the system. The system was kept at 110°C under stirring for 20 hours to perform a surface esterification on the CNCs. Following the esterification, the excess 4-pentenoic acid was removed using centrifugation, decanting and replacement of solvent in two iterations (10,000 rpm, 4°C, 15 min). The grafted CNCs were washed with ethanol 3 times to remove any unreacted acid by centrifugation. All grafted CNCs will be referred to as PA-g-CNCs.

2.2.2 Fabrication of 4-Pentenoic acid-g-CNC/Alginate/ACVA Composites

PA-g-CNC/alginate/ACVA composites were made by soaking 0.6 g of sodium alginate powder in 20 mL DI-H₂O overnight and stirring mildly for 2 hours to form a homogeneous suspension. 120 mL of sonicated 1 wt% CNC or PA-g-CNCs suspensions were mixed with 0.3g of ACVA for 10 minutes and then sonicated for 10 minutes. Suspensions of varying ratios of CNC+ACVA to sodium alginate were made with the amounts highlighted in Table 1 with 0.25% ACVA solution also added to the alginate matrix. PA-g-CNC and alginate suspensions were stirred for 30 minutes. The suspensions were solvent casted and allowed to dry at ambient conditions for 48 hours and then at 45°C for 24 hours. Dried

films were then soaked overnight in CaCl₂ solution with concentration of 0.45M CaCl₂ and rinsed. The crosslinked films were dried again at ambient conditions for 24 hours under fume hood evaporation. All composites were exposed to ultraviolet radiation for 30 minutes, 1 hour, and 2 hours following drying to induce crosslinking between the PA-g-CNCs.

Table 1. Amounts of CNC, PA-g-CNC, and sodium alginate for fabrication of composites

Ratio PA-g-CNC:Alginate	3 wt% Sodium alginate	1 wt% PA-g-CNC
	solution(mL)	suspension + ACVA (mL)
Alginate	20	0
10:90	18	6
30:70	14	18
50:50	10	30

2.3 Characterization of Grafted CNCs

2.3.1 Atomic Force Microscopy (AFM)

Suspensions of approximately 0.2 mL 1x10⁻⁴% wt of CNC and PA-g-CNC were prepared, and placed on the surface of a cleaved mica plate. The CNC and PA-g-CNC coated mica plates were dried overnight at ambient conditions, and then analyzed using atomic force microscopy. Images were acquired using tapping mode with a Nanoscope IIA microscope from Veeco Instruments (Plainview, New York, USA) at a frequency of ~265-340 Hz. Silicon cantilevers with a curvature of 10-15 nm were used (OTESPA®, Bruker, Billerica, Massachusetts, USA). AFM images were analyzed ImageJ (U. S. National Institutes of Health, Bethesda, Maryland, USA). At least 50 measurements were performed to obtain a representative average.

2.3.2 Dynamic Light Scattering (DLS)

Dynamic light scattering to determine the size of the nanoparticles was carried out using a Vasco Particle Size Meter (Cordouan Technologies, Pessac, France). Ten measurements with a 60-time step and a noise ratio of 1.06 were carried out for each sample in triplicate. The polydispersion index of the DLS measurements needs to be under 0.2 in order to determine if the measurements are accurate. The measurements were collected and analyzed using nanoQ software (Cordouan Technologies, Pessac, France).

2.3.3 X-Ray Diffraction (XRD)

The crystallinity of lyophilized CNC and PA-g-CNC samples were measured using X-ray diffraction (XRD). XRD diffractogram patterns were measured using a PW 1720 X-ray generator (Phillips, Eindhoven, Netherlands) at 45 kV and 40mA with Cu K α radiation and a wavelength of 0.154 nm in the range of $2\theta=6-56^\circ$ with a fixed step interval. The samples were lyophilized and ground into a powder using a mortar and pestle. The crystallinity index was calculated according to the following equation,

$$C_I^{XRD} = \frac{I_{002} - I_{am}}{I_{002}} * 100 \quad (\text{Eq. 1})$$

and corresponds to the ratio of the interference of the [002] crystal planes, which was subtracted by the amorphous regions observed at 18° , and the total peak height [002] of the crystal planes. (I_{002}) observed at 22.5° [69].

2.3.4 Thermogravimetric Analysis (TGA)

Thermogravimetric measurements were performed with a Perkin Elmer STA 6000 (Waltham, Massachusetts, USA). The temperature ranged from 25°C to 900°C with a heating rate of $10^\circ\text{C}/\text{min}$. The tests were carried out under atmospheric conditions ($20\text{mL}/\text{min}$). All results were analyzed with Pyris Series software (Perkin Elmer, Waltham, Massachusetts, USA).

2.3.5 Fourier Transform Infrared Spectroscopy (FTIR)

Fourier transform infrared spectroscopy (FTIR) was done on KBr pellets of modified and unmodified CNCs using a Perkin Elmer Spectrum One spectrometer (Waltham, Massachusetts, USA). 32 scans from $6000-400\text{ cm}^{-1}$ with a resolution of 1 cm^{-1} were carried out. The spectra were normalized with respect to 1100 cm^{-1} , and analyzed using Spectrum software (Perkin Elmer, Waltham, Massachusetts, USA).

2.3.6 Solid state carbon-13 nuclear magnetic resonance (^{13}C NMR)

^{13}C NMR was performed on a Bruker AVANCE 400 spectrometer. Samples were placed in 4 mm ZrO₂ rotors. All spectra were recorded using a combination of cross-polarization, high power proton decoupling and magic angle spinning (CP/MAS). ^{13}C NMR spectra were acquired at 298 K, with a 4-mm probe operating at 100.13 MHz. The chemical shift values were measured with respect to TMS via glycine as a secondary reference with the carbonyl signal set to 176.03 ppm.

For modified CNCs, experiments were conducted with CP contact times from 0.05 to 12 ms, MAS of 14 kHz (to avoid SSB overlapping with grafted material peaks), and repetition time of 2 s, and from these experiments the polarization curves were built for each NMR signal to determine its integral by extrapolation to origin.

2.4 Characterization of PA-g-CNC/Alginate/ACVA composites

2.4.1 Water Uptake

Samples were placed in DI-H₂O for 24 hours, removed, and weighed following excess water removal between two sheets of absorbent paper. The liquid uptake was calculated using the following formula:

$$\text{Water Uptake } (W_p) = \frac{T_t - T_0}{T_0} * 100 \quad (\text{Eq. 2})$$

Where T is the thickness of the composite film at 0 and 24 hours after soaking in DI-H₂O. All samples were done in triplicate and are reported as mean \pm standard deviation.

2.4.2 Mechanical Testing

Films were dried and conditioned at least 24 hours before analysis in a temperature and humidity controlled room at 23°C and 50% humidity. Mechanical properties of the samples were measured using a DMA Q800 by TA Instruments (New Castle, Delaware, USA). The distance between the clamps was 10 mm with a width of approximately 5 mm. Samples were tested in both dry and wet conditions at 37°C, with an additional isothermal step at 37°C for 5 minutes before each test. Samples underwent rectangular tension measurements with a force ramp rate of 0.25 N/min and preload force of 0.01 N. The stress vs strain curves were measured and analyzed using TA Orchestrator (New Castle, Delaware, USA).

3. Results and Discussion

3.1 Dimensional Analysis of CNCs

The morphological results obtained by AFM are shown in Figure 1. It has been shown that grafted CNCs retain their rod-like shape following chemical modification. Slight increase in the length and

width can be shown following chemical functionalization, which can be attributed to the higher aggregation or swelling of the CNCs during the grafting procedure.

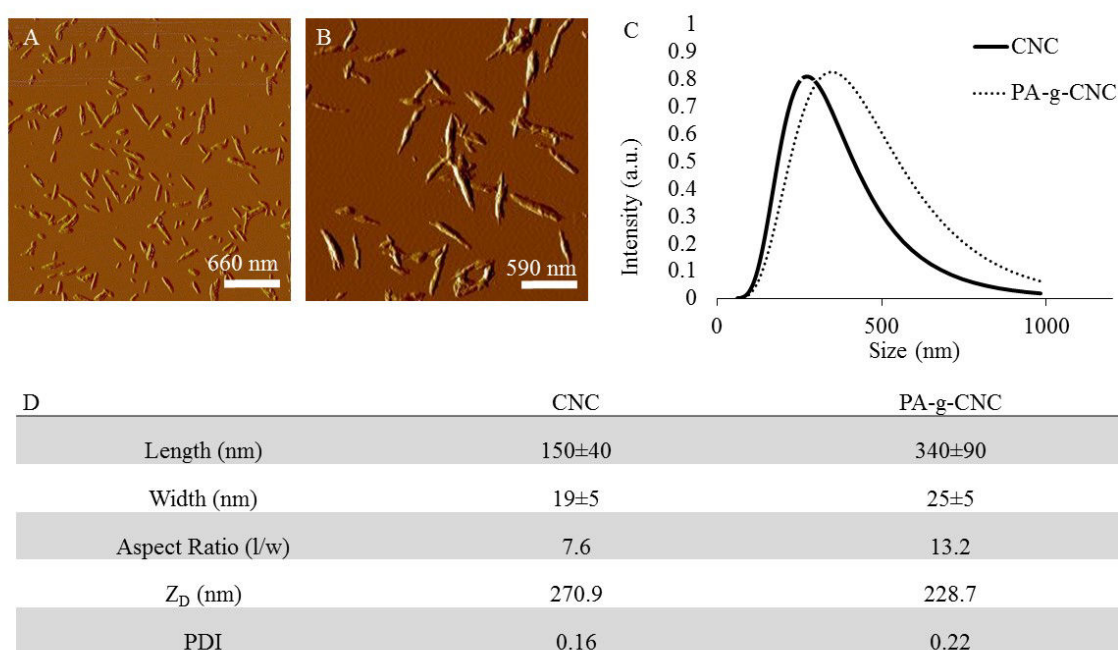


Figure 1. CNC AFM images from suspensions of 0.0001 wt% of A) CNC, B) PA-g-CNC acquired by tapping mode in air. C) Size distribution of CNC and PA-g-CNC nanoparticles from 0.001 wt% suspensions in DI-H₂O as determined by DLS. D) Length and width measurements of CNCs and PA-gCNCs as determined by ImageJ analysis of AFM images from N=25, and Hydrodynamic diameter (Z_D), polydispersity index (PDI) determined by dynamic light scattering.

The DLS results, which include the Z_D , or hydrodynamic diameter and polydispersity index (PDI), are also shown in Figure 1. The CNCs and PA-g-CNCs size distribution, as seen in Figure 1 have a wide range and follow a Gaussian distribution. In regards to the average size of the particles, PA-g-CNCs have a larger average, Z_D , compared to CNCs, which indicate a larger diameter. These results are in agreement with the AFM image analysis, and further indicate the influence of the addition of 4-pentenoic acid to the surface of the CNCs.

The PDI measurement for the suspension shows the degree of homogeneity within the size distribution of the sample. The closer the PDI value is to 0 the more homogeneous the sample, while values closer to 1 indicate that the sample has a wide size distribution. The low PDI reported of the CNCs and 4-pentenoic-g-CNCs signifies that the samples are mono-dispersed. These results cannot be assumed to be conclusive, because DLS measurements require that the particles have a spherical shape, and both the modified and neat CNCs are known to be rod-like materials. DLS is used in our results to confirm that the isolated CNCs are in fact nanoparticles, and follow a Gaussian size distribution.

3.2 Characterization of Functionalized CNCs

To confirm the “swelling” of grafted CNCs is due to a change in crystallinity, X-ray diffraction was performed and the results are shown in Figure 2. It was reported by Sèbe et al. that cellulose I has typical peaks at 15.7° and 22.6° , while cellulose II has peaks located at 12.2° and 20.1° [70], which are present in both samples. It is well known that this CNCs coming from the University of Maine contain these two allomorphs. The crystallinity index was calculated for commercial CNCs and PA-g-CNCs, with PA-g-CNCs exhibiting a lower crystallinity when compared to CNCs (77% vs. 72%). This reduction can be attributed to the exposure of the CNCs to the acidic conditions necessary for the grafting, which causes continued hydrolysis of the CNCs. This reduction in crystallinity is limited and the grafted PA-g-CNCs still retain their structure as shown by the AFM images in the previous section. These two results in conjunction suggest the grafted CNCs are not degraded or have lost their crystalline order.

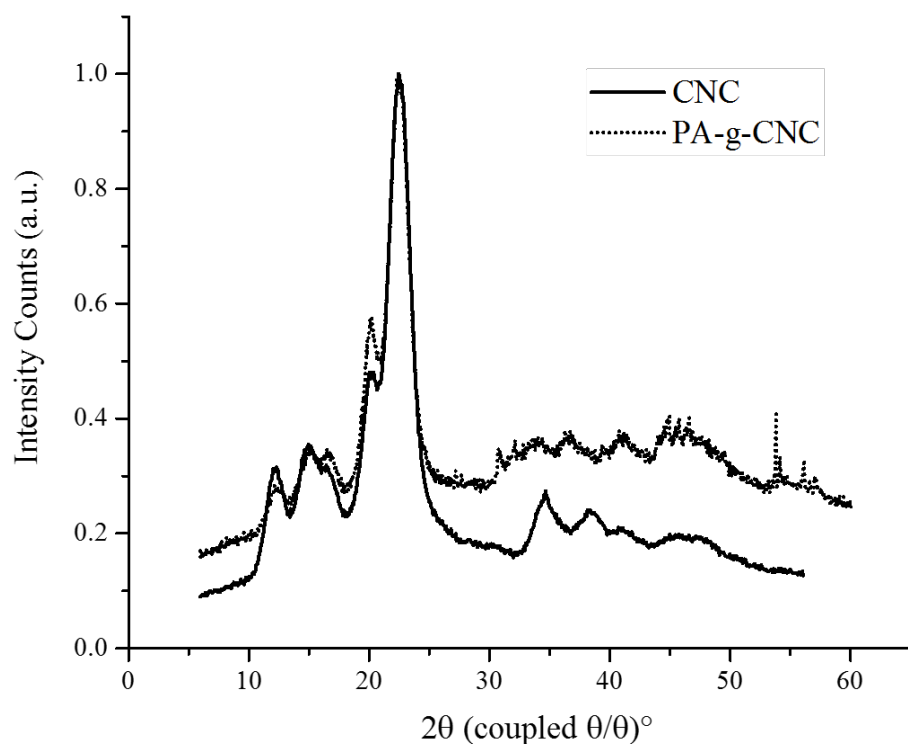


Figure 2. X-ray diffraction spectrograms of CNC and PA-g-CNCs obtained from powder and normalized to the maximum

CNCs can be used in a variety of applications with one of those applications as a reinforcement tool in materials. In material processing, thermal stability is a must in order to have materials which can withstand typical processing conditions, which can include melt processing of polymers [70]. Thermogravimetric analysis curves of CNC and PA-g-CNC are shown in Figure 3. The loss of weight under 100 °C can be attributed to the evaporation of residual water within the samples, which is approximately 5-6 % of the sample mass [71]. Samples of pure cellulose exhibit a single weight loss event, while samples with surface groups, such as sulfate groups, typically have two weight loss events, which are shown by the peak derivatives of the thermogram curve. The first weight loss event for the CNC can be attributed to the sulfate groups attached to the surface of CNC, while the second event is attributed to the –OH groups [72]. The increase in degradation of the first weight loss event in modified CNCs compared to neat CNCs is usually due to the reduction of sulfate groups on the surface of the CNCs because of the esterification of 4-pentenoic acid as cited by Beck et al [73]. The

functionalization of the CNCs by 4-pentenoic acid did not negatively affect the thermal stability of the CNCs, and in fact slightly improved thermal stability.

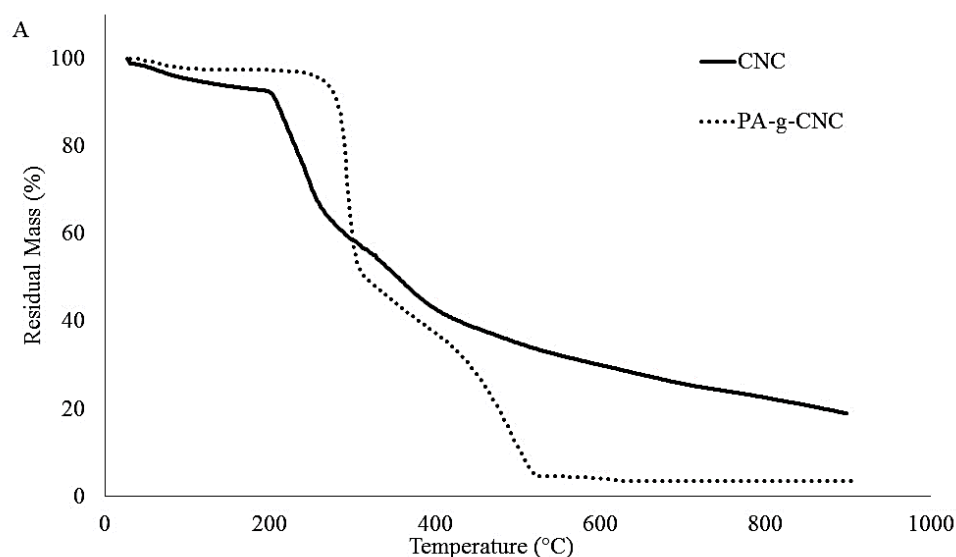


Figure 3. A) TGA thermograms of PA-g-CNC measured from 30-900 °C with a temperature rate increase of 10 °C per minute under an atmosphere of air.

Following chemical grafting FTIR was performed on the neat and functionalized CNCs. Both the CNC and 4-pentenoic acid-g-CNC samples exhibit peaks at 1061 (C-O stretching) and 897 cm^{-1} (C-H rock vibrations) [74], which are commonly associated with cellulose. The appearance of new peaks within the spectra for PA-g-CNC indicates that 4-pentenoic acid has been grafted to CNCs through esterification. The appearance of a peak at 1275 cm^{-1} for the PA-g-CNC sample indicates the presence of an asymmetric =C-O-C group, which occurs in esters. Other indications of the presence of grafted 4-pentenoic acid are the asymmetric peaks present at 2925 and 2850 cm^{-1} , which are indicative of CH_2 groups present in the functionalized CNCs. It has been noted that the band at approximately 1730 cm^{-1} appeared in PA-g-CNCs. This wavelength corresponds to the stretching of the C=O bond of the ester of the carboxylic acid, while the neat CNC does not show the addition of the ester bond through esterification. This difference in spectra indicates that 4-pentenoic acid has been grafted to the neat cellulose nanocrystals.

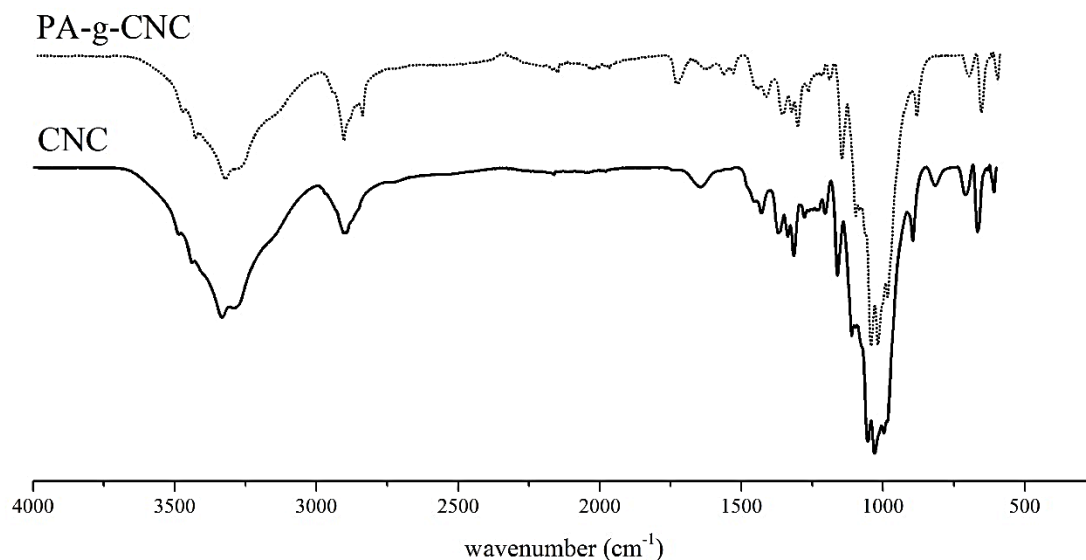


Figure 4. FTIR spectrum of CNC and PA-g-CNC

In order to confirm such grafting, solid state ^{13}C NMR was performed on the neat and modified CNC samples in order to have further proof of the grafting on CNC. The carbon signals attributed to cellulose range from 60 to 106 ppm. The carbon signals found between 70-75 ppm, C_2 , C_3 , and C_5 are not needed for the $\beta(1-4)$ linkage in cellulose.

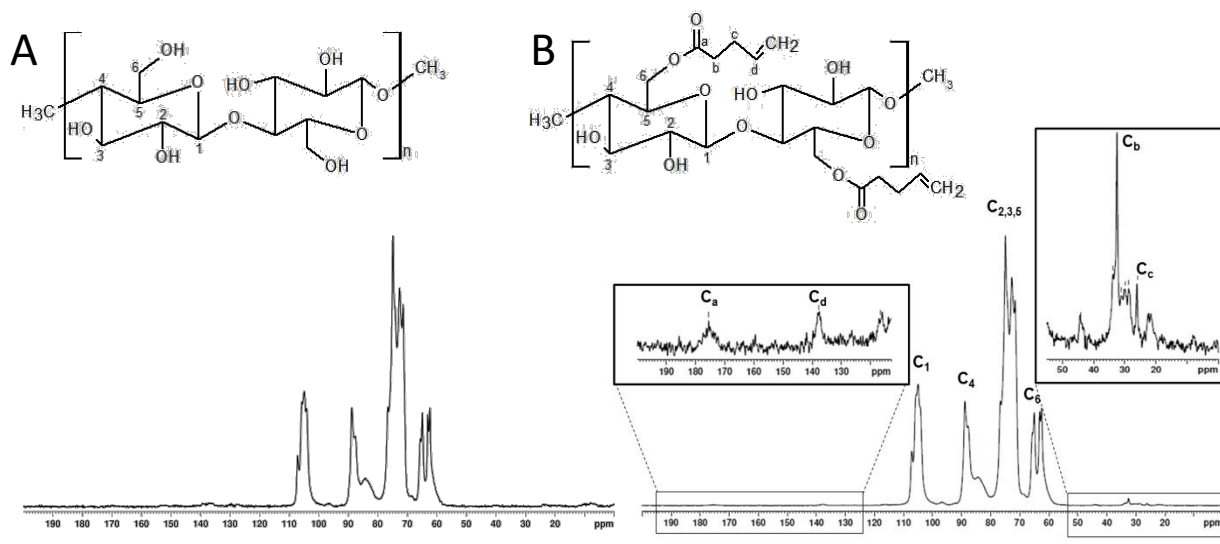


Figure 5. ^{13}C solid state NMR of A) CNC and B) PA-g-CNC

After grafting of 4-pentenoic acid, four new resonances peaks occurred. The carbon from the carbonyl group (C_a) was detected at the highest frequency (175 ppm), while at low frequency the additional methylene groups were detected for C_b and C_c (32 and 26 ppm). While the allyl group appears at 137 ppm. These additional resonance peaks confirm an efficient grafting of 4-pentenoic acid to CNCs.

With the addition of grafted 4-pentenoic acid to the surface of CNCs there was no noted shift in the peak signals associated with CNCs. It must be noted that quantification of the amount of 4-pentenoic acid grafted could not be determined by ^{13}C NMR, but confirms the presence of grafted CNCs.

3.3. Characterization of PA-g-CNC/alginate/ACVA Composites

Previous sections displayed that CNCs were functionalized with 4-pentenoic acid using a one step process with environmentally friendly solvents. To further verify that the CNCs were functionalized with 4-pentenoic acid, composites of alginate, PA-g-CNCs, and ACVA were fabricated. ACVA is a water soluble azo-initiator and is expected to crosslink the PA-g-CNCs once exposed to UV radiation. The efficiency of crosslinking of PA-g-CNCs within the alginate matrix was studied by measuring the increase in thickness of the composite films once exposed to water and mechanical testing in wet and dry conditions.

3.3.1 Indirect Confirmation of Crosslinking

To determine if the addition of ACVA and sequential UV exposure for differing amounts of time induced crosslinking by free-radical polymerization, alginate and PA-g-CNC:Alginate composites were exposed to DI- H_2O for 24 hours, and the percent change in the thickness of the composites was measured. If there was a reduction in the amount of change in thickness from un-crosslinked samples to UV-exposed samples, then it can be inferred that crosslinking has occurred.

As seen in Figure 6, a change in the thickness of the samples following crosslinking and water exposure occurs in the alginate and composites. A controlled decrease with increased UV exposure time does not occur in the samples, indicating that crosslinking is not dependent on UV exposure time. But the apparent changes in thickness are dependent on the amount of modified CNCs added to the alginate with the most pronounced differences in 50:50 PA-g-CNCs. This suggests that by controlling the amount of PA-g-CNCs added to alginate the amount of crosslinking can be modified and tuned.

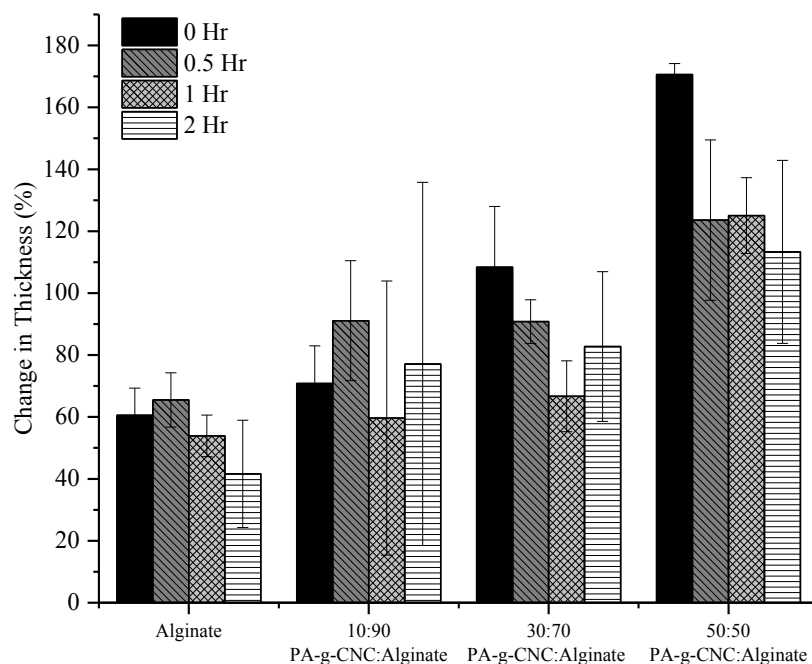


Figure 6. Change in thickness of Alginate and PA-g-CNC:Alginate composites following 24 hours in DI-H₂O measured in percent

Meanwhile, the addition of PA-g-CNCs did cause an increase in the amount of water uptake compared to alginate. This can be explained by a possible disturbance or interruption of the “egg-box” structure occurring inside the alginate following “ionic crosslinking” by calcium ions [75]. The introduction of the PA-g-CNCs hinders the formation of the “egg-box” structure, which in turn causes an increase in the change of thickness. Interestingly there was even apparent crosslinking depending on the time of UV exposure within the alginate samples which suggests that the ACVA causes a crosslinking between the M- and G-chains of alginate, but cannot be determined to be definite because of the high.

3.3.2 Mechanical Analysis: Tensile Testing

Further indication of possible crosslinking caused by azo-initiated free-radical polymerization was determined using mechanical testing of the alginate and PA-g-CNC:Alginate composites in both dry and wet conditions. All testing was conducted at 37°C in both dry and wet conditions for envisioned use in biomedical applications.

When tested at 37°C in dry conditions there was a thermally-induced contraction of the samples as indicated by the elongation at break as seen in Table 2. While the elongation at break increased for

samples with PA-g-CNCs, the Young's modulus only increased when compared to alginate for some of the composites with certain exposure time. The most apparent differences in Young's modulus compared to alginate occurred in the 10:90 PA-g-CNC:Alginate samples for all UV exposure times. This increase in Young's modulus indicates that the crosslinking of 10:90 PA-g-CNC:Alginate samples is more pronounced when compared to alginate and the other nanocomposites. This increase in stiffness of the 10:90 PA-g-CNC:Alginate composites when compared to alginate and the other nanocomposites shows that with increased functionalized CNC content the influence of crosslinking on the mechanical properties when tested in dry conditions lessens. This can be explained once again by the increased disruption of the "egg-box" structure and degradation of crosslinking with increased amount of PA-g-CNCs added to alginate.

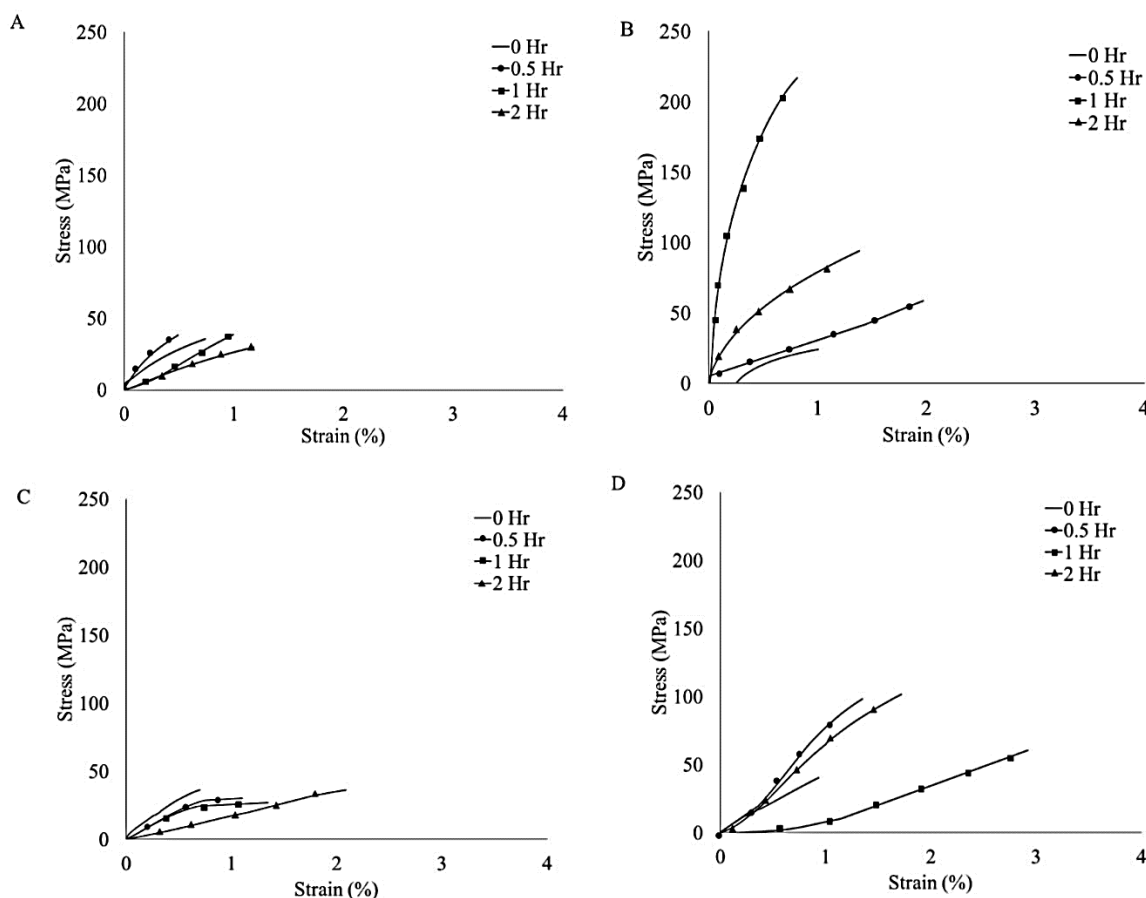


Figure 7. Stress-strain curves of (A) alginate, (B) 10:90 PA-g-CNC:Alginate, (C) 30:70 PA-g-CNC:Alginate, and (D) 50:50 PA-g-CNC:Alginate tested at 37°C following UV exposure for 0.5, 1, and 2 hours. All graphs were normalized to start with a zero strain.

For a majority of the samples, alginate and composites, there was an increase in the Young's modulus from no UV exposure to 0.5 hour of UV exposure followed by a decrease for later times. This indicates that an optimal crosslinking time for dry conditions is 30 minutes. Following 30 minutes of UV exposure there is a decrease in the Young's modulus of the sample indicating that some possible degradation of the samples is occurring. This is especially true of 30:70 PA-g-CNC:Alginate composites.

Since the use of CNCs in biomedical applications has increased in recent years and alginate is a well-researched biomaterial, the composites were tested in physiological-like aqueous conditions using DI-H₂O. As seen in Figure 8, the stress-strain curves follow a more traditional curve, without a thermally induced contraction. While there is a decrease in the Young's modulus and increase in the elongation at break compared to testing in dry conditions, this is expected, and can be attributed to the hydrophilic nature of alginate and CNCs.

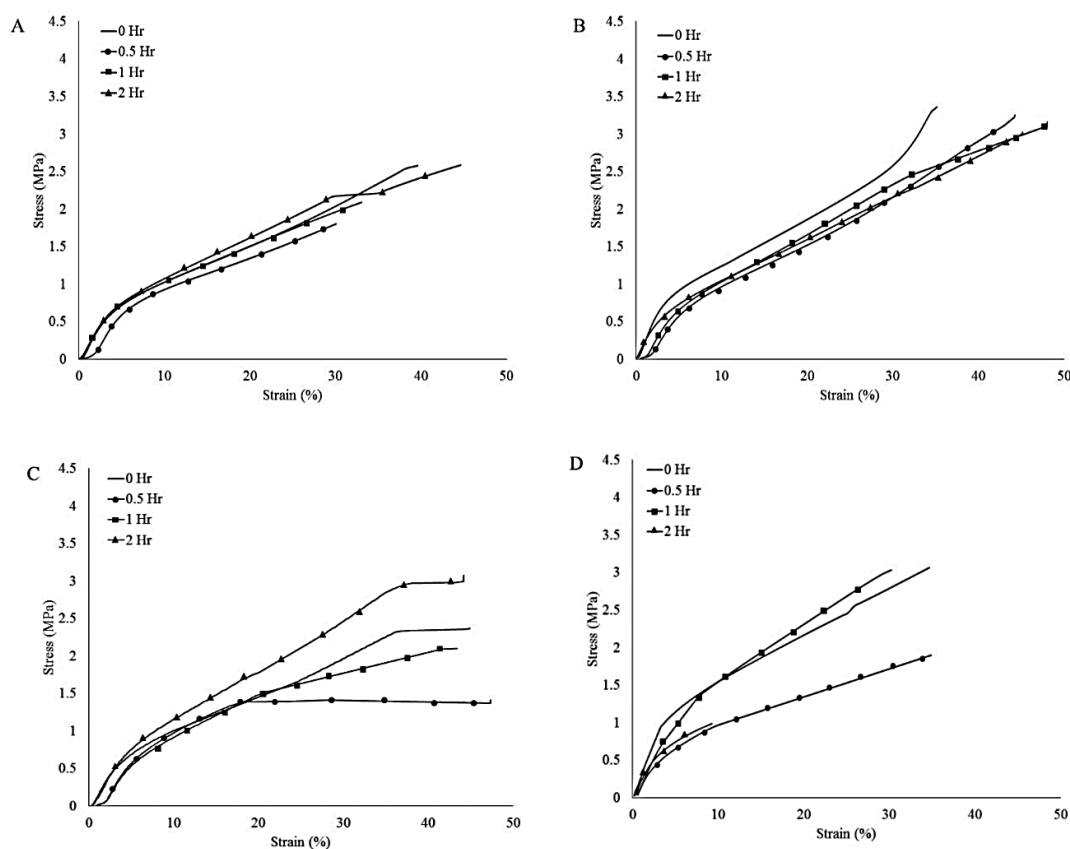


Figure 8. Stress-strain curves of (A) alginate, (B) 10:90 PA-g-CNC:Alginate, (C) 30:70 PA-g-CNC:Alginate, and (D) 50:50 PA-g-CNC:Alginate tested at 37°C in DI-H₂O following UV exposure for 0.5, 1, and 2 hours.

When compared to alginate all the nanocomposites have an increased Young's modulus with or without UV exposure. This shows that the addition of PA-g-CNCs causes a positive change in the mechanical properties of alginate that is not dependent on the UV-induced crosslinking. While there were not significant changes with the Young's modulus following UV exposure because of the large standard deviation in all the composites, there was some increases in Young's modulus in certain samples with specific levels of UV exposure. The only recorded increase in Young's modulus occurred for 30:70 PA-g-CNC:Alginate when exposed for 1 hour. This increase in the Young's modulus can be related to the results of thickness change when exposed to DI-H₂O, because following 1 hour of UV exposure the largest difference occurred between the crosslinked and un-crosslinked sample.

Table 2. Elongation at break and Young's modulus of Alginate and PA-g-CNC:Alginate composites as determined by tensile testing in dry and wet conditions at 37°C following UV exposure

	UV Exposure Time (hr)	Dry Conditions at 37°C		Wet Conditions at 37°C	
		Elongation at Break (%)	Young's Modulus (GPa)	Elongation at Break (%)	Young's Modulus (MPa)
Alginate	0	-1.8±2.0	5.6±3.0	42.7±2.7	16.4±1.5
	0.5	-0.7±1.2	9.0±4.3	41.8±4.3	15.4±2.0
	1	0.1±0.7	3.6±1.9	41.2±4.3	16.8±1.0
	2	-1.0±1.6	4.1±2.4	40.3±7.2	21.1±5.2
10:90 PA-g- CNC:Alginate	0	0.9±1.0	9.1±2.3	44.2±0.4	28.5±3.4
	0.5	0.7±1.2	19.3±1.5	46.0±1.9	17.7±1.7
	1	-2.6±1.5	19.1±3.4	46.0±1.8	21.3±4.2
	2	-0.9±0.2	10.7±5.7	45.0±0.2	22.0±5.2
30:70 PA-g- CNC:Alginate	0	-2.3±0.6	19.1±1.2	44.6±0.5	20.7±2.4
	0.5	-0.6±0.9	4.2±1.5	46.3±1.7	19.0±3.9
	1	-1.3±1.0	4.3±2.3	46.0±1.8	21.3±5.0
	2	-0.6±0.3	1.8±1.5	44.6±0.4	20.5±8.6
50:50 PA-g- CNC:Alginate	0	-1.1±0.2	4.2±0.5	34.7±11.5	29.7±18.1
	0.5	-0.5±0.5	8.4±2.2	34.9±11.6	23.0±5.09
	1	1.3±0.1	1.4±0.5	30.3±9.2	24.9±6.6
	2	-0.2±0.4	6.5±3.3	9.3±4.2	25.2±10.0

For tensile testing, it can be said that in dry conditions the influence of UV-induced crosslinking has a stronger effect on the mechanical properties of alginate, but differed when submerged and tested in liquid. When tested in DI-H₂O the mechanical properties in all composites decreased. This

difference in performance is well known and can be explained by possible leaching of Ca^{+2} ions from the composites, which causes a degradation of the “egg-box” crosslinked structure of alginate [76]. It is hypothesized that the lack of variation between the nanocomposites when mechanically tested and the change in thickness experiments were caused by the lack of applied tension in the water uptake tests. It is suggested that the tensile force applied to the composites causes an easier infiltration of the DI- H_2O within the crosslinked structure of the alginate influenced by ionic coordination of the Ca^{+2} ions and azo-induced radical polymerization. The introduction of water causes a degradation of both types of crosslinking, and this degradation possibly occurs more quickly during tensile testing.

4. Conclusion

A UV-stimuli responsive functionalized CNC and alginate composite was produced and analyzed in physiological conditions for future use in biomedical applications. Functionalized CNCs (PA-g-CNCs) were produced through a simple, environmentally friendly method using 4-pentenoic acid as the solvent and grafting agent following solvent exchange of sulfuric acid derived wood CNCs. The presence of 4-pentenoic acid on the surface of CNCs did not cause a change in the morphology and crystallinity of the CNCs as shown by AFM, DLS, and XRD analysis. Bulk analysis of the PA-g-CNCs indicates the presence of 4-pentenoic acid on the surface the CNCs through TGA, FTIR, and ^{13}C NMR, but limited amount of grafting occurred without any possible quantification. These functionalized CNCs were used to create stimuli-responsive alginate composites through the free radical polymerization of the double bond present on the PA-g-CNC by the azo-initiator ACVA when exposed to UV radiation.

Overall, the addition of PA-g-CNC causes an increase in the mechanical properties of alginate in wet conditions without any apparent dependence in the azo-initiated crosslinking, but crosslinking does occur as indicated by the changes in the thickness of the nanocomposites when submerged in DI- H_2O for 24 hours. In comparison to testing in dry conditions, the addition of PA-g-CNCs and sequential UV-induced crosslinking does cause an improvement of the mechanical properties, especially for 10:90 PA-g-CNC:Alginate composites.

5. Acknowledgements

LGP2 is part of the LabEx Tec 21 (Investissements d’Avenir - grant agreement n°ANR-11-LABX-0030) and of the PolyNat Carnot Institutes (Investissements d’Avenir - grant agreements n° ANR-11-

CARN-030-01). This work been partially supported by the LabEx Tec 21 (Investissements d'Avenir - grant agreement n°ANR-11-LABX-0030).

6. References

- [1] Favier V, Canova G, Cavaillé J, Chanzy H, Dufresne A, Gauthier C. Nanocomposite materials from latex and cellulose whiskers. *Polymers for Advanced Technologies*. 1995;6:351-5.
- [2] Rånby B, Ribí E. Über den feinebau der zellulose. *Experientia*. 1950;6:12-4.
- [3] Yu H, Qin Z, Liang B, Liu N, Zhou Z, Chen L. Facile extraction of thermally stable cellulose nanocrystals with a high yield of 93% through hydrochloric acid hydrolysis under hydrothermal conditions. *Journal of Materials Chemistry A*. 2013;1:3938-44.
- [4] Camarero Espinosa S, Kuhnt T, Foster EJ, Weder C. Isolation of thermally stable cellulose nanocrystals by phosphoric acid hydrolysis. *Biomacromolecules*. 2013;14:1223-30.
- [5] Novo LP, Bras J, García A, Belgacem N, Curvelo AA. Subcritical water: A method for green production of cellulose nanocrystals. *ACS Sustainable Chemistry & Engineering*. 2015;3:2839-46.
- [6] Klemm D, Schumann D, Kramer F, Heßler N, Koth D, Sultanova B. Nanocellulose materials—Different cellulose, different functionality. *Macromolecular symposia: Wiley Online Library*; 2009. p. 60-71.
- [7] Deepa B, Abraham E, Cordeiro N, Mozetic M, Mathew AP, Oksman K, et al. Utilization of various lignocellulosic biomass for the production of nanocellulose: a comparative study. *Cellulose*. 2015;22:1075-90.
- [8] Sacui IA, Nieuwendaal RC, Burnett DJ, Stranick SJ, Jorfi M, Weder C, et al. Comparison of the properties of cellulose nanocrystals and cellulose nanofibrils isolated from bacteria, tunicate, and wood processed using acid, enzymatic, mechanical, and oxidative methods. *ACS Applied Materials & Interfaces*. 2014;6:6127-38.
- [9] García A, Gandini A, Labidi J, Belgacem N, Bras J. Industrial and crop wastes: A new source for nanocellulose biorefinery. *Industrial Crops and Products*. 2016;93:26-38.
- [10] Mariano M, El Kissi N, Dufresne A. Cellulose nanocrystals and related nanocomposites: review of some properties and challenges. *Journal of Polymer Science Part B: Polymer Physics*. 2014;52:791-806.
- [11] Azizi Samir MAS, Alloin F, Dufresne A. Review of recent research into cellulosic whiskers, their properties and their application in nanocomposite field. *Biomacromolecules*. 2005;6:612-26.

- [12] Moon RJ, Martini A, Nairn J, Simonsen J, Youngblood J. Cellulose nanomaterials review: structure, properties and nanocomposites. *Chemical Society Reviews*. 2011;40:3941-94.
- [13] Hubbe MA, Rojas OJ, Lucia LA, Sain M. Cellulosic nanocomposites: a review. *BioResources*. 2008;3:929-80.
- [14] Siqueira G, Bras J, Dufresne A. Cellulosic bionanocomposites: a review of preparation, properties and applications. *Polymers*. 2010;2:728-65.
- [15] Peresin MS, Habibi Y, Zoppe JO, Pawlak JJ, Rojas OJ. Nanofiber composites of polyvinyl alcohol and cellulose nanocrystals: manufacture and characterization. *Biomacromolecules*. 2010;11:674-81.
- [16] Roohani M, Habibi Y, Belgacem NM, Ebrahim G, Karimi AN, Dufresne A. Cellulose whiskers reinforced polyvinyl alcohol copolymers nanocomposites. *European Polymer Journal*. 2008;44:2489-98.
- [17] Bilbao-Sainz C, Bras J, Williams T, Sénechal T, Orts W. HPMC reinforced with different cellulose nano-particles. *Carbohydrate Polymers*. 2011;86:1549-57.
- [18] Siqueira G, Frascini C, Bras J, Dufresne A, Prud'homme R, Laborie M-P. Impact of the nature and shape of cellulosic nanoparticles on the isothermal crystallization kinetics of poly (ϵ -caprolactone). *European Polymer Journal*. 2011;47:2216-27.
- [19] Oksman K, Mathew A, Bondeson D, Kvien I. Manufacturing process of cellulose whiskers/polylactic acid nanocomposites. *Composites Science and Technology*. 2006;66:2776-84.
- [20] Mathew AP, Oksman K, Sain M. The effect of morphology and chemical characteristics of cellulose reinforcements on the crystallinity of polylactic acid. *Journal of Applied Polymer Science*. 2006;101:300-10.
- [21] Mariano M, El Kissi N, Dufresne A. Cellulose nanocrystal reinforced oxidized natural rubber nanocomposites. *Carbohydrate Polymers*. 2016;137:174-83.
- [22] Pasquini D, de Morais Teixeira E, da Silva Curvelo AA, Belgacem MN, Dufresne A. Extraction of cellulose whiskers from cassava bagasse and their applications as reinforcing agent in natural rubber. *Industrial Crops and Products*. 2010;32:486-90.
- [23] Bras J, Hassan ML, Bruzesse C, Hassan EA, El-Wakil NA, Dufresne A. Mechanical, barrier, and biodegradability properties of bagasse cellulose whiskers reinforced natural rubber nanocomposites. *Industrial Crops and Products*. 2010;32:627-33.
- [24] Abraham E, Thomas MS, John C, Pothen L, Shoseyov O, Thomas S. Green nanocomposites of natural rubber/nanocellulose: membrane transport, rheological and thermal degradation characterisations. *Industrial Crops and Products*. 2013;51:415-24.

- [25] Siqueira G, Abdillahi H, Bras J, Dufresne A. High reinforcing capability cellulose nanocrystals extracted from *Syngonanthus nitens* (Capim Dourado). *Cellulose*. 2010;17:289-98.
- [26] Siqueira G, Tapin-Lingua S, Bras J, da Silva Perez D, Dufresne A. Mechanical properties of natural rubber nanocomposites reinforced with cellulosic nanoparticles obtained from combined mechanical shearing, and enzymatic and acid hydrolysis of sisal fibers. *Cellulose*. 2011;18:57-65.
- [27] Huq T, Salmieri S, Khan A, Khan RA, Le Tien C, Riedl B, et al. Nanocrystalline cellulose (NCC) reinforced alginate based biodegradable nanocomposite film. *Carbohydrate Polymers*. 2012;90:1757-63.
- [28] Abdollahi M, Alboofetileh M, Rezaei M, Behrooz R. Comparing physico-mechanical and thermal properties of alginate nanocomposite films reinforced with organic and/or inorganic nanofillers. *Food Hydrocolloids*. 2013;32:416-24.
- [29] Lin N, Bruzzese C, Dufresne A. TEMPO-oxidized nanocellulose participating as crosslinking aid for alginate-based sponges. *ACS Appl Mater Interfaces*. 2012;4:4948-59.
- [30] Ureña-Benavides EE, Brown PJ, Kitchens CL. Effect of jet stretch and particle load on cellulose nanocrystal–alginate nanocomposite fibers. *Langmuir*. 2010;26:14263-70.
- [31] George M, Abraham TE. Polyionic hydrocolloids for the intestinal delivery of protein drugs: alginate and chitosan—a review. *Journal of Controlled Release*. 2006;114:1-14.
- [32] Lee KY, Mooney DJ. Hydrogels for tissue engineering. *Chemical Reviews*. 2001;101:1869-80.
- [33] Drury JL, Mooney DJ. Hydrogels for tissue engineering: scaffold design variables and applications. *Biomaterials*. 2003;24:4337-51.
- [34] Kuo CK, Ma PX. Ionically crosslinked alginate hydrogels as scaffolds for tissue engineering: Part 1. Structure, gelation rate and mechanical properties. *Biomaterials*. 2001;22:511-21.
- [35] Barnett S, Varley S. The effects of calcium alginate on wound healing. *Annals of the Royal College of Surgeons of England*. 1987;69:153.
- [36] Boateng JS, Matthews KH, Stevens HN, Eccleston GM. Wound healing dressings and drug delivery systems: a review. *Journal of Pharmaceutical Sciences*. 2008;97:2892-923.
- [37] Tønnesen HH, Karlsen J. Alginate in drug delivery systems. *Drug Development and Industrial Pharmacy*. 2002;28:621-30.
- [38] Choi B, Park HJ, Hwang S, Park J. Preparation of alginate beads for floating drug delivery system: effects of CO₂ gas-forming agents. *International Journal of Pharmaceutics*. 2002;239:81-91.
- [39] Stockwell A, Davis S, Walker S. In vitro evaluation of alginate gel systems as sustained release drug delivery systems. *Journal of Controlled Release*. 1986;3:167-75.

- [40] Drury JL, Dennis RG, Mooney DJ. The tensile properties of alginate hydrogels. *Biomaterials*. 2004;25:3187-99.
- [41] Lee KY, Rowley JA, Eiselt P, Moy EM, Bouhadir KH, Mooney DJ. Controlling mechanical and swelling properties of alginate hydrogels independently by cross-linker type and cross-linking density. *Macromolecules*. 2000;33:4291-4.
- [42] Habibi Y, Chanzy H, and Vignon, M.R. TEMPO-mediated surface oxidation of cellulose whiskers. *Cellulose*. 2006;6:679-87.
- [43] Saito T, Nishiyama Y, Putaux J-L, Vignon M, Isogai A. Homogeneous suspensions of individualized microfibrils from TEMPO-catalyzed oxidation of native cellulose. *Biomacromolecules*. 2006;7:1687-91.
- [44] Heux L, Chauve G, Bonini C. Nonflocculating and chiral-nematic self-ordering of cellulose microcrystals suspensions in nonpolar solvents. *Langmuir*. 2000;16:8210-2.
- [45] Araki J, Wada M, Kuga S. Steric Stabilization of a Cellulose Microcrystal Suspension by Poly(ethylene glycol) Grafting. *Langmuir*. 2001;17:21-7.
- [46] Siqueira G, Bras J, Dufresne A. New process of chemical grafting of cellulose nanoparticles with a long chain isocyanate. *Langmuir*. 2009;26:402-11.
- [47] Habibi Y. Key advances in the chemical modification of nanocelluloses. *Chemical Society Reviews*. 2014;43:1519-42.
- [48] Habibi Y, Lucia LA, Rojas OJ. Cellulose nanocrystals: chemistry, self-assembly, and applications. *Chemical Reviews*. 2010;110:3479-500.
- [49] Eyley S, Thielemans W. Surface modification of cellulose nanocrystals. *Nanoscale*. 2014;6:7764-79.
- [50] Braun B, Dorgan JR. Single-step method for the isolation and surface functionalization of cellulosic nanowhiskers. *Biomacromolecules*. 2008;10:334-41.
- [51] Sobkowicz MJ, Braun B, Dorgan JR. Decorating in green: surface esterification of carbon and cellulosic nanoparticles. *Green Chemistry*. 2009;11:680-2.
- [52] Cetin NS, Tingaut P, Özmen N, Henry N, Harper D, Dadmun M, et al. Acetylation of cellulose nanowhiskers with vinyl acetate under moderate conditions. *Macromolecular bioscience*. 2009;9:997-1003.
- [53] Sassi J-F, Chanzy H. Ultrastructural aspects of the acetylation of cellulose. *Cellulose*. 1995;2:111-27.

- [54] Yuan H, Nishiyama Y, Wada M, Kuga S. Surface acylation of cellulose whiskers by drying aqueous emulsion. *Biomacromolecules*. 2006;7:696-700.
- [55] Berlio S, Molina-Boisseau S, Nishiyama Y, Heux L. Gas-phase surface esterification of cellulose microfibrils and whiskers. *Biomacromolecules*. 2009;10:2144-51.
- [56] Espino-Perez E, Domenek S, Belgacem N, Sillard C, Bras J. Green process for chemical functionalization of nanocellulose with carboxylic acids. *Biomacromolecules*. 2014;15:4551-60.
- [57] Boujemaoui A, Mongkhontreerat S, Malmström E, Carlmark A. Preparation and characterization of functionalized cellulose nanocrystals. *Carbohydrate Polymers*. 2015;115:457-64.
- [58] Capadona JR, Shanmuganathan K, Tyler DJ, Rowan SJ, Weder C. Stimuli-responsive polymer nanocomposites inspired by the sea cucumber dermis. *Science*. 2008;319:1370-4.
- [59] Dagnon KL, Shanmuganathan K, Weder C, Rowan SJ. Water-triggered modulus changes of cellulose nanofiber nanocomposites with hydrophobic polymer matrices. *Macromolecules*. 2012;45:4707-15.
- [60] Jorfi M, Roberts MN, Foster EJ, Weder C. Physiologically responsive, mechanically adaptive bio-nanocomposites for biomedical applications. *ACS Applied Materials & Interfaces*. 2013;5:1517-26.
- [61] Mendez J, Annamalai PK, Eichhorn SJ, Rusli R, Rowan SJ, Foster EJ, et al. Bioinspired mechanically adaptive polymer nanocomposites with water-activated shape-memory effect. *Macromolecules*. 2011;44:6827-35.
- [62] Way AE, Hsu L, Shanmuganathan K, Weder C, Rowan SJ. pH-responsive cellulose nanocrystal gels and nanocomposites. *ACS Macro Letters*. 2012;1:1001-6.
- [63] Cha R, He Z, Ni Y. Preparation and characterization of thermal/pH-sensitive hydrogel from carboxylated nanocrystalline cellulose. *Carbohydrate Polymers*. 2012;88:713-8.
- [64] Azzam F, Heux L, Putaux J-L, Jean B. Preparation by grafting onto, characterization, and properties of thermally responsive polymer-decorated cellulose nanocrystals. *Biomacromolecules*. 2010;11:3652-9.
- [65] McKee JR, Hietala S, Seitsonen J, Laine J, Kontturi E, Ikkala O. Thermoresponsive nanocellulose hydrogels with tunable mechanical properties. *ACS Macro Letters*. 2014;3:266-70.
- [66] Biyani MV, Jorfi M, Weder C, Foster EJ. Light-stimulated mechanically switchable, photopatternable cellulose nanocomposites. *Polymer Chemistry*. 2014;5:5716-24.
- [67] Biyani MV, Weder C, Foster EJ. Photoswitchable nanocomposites made from coumarin-functionalized cellulose nanocrystals. *Polymer Chemistry*. 2014;5:5501-8.

- [68] Fox JD, Capadona JR, Marasco PD, Rowan SJ. Bioinspired water-enhanced mechanical gradient nanocomposite films that mimic the architecture and properties of the squid beak. *Journal of the American Chemical Society*. 2013;135:5167-74.
- [69] Segal L, Creely J, Martin Jr A, Conrad C. An empirical method for estimating the degree of crystallinity of native cellulose using the X-ray diffractometer. *Textile Research Journal*. 1959;29:786-94.
- [70] Lin N, Dufresne A. Surface chemistry, morphological analysis and properties of cellulose nanocrystals with gradiented sulfation degrees. *Nanoscale*. 2014;6:5384-93.
- [71] Neto WPF, Silvério HA, Dantas NO, Pasquini D. Extraction and characterization of cellulose nanocrystals from agro-industrial residue—Soy hulls. *Industrial Crops and Products*. 2013;42:480-8.
- [72] Roman M, Winter WT. Effect of sulfate groups from sulfuric acid hydrolysis on the thermal degradation behavior of bacterial cellulose. *Biomacromolecules*. 2004;5:1671-7.
- [73] Beck S, Bouchard J. Auto-catalyzed acidic desulfation of cellulose nanocrystals. *Nordic Pulp & Paper Research Journal*. 2014;29:6-14.
- [74] Alemdar A, Sain M. Isolation and characterization of nanofibers from agricultural residues—Wheat straw and soy hulls. *Bioresource Technology*. 2008;99:1664-71.
- [75] Grant GT, Morris ER, Rees DA, Smith PJ, Thom D. Biological interactions between polysaccharides and divalent cations: the egg-box model. *FEBS Letters*. 1973;32:195-8.
- [76] Bajpai SK, Sharma S. Investigation of swelling/degradation behaviour of alginate beads crosslinked with Ca^{2+} and Ba^{2+} ions. *Reactive and Functional Polymers*. 2004;59:129-40.

Chapter 3.3 Incorporation and Release of Bovine Serum Albumin from Cellulose Nanofiber Films for Growth Factor Release Applications

Abstract	192
1. Introduction	193
2. Materials and Methods	195
2.1 Materials	195
2.2 Methods	195
2.2.1 Incorporation of BSA into CNF Films	195
2.2.1.2 Fabrication of BSA-CNF Films	195
2.2.1.2 Diffusion of BSA into CNF Films	196
2.2.2 Characterization of CNF and BSA	196
2.2.2.1 Atomic Force Microscopy (AFM)	196
2.2.2.2 Optical Microscopy	197
2.2.2.3 Dynamic Light Scattering (DLS)	197
2.2.3 Characterization of BSA-CNF Films	197
2.2.3.1 Scanning Electron Microscopy (SEM)	197
2.2.3.2 Fourier Transform Infrared Spectroscopy (FTIR)	197
2.2.3.3 Release Profile of BSA	198
3. Results and Discussion	198
3.1 Characterization of Raw Materials	198
3.2 Loading and Release of BSA by CNF Films	200
3.2.1 Influence of BSA in CNF Film Properties	200
3.2.2 Release Profile of BSA	203
4. Conclusion	205
5. Acknowledgements	205
6. References	205

Incorporation and Release of Bovine Serum Albumin from Cellulose Nanofiber Films for Growth Factor Release Applications

Megan Smyth^{a,b}, E. Johan Foster^c, Julien Bras^{a,b,d}

a. CNRS, LGP2, 461 Rue de la Papeterie, 38402, Saint-Martin-d'Hères, France

b. Université Grenoble Alpes, LGP2, 38000, Grenoble, France

c. Virginia Polytechnic Institute and State University (Virginia Tech), Macromolecules Innovation Institute (MII), Department of Materials Science and Engineering, Blacksburg, Virginia 24061, USA

d. Institut Universitaire de France, 75005, Paris, France

Abstract

Cellulose nanofiber (CNF) films with bovine serum albumin (BSA) incorporated by two different manners were created. The use of CNF as an antimicrobial or drug carrier has gained interest in recent years because of its nanoporous material properties, as well as being biocompatible and renewable. In this work, the use of BSA as a model protein for growth factor delivery by CNF films was studied for the first time. CNF films loaded with BSA by two processes were compared in physiological conditions for possible future use in cell culture as a growth factor carrier. It is suggested that the release profile of BSA from CNF is dependent on loading technique and amount of BSA added.

1. Introduction

The use of cellulose nanofibers (CNF) as a delivery system for drugs or antimicrobial agents has gained interest in recent years. This can be attributed to intrinsic properties of this nanoscaled cellulose such as: renewability, relative low-cost, sustainability, biocompatibility, and biodegradability [1, 2]. CNF is one type of nanocellulose and can be produced in a variety of ways, and depending on production conditions such as source, pre-treatments, mechanical treatments, and post-treatments the properties of the CNF can strongly differ. These properties include surface charge, crystallinity, morphology, and chemical surface groups [3, 4]. Compared to the other type of vegetal-based nanocellulose, cellulose nanocrystals (CNCs), CNF is less crystalline, flexible, and has dimensions of approximately several microns in length and 20-60 nm in diameter depending on the production conditions. CNF has been studied as an additive filler in nanocomposites [5, 6], stabilizer in dispersions [7], use in electronic devices [8, 9], but more importantly for this application as barrier films [10-12]. The use of CNF as a barrier film is facilitated by the nanoporous structure that CNF creates upon drying [13-15]. This

nanostructure, also called nanopaper, is due to the hydrogen bonding occurring between the surface of the nanofibers that produces an intertwined network of CNF. This network can be used to entrap active molecules such as drugs, antimicrobial agents, proteins, and growth factors [3, 16]. The first instance of CNF films used for drug delivery was done less than five years ago by Kolakovic et al. in 2013, and they determined that drug delivery was dependent on the diffusion control by the structure of the CNF. The CNF facilitated a controlled release over 3 months, with very small amounts being released every 24 hours [17]. Other techniques, besides incorporation through diffusion or mixing formation, have been employed to impart releasable factors to CNF such as: microencapsulation of an active compound and then embedding the microcapsule into a CNF [18-20], multilayered systems or coatings of CNF with cyclodextrins [21-23], and grafting of active agents to surface of CNF [24, 25]. Concerning entrapment, Valo et al. showed that protein coated drug particle release from CNF aerogels is dependent on CNF source [20], and Lavonie et al. proved that cyclodextrin and caffeine can be entrapped within CNF-based paper coatings with controlled release [22, 23, 26]. These last two examples are of importance to food packaging applications.

The use of CNF in biomedical applications has gained interest in recent years because of its favorable properties like low cytotoxicity, renewability, and biocompatibility [27]. While CNF membranes have been used as carriers for drug delivery [13, 16, 28-30], there has not been a focus on the use of CNF films for the release of proteins or growth factors. Growth factors are commonly employed in the development of biocompatible materials, also called biomaterials, for tissue engineering applications. These peptide regulator molecules are found in all tissues and can mediate the effect of hormones on cells, cell-cell metabolic activity, as well as differentiation [31]. Cell fate or differentiation can be determined by growth factors, which can be added in culture *in vitro*, but during *in vivo* are either secreted by the individual cell or by nearby niche cells. Growth factors are closely regulated during the cell differentiation process [32]. The use of growth factors for controlled release in biomedical applications has been extensively reviewed [31, 33-35], and are most commonly incorporated by tethering to the substrate [36], heparin-mediated release [37], hydrogel entrapment [38-40], and encapsulation by emulsion [41-43].

Bovine serum albumin (BSA) is a commonly used model protein in release studies. The only instance of BSA used in combination with nanocellulose for controlled release was conducted by Müller et al. in 2013. This study compared the loading and release profile of BSA in solution from bacterial nanocellulose (BNC) membrane, as hydrogels or freeze-dried aerogels. They determined that the controlled release of BSA from BNC was dependent on the time, temperature, concentration, and pre-

swelling conditions, but that BNC hydrogels had a higher capacity for BSA uptake compared to the aerogels. These results suggested that BNC can be modulated to control BSA release [44]. One drawback of this study is the difficulty to process BNC compared to CNF, and the limited amount of BSA introduced into the BNC construct.

This study investigates the use of thin CNF films for the moderated release of BSA in physiological conditions, which was added in two different manners – diffusion loading and by mixing. Determination of BSA loading influence was analyzed using Fourier transform infrared spectroscopy, scanning electron microscopy, and bicinchoninic acid (BCA) assay.

2. Materials and Methods

2.1 Materials

A 2 % wt suspension of enzymatically pre-treated CNF from wood pulp (Domsjö) was purchased from Centre Technique du Papier (CTP) (France). Bovine serum albumin (BSA), calcium chloride (CaCl_2), phosphate buffer solution (PBS), bicinchoninic acid (BCA), and Copper (II) sulfate pentahydrate were purchased from Sigma-Aldrich (USA).

2.2 Methods

2.2.1 Incorporation of BSA into CNF Films

Two techniques were used to introduce BSA into CNF films. One, which will be referred to as *BSA-CNF Films* and *Diffusion of BSA into CNF Films*.

2.2.1.2 Fabrication of BSA-CNF Films

BSA was added to a 1 wt% suspension of CNF at 0.1 wt% (10:1 CNF:BSA w:w dry content), 0.25 wt% (4:1 CNF:BSA w:w dry content), and 0.5 wt% (2:1 CNF:BSA w:w dry content) by ultraturax for 2 minutes. Following mixing, the suspensions were casted into a 12-well plate and placed in a desiccator under vacuum for 30 minutes. Followed by drying for 12 hours at 37°C at ambient relative humidity. A similar protocol was done for CNF films without any BSA. Density or basis weight of CNF and BSA-CNF films was determined using the following equation:

$$\text{Density (g/m}^2\text{)} = \frac{\text{Mass of CNF film/Composite}}{\text{Area of CNF film/Composite}} \quad (\text{Eq 1.})$$

Results are reported as average of three samples.

2.2.1.2 Diffusion of BSA into CNF Films

Following the protocol of Müller et al with some modification [44]. CNF films were prepared by solvent casting a 1% wt suspension of CNF onto a teflon mold and allowed to dry at ambient conditions for 5 days. 22 mm diameter specimens from CNF films were pre-soaked in deionized water (DI-H₂O) for 1 hour at room temperature. CNF samples were then placed into 10 mL of BSA solutions of 0.1 wt%, 0.25 wt%, 0.5 wt%, and 1 wt% in PBS for 48 hours at 37°C under shaking (50 rpm).

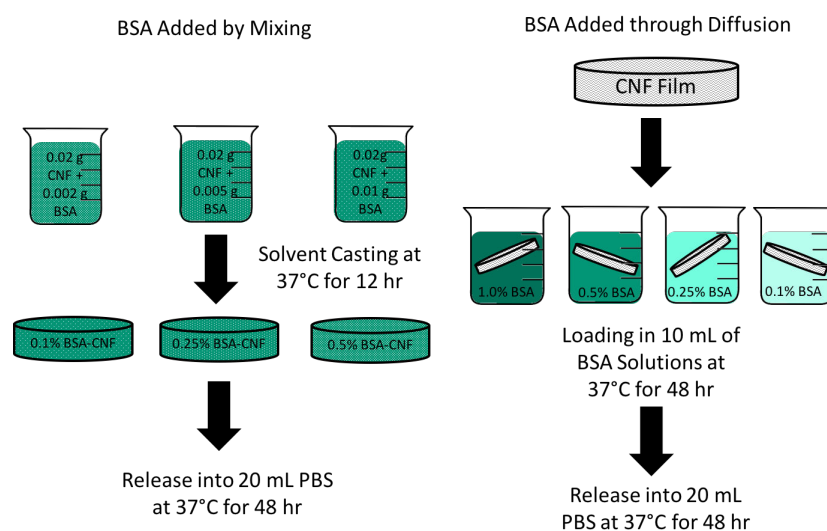


Figure 1. Schematic of CNF-BSA film fabrication and loading of CNF with BSA by diffusion

2.2.2 Characterization of CNF and BSA

2.2.2.1 Atomic Force Microscopy (AFM)

A suspension of approximately 0.2 mL 0.0001 wt% of CNF was prepared, and placed on the surface of a cleaved mica plate. The CNF coated mica plate were dried overnight at ambient conditions, and then analyzed using atomic force microscopy. Images were acquired using tapping mode with a Nanoscope IIA microscope from Veeco Instruments (Plainview, New York, USA) at a frequency of 265-340 Hz. Silicon cantilevers with a curvature of 10-15 nm were used (OTESPA®, Bruker, Billerica, Massachusetts, USA). AFM images were analyzed using Nanoscope Analysis (Plainview, New York, USA) and ImageJ (U. S. National Institutes of Health, Bethesda, Maryland, USA).

2.2.2.2 Optical Microscopy

A dilute suspension of CNF was prepared and placed between a glass lamina for optical microscopy imaging to characterize the quality of the CNF. Images were acquired using a Zeiss Imager.M1m Axio microscope (Zeiss, Germany) and analyzed using Axiovision SE64 (Zeiss, Germany).

2.2.2.3 Dynamic Light Scattering (DLS)

To determine the size of the nanoparticles, dynamic light scattering was carried out using a Vasco Particle Size Meter (Cordouan Technologies, Pessac, France). Ten measurements with 60 second time step and a noise ratio of 1.06 were carried out for each sample in triplicate. The polydispersion index of the DLS measurements was under 0.2 in order to determine if the measurements are precise. The measurements were collected and analyzed using nanoQ software (Cordouan Technologies, Pessac, France). The cumulative method was used at the hydrodynamic diameter (z^*) was measured. DLS analysis does not measure the actual dimensions of the particle, only the change in intensity of the scattered light to calculate the hydrodynamic diameter. All results are reported in average \pm standard deviation from three separate scans.

2.2.3 Characterization of BSA-CNF Films

2.2.3.1 Scanning Electron Microscopy (SEM)

SEM images of the BSA-CNF films and solvent casted CNF film for thickness measurements and to observe possible BSA incorporation were obtained using a Quanta200[®] (Netherlands). Samples were attached to a holder, coated with a thin layer of Au/Pb to create a conductive charge, and scanned using an accelerated voltage of 10 kV and a working distance of 10.3 mm. An Everhart Thornley-Secondary electron detector (ETD) was employed. 50 thickness measurements for each sample was performed using ImageJ (U.S. National Institute of Health, USA) with values reported as average \pm standard deviation.

2.2.3.2 Fourier Transform Infrared Spectroscopy (FTIR)

Fourier Transform Infrared Spectroscopy (FTIR) was done on BSA-CNF composite films using a Perkin Elmer Spectrum One spectrometer (Waltham, Massachusetts, USA). 32 scans from 4000-500 cm^{-1} with a resolution of 1 cm^{-1} were carried out and analyzed using Spectrum software (Perkin Elmer, Waltham, Massachusetts, USA).

2.2.3.3 Release Profile of BSA

Release of BSA in physiological conditions was conducted following a modified protocol of Müller et al. [44]. Specimens of CNF with diameter of 22 mm with BSA incorporated by mixing or diffusion were placed into 20 mL of PBS at 37 °C for 48 hours under shaking (70 rpm) with 100 µL aliquots taken at numerous time points (1, 5, 10, 15, 20, 30 minutes, 1, 2, 3, 4, 24, and 48 hours) to determine the release profile of BSA from CNF. The release profile of BSA from CNF films was analyzed using bicinchoninic acid (BCA) assay. The BCA assay reagent is comprised of BCA and Copper (II) sulfate pentahydrate in 50:1 ratio. A calibration curve of BSA from 0 to 5000 µg/mL was created from a stock-solution of 2 mg/mL of BSA. 20 µL of each aliquot was transferred to a 96-well plate and 180 µL of the BCA assay reagent was added. The samples were conditioned at 60°C for 30 minutes, and the absorbance was read at 562 nm. All results were conducted in triplicate.

3. Results and Discussion

3.1 Characterization of Raw Materials

Commercial cellulose nanofibers produced from enzymatically pre-treated softwood pulp was previously characterized by Bardet et al. to determine the morphology and crystallinity. CNF fibers diameter of approximately 5 nm and a crystallinity index of 77% [45]. The CNF fibers were composed of 88% cellulose as reported in a previous study by the authors reported in Chapter 4.2, which is in accordance with literature [46]. As seen in Figure 2, following fibrillation that CNF suspension still retains larger fibers (A-C) and is heterogeneous. This heterogeneity can negatively contribute to the quality of the CNF, which can affect the material properties of the CNF films.

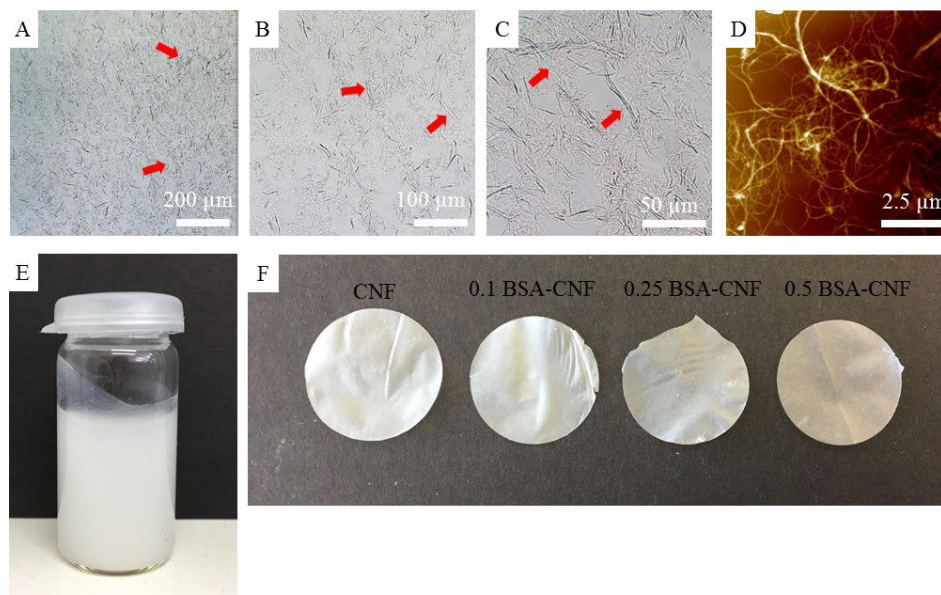


Figure 2. Optical microscopy (A-C) and AFM (D) images of CNF suspension displaying the fibrillation of CNF with residual fiber content as seen in the optical microscopy images. Images of (E) 1 wt% CNF suspension and (F) CNF and BSA-CNF films

Another study by the authors (Chapter 3.4) explored the mechanical and material properties of CNF films in aqueous conditions. The porosity of CNF films, casted in ambient conditions for 5 days, in water was determined by thermoporometry using a technique developed by Driemeier et al.[47]. It was reported that solvent-casted CNF films had pores with sizes between 1-200 nm, without any specific characteristics in a certain size range (Chapter 4.2). Dynamic light scattering of BSA within water shows that BSA has a diameter of 42 ± 11 nm, which is between the size of the pores present in the CNF films. This indicates that BSA particles are small enough to fit within CNF pores when CNF is exposed to liquid, which helps in the diffusion of BSA into CNF for future release.

3.2 Loading and Release of BSA by CNF Films

3.2.1 Influence of BSA in CNF Film Properties

The BSA-CNF films were characterized to determine if the adsorption of BSA occurred. The introduction of BSA to CNF by mixing and solvent casting caused morphological and chemical changes the introduction of BSA to CNF.

Table 1. Characterization of CNF, BSA-CNF films, and Release of BSA

	Thickness (μm)	Basis Weight (g/m^2)	BSA Loaded (μg)	BSA Released (μg)
CNF	24.4 ± 1.6	38.6		
CNF + 0.1% BSA			~ 7000	~ 100
CNF + 0.25% BSA			~ 10000	~ 300
CNF + 0.5% BSA			~ 12000	~ 220
CNF + 1.0% BSA			~ 13000	~ 300
0.1 BSA-CNF	14.1 ± 0.8	40.9	~ 2000	~ 150
0.25 BSA-CNF	11.8 ± 0.6	41.1	~ 5000	~ 650
0.5 BSA-CNF	12.8 ± 0.9	47.9	~ 10000	~ 1500

The addition of BSA caused a slight decrease in the thickness of the CNF samples when compared to CNF prepared in the same manner, but without any BSA. This decrease can be because of a possible higher removal of air during film preparation. The addition of BSA to the CNF caused a “bubbling” of the solution when put under vacuum because the BSA, which consists of proteins, absorbs on the boundary surface and can act as a type of foam stabilizer [48]. The removal of this increased gas by vacuum cause the films to become denser than with just CNF alone. CNF films had a thickness of $24.4 \pm 1.6 \mu\text{m}$, while BSA-CNF composite films had thicknesses of $14.1 \pm 0.8 \mu\text{m}$, $11.8 \pm 0.6 \mu\text{m}$, and $12.8 \pm 0.9 \mu\text{m}$, for 0.1% BSA-CNF, 0.25% BSA-CNF, and 0.5% BSA-CNF, respectively.

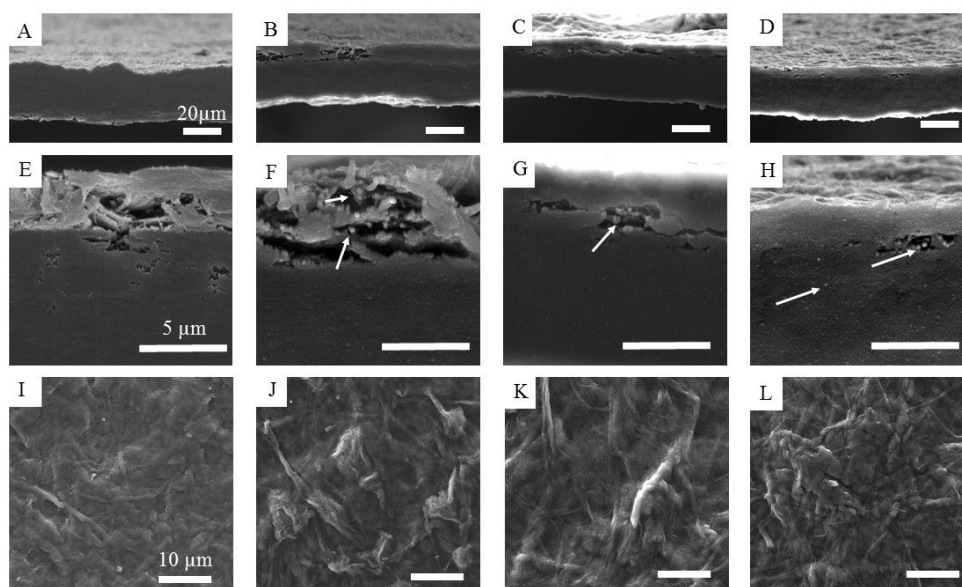


Figure 3. SEM images of solvent casted (A, E, I) CNF films with (B, F, J) 0.1% BSA, (C, G, K) 0.25% BSA, and (D, H, L) 0.5% BSA added. A-H are images to show the inner structure of cut CNF films with round, BSA particles present. I-L are surface images with BSA entrapped within the fiber structure

As seen in the images in Figure 3, the addition of the BSA to the CNF coincides with the appearance of circular BSA particles on the surface of the CNF. This is especially evident in the images of the thickness of the BSA-CNF samples. The BSA is shown to attach to the CNF fibers and remain entrapped within the composite upon solvent casting.

The FTIR spectra of BSA, CNF, and BSA-CNF films were analyzed to determine the presence of BSA. As seen in Figure 4, BSA has distinct peaks at 1650 cm^{-1} and 1540 cm^{-1} due to two distinct amide bands. The bending vibration of N-H, or amide band II, is present at 1540 cm^{-1} , and at 1650 cm^{-1} is the amide I band, which corresponds to the stretching vibrations of C=O bonds [49]. This peak at 1650 cm^{-1} is also present in the CNF sample, but is not as pronounced as in BSA and BSA-CNF films which indicates that BSA has been incorporated into the CNF films.

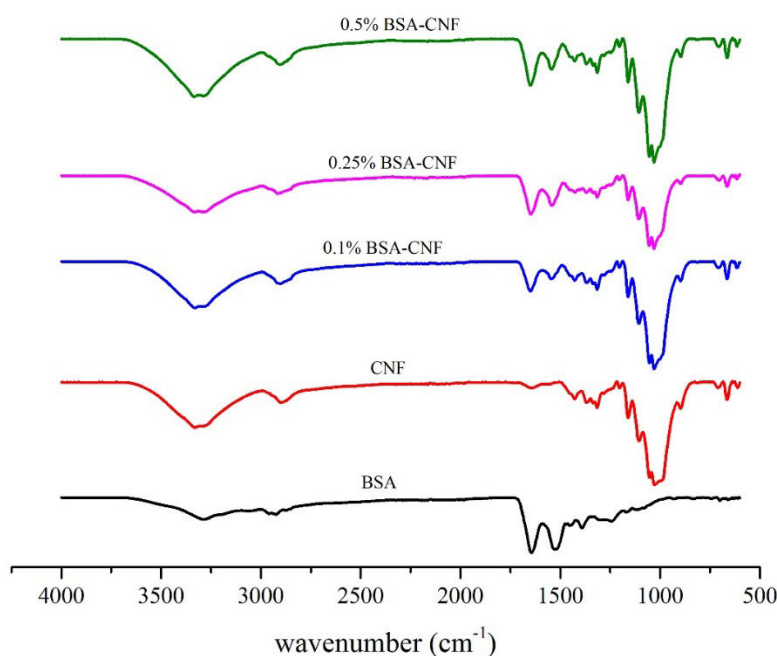


Figure 4. FTIR spectra of BSA, CNF, 0.1% BSA-CNF, 0.25% BSA-CNF, and 0.5% BSA-CNF with apparent peaks indicating the incorporation of BSA within the BSA-CNF films

While all of the spectra exhibit C-H vibrations between $2800\text{--}3050\text{ cm}^{-1}$, they are more intense for the cellulose based samples because of the asymmetric and symmetric CH_2 groups present in the CNF. Characteristic peaks of cellulose include C-O stretching at 1061 cm^{-1} and at 897 cm^{-1} for the C-H

rocking [50]. These peaks are only present in the CNF and BSA-CNF films, which indicates that the addition of the BSA does not change the chemical structure of the CNF.

The amount of BSA released and the amount loaded into the CNF can be controlled by the fabrication technique, and even for loading time in the case of CNF soaked in BSA. The uptake of the BSA increases with time as shown in Figure 6. The amount of BSA loaded into solvent casted CNF films, as determined by BCA assay, was higher compared to when BSA was mixed and solvent casted with CNF. While the amount of BSA added to the CNF film increased with increased BSA content, the range was still approximately 7000-13000 μg with less variance with CNF immersed in suspensions with higher amounts of BSA.

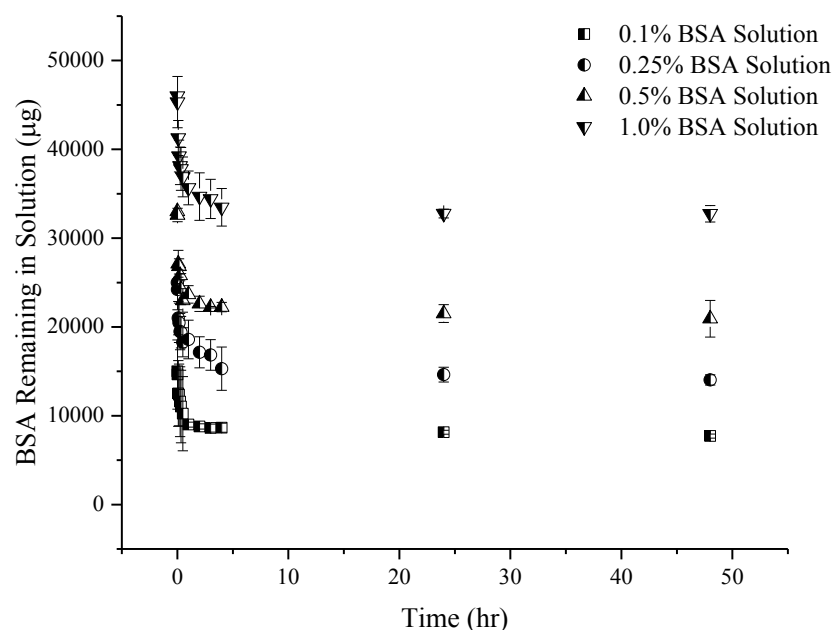


Figure 5. Amount of BSA remaining in solution during CNF film loading by diffusion for 48 hours in PBS at 37°C as determined by BCA assay

This dependence on protein concentration and loading time is a similar conclusion made by Müller et al. using a similar loading protocol, but in this case using BNC hydrogels and aerogels. The amount loaded into the BNC constructs ranged from 500-18000 μg depending on the protein amount and if the BNC was freeze dried or never dried. These values are in accordance to what has been reported, even for thin CNF films with less volume and porosity.

3.2.2 Release Profile of BSA

BSA-CNF films and CNF films with BSA loaded by diffusion were exposed for 48 hours at 37°C in PBS to replicate physiological-like or cell culture conditions. The amount of BSA released from the samples prepared in different manners are presented in Figure 6. As noted in the figure, amount of BSA released is dependent on the amount of loading, and technique of incorporation. The amount of BSA loaded by diffusion was determined using a BCA assay and is reported in Figure 5 following a modified protocol of Müller et al. [44].

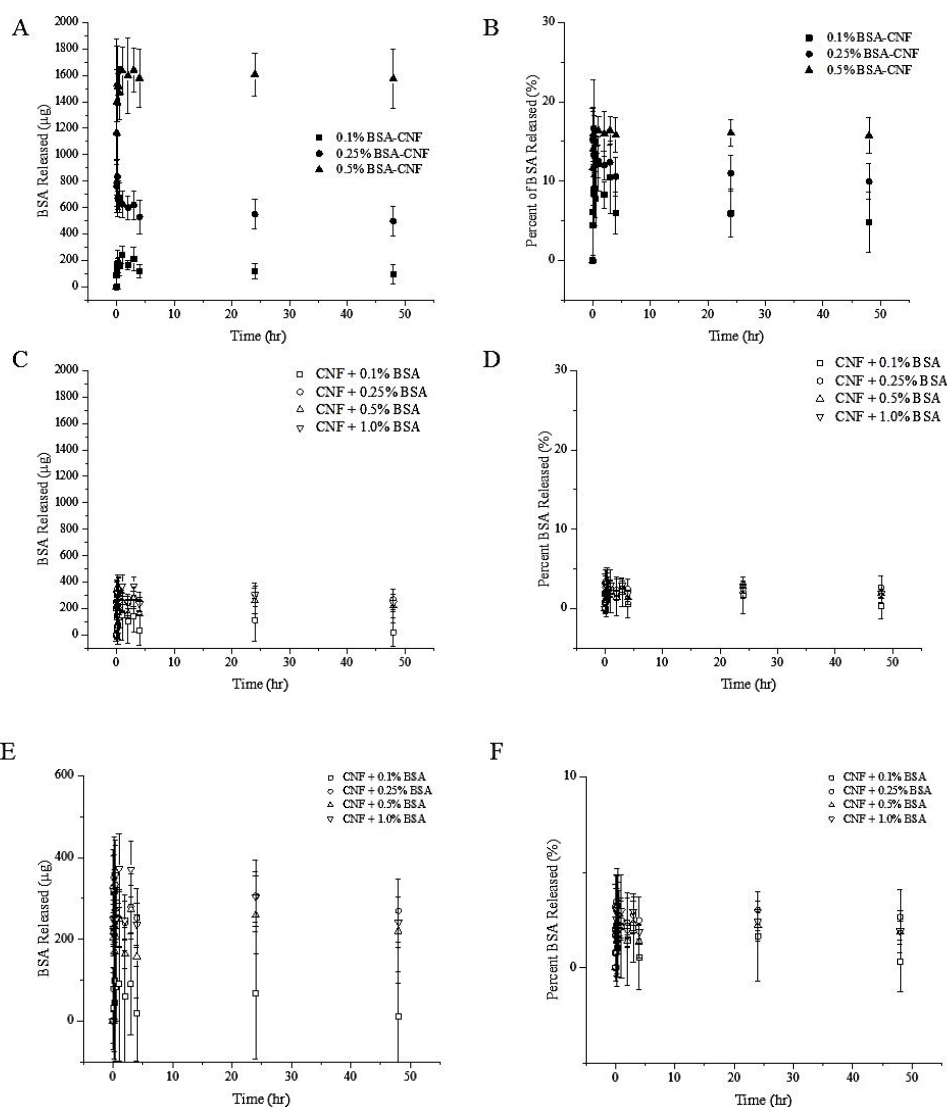


Figure 6. Release of BSA from CNF in A, C) micrograms, B, D) percentage of CNF added for A, B) BSA-CNF composites and C, D) BSA added by diffusion for 48 hours in PBS at 37°C as determined by BCA assay with a zoom from E) 0-600 µg and F) 0-10% for CNF+BSA solutions.

CNF films loaded by diffusion had a lower percentage of release of the incorporated BSA compared to BSA-CNF composites. The amount of loading within the samples was higher, but the release was much lower. This small amount of release can be attributed to the fact that BSA remains entrapped within the already hydrated sample. The BSA-CNF films are dry, and with exposure to PBS become swollen and release any incorporated BSA. For BSA-CNF films a larger amount of the BSA within each sample was released (~5-15%). The percentage released was lower for samples with lower BSA amounts. This can be caused by the increased entrapment by the CNF fibers since there is a higher proportion of CNF fibers compared to BSA particles.

All samples had an initial burst release which plateau around 3 hours and remained at this level until the end of the test at 48 hours. While the percentage and amount of BSA released for samples prepared by diffusion was much lower than reported for BNC hydrogels and areogels (175 μg vs. 4 mg), this can be attributed to the fact that the CNF films are much less porous than the BNC hydrogels and areogels and have a smaller volume ($1.22 \times 10^{-4} \text{ cm}^3$ vs. 1.06 cm^3). This lower percentage can also be due to more BSA remaining entrapped within the fibers of the CNF films after 48 hours in PBS at 37°C. The BSA that remains following release can be of importance in applications where a washing step is required, or where prolonged release following media replacement is necessary which is a common requirement in many biomedical applications.

The differing fabrication techniques display that the amount of BSA released can be controlled. The amount of BSA released ranges from approximately 20 μg to 1700 μg depending on the amount of BSA added and the technique with CNF loaded by diffusion released less BSA. This can be of importance to researchers if the amount of growth factor or protein concentration needs to be within a specific range. Overall, with increased BSA amount either mixed during the creation of BSA-CNF films or added by diffusion causes an increase in the amount released.

Müller et al. reported a dependence on the type of BNC-based construct (freeze dried areogels vs. never dried hydrogels) for the amount of BSA loaded and released. BNC hydrogels allowed for a higher amount of BSA to be loaded via diffusion and therefore have a higher amount released. The percentage of release is much higher for the BNC hydrogels and aerogels compared to what has been reported in this study. This lack of complete release of BSA from the CNF films compared to the BNC hydrogels and aerogels demonstrates that CNF has a stronger adsorption of the BSA to the surface of the fibers as characterized by SEM in Section 3.2.1. This interaction can be of use to researchers for long term cell culture where media replacement is required since it was determined that the BNC constructs do

not retain more than 1000 μg after release for 48 hours [44]. The use of these films within cell culture or differentiation applications can benefit from this moderate release since expansion of cell lines or differentiation requires cell media to be changed approximately every 48 to 72 hours. Because the BSA remains within the CNF films after this time, additional BSA can be released with the introduction of new aqueous media, which cannot occur within the BNC constructs.

4. Conclusion

The use of BSA as a model protein for growth factor delivery has long been of use to researchers. In this work, the release profile of BSA added to CNF by diffusion or mixing in CNF suspension to create BSA-CNF films was compared. It has been shown that BSA is easily incorporated into the BSA-CNF films by SEM and FTIR with qualitative results. BSA can be loaded into CNF films by diffusion as illustrated by the decrease of the amount of BSA in solution as shown by BCA assay. The amount of BSA released by either film or diffusion is dependent on the amount of BSA within the CNF film. BSA-CNF films formed by mixing have a larger amount and percentage of BSA released compared to CNF films loaded by diffusion, but both samples have a low percentage of release. This can be caused by possible high entrapment of the BSA by the CNF fibers within the film. Overall, these results show that CNF films can be used to release BSA in controlled amounts depending on concentration of BSA added and fabrication technique, which can be advantageous for applications which require media changes such as cell culture, expansion, and differentiation.

5. Acknowledgements

LGP2 is part of the LabEx Tec 21 (Investissements d'Avenir - grant agreement n°ANR-11-LABX-0030) and of the PolyNat Carnot Institutes (Investissements d'Avenir - grant agreements n° ANR-11-CARN-030-01). This work been partially supported by the LabEx Tec 21 (Investissements d'Avenir - grant agreement n°ANR-11-LABX-0030). AFM image of CNF suspension was used with permission from Charlene Reverdy.

6. References

- [1] Klemm D, Kramer F, Moritz S, Lindström T, Ankerfors M, Gray D, et al. Nanocelluloses: A new family of nature-based materials. *Angewandte Chemie International Edition*. 2011;50:5438-66.
- [2] Dufresne A. Nanocellulose: a new ageless bionanomaterial. *Materials Today*. 2013;16:220-7.

- [3] Jonoobi M, Oladi R, Davoudpour Y, Oksman K, Dufresne A, Hamzeh Y, et al. Different preparation methods and properties of nanostructured cellulose from various natural resources and residues: a review. *Cellulose*. 2015;22:935-69.
- [4] Klemm D, Schumann D, Kramer F, Heßler N, Koth D, Sultanova B. Nanocellulose materials—Different cellulose, different functionality. *Macromolecular symposia*: Wiley Online Library; 2009. p. 60-71.
- [5] Siqueira G, Tapin-Lingua S, Bras J, da Silva Perez D, Dufresne A. Mechanical properties of natural rubber nanocomposites reinforced with cellulosic nanoparticles obtained from combined mechanical shearing, and enzymatic and acid hydrolysis of sisal fibers. *Cellulose*. 2011;18:57-65.
- [6] Siqueira G, Bras J, Dufresne A. Cellulosic bionanocomposites: a review of preparation, properties and applications. *Polymers*. 2010;2:728-65.
- [7] Andresen M, Johansson L-S, Tanem BS, Stenius P. Properties and characterization of hydrophobized microfibrillated cellulose. *Cellulose*. 2006;13:665-77.
- [8] Torvinen K, Sievänen J, Hjelt T, Hellén E. Smooth and flexible filler-nanocellulose composite structure for printed electronics applications. *Cellulose*. 2012;19:821-9.
- [9] Hoeng F, Denneulin A, Bras J. Use of nanocellulose in printed electronics: a review. *Nanoscale*. 2016;8:13131-54.
- [10] Lavoine N, Desloges I, Dufresne A, Bras J. Microfibrillated cellulose - its barrier properties and applications in cellulosic materials: a review. *Carbohydrate Polymers*. 2012;90:735-64.
- [11] Siró I, Plackett D. Microfibrillated cellulose and new nanocomposite materials: a review. *Cellulose*. 2010;17:459-94.
- [12] Minelli M, Baschetti MG, Doghieri F, Ankerfors M, Lindström T, Siró I, et al. Investigation of mass transport properties of microfibrillated cellulose (MFC) films. *Journal of Membrane Science*. 2010;358:67-75.
- [13] Lavoine N, Desloges I, Bras J. Microfibrillated cellulose coatings as new release systems for active packaging. *Carbohydrate Polymers*. 2014;103:528-37.
- [14] Sehaqui H, Zhou Q, Ikkala O, Berglund LA. Strong and tough cellulose nanopaper with high specific surface area and porosity. *Biomacromolecules*. 2011;12:3638-44.
- [15] Sehaqui H, Zhou Q, Berglund LA. High-porosity aerogels of high specific surface area prepared from nanofibrillated cellulose (NFC). *Composites Science and Technology*. 2011;71:1593-9.

- [16] Kolakovic R, Peltonen L, Laukkanen A, Hirvonen J, Laaksonen T. Nanofibrillar cellulose films for controlled drug delivery. *European Journal of Pharmaceutics and Biopharmaceutics*. 2012;82:308-15.
- [17] Kolakovic R, Peltonen L, Laukkanen A, Hellman M, Laaksonen P, Linder MB, et al. Evaluation of drug interactions with nanofibrillar cellulose. *European Journal of Pharmaceutics and Biopharmaceutics*. 2013;85:1238-44.
- [18] Zhai F, Li D, Zhang C, Wang X, Li R. Synthesis and characterization of polyoxometalates loaded starch nanocomplex and its antitumoral activity. *European journal of medicinal chemistry*. 2008;43:1911-7.
- [19] Marques HMC. A review on cyclodextrin encapsulation of essential oils and volatiles. *Flavour and fragrance journal*. 2010;25:313-26.
- [20] Valo H, Arola S, Laaksonen P, Torkkeli M, Peltonen L, Linder MB, et al. Drug release from nanoparticles embedded in four different nanofibrillar cellulose aerogels. *European Journal of Pharmaceutical Sciences*. 2013;50:69-77.
- [21] Liu K, Chen L, Huang L, Ni Y, Sun B. Enhancing antibacterium and strength of cellulosic paper by coating triclosan-loaded nanofibrillated cellulose (NFC). *Carbohydrate Polymers*. 2015;117:996-1001.
- [22] Lavoine N, Guillard V, Desloges I, Gontard N, Bras J. Active bio-based food-packaging: Diffusion and release of active substances through and from cellulose nanofiber coating toward food-packaging design. *Carbohydrate Polymers*. 2016;149:40-50.
- [23] Lavoine N, Tabary N, Desloges I, Martel B, Bras J. Controlled release of chlorhexidine digluconate using β -cyclodextrin and microfibrillated cellulose. *Colloids and Surfaces B: Biointerfaces*. 2014;121:196-205.
- [24] Saini S, Belgacem MN, Salon M-CB, Bras J. Non leaching biomimetic antimicrobial surfaces via surface functionalisation of cellulose nanofibers with aminosilane. *Cellulose*. 2016;23:795-810.
- [25] Saini S, Belgacem N, Mendes J, Elegir G, Bras J. Contact antimicrobial surface obtained by chemical grafting of microfibrillated cellulose in aqueous solution limiting antibiotic release. *ACS Applied Materials & Interfaces*. 2015;7:18076-85.
- [26] Lavoine N, Desloges I, Sillard C, Bras J. Controlled release and long-term antibacterial activity of chlorhexidine digluconate through the nanoporous network of microfibrillated cellulose. *Cellulose*. 2014;21:4429-42.

- [27] Jorfi M, Foster EJ. Recent advances in nanocellulose for biomedical applications. *Journal of Applied Polymer Science*. 2015;132:41719.
- [28] Kolakovic R, Peltonen L, Laaksonen T, Putkisto K, Laukkanen A, Hirvonen J. Spray-dried cellulose nanofibers as novel tablet excipient. *Aaps Pharmscitech*. 2011;12:1366-73.
- [29] Kolakovic R, Laaksonen T, Peltonen L, Laukkanen A, Hirvonen J. Spray-dried nanofibrillar cellulose microparticles for sustained drug release. *International Journal of Pharmaceutics*. 2012;430:47-55.
- [30] Cozzolino CA, Nilsson F, Iotti M, Sacchi B, Piga A, Farris S. Exploiting the nano-sized features of microfibrillated cellulose (MFC) for the development of controlled-release packaging. *Colloids and Surfaces B: Biointerfaces*. 2013;110:208-16.
- [31] Lind M. Growth factors: possible new clinical tools: a review. *Acta Orthopaedica Scandinavica*. 1996;67:407-17.
- [32] Murry CE, Keller G. Differentiation of embryonic stem cells to clinically relevant populations: lessons from embryonic development. *Cell*. 2008;132:661-80.
- [33] Discher DE, Mooney DJ, Zandstra PW. Growth factors, matrices, and forces combine and control stem cells. *Science*. 2009;324:1673-7.
- [34] Whitaker M, Quirk R, Howdle S, Shakesheff K. Growth factor release from tissue engineering scaffolds. *Journal of Pharmacy and Pharmacology*. 2001;53:1427-37.
- [35] Tabata Y. Tissue regeneration based on growth factor release. *Tissue Engineering*. 2003;9:5-15.
- [36] Hui EE, Bhatia SN. Micromechanical control of cell–cell interactions. *Proceedings of the National Academy of Sciences*. 2007;104:5722-6.
- [37] Sakiyama-Elbert SE, Hubbell JA. Controlled release of nerve growth factor from a heparin-containing fibrin-based cell ingrowth matrix. *Journal of Controlled Release*. 2000;69:149-58.
- [38] Drumheller PD, Elbert DL, Hubbell JA. Multifunctional poly (ethylene glycol) semi-interpenetrating polymer networks as highly selective adhesive substrates for bioadhesive peptide grafting. *Biotechnology and Bioengineering*. 1994;43:772-80.
- [39] Cruise GM, Scharp DS, Hubbell JA. Characterization of permeability and network structure of interfacially photopolymerized poly (ethylene glycol) diacrylate hydrogels. *Biomaterials*. 1998;19:1287-94.
- [40] Park H, Temenoff JS, Holland TA, Tabata Y, Mikos AG. Delivery of TGF- β 1 and chondrocytes via injectable, biodegradable hydrogels for cartilage tissue engineering applications. *Biomaterials*. 2005;26:7095-103.

- [41] Park YJ, Lee YM, Park SN, Sheen SY, Chung CP, Lee SJ. Platelet derived growth factor releasing chitosan sponge for periodontal bone regeneration. *Biomaterials*. 2000;21:153-9.
- [42] Park YJ, Lee YM, Lee JY, Seol YJ, Chung CP, Lee SJ. Controlled release of platelet-derived growth factor-BB from chondroitin sulfate–chitosan sponge for guided bone regeneration. *Journal of Controlled Release*. 2000;67:385-94.
- [43] Benoit J-P, Faisant N, Venier-Julienne M-C, Menei P. Development of microspheres for neurological disorders: from basics to clinical applications. *Journal of Controlled Release*. 2000;65:285-96.
- [44] Müller A, Ni Z, Hessler N, Wesarg F, Müller FA, Kralisch D, et al. The biopolymer bacterial nanocellulose as drug delivery system: investigation of drug loading and release using the model protein albumin. *Journal of Pharmaceutical Sciences*. 2013;102:579-92.
- [45] Bardet R, Reverdy C, Belgacem N, Leirset I, Syverud K, Bardet M, et al. Substitution of nanoclay in high gas barrier films of cellulose nanofibrils with cellulose nanocrystals and thermal treatment. *Cellulose*. 2015;22:1227-41.
- [46] Nordli HR, Chinga-Carrasco G, Rokstad AM, Pukstad B. Producing ultrapure wood cellulose nanofibrils and evaluating the cytotoxicity using human skin cells. *Carbohydrate Polymers*. 2016;150:65-73.
- [47] Driemeier C, Mendes FM, Oliveira MM. Dynamic vapor sorption and thermoporometry to probe water in celluloses. *Cellulose*. 2012;19:1051-63.
- [48] Krzan M, Caps H, Vandewalle N. High stability of the bovine serum albumine foams evidenced in Hele–Shaw cell. *Colloids and Surfaces A: Physicochemical and Engineering Aspects*. 2013;438:112-8.
- [49] Grdadolnik J, Maréchal Y. Bovine serum albumin observed by infrared spectrometry. I. Methodology, structural investigation, and water uptake. *Biopolymers*. 2001;62:40-53.
- [50] Alemdar A, Sain M. Isolation and characterization of nanofibers from agricultural residues–Wheat straw and soy hulls. *Bioresource Technology*. 2008;99:1664-71.

Chapter 3.4 Mechanical Properties of Thin Cellulose Nanofiber Films in Liquid

This subchapter is based on *CELLDIFF: Stimuli Responsive Nanocellulose based Matrices for Differentiating Cell Growth*. 251st American Chemical Society National Meeting and Exposition. San Diego, California, United States. March 2016 and *Tunable Structural and Mechanical Properties of Cellulose Nanofiber Substrates in Aqueous Conditions for Stem Cell Culture*. **Biomacromolecules**. (2017).

Abstract	213
1. Introduction	213
2. Materials and Methods	214
2.1 Materials	214
2.2 Methods	214
2.2.1 Characterization of CNF Fibers.....	214
2.2.2 Production of CNF Films	215
2.2.3 CNF Film Characterization.....	215
2.2.3.1 Optical Properties	215
2.2.3.2 Mechanical Tests	215
2.2.4 MSC Cell Culture on CNF Films	216
2.2.4.1 DAPI-Phalloidin Staining	216
3. Results and Discussion.....	216
3.1 Characterization of CNF Fibers and Films	216
3.2 Effect of PBS on CNF Mechanical Properties	218
3.3 Perspectives: From CNF Films to Cells.....	221
4. Conclusion	222
5. Acknowledgements.....	222
6. References	222

Mechanical Properties of Thin Cellulose Nanofiber Films in Liquid

Megan Smyth^{a,b}, E. Johan Foster^c, Julien Bras^{a,b,d}

a. CNRS, LGP2, 461 Rue de la Papeterie, 38402, Saint-Martin-d'Hères, France

b. Université Grenoble Alpes, LGP2, 38000, Grenoble, France

c. Virginia Polytechnic Institute and State University (Virginia Tech), Macromolecules Innovation Institute (MII), Department of Materials Science and Engineering, Blacksburg, Virginia 24061, USA

d. Institut Universitaire de France, 75005, Paris, France

Abstract

Cellulose nanofiber (CNF)-based nanopapers were produced with varying mechanical properties by differing conditions used during fabrication. Through heat exposure, or curing, CNF film mechanical properties were changed when tested in a liquid state mimicking physiological conditions. It was shown that the Young's modulus and storage modulus of CNF films was dependent on the basis weight of the CNF nanostructures and curing step with some samples having an increase of E from 6 to 90 MPa following curing. It must be noted that with increased fiber amount there is a possible reduction in the mechanical properties due to a possible degradation of hydrogen bonding caused by hornification once exposed to liquid. It is suggested that the mechanical properties of CNF within a liquid state can be easily tuned in regards to Young's modulus and storage modulus.

1. Introduction

The use of cellulose, or more specifically nanocellulose, within biomedical applications has increased in recent years as characterized by review articles [1-3]. While research using both cellulose nanocrystals (CNCs) and cellulose nanofibers (CNF) in biomedicine has increased, there is little knowledge on the mechanical properties of these materials in cell culture conditions. Cellulose has long been of interest to researchers for biomedical applications because of its properties such as biocompatibility, low cytotoxicity, renewability, and biodegradation properties [1]. The most common form of nanocellulose used in biomedical applications is bacterial nanocellulose (BNC), which is favorable because of its lack of lignin and hemicellulose content, but it is expensive and difficult to upscale production [4, 5]. CNF, which is derived from biomass, was first discovered in the 1980s by Turbak [6] through mechanical

disintegration and enzymatic pretreatment. The properties of CNF has been thoroughly reviewed in the numerous review articles [7-12] and books [13].

CNF, which contains some amorphous regions of the cellulose fibers, is flexible and has dimensions of approximately 20-60 nm and length of several microns [7]. The properties of these fibers, such as crystallinity, surface charge, and mechanical properties are dependent on the CNF source and means of production [14]. The surface of CNF fibers has numerous hydrogen bonds on the surface. These bonds are the cause of entanglement between fibers which can lead to the formation of nanostructured substrate that is commonly referred to as nanopaper. CNF-based nanopapers are known for their barrier properties and are outlined in a review by Lavoine et al. [7]. Nanopapers can be produced by different means [15, 16] which can impart differing barrier and structural properties [17-19]. These structural properties can then influence the mechanical properties within wet conditions. To the best of the authors' knowledge there has not been any previous studies to explore this relationship.

In this study, CNF films produced by solvent-casting in ambient conditions were modified by an extra curing step to see if the hornification of CNF fibers causes a change in the mechanical properties of CNF nanopaper when tested in physiological-like conditions for future biomedical applications.

2. Materials and Methods

2.1 Materials

A 2 % wt suspension of enzymatically pre-treated CNF from wood pulp (Domsjö) was purchased from Centre Technique du Papier (CTP) (France). Phosphate buffer solution (PBS) was purchased from Sigma-Aldrich (USA).

2.2 Methods

2.2.1 Characterization of CNF Fibers

A dilute suspension of CNF was prepared and placed between a glass lamina for optical microscopy imaging to characterize the quality of the CNF. Images were acquired using a Ziess Imager.M1m Axio microscope (Ziess, Germany) and analyzed using Axiovision SE64 (Ziess, Germany).

2.2.2 Production of CNF Films

CNF films with varying fiber content were produced by casting 1% wt solution of CNF onto a teflon mold and allowed to dry at ambient conditions for 5 days (AC-CNF) followed by curing for 2 (2hC-CNF) hours at 150°C following a modified protocol by Bardet et al. [17, 19]. Basis weight was determined by the following equation:

$$\text{Basis Weight} \left(\frac{g}{m^2} \right) = \frac{\text{Mass of CNF film}}{\text{Area of CNF film}} \quad (\text{Eq. 1})$$

2.2.3 CNF Film Characterization

2.2.3.1 Optical Properties

Films were analyzed with UV spectroscopy. The films were loaded into the spectrometer with a film holder. The absorbance from 300-800 nm was measured with ten scans in spectrum mode with a UV Spectrometer (Shimadzu, Kyoto, Japan) with a normal incidence and repeated in triplicate.

2.2.3.2 Mechanical Tests

Tensile tests and dynamic mechanical analysis (DMA) were measured using a TA Instruments RSA 3 (USA) with a submersion clamp system designed internally. CNF films were tested in physiological-like conditions, i.e. in aqueous environment. For physiological-like conditions, CNF films were conditioned for 24 hours in PBS prior to mechanical tests. Samples underwent rectangular tension measurements, frequency dependent dynamic mechanical analysis, and compression testing in PBS at 37°C. The distance between the clamps for the tension was 10 mm, and the films had a width of approximately 5 mm and thickness of 0.2 mm. Samples underwent rectangular tension measurements at a rate of 0.001 mm/s at 37°C. For dynamic mechanical analysis, films were tested with an angular frequency from 0.1-15 Hz at 37°C with a constant strain of 0.03 mm. For compression testing, samples had dimensions of 15 mm in diameter and thickness of approximately 0.2 mm with an angular frequency of 0.1-20 Hz and constant strain of 10 mm. The stress vs strain and frequency dependent curves were measured and analyzed using TA Orchestrator (USA). Results were done in triplicate.

2.2.4 MSC Cell Culture on CNF Films

Cell culture studies were performed with BALB/c D1 murine bone marrow mesenchymal stem cells (D1 MSCs) (American Type Culture Collection, ATCC, France). Cells were cultured in α MEM supplemented with 10% heat-inactivated fetal bovine serum, 1% penicillin streptomycin mixture and 2 mM L-Glutamine. CNF films were sterilized with UV exposure prior to cell seeding and rinsed twice with DI-H₂O. Cells were seeded at a density of 20,000 cells/cm² for 24 hours for DAPI-phalloidin assay in a humidified atmosphere of 5% CO₂ at 37 °C.

2.2.4.1 DAPI-Phalloidin Staining

4,6-Diaminidino-2-phenylindole-dilactate (DAPI, 20 mg/mL, Sigma-Aldrich, USA) and phalloidintetramethylrhod B isothiocyanate dyes (phalloidin, 10 mg/mL, Sigma-Aldrich, USA) were used to determine the adhesion of cells at 6 hours and 24 hours following seeding on CNF substrates and a glass control. At each time point, the culture media was moved and the samples were fixed with 3.7% paraformaldehyde. The paraformaldehyde was removed after 20 min at room temperature and washed twice with PBS. The phalloidin/DAPI solution was added for 45 min at room temperature (12.5 μ g/mL phalloidin, 10 μ g/mL DAPI). The samples were then washed three times with PBS, mounted with anti-fade reagent, which is 24% glycerol, 9.6% mowiol 4-88 in tris buffered saline (TBS). Followed by confocal laser scanning microscopy (Zeiss, Germany) 24 hours later.

3. Results and Discussion

3.1 Characterization of CNF Fibers and Films

Bardet et al. characterized the Domsjö pulp CNF suspension which was enzymatically pretreated to determine the crystallinity and morphology. It was determined that the CNF had a crystallinity index of 77% and a diameter of approximately 14 ± 5 nm, which is in accordance with CNF properties [17]. Figure 1 displays optical microscopy images of CNF suspension to show the amount of fibrillation (A-C). As seen in the images, large fibers remain within the suspension. This heterogeneity can cause defects within the nanopaper structure, which can negatively impact the mechanical properties.

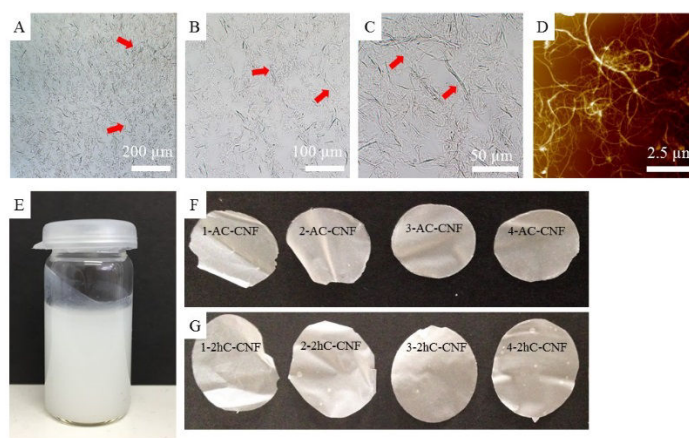


Figure 1. Optical microscopy (A-C) and AFM (D) images of CNF suspension displaying the fibrillation of CNF with residual fiber content as seen in the optical microscopy images. Images of (E) 1 wt% CNF suspension (F) AC-CNF Films, and (G) 2hC-CNF Films

The transparency of CNF films can be an indication of the quality of CNF fibers as well as degree of fibrillation. To study this, the transmission CNF films with differing basis weight and after curing was determined using UV-Visible spectroscopy. As seen in Figure 2, the addition of CNF fibers causes a decrease in the transparency of AC-CNF films because of the increase of entanglement. While the addition of CNF to 2hC-CNF films did not have a clear trend, but with maximum CNF content there is a large decrease in transmission which could be cause by discoloration during the hornification process.

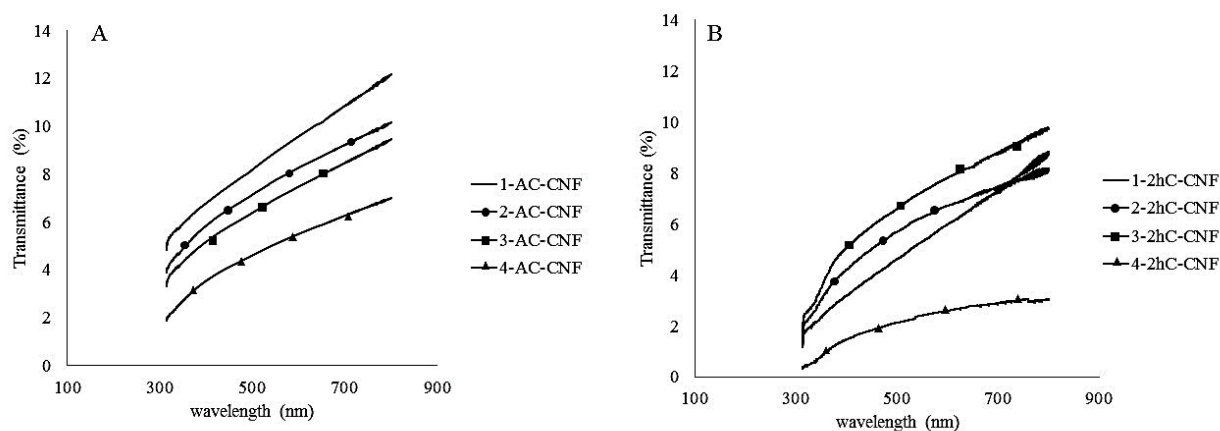


Figure 2. Transmission spectra of (A) AC-CNF films and (B) 2hC-CNF films as measured by UV-Visible spectrography from 100-900 nm.

3.2 Effect of PBS on CNF Mechanical Properties

CNF films with different drying applications were tested to determine the effect of curing on the mechanical properties. Based on literature [17], such curing treatment modifies the structures of this entangled network of CNF. Others called it densification by hornification due to the increase in number of strong hydrogen bonds and by the elimination of water. This densification is illustrated by the changes in basis weight of the films with the same fiber content from AC-CNF to 2hC-CNF with less basis weight for the samples which underwent curing. This change in weight can be attributed to the evaporation of water within the films during exposure to 150°C. The removal of entrapped water within the fiber network can possibly lead to improvement of the mechanical properties in liquid because of the increased hydrogen bonding between the fibers. To determine if this indeed happens CNF films were tested in physiological conditions in an ionic liquid (PBS) at 37°C with a variety of mechanical tests with the results summarized in Table 1.

Table 1. A) Amount of Fibers (g), Basis weight (g/m²), elongation at break (%), Young's modulus (MPa), storage modulus (MPa), compression storage modulus (MPa) of CNF films as-cast (AC) or after 2h curing (2hC) following mechanical testing at physiological conditions at 37°C in PBS.

Sample	Mass of Fibers Prior to Casting (g)	Basis Weight (g/m ²)	Elongation at Break in PBS (%)	Young's Modulus in PBS (MPa)	Storage Modulus at 0.5Hz for DMA in PBS (MPa)	Storage Modulus at 0.5Hz for Compression Testing in PBS (MPa)
1-AC-CNF	0.15	24	---	---	19 ± 5	0.38 ± 0.20
2-AC-CNF	0.25	44	4.43 ± 1.11	6 ± 1	34 ± 3	0.66 ± 0.15
3-AC-CNF	0.30	58	3.77 ± 1.30	30 ± 4	170 ± 55	0.88 ± 0.08
4-AC-CNF	0.50	102	3.14 ± 0.89	83 ± 2	107 ± 8	1.39 ± 0.16
1-2hC-CNF	0.15	13	---	---	2908 ± 285	0.26 ± 0.03
2-2hC-CNF	0.25	20	2.54 ± 0.56	90 ± 2	357 ± 156	0.19 ± 0.09
3-2hC-CNF	0.30	33	2.72 ± 0.10	72 ± 7	163 ± 66	1.29 ± 0.16
4-2hC-CNF	0.50	61	5.31 ± 0.72	43 ± 3	86 ± 24	0.95 ± 0.05

As shown in the table, there are different mechanical properties of the films depending on the basis weight and the Young's modulus varies in regards to cured films. The general trend is that with curing the films had a higher modulus compared to the as casted films. The most evident increase in the

Young's modulus from AC-CNF to 2hC-CNF occurred in samples 2-AC-CNF and 2-2hC-CNF as seen in Table 1. While it would be expected that with increased fiber content the Young's modulus would increase this was not the case for samples which underwent curing. The decrease in Young's modulus from 2-2hC-CNF to 4-2hC-CNF could be due to a higher influence of the liquid on the swelling of the fibers and therefore disturbance of the hydrogen bonds.

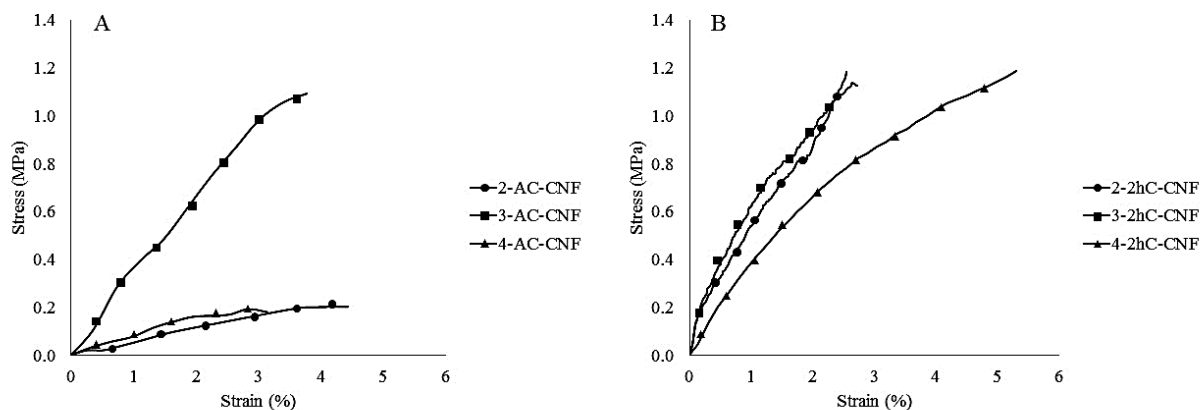


Figure 3. Stress-strain testing of (A) AC-CNF films and (B) 2hC-CNF films in aqueous conditions in PBS at 37°C.

CNF films underwent frequency dependent dynamic mechanical analysis and compression testing to determine the viscoelastic behaviors of CNF films. It has been shown that these mechanical tests can be used to determine the characteristics of the biomaterial in physiological conditions [20-23]. Dynamic mechanical analysis of CNF films showed that overall curing caused an increase in the storage modulus for all samples except in the case of 3-AC-CNF. For AC-CNF films an increase in basis weight caused an overall increase in storage modulus, but this trend was not the same for 2hC-CNF films. This can once again be attributed to a possible reduction in hydrogen bonding when tested in PBS. This mechanical test, which has a rectangular tension orientation, could cause a stretching of the films which could loosen the entanglement of CNF fibers and has a higher effect on 2hC-CNF films.

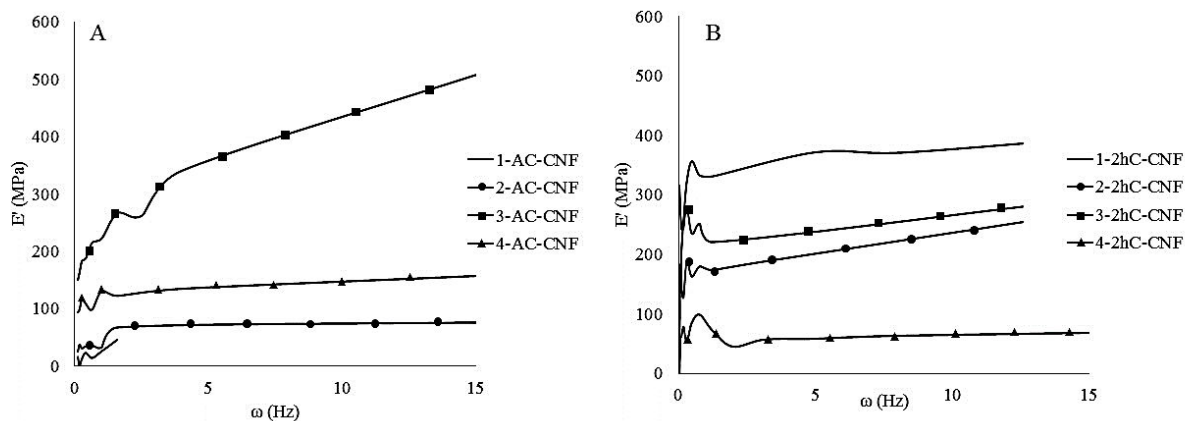


Figure 4. Frequency dependent dynamic mechanical analysis from 0.5-15 Hz with 0.03 mm applied strain in aqueous conditions in PBS at 37°C for AC-CNF films (A) and 2hC-CNF films (B).

The same trend, a decrease with increased basis weight, was not apparent when tested in a compressive state (Figure 5). In a compressive state, there is less energy stored within the samples when compared to dynamic mechanical analysis. With increased basis weight there is an increase in the storage modulus for both AC-CNF and 2hC-CNF. When comparing AC-CNF films and 2hC-CNF films there is an increase in the storage modulus for 1-CNF and 3-CNF samples and similar results occurring with 4-CNF samples. While there is improvement in the mechanical properties overall after curing, this improvement is not quite as pronounced when compared to Young's modulus obtained by tensile testing. The differences in the values of storage modulus in dynamic mechanical testing and compression testing can be explained by the lack of restorative force within the thin CNF nanopaper because of the small thicknesses of the films.

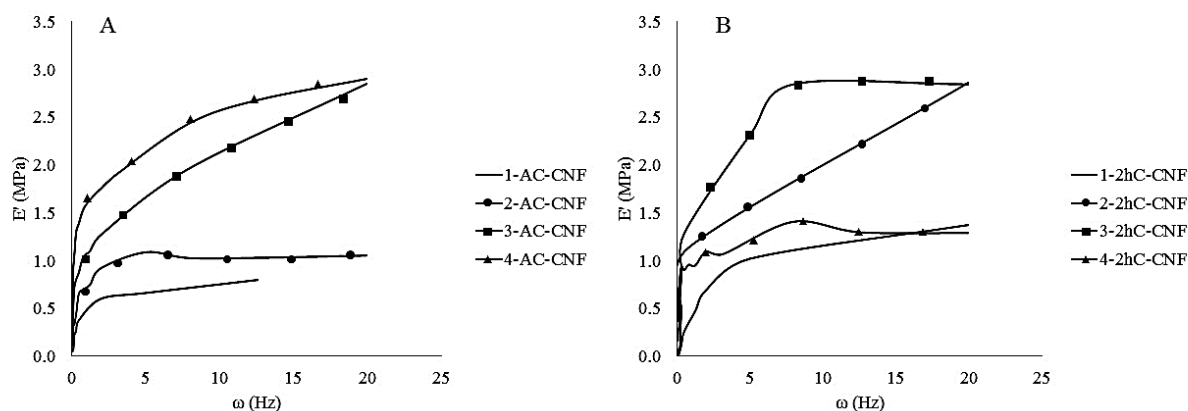


Figure 5. Compression Frequency dependent dynamic mechanical analysis from 0.5-20 Hz with 10 mm applied strain in aqueous conditions in PBS at 37°C for AC-CNF Films (A) and 2hC-CNF films (B).

It is worth noting that with similar raw material, a significant difference in mechanical properties (E in PBS is between 6 and 90 MPa) can result. This kind of ability to vary the properties is not common, even within the CNF field, with only few scientific papers dealing with such an approach [17, 19]. But what is important to highlight is that with just changing the fabrication methods (i.e. increased fiber content and curing) differing mechanical properties can be achieved which could be of interest to researchers.

3.3 Perspectives: From CNF Films to Cells

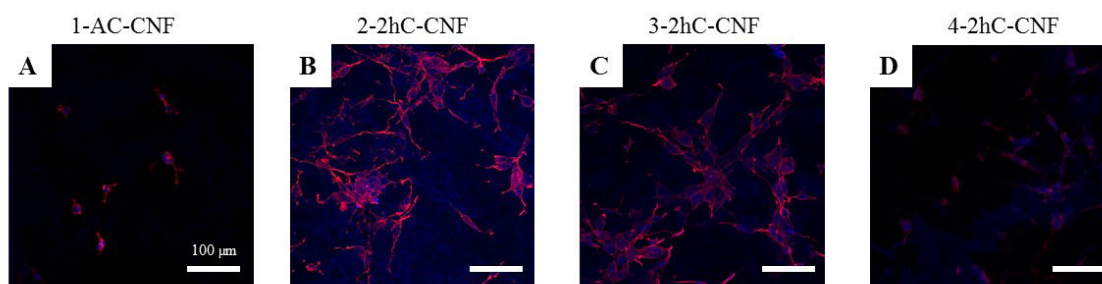


Figure 6. MSCs interactions with the CNF with different basis weight were assessed after 24 h of culture by staining the cell nucleus and cytoskeleton (DAPI and phalloidin). B) 1-AC-CNF, C) 2-2hC-CNF, D) 3-2hC-CNF, and E) 4-2hC-CNF as measured by confocal laser scanning microscopy

It is already recognized that mechanical values are crucial for cell growth and differences might be interesting for stem cell differentiation [24] which lead to preliminary tests being conducted to determine if it was possible to culture MSCs with these different CNF substrates. MSCs were cultured for 24 hours, stained with Phalloidin/DAPI and observed using confocal microscopy as shown in Figure 6. Thinner films allowed imaging and showed cell attachment for the high mechanical property substrates, but low attachment for the as-cast films with the same fiber amount. This result is promising because of the apparent attachment of the cells to the CNF, but it is difficult to say if this qualitative difference is due to mechanical properties or to other substrate properties. Further exploration of the effect of the material and mechanical properties of cured CNF films on the behavior of MSCs will be presented in Chapter 4.2.

4. Conclusion

The mechanical properties of CNF films with varying basis weights can easily be changed by the application of a curing step at an elevated temperature. This treatment causes a change in the density of the CNF films, as well as the transparency. While there is not a clear relationship between the changes in mechanical properties with increased basis weight, this could be attributed to lack of characterization tools to determine the amount of hydrogen bonding between individual nanofibers. It is suggested that with the increased number of fibers there is a higher disturbance of hydrogen bonding when tested in physiological conditions, but that the mechanical properties can be easily tuned by changing the amount of fibers and by subsequent curing. The variation in the Young's and storage moduli between AC-CNF films and 2hC-CNF films could be of interest to researchers for biomedical applications or other applications of CNF.

5. Acknowledgements

LGP2 is part of the LabEx Tec 21 (Investissements d'Avenir - grant agreement n°ANR-11-LABX-0030) and of the PolyNat Carnot Institutes (Investissements d'Avenir - grant agreements n° ANR-11-CARN-030-01). LMGP is part of the LabEx Centre of Excellence of Multifunctional Architected Materials "CEMAM" (ANR 10-LABX-44-01). This work been partially supported by the LabEx Tec 21 (Investissements d'Avenir - grant agreement n°ANR-11-LABX-0030). AFM image of CNF suspension was used with permission from Charlène Reverdy.

6. References

- [1] Jorfi M, Foster EJ. Recent advances in nanocellulose for biomedical applications. *Journal of Applied Polymer Science*. 2015;132:41719.
- [2] Lin N, Dufresne A. Nanocellulose in biomedicine: Current status and future prospect. *European Polymer Journal*. 2014;59:302-25.
- [3] Domingues RM, Gomes ME, Reis RL. The potential of cellulose nanocrystals in tissue engineering strategies. *Biomacromolecules*. 2014;15:2327-46.
- [4] Petersen N, Gatenholm P. Bacterial cellulose-based materials and medical devices: current state and perspectives. *Applied Microbiology and Biotechnology*. 2011;91:1277-86.
- [5] Dufresne A. Nanocellulose: a new ageless bionanomaterial. *Materials Today*. 2013;16:220-7.

- [6] Turbak AF, Snyder FW, Sandberg KR. Microfibrillated cellulose, a new cellulose product: properties, uses, and commercial potential. *J Appl Polym Sci: Appl Polym Symp*;(United States): ITT Rayonier Inc., Shelton, WA; 1983.
- [7] Lavoine N, Desloges I, Dufresne A, Bras J. Microfibrillated cellulose - its barrier properties and applications in cellulosic materials: a review. *Carbohydrate Polymers*. 2012;90:735-64.
- [8] Siró I, Plackett D. Microfibrillated cellulose and new nanocomposite materials: a review. *Cellulose*. 2010;17:459-94.
- [9] Moon RJ, Martini A, Nairn J, Simonsen J, Youngblood J. Cellulose nanomaterials review: structure, properties and nanocomposites. *Chemical Society Reviews*. 2011;40:3941-94.
- [10] Eichhorn SJ, Dufresne A, Aranguren M, Marcovich NE, Capadona JR, Rowan SJ, et al. Review: current international research into cellulose nanofibres and nanocomposites. *Journal of Materials Science*. 2010;45:1-33.
- [11] Mariano M, El Kissi N, Dufresne A. Cellulose nanocrystals and related nanocomposites: review of some properties and challenges. *Journal of Polymer Science Part B: Polymer Physics*. 2014;52:791-806.
- [12] Hoeng F, Denneulin A, Bras J. Use of nanocellulose in printed electronics: a review. *Nanoscale*. 2016;8:13131-54.
- [13] Dufresne A. *Nanocellulose: from nature to high performance tailored materials*: Walter de Gruyter; 2013.
- [14] Nechyporchuk O, Belgacem MN, Bras J. Production of cellulose nanofibrils: a review of recent advances. *Industrial Crops and Products*. 2016;93:2-25.
- [15] Sehaqui H, Morimune S, Nishino T, Berglund LA. Stretchable and strong cellulose nanopaper structures based on polymer-coated nanofiber networks: An alternative to nonwoven porous membranes from electrospinning. *Biomacromolecules*. 2012;13:3661-7.
- [16] Sehaqui H, Ezekiel Mushi N, Morimune S, Salajkova M, Nishino T, Berglund LA. Cellulose nanofiber orientation in nanopaper and nanocomposites by cold drawing. *ACS Applied Materials & Interfaces*. 2012;4:1043-9.
- [17] Bardet R, Reverdy C, Belgacem N, Leirset I, Syverud K, Bardet M, et al. Substitution of nanoclay in high gas barrier films of cellulose nanofibrils with cellulose nanocrystals and thermal treatment. *Cellulose*. 2015;22:1227-41.
- [18] Bardet R, Belgacem N, Bras J. Flexibility and color monitoring of cellulose nanocrystal iridescent solid films using anionic or neutral polymers. *ACS Appl Mater Interfaces*. 2015;7:4010-8.

- [19] Bardet R, Belgacem MN, Bras J. Different strategies for obtaining high opacity films of MFC with TiO₂ pigments. *Cellulose*. 2013;20:3025-37.
- [20] Caridade SG, Merino EG, Alves NM, Mano JF. Bioactivity and viscoelastic characterization of chitosan/bioglass® composite membranes. *Macromolecular bioscience*. 2012;12:1106-13.
- [21] Caridade SG, Merino EG, Alves NM, de Zea Bermudez V, Boccaccini AR, Mano JF. Chitosan membranes containing micro or nano-size bioactive glass particles: evolution of biomineralization followed by in situ dynamic mechanical analysis. *Journal of the mechanical behavior of biomedical materials*. 2013;20:173-83.
- [22] Malheiro VN, Caridade SG, Alves NM, Mano JF. New poly (ϵ -caprolactone)/chitosan blend fibers for tissue engineering applications. *Acta biomaterialia*. 2010;6:418-28.
- [23] Silva JM, Duarte ARC, Caridade SG, Picart C, Reis RL, Mano JoF. Tailored freestanding multilayered membranes based on chitosan and alginate. *Biomacromolecules*. 2014;15:3817.
- [24] Engler AJ, Sen S, Sweeney HL, Discher DE. Matrix elasticity directs stem cell lineage specification. *Cell*. 2006;126:677-89.

Figures and Tables

Figures

Chapter 3.1

Figure 1. Schematic representation of preparation of CNC:Alginate and CNC-T:Alginate nanocomposites and characterization

Figure 2. Conductimetric titration of CNC-T to determine amount of hydroxyl groups added to CNC after TEMPO-mediated oxidation.

Figure 3. CNC AFM images of A) CNC B) CNC-T, C) length and width measurements of CNCs and CNC-Ts

Figure 4. XRD spectra of CNC and CNC-T obtained from powder

Figure 5. Thermograms of A) CNC:Alginate composites and B) CNC-T:Alginate composites with indicative curves of cellulose degradation with composites with CNCs. C) Weight loss in percent for samples at 100, 200, 300, 400, 500, and 600°C.

Figure 6. Optical images of A) Alginate, B) 10:90 CNC:Alginate, C) 30:70 CNC:Alginate, D) 50:50 CNC:Alginate, E) 70:30 CNC:Alginate, F) 10:90 CNC-T:Alginate, G) 30:70 CNC-T:Alginate, H) 50:50 CNC-T:Alginate, and I) 70:30 CNC-T:Alginate with noticeable increase of opaqueness with increased CNC and CNC-T amounts in the composites. Transmittance versus wavelength as measured by UV-Vis spectroscopy for J) CNC:Alginate and K) CNC-T:Alginate composites.

Figure 7. The percentage of swelling due to A,) water and B,D) D-PBS uptake in CNC:Alginate (A,B) CNC-T:Alginate (C,D) for various time points until 24 hours.

Figure 8. Storage modulus of 30:70 CNC:Alginate composites crosslinked with varying molarity of calcium chloride measured at 50% relative humidity for 15 hours at constant frequency of 1Hz and constant strain of 3%.

Figure 9. Storage modulus of 30:70 CNC:Alginate composites measured at 10%, 30%, 50%, and 70% relative humidity for 15 hours at constant frequency of 1 Hz and constant strain of 3%.

Figure 10. Stress-strain curves of in ambient conditions (A, B), in aqueous conditions in DI-H₂O (C,E) and D-PBS (D,F) at 37°C for CNC:Alginate composites (A,C,D) and CNC-T:Alginate composites (B,E,F).

Figure 11. Schematic representation of improved crosslinking with CNC-T versus CNC in D-PBS. For CNC-T:Alginate composites there is improved interaction between the Ca²⁺ ions, the ions present

in D-PBS and CNC-Ts which causes less Ca^{2+} ions to be leached from the composites compared to CNC-based systems in D-PBS and also DI- H_2O

Chapter 3.2

Figure 1. CNC AFM images from suspensions of 0.0001 wt% of A) CNC, B) PA-g-CNC r. C) Size distribution of CNC and PA-g-CNC nanoparticles DI- H_2O as determined by DLS. D) Length and width measurements of CNCs and PA-gCNCs, and Hydrodynamic diameter (ZD), polydispersity index (PDI) determined by dynamic light scattering.

Figure 2. X-ray diffraction spectrograms of CNC and PA-g-CNCs obtained from powder

Figure 3. A) TGA thermograms of PA-g-CNC measured from 30-900 °C with a temperature rate increase of 10 °C per minute under air.

Figure 4. FTIR spectrum of CNC and PA-g-CNC

Figure 5. ^{13}C solid state NMR of A) CNC and B) PA-g-CNC

Figure 6. Change in thickness of Alginate and PA-g-CNC:Alginate composites following 24 hours in DI- H_2O measured in percent

Figure 7. Stress-strain curves of (A) alginate, (B) 10:90 PA-g-CNC:Alginate, (C) 30:70 PA-g-CNC:Alginate, and (D) 50:50 PA-g-CNC:Alginate tested at 37°C following UV exposure for 0.5, 1, and 2 hours. All graphs were normalized to start with a zero strain.

Figure 8. Stress-strain curves of (A) alginate, (B) 10:90 PA-g-CNC:Alginate, (C) 30:70 PA-g-CNC:Alginate, and (D) 50:50 PA-g-CNC:Alginate tested at 37°C in DI- H_2O following UV exposure for 0.5, 1, and 2 hours

Chapter 3.3

Figure 1. Schematic of CNF-BSA film fabrication (A) and loading of CNF with BSA by diffusion (B)

Figure 2. Optical microscopy (A-C) and AFM (D) images of CNF suspension displaying the fibrillation of CNF with residual fiber content as seen in the optical microscopy images. Images of (E) 1 wt% CNF suspension and (F) CNF and BSA-CNF films.

Figure 3. Dynamic light scattering spectrum for BSA solution with an average size of 42 ± 11 nm and polydispersion index of 0.15 ± 0.01 , which indicates the BSA is uniformly dispersed without varying size.

Figure 4. SEM images of solvent casted (A, E, I) CNF films with (B, F, J) 0.1% BSA, (C, G, K) 0.25% BSA, and (D, H, L) 0.5% BSA added. A-H are images to show the inner structure of cut CNF films

with round, BSA particles present. I-L are surface images with BSA entrapped within the fiber structure.

Figure 5. FTIR spectra of BSA, CNF, 0.1% BSA-CNF, 0.25% BSA-CNF, and 0.5% BSA-CNF with apparent peaks indicating the incorporation of BSA within the BSA-CNF films
Figure 6. Amount of BSA remaining in solution during CNF film loading by diffusion for 48 hours in PBS at 37°C as determined by BCA assay

Figure 7. Release of BSA from CNF in A, B) micrograms, C, D) percentage of CNF added for A, C) BSA-CNF composites and B, D) BSA added by diffusion for 48 hours in PBS at 37°C as determined by BCA assay

Chapter 3.4

Figure 1. Optical microscopy (A-C) and AFM (D) images of CNF suspension displaying the fibrillation of CNF with residual fiber content as seen in the optical microscopy images. Images of (E) 1 wt% CNF suspension (F) AC-CNF Films, and (G) 2hC-CNF Films

Figure 2. Transmission spectra of (A) AC-CNF films and (B) 2hC-CNF films as measured by UV-Visible spectrography from 100-900 nm.

Figure 3. Stress-strain testing of (A) AC-CNF films and (B) 2hC-CNF films in aqueous conditions in PBS at 37°C.

Figure 4. Frequency dependent dynamic mechanical analysis from 0.5-15 Hz with 0.03 mm applied strain in aqueous conditions in PBS at 37°C for AC-CNF films (A) and 2hC-CNF films (B).

Figure 5. Compression Frequency dependent dynamic mechanical analysis from 0.5-20 Hz with 10 mm applied strain in aqueous conditions in PBS at 37°C for AC-CNF Films (A) and 2hC-CNF films (B).

Figure 6. D1 MSCs interactions with the CNF with different basis weight were assessed after 24 h of culture by staining the cell nucleus and cytoskeleton (DAPI and phalloidin). B) 1-AC-CNF, C) 2-2hC-CNF, D) 3-2hC-CNF, and E) 4-2hC-CNF as measured by confocal laser scanning microscopy

Tables

Chapter 3.1

Table 1. Amounts of CNC, CNC-T, and sodium alginate for fabrication of composites

Table 2. Determination of amount of Ca^{+2} remaining within CNC:Alginate or CNC-T:Alginate composites following 24 hours in DI- H_2O or D-PBS by complexometric titration using EDTA.

Table 3. Mechanical properties of Alginate, CNC:Alginate composites, and CNC-T:Alginate composites in dry conditions, DI-H₂O, and D-PBS

Chapter 3.2

Table 1. Amounts of CNC, PA-g-CNC, and sodium alginate for fabrication of composites

Table 2. Elongation at break and Young's modulus of Alginate and PA-g-CNC:Alginate composites as determined by tensile testing in dry and wet conditions at 37°C following UV exposure

Chapter 3.3

Table 1. Characterization of CNF, BSA-CNF films, and Release of BSA

Chapter 3.4

Table 1. A) Amount of Fibers (g), Basis weight (g/m²), elongation at break (%), Young's modulus (MPa), storage modulus (MPa), compression storage modulus (MPa) of CNF films as-cast (AC) or after 2h curing (2hC) following mechanical testing at physiological conditions at 37°C in PBS.

Chapter 4. The Influence of Nanocellulose on Stem Cell Behavior in Culture

Chapter 4. The Influence of Nanocellulose on Stem Cell Behavior in Culture

1. Modulation of Mechanical Properties of Cellulose Nanocrystal Composites for use in Stem Cell Culture	231
2. Tunable Structural and Mechanical Properties of Cellulose Nanofiber Substrates in Liquid for Stem Cell Culture	255
Figures and Tables	283

Chapter 4.1 Modulation of Mechanical Properties of Cellulose Nanocrystal Composites for use in Stem Cell Culture

This subchapter is based on *The effect of hydration on the material and mechanical properties of cellulose nanocrystal-alginate composites*. **Carbohydrate Polymers**. Under Revision

Abstract	233
1. Introduction.....	233
2. Materials and Methods	235
2.1 Materials	235
2.2 Methods	235
2.2.1 Fabrication of CNC:Alginate and CNC-T:Alginate Films	235
2.2.2 Atomic Force Microscopy (AFM)	236
2.2.3 Dynamic Mechanical Analysis (DMA)	236
2.2.4 Cell Culture	236
2.2.5 Phalloidin Staining	236
2.2.6 MTT Assay	237
2.2.7 Statistical Analysis	237
3. Results and Discussion.....	238
3.1 Characterization of CNC:Alginate and CNC-T:Alginate Composites	238
3.1.1 Surface Roughness of CNC:Alginate and CNC-T:Alginate Composites	238
3.1.2 Dynamic Mechanical Analysis in Physiological Conditions	239
3.2 MSC Cell Culture with CNC:Alginate and CNC-T:Alginate Composites	242
3.2.1 Cell Adhesion	242
3.2.2 MSC Viability	246
4. Conclusion	248
5. Acknowledgements.....	249
6. References	249

Modulation of Mechanical Properties of Cellulose Nanocrystal Composites for use in Stem Cell Culture

Megan Smyth^{a,b}, Marie-Stella M'Bengue^{a,b}, Catherine Picart^{c,d}, Julien Bras^{a,b,e}, E. Johan Foster^f

a. CNRS, LGP2, 461 Rue de la Papeterie, 38402, Saint-Martin-d'Hères, France

b. Université Grenoble Alpes, LGP2, 38000 Grenoble, France

c. CNRS, UMR 5628, LMGP, 38016 Grenoble, France

d. Université Grenoble Alpes, Grenoble Institute of Technology, 38016 Grenoble, France

e. Institut Universitaire de France, 75005 Paris, France

f. Virginia Polytechnic Institute and State University (Virginia Tech), Macromolecules Innovation Institute (MII), Department of Materials Science and Engineering, Blacksburg, Virginia 24061, USA

Abstract

Cellulose nanocrystal-alginate composites with material properties such as roughness and storage modulus were produced with varying ratios of cellulose nanocrystals (CNCs) and TEMPO-mediated oxidized nanocrystals (CNC-Ts). In this study, the adhesion and viability of mesenchymal stem cells (MSCs) cultured on these nanocomposites will be presented. It is well-known by biomedical researchers that alginate is not a favorable material for cell adhesion. The adhesion of MSCs after 6 and 24 hours was conditional on the amount of CNCs added to the alginate in cell culture conditions as measured by cell area, cell aspect ratio, and area fraction of cells adhered to the culture surface. Viability of D1/BALBc MSCs were assessed for 24 and 48 hours, and it was shown that the viability varied significantly, with higher levels of significance for nanocomposites with unmodified CNCs. These results suggest the addition of CNCs or CNC-Ts can affect MSC behavior in cell culture, and that CNC-Alginate and CNC-T-Alginate composites are promising materials for future cell studies.

1. Introduction

The use of cellulose, which is considered to be the world's most abundant polymer [1] with one gigaton produced annually, in biomedical applications has gained interest in recent years, especially the use of cellulose nanocrystals (CNCs) for tissue engineering applications [2]. CNCs are most commonly extracted from cellulose fibers by acid hydrolysis [3], which have favorable properties including; biodegradability, biocompatibility, and high mechanical properties for use in nanocomposites. The use of CNCs in nanocomposites has been of interest for researchers since the mid-1990s [4, 5], with

previous research focusing on the use of soluble polymers, such as latex, polyvinyl alcohol, and HPMC [6-11], with more recent research focusing on alginate and other biosourced polymers [12, 13].

As with cellulose nanocrystals, alginate is also derived from a biomass. In this case brown algae, which contains 1,4-linked β -D-mannuronate (M) and α -L-guluronate (G) chains in variable ratios. Crosslinking of alginate is caused by the ionic interaction of G-chains with multivalent cationic ions, which induces gelation [14]. Alginate is a commonly used biomaterial that is known to be biocompatible, relatively non-toxic, cost-effective, and have controlled gelation [15]. While alginate is frequently used in biomedical applications ranging from tissue engineering [16-18] to drug delivery [19-21], there are many problems associated with this material because of its high hydrophilicity such degradation [22-26], low mechanical properties [27, 28], and lack of cell adhesion because of the prevention of protein deposition onto the surface [29]. To improve upon cell adhesion differing techniques have been employed such as the crosslinking of RGD ligands to the surface of the alginate [30-32], or incorporation of transforming growth factor beta (TGF- β) [33-35]. The adhesion of cells onto the surface of biomaterials is controlled by the interaction between molecules at the material surface and the transmembrane receptors of the cells [36]. This is especially important in anchorage dependent cells like mesenchymal stem cells (MSCs) [37, 38]. Alginate does not induce high levels of adhesion, and MSCs cultured in alginate hydrogels usually aggregate into multicellular clusters [39].

In this work, mechanical reinforcement of alginate will be explored through the addition of nanocellulose crystals. Dynamic mechanical analysis, or DMA, is a suitable means of investigating the mechanical properties of polymer based materials in biomedical applications [40], and is important to gain an understanding of the viscoelastic nature of the biomaterial because it relates to the functionality and the biocompatibility of the material. These mechanical properties can even influence cell growth and differentiation [41]. The use of mechanically-modified alginate by the addition of filler for use as a cell culture substrate has not been studied previously. Previous studies have focused on the effect of mechanically adaptive alginate hydrogels by variation of M- and G-chain ratios [42] and UV-induced crosslinking [43] on cell viability. While other studies have already shown the use of reinforcement materials such as cellulose [44-46], chitosan [47], and also CNCs [12, 13] with alginate, but not for biomedical applications or use in cell culture.

Alginate and cellulose nanocrystal composites with varying mechanical and material properties were created using unmodified CNCs and TEMPO-mediated oxidized CNCs. Previous work by the authors has characterized various aspects of these composites (Chapter 3.1). In this study, further mechanical

and material characterization of alginate and cellulose nanocrystal composites and their effect MSC viability and adhesion will be presented.

2. Materials and Methods

2.1 Materials

Sodium alginate from brown algae, calcium chloride (CaCl_2), Dubecco's Phosphate Buffer Solution (D-PBS), (2,2,6,6-tetramethylpiperidin-1-yl)oxyl (TEMPO), Minimum Essential Medium Eagle (α MEM), 4phalloidintetramethylrhod B isothiocyanate dyes (Phalloidin), glycerol, mowiol 4-88, tris buffer saline (TBS), thiazolyl blue tetrazolium bromide (MTT), and dimethyl sulfoxide (DMSO) were purchased from Sigma-Aldrich France Ltd. (France). Cellulose nanocrystals (CNCs) were purchased from University of Maine Process Development Center (USA). The CNCs were extracted from wood pulp using sulfuric acid hydrolysis. BALB/c D1 murine bone marrow mesenchymal stem cells were purchased from American Type Culture Collection (France). 10% heat-inactivated fetal bovine serum (FBS) was acquired from PAA Laboratories (Austria), and penicillin streptomycin mixture and L-Glutamine were purchased from Invitrogen (USA). All materials were used without any modification.

2.2 Methods

2.2.1 Fabrication of CNC:Alginate and CNC-T:Alginate Films

CNC:Alginate and CNC-T:Alginate composites were made following a modified protocol of Lin et al. [12], which was also reported in previous work conducted by the authors (Chapter 3.1). A 3 wt% solution of sodium alginate was added to 1 wt% CNC or CNC-T in varying ratios under stirring for 30 minutes following Table 1. CNC:alginate suspensions were solvent casted and allowed to dry at ambient conditions for 48 hours and then at 45°C for 24 hours. Dried films were then soaked overnight in a 0.45M CaCl_2 solution and rinsed. The crosslinked films were dried again at ambient conditions for 24 hours under fume hood evaporation.

Table 1. Amounts of CNC, CNC-T, and sodium alginate for fabrication of composites

Ratio CNC (or CNC-T):Alginate	3 wt% Sodium Alginate Solution (mL)	1 wt% CNC (or CNC-T) Suspension (mL)
Alginate	20	0
10:90	18	6
30:70	14	18
50:50	10	30
70:30	6	42

2.2.2 Atomic Force Microscopy (AFM)

Films of CNC:Alginate and CNC-T:Alginate were fixed to metal plates prior to image. Images were acquired using tapping mode with a Nanoscope IIA microscope from Veeco Instruments (Plainview, New York, USA) at a frequency of 265-340 Hz. Silicon cantilevers with a curvature of 10-15 nm were used (OTESPA®, Bruker, Billerica, Massachusetts, USA). AFM images were analyzed using Nanoscope Analysis (Plainview, New York, USA). Roughness measurements (R_{rms} root mean square deviation) were obtained by Image J® (U. S. National Institutes of Health, Bethesda, Maryland, USA) in triplicate.

2.2.3 Dynamic Mechanical Analysis (DMA)

Samples were also measured in immersion conditions, in D-PBS at 37°C thanks to a specially designed device allowing dipping of samples and clamp and temperature monitoring. A frequency scan from 0.05-20 Hz and a constant strain of 10 mm was used. Compression testing was conducted at 37°C from 0.05-30 Hz with a constant strain of 10% in D-PBS.

2.2.4 Cell Culture

Cell culture studies were performed with BALB/c D1 murine bone marrow mesenchymal stem cells (MSCs) (American Type Culture Collection, ATCC, France). Cells were cultured in α MEM supplemented with 10% heat-inactivated fetal bovine serum, 1% penicillin streptomycin mixture and 2 mM L-Glutamine. CNC:Alginate composites were sterilized with UV exposure prior to cell seeding and rinsed twice with DI-H₂O. Cells were seeded at a density of 10,000 cells/cm² for 6 hours and 24 hours for phalloidin assay, and 24 hours and 48 hours for MTT analysis in a humidified atmosphere of 5% CO₂ at 37 °C.

2.2.5 Phalloidin Staining

Phalloidintetramethylrhod B isothiocyanate dye (phalloidin, 10 mg/mL, Sigma-Aldrich, USA) was used to determine the adhesion of cells at 6 hours and 24 hours following seeding on CNF substrates and a glass control. At each time point, the culture media was moved and the samples were fixed with 3.7% paraformaldehyde. The paraformaldehyde was removed after 20 min at room temperature and washed twice with PBS. The phalloidin solution was added for 45 min at room temperature (12.5 μ g/mL phalloidin). The samples were then washed three times with PBS, mounted with anti-fade

reagent, which is 24% glycerol, 9.6% mowiol 4-88 in tris buffered saline (TBS). Followed by analysis by confocal laser scanning microscopy (Zeiss, Germany) 6 and 24 hours later. The cell surface area and aspect ratio were analyzed using ImageJ with a sample size of 300 cells per condition from two independent experiments. Cell surface area and aspect ratio measurements were done by measuring clearly defined individual cells using the tracing tool in ImageJ after calibrating the scale and thresholding each image. Percentage of cells attached was measured using tile scan of a single well in triplicate with the area fraction of the well covered by the cells measured by ImageJ.

2.2.6 MTT Assay

Thiazolyl blue tetrazolium bromide (MTT, 2.5 mg/mL, Sigma Aldrich, USA) was used to perform a MTT assay on two independent experiments to measure the mitochondrial activity of MSCs after 24 hours and 48 hours post seeding on CNC/Alginate, CNC-T/Alginate composites or tissue culture polystyrene (TCPS) control. MTT solution was added to the cells and incubated in media for 1.5 hours. After 1.5 hours, the growth media was removed and 200 μ L of dimethyl sulfoxide (DMSO) was added to solubilize the formazan crystals formed in the reduction of MTT. 200 μ L of the formazan solution was added to a microplate reader. The absorbance of each sample was read at 550 nm. The samples were imaged using optical microscopy (Zeiss, Germany).

2.2.7 Statistical Analysis

All experiments were carried out in triplicate unless otherwise noted. All results are presented with mean \pm standard deviation unless otherwise noted. Statistical analysis of cell studies was performed in Originlab using a Kolmogorov-Smirnov test for normality. For the cell area and aspect ratio results following the Phalloidin assay, the samples did not follow a normal distribution and were normalized using a Box-Cox transformation. Following the normalization transformation, a Kolmogorov-Smirnov test was repeated. Normalized results were analyzed by two-way ANOVA with post-hoc testing using a Bonferroni test.

3. Results and Discussion

3.1 Characterization of CNC:Alginate and CNC-T:Alginate Composites

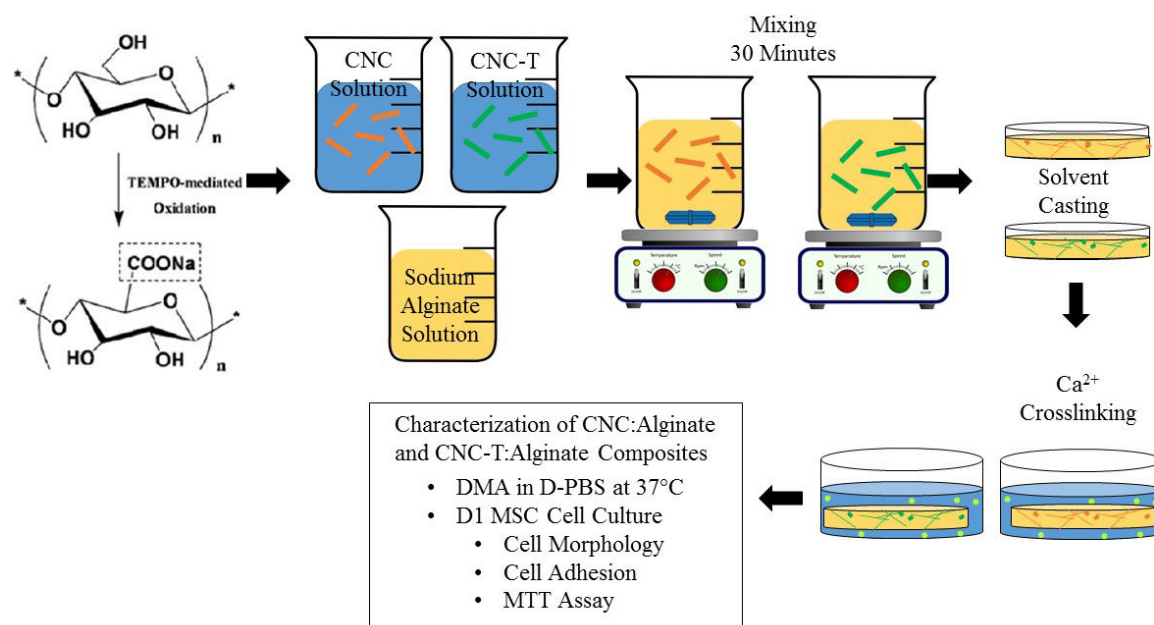


Figure 1. Schematic Representation of Nanocomposite Fabrication and Characterization

3.1.1 Surface Roughness of CNC:Alginate and CNC-T:Alginate Composites

Atomic force microscopy was performed on alginate, CNC:Alginate, and CNC-T:Alginate composites to characterize their surface roughness, and to determine if the addition of nanocellulose causes an increase in the roughness. Figure 2 shows the AFM images of the composites following fabrication: crosslinking and drying. The reported roughness values from root-mean-square analysis of AFM images of shows that for micro scale roughness there is no significant difference between the roughness. This indicates that for future cell studies that the roughness of the surface should not influence cell attachment or viability.

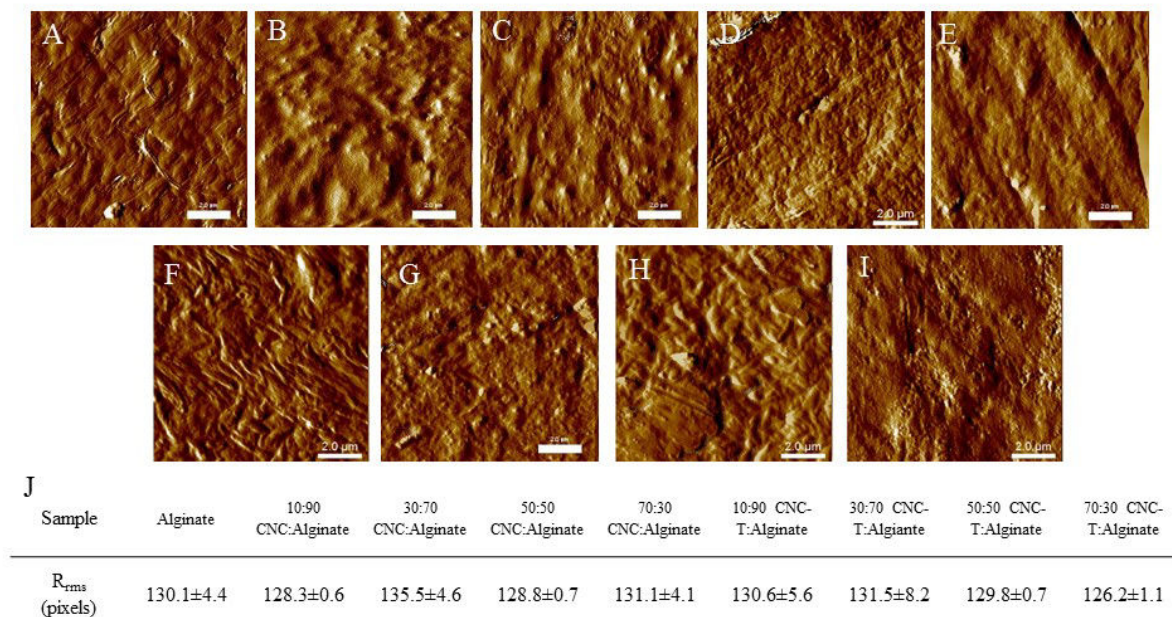


Figure 2. Atomic force microscopy images of the surface of the CNC:Alginate composites A) Alginate, B) 10:90 CNC:Alginate, C) 30:70 CNC:Alginate, D) 50:50 CNC:Alginate and CNC-T:Alginate composites F) 10:90 CNC-T:Alginate, G) 30:70 CNC-T:Alginate, H) 50:50 CNC-T:Alginate, and I) 70:30 CNC-T:Alginate taken by tapping mode in air. Images dimensions of 10x10 μm . J) root mean square roughness measurements measured in pixels by ImageJ of the surface of the composite films

3.1.2 Dynamic Mechanical Analysis in Physiological Conditions

Two different dynamic mechanical analyses were done on the CNC:Alginate and CNC-T:Alginate composites immersed in D-PBS. Frequency dependent tests with rectangular orientation with applied tension will be further described as frequency-dependent testing. A frequency-dependent test can determine the viscoelastic properties of the composites that are comparable to what occurs in the body. Compression testing on circular samples of the composites were done to see the effect of hydration on the storage modulus in a compressive state and if these results differed from the frequency dependent tests. Both types of tests had a frequency of 0.5-20 Hz with a constant strain of 3% in 37°C. It has been shown that this type of mechanical testing is an appropriate method to determine the characteristics of the biomaterial in physiological conditions [48-51].

The storage modulus (E') of the composites and alginate were determined as a function of frequency. With an increase in frequency, there is a slight change in the storage modulus of the composites. While alginate films display a slight increase in the storage modulus, the addition of CNCs or CNC-Ts does not cause a similar increase. The storage modulus remains constant until approximately 7 Hz and then

begins to decrease. This decrease is not dependent on the modification of CNCs, but is more pronounced for 10:90 CNC-T:Alginate composites.

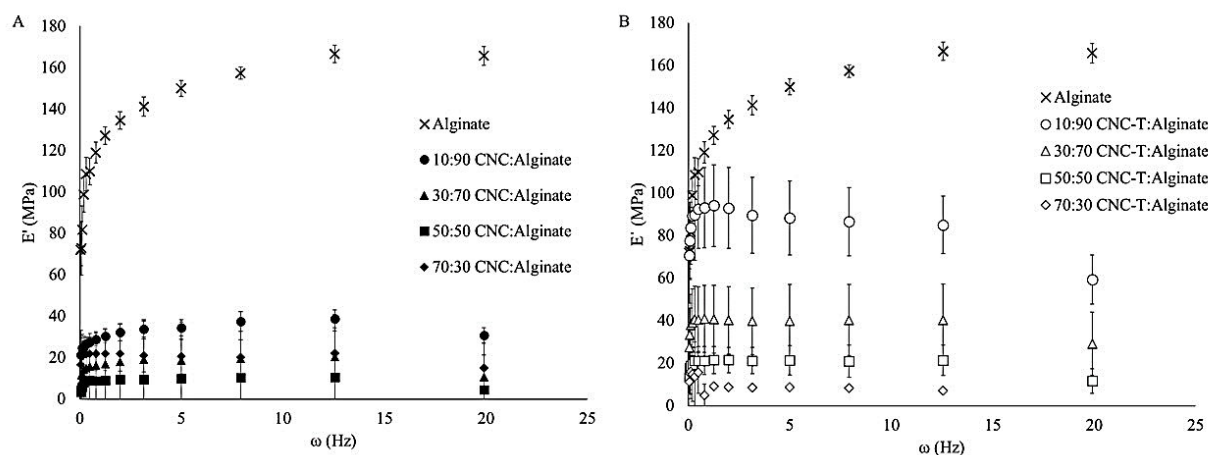


Figure 3. Frequency dependent dynamic mechanical analysis from 0.5-20 Hz with 3% applied strain in aqueous conditions in D-PBS at 37°C for CNC:Alginate composites (A) and CNC-T:Alginate composites (B). With apparent decreases in storage modulus for all of the nanocomposites, which can be caused by the orientation of the samples with increased exposure of the “egg-box” structure to ions present in D-PBS.

Cellulose nanocrystals, either unmodified or oxidized, have a negative impact on the storage modulus of the alginate, this negative impact is less with CNC-T:Alginate composites. This can be possibly explained by the interaction between the carboxyl groups of the CNC-T with the “egg-box” structure of the crosslinked alginate. This concept was further analyzed and explained by Lin et al. with alginate-CNC-T sponges in a dry state [12] and previous work by the authors, which analyzed the effect of hydration on cellulose nanocrystal-alginate composites. It was determined by tensile testing and complexometric titration that the addition of CNC-T improved the elongation at break and Young’s modulus when compared to CNCs and prevents less Ca^{2+} leaching from the composites because of increased ionic interactions with the “egg box” structure [52].

While the addition of CNCs or CNC-Ts does not improve the viscoelastic behavior of alginate, interestingly, the addition of nanocellulose causes a systematic decrease in the storage modulus. With increased CNC or CNC-T content the storage modulus decreases. This could be of use to create systems in which the storage modulus of alginate systems can be controlled.

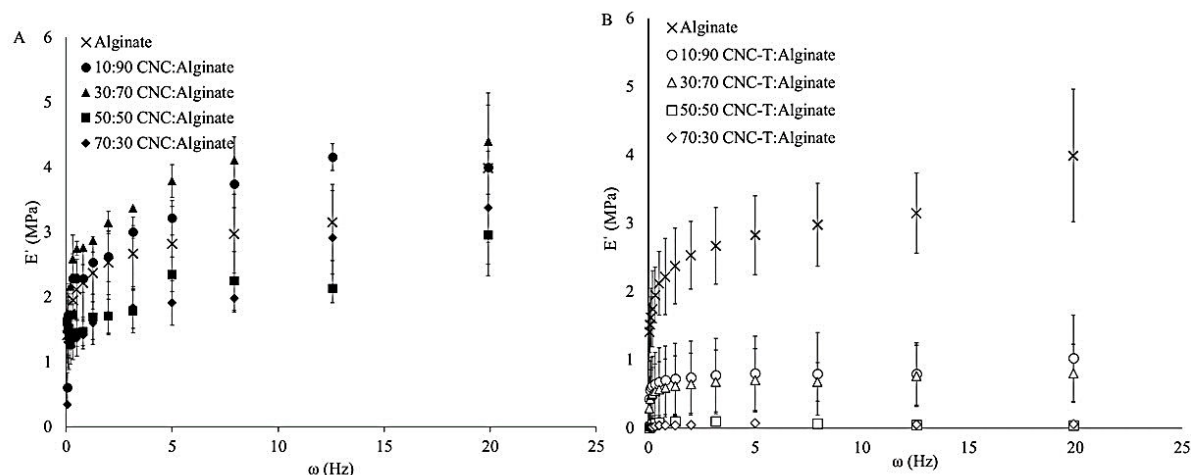


Figure 4. Compression Frequency dependent dynamic mechanical analysis from 0.5-20 Hz with 3% applied strain in aqueous conditions in D-PBS at 37°C for CNC:Alginate composites (A) and CNC-T:Alginate composites (B). With apparent decreases in storage modulus for a majority of nanocomposites, except 10:90 CNC:Alginate and 30:70 CNC:Alginate.

Compression testing of the alginate-based composites produces differing results when compared to frequency dependent testing. This difference is a lessening of the storage modulus, but also a change in the trends. Compared with frequency-dependent testing, which showed a decrease in storage modulus with increased frequency, compression testing shows an increase in storage modulus with increased frequency. This increase in storage modulus in relation to frequency is more pronounced with CNC:Alginate composites. With applied compression, there is less energy stored within the composites when compared to frequency-dependent applied tension. While CNC-T-based composites still have a storage modulus less than alginate that is dependent on the amount of CNC-Ts, CNC-based composites do not follow a similar trend. For CNC:Alginate composites of 10:90 and 30:70 ratios there is an improvement of the storage modulus. This indicates that in a compressive state the addition of CNCs to a certain ratio improves the storage modulus, but decreases after maximum improvement. Once again, while the addition of CNCs or CNC-Ts do not improve the storage modulus in a majority of systems, it can be used to create tunable structures. The differences in the values of storage modulus in frequency-dependent and compression testing can be explained by the lack of restorative force in the alginate and alginate composite films. The dimensions of the films (i.e. small thickness) could prevent a noticeable effect of this material property.

3.2 MSC Cell Culture with CNC:Alginate and CNC-T:Alginate Composites

3.2.1 Cell Adhesion

Cell adhesion is a critical aspect to determine if a biomaterial is biocompatible or not. The adhesion and morphology of MSCs were studied in order to see if the addition of CNCs or CNC-Ts had an effect on the MSCs compared to unmodified alginate substrates.

The cell morphology, surface area, aspect ratio, and area fraction covered by MSCs were determined by Phalloidin staining at 6 h and 24 h following cell seeding. As seen in Figure 5, the addition of CNC or CNC-T causes a change in the MSCs morphology compared to alginate. This was quantified by measuring the area and aspect ratio of the cells, with more elongated cells displaying a higher aspect ratio.

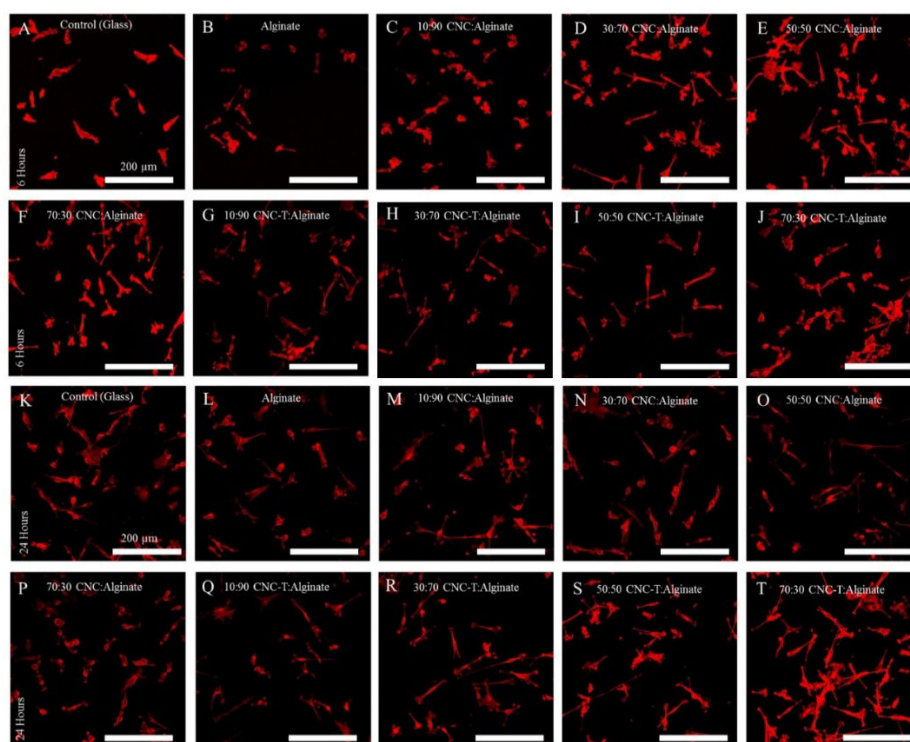


Figure 5. Confocal microscopy images of D1 MSCs stained for actin seeded on A, K) Control (Glass) B, L) Alginate, C, M) 10:90 CNC:Alginate, D, N) 30:90 CNC:Alginate, E, O) 50:50 CNC:Alginate, F, P) 70:30 CNC:Alginate, G, Q) 10:90 CNC-T:Alginate, H, R) 30:70 CNC-T:Alginate, I, S) 50:50 CNC-T:Alginate, and J, T) 70:30 CNC-T:Alginate at A-J) at 6h and K-T) 24h post-seeding with a scale bar of 200 μm

Cell area at 6 h was not widely affected by culturing MSCs on any of the alginate substrates. 30:70 CNC:Alginate versus 30:70 CNC-T:Alginate. Interestingly, only this composition had a significant

difference in cell area at 6h with 30:70 CNC:Alginate having 17% less area compared to 30:70 CNC-T:Alginate. In comparison with the control at 6h, 10:90 CNC:Alginate, 70:30 CNC:Alginate, and 70:30 CNC-T:Alginate had less cell area (-20%, -19%, and -19%, respectively $p<0.05$). From 6h to 24h only some of the tested substrates had a significant increase in cell area (control, alginate, all of the CNC:Alginate substrates, 10:90 CNC-T:Alginate, and 70:30 CNC-T:Alginate). This lack of cell area change within the substrates with CNC-T indicates that the cells maintain a similar shape at 6h and at 24h. This is supported in the results presented for aspect ratio. For the same substrates that did not have a significant increase in cell area, there is not a significant increase in cell aspect ratio.

There were more pronounced significant changes at 24h versus the control and alginate, but also between CNC:Alginate and CNC-T:Alginate substrates with the same composition. Only 50:50 CNC:Alginate vs. 50:50 CNC-T:Alginate had any significant differences with the CNC-T:Alginate substrate having 16% less area compared to the CNC:Alginate substrate. In comparison to alginate, CNC-T:Alginate substrates had more significant differences in cell area (30:70 -17% , 50:50 -24% , and 70:30 -11%, $p<0.05$). When compared with the control at 24h only 50:50 CNC:Alginate, 70:30 CNC:Alginate, and 30:70, 50:50, and 70:30 CNC-T:Alginate had significantly less cell area (-14%, -18%, -19%, -26%, and -13%, respectively $p<0.05$). This decrease in cell area can be related to changes in the cell aspect ratio with cells becoming more elongated and not spreading in a similar manner to the control, but only 30:70 CNC:Alginate in this instance has a significant increase in cell aspect ratio compared to the control at 24 h (+21%, $p<0.05$).

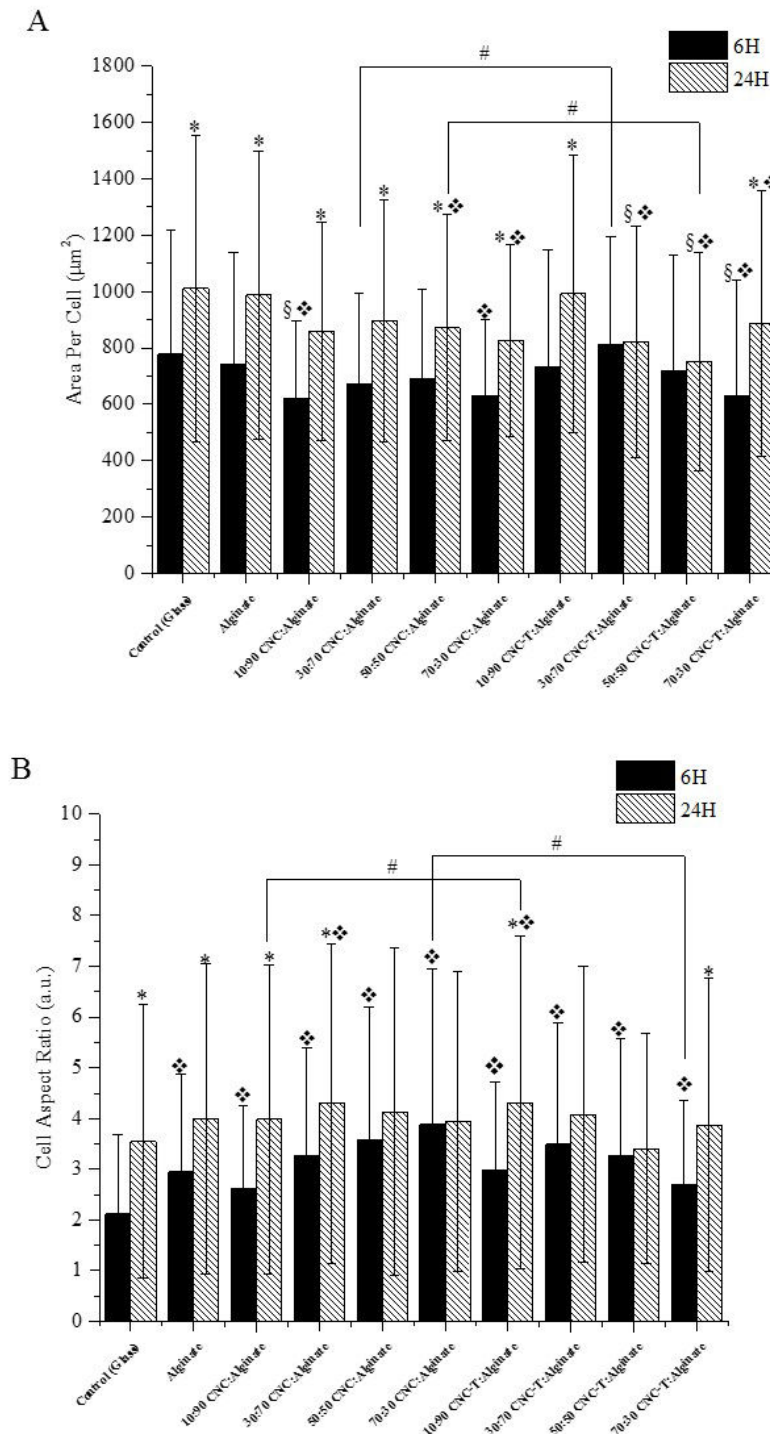


Figure 6. A) surface area per cell and B) cell aspect ratio as measured by ImageJ (N=300) for two independent experiments. * $p < 0.05$ significance between 6h and 24h for same substrate, # $p < 0.05$ significance between composites with same ratio of nanocellulose at the same time point, ¶ $p < 0.05$ significance between control (glass) and composite at same time point, § $p < 0.05$ significance between alginate and composite at same time point. Where significant decreases in cell area occur in 10:90 CNC:Alginate and 50:50 CNC-T:Alginate samples with less cell spreading.

At 6 hours post-seeding, significant higher aspect ratios were observed for all the substrates when compared to the control group (Figure 5B). With 50:50 CNC:Alginate, 70:30 CNC:Alginate, 30:70 CNC-T:Alginate, and 50:50 CNC-T:Alginate the aspect ratio of the cells remains similar between 6 and 24 hours. This lack of change in the aspect ratio suggests that the cells maintain the same shape, and do not further increase their cytoplasmic extensions. Cells on the other substrates developed long cytoplasmic extensions attached to the cellulose surface between 6 and 24 hours which is supported by an increase of the cell aspect ratio as seen in Figure 5. Interestingly, there is no significant difference reported for any of the substrates with nanocellulose added compared to alginate. This suggests that cells seeded on alginate and the composites have a similar cell aspect ratio at both 6 and 24 hours. When comparing composites with the same ratio of nanocellulose only ratios of 70:30 at 6h and 10:90 at 24h have significant differences (44%, 8%, respectively $p < 0.05$). The lack of differences with the other substrates for cell aspect ratio and area, as reported earlier, indicates that the TEMPO-mediated oxidation of CNCs does not cause a difference in cell behavior.

The changes in cell area and aspect ratio on CNC:Alginate and CNC-T:Alginate compared to the control suggests that alginate composites have properties that allows MSCs to more quickly spread and form cytoplasmic extension compared to the control. The lack of significant differences with the alginate can possibly be attributed to the lack of difference in surface roughness of the samples as indicated by AFM, but also shows that the decrease in storage modulus as measured by DMA also does not have a pronounced effect on MSC behavior.

To determine if the addition of nanocellulose improves the spreading of cells adhering to the surface of alginate, the area fraction of the well plate covered by MSCs was determined. As seen in Figure 6, the addition of CNCs or CNC-Ts does cause an improvement in the area covered by cells adhering to the surface when compared to alginate. All samples had a reported improvement in the amount adhered to the surface at 6 and 24 hours, but only a few composites with reported significance. For example, only 30:70 CNC:Alginate and 50:50 CNC:Alginate increased compared to alginate at 24 hours (+126% 30:70 CNC:Alginate, +205% 50:50 CNC:Alginate vs. Alginate, $p < 0.05$).

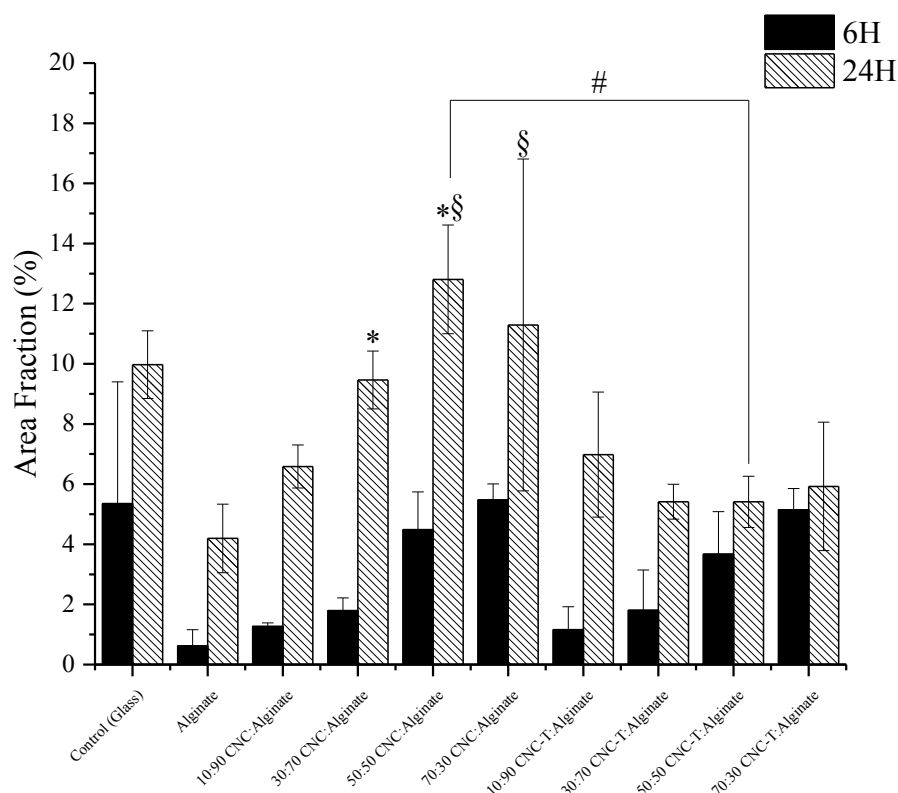


Figure 7. Area fraction of well surface area covered by D1 MSCs seeded at a density of 10,000 cells/cm² on TCPS (Control), Alginate, CNC:Alginate composites, and CNC-T:Alginate composites (N=3 per group). *p<0.05 significance between 6h and 24h for same substrate, #p<0.05 significance between composites with same ratio of nanocellulose at the same time point, §p<0.05 significance between alginate and composite at same time point. Where a significant increase in area fraction covered by cells is apparent with nanocomposites with CNCs at higher ratios compared to alginate

This displays that only unmodified CNCs at higher ratios cause an increase in the adhesion of MSCs, but the same trends do not follow for cell morphology, but that the addition of a bulk filler like nanocellulose are able improve the adhesion properties of alginate.

3.2.2 MSC Viability

The effect of CNC:Alginate and CNC-T:Alginate composites on the mitochondrial activity of MSCs was evaluated *in vitro* using an MTT assay. Cell viability was measured 24 and 48 hours post seeding. All alginate-based composites had a significant lower viability compared to the control at 24h and 48h post-seeding. The lessening of the percentage of viable cells compared to the control can be explained by the formation of cellular clusters on the surface of the alginate and alginate-based composites and shown in Figure 8. This is a common phenomenon that occurs with culturing of

cells onto alginate [39], which is why many researchers prefer to culture cells into alginate microspheres or attach RGD ligands to the surface to improve adhesion [31].

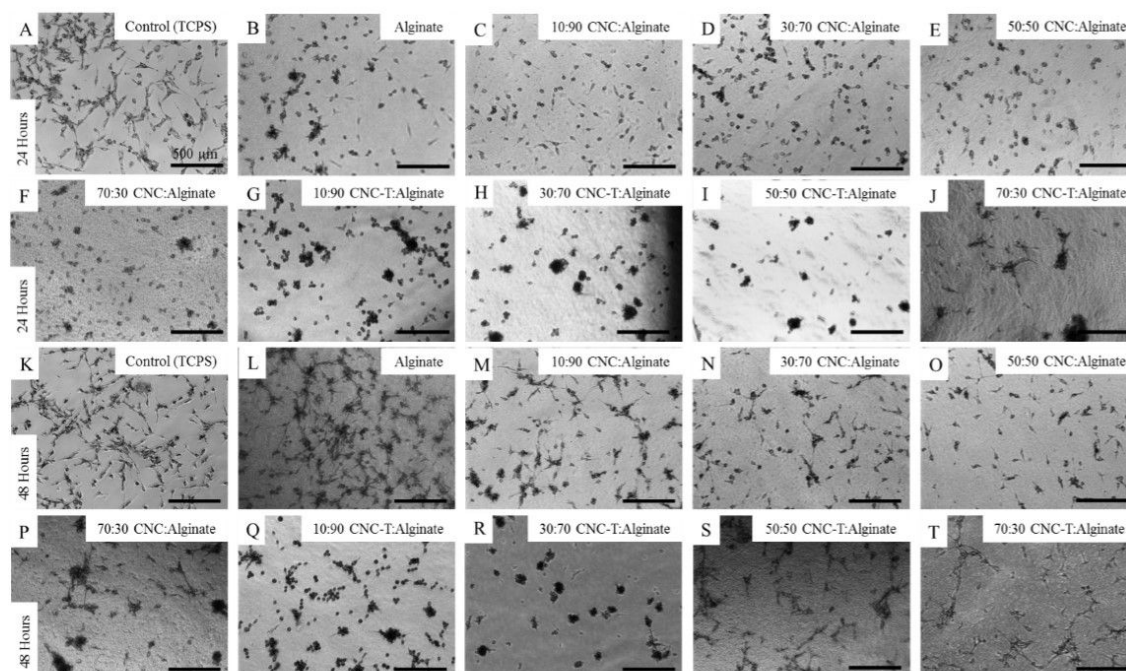


Figure 8. Microscopy images of D1 MSCs following formazan crystal formation A, K) Control (TCPS), B, L) Alginate, C, M) 10:90 CNC:Alginate, D, N) 30:90 CNC:Algiante, E, O) 50:50 CNC:Alginate, F, P) 70:30 CNC:Algiante, G, Q) 10:90 CNC-T:Alginate, H, R) 30:70 CNC-T:Alginate, I, S) 50:50 CNC-T:Alginate, and J, T) 70:30 CNC-T:Alginate at A-J) at 24h and K-T) 48h post-seeding with a scale bar of 500 μm

A significant percent of viable cells increased between 24 and 48 hours for 10:90 CNC:Algiante, 30:70 CNC:Alginate, 50:50 CNC:Alginate, and the control (+423%, +245%, +57%, +223% respectively; $p < 0.05$). The increased viability of MSCs with time shows that the cells remain viable, and continue to proliferation on the surface of the alginate-based composites. Interestingly, compared to alginate at 48 hours, most the composites had higher cell viability (except 30:70 CNC-T:Alginate), but only on 10:90 CNC:Alginate had a significant higher viability at 48 h post seeding (+87% $p < 0.05$ vs. alginate).

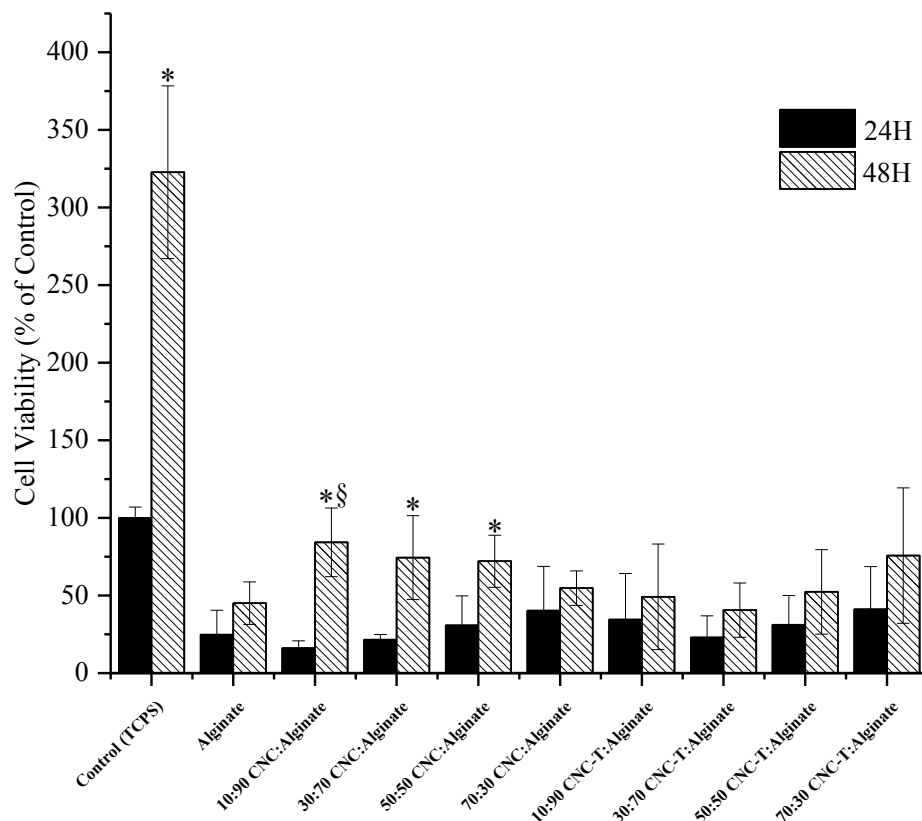


Figure 9. MTT assay results reported in % of control to monitor cell proliferation and viability following 24h and 48h incubation of 10,000 cells/cm² on TCPS (Control), Alginate, CNC:Alginate composites, and CNC-T:Alginate composites (N=12 per group) from 2 independent experiments. *p<0.05 significance between 24h and 48h for same substrate, #p<0.05 significance between composites with same ratio of nanocellulose at the same time point, § p<0.05 significance between alginate and composite at same time point. All samples (alginate and composites) have 24h and 48h significance with the TCPS control. Only instance of significant increases compared to alginate occurs in the 10:90 CNC:Alginate sample, but an overall trend of increased viability does exist.

These changes show that the addition of nanocellulose can actually increase the viability of MSCs when cultured on alginate. These results indicate that future tests using CNCs and alginate to create microspheres could prove to be advantageous for cell viability. Or in other words, the addition of nanocellulose does not have a negative effect on the cell viability characteristics of alginate.

4. Conclusion

The addition of CNCs or TEMPO-mediated oxidized CNCs causes a change in the characteristics of alginate when tested in physiological conditions and in regards to stem cell behavior. While there is

not a systematic improvement of the mechanical properties as measured in PBS at 37°C, there are changes in the properties. These changes, as well as previously reported data, indicate that the use of nanocellulose for a bulk filler in alginate can improve the mechanical properties, but only in certain fabrication ratios. These composites were tested with MSCs to determine if the nanocomposites have affect cell behavior such as cell morphology, adhesion, and viability. There were few reported significant difference between alginate and the cellulose nanocrystal-alginate nanocomposites. These reported differences in cell adhesion and viability indicate that CNCs and CNC-Ts can be used to improve the properties of alginate in cell culture. Especially in regards to adhesion and viability with low ratios of unmodified CNCs.

5. Acknowledgments

This work has been partially supported by the LabEx Tec 21 (Investissements d'Avenir, Grant Agreement ANR-11-LABX- 0030 and by FAPESP Grant13/07932-6. LGP2 is part of the PolyNat Carnot Institut (Investissements d'Avenir, Grant Agreement ANR-16-CARN-0025-01). LMGP is part of the LabEx Centre of Excellence of Multifunctional Architected Materials “CEMAM” (ANR 10-LABX-44-01). C.P. and J.B. are members of the Institute Universitaire de France whose support is acknowledged. The confocal laser microscope was bought on a European Research Council grant (FP7/2007-2013) / ERC GA259370. The authors would like to thank Isabelle Paintrand of LMGP for her assistance with the confocal microscope.

6. References

- [1] Urruzola I, Robles E, Serrano L, Labidi J. Nanopaper from almond (*Prunus dulcis*) shell. *Cellulose*. 2014;21:1619-29.
- [2] Domingues RM, Gomes ME, Reis RL. The potential of cellulose nanocrystals in tissue engineering strategies. *Biomacromolecules*. 2014;15:2327-46.
- [3] Rånby B, Ribi E. Über den feinkbau der zellulose. *Experientia*. 1950;6:12-4.
- [4] Favier V, Dendievel R, Canova G, Cavaille J, Gilormini P. Simulation and modeling of three-dimensional percolating structures: case of a latex matrix reinforced by a network of cellulose fibers. *Acta Materialia*. 1997;45:1557-65.
- [5] Favier V, Canova G, Cavaillé J, Chanzy H, Dufresne A, Gauthier C. Nanocomposite materials from latex and cellulose whiskers. *Polymers for Advanced Technologies*. 1995;6:351-5.

- [6] Bilbao-Sainz C, Bras J, Williams T, Sénechal T, Orts W. HPMC reinforced with different cellulose nano-particles. *Carbohydrate Polymers*. 2011;86:1549-57.
- [7] Peresin MS, Habibi Y, Zoppe JO, Pawlak JJ, Rojas OJ. Nanofiber composites of polyvinyl alcohol and cellulose nanocrystals: manufacture and characterization. *Biomacromolecules*. 2010;11:674-81.
- [8] Jorfi M, Roberts MN, Foster EJ, Weder C. Physiologically responsive, mechanically adaptive bio-nanocomposites for biomedical applications. *ACS Applied Materials & Interfaces*. 2013;5:1517-26.
- [9] Mariano M, El Kissi N, Dufresne A. Cellulose nanocrystal reinforced oxidized natural rubber nanocomposites. *Carbohydrate Polymers*. 2016;137:174-83.
- [10] Annamalai PK, Dagnon KL, Monemian S, Foster EJ, Rowan SJ, Weder C. Water-Responsive Mechanically Adaptive Nanocomposites Based on Styrene–Butadiene Rubber and Cellulose Nanocrystals Processing Matters. *ACS Applied Materials & Interfaces*. 2014;6:967-76.
- [11] Roohani M, Habibi Y, Belgacem NM, Ebrahim G, Karimi AN, Dufresne A. Cellulose whiskers reinforced polyvinyl alcohol copolymers nanocomposites. *European Polymer Journal*. 2008;44:2489-98.
- [12] Lin N, Bruzzese C, Dufresne A. TEMPO-oxidized nanocellulose participating as crosslinking aid for alginate-based sponges. *ACS Appl Mater Interfaces*. 2012;4:4948-59.
- [13] Huq T, Salmieri S, Khan A, Khan RA, Le Tien C, Riedl B, et al. Nanocrystalline cellulose (NCC) reinforced alginate based biodegradable nanocomposite film. *Carbohydrate Polymers*. 2012;90:1757-63.
- [14] George M, Abraham TE. Polyionic hydrocolloids for the intestinal delivery of protein drugs: alginate and chitosan—a review. *Journal of Controlled Release*. 2006;114:1-14.
- [15] Gombotz WR, Wee SF. Protein release from alginate matrices. *Advanced Drug Delivery Reviews*. 2012;64:194-205.
- [16] Lee KY, Mooney DJ. Hydrogels for tissue engineering. *Chemical Reviews*. 2001;101:1869-80.
- [17] Drury JL, Mooney DJ. Hydrogels for tissue engineering: scaffold design variables and applications. *Biomaterials*. 2003;24:4337-51.
- [18] Kuo CK, Ma PX. Ionically crosslinked alginate hydrogels as scaffolds for tissue engineering: Part 1. Structure, gelation rate and mechanical properties. *Biomaterials*. 2001;22:511-21.
- [19] Tønnesen HH, Karlsen J. Alginate in drug delivery systems. *Drug Development and Industrial Pharmacy*. 2002;28:621-30.
- [20] Choi B, Park HJ, Hwang S, Park J. Preparation of alginate beads for floating drug delivery system: effects of CO₂ gas-forming agents. *International Journal of Pharmaceutics*. 2002;239:81-91.

- [21] Stockwell A, Davis S, Walker S. In vitro evaluation of alginate gel systems as sustained release drug delivery systems. *Journal of Controlled Release*. 1986;3:167-75.
- [22] Simmons CA, Alsberg E, Hsiong S, Kim WJ, Mooney DJ. Dual growth factor delivery and controlled scaffold degradation enhance in vivo bone formation by transplanted bone marrow stromal cells. *Bone*. 2004;35:562-9.
- [23] Alsberg E, Kong H, Hirano Y, Smith M, Albeiruti A, Mooney D. Regulating bone formation via controlled scaffold degradation. *Journal of dental research*. 2003;82:903-8.
- [24] Bouhadir KH, Lee KY, Alsberg E, Damm KL, Anderson KW, Mooney DJ. Degradation of partially oxidized alginate and its potential application for tissue engineering. *Biotechnology Progress*. 2001;17:945-50.
- [25] Bajpai SK, Sharma S. Investigation of swelling/degradation behaviour of alginate beads crosslinked with Ca^{2+} and Ba^{2+} ions. *Reactive and Functional Polymers*. 2004;59:129-40.
- [26] Shoichet MS, Li RH, White ML, Winn SR. Stability of hydrogels used in cell encapsulation: An in vitro comparison of alginate and agarose. *Biotechnology and Bioengineering*. 1996;50:374-81.
- [27] Drury JL, Dennis RG, Mooney DJ. The tensile properties of alginate hydrogels. *Biomaterials*. 2004;25:3187-99.
- [28] Lee KY, Rowley JA, Eiselt P, Moy EM, Bouhadir KH, Mooney DJ. Controlling mechanical and swelling properties of alginate hydrogels independently by cross-linker type and cross-linking density. *Macromolecules*. 2000;33:4291-4.
- [29] Smetana K. Cell biology of hydrogels. *Biomaterials*. 1993;14:1046-50.
- [30] Rowley JA, Madlambayan G, Mooney DJ. Alginate hydrogels as synthetic extracellular matrix materials. *Biomaterials*. 1999;20:45-53.
- [31] Rowley JA, Mooney DJ. Alginate type and RGD density control myoblast phenotype. *Journal of biomedical materials research*. 2002;60:217-23.
- [32] Yu J, Du KT, Fang Q, Gu Y, Mihardja SS, Sievers RE, et al. The use of human mesenchymal stem cells encapsulated in RGD modified alginate microspheres in the repair of myocardial infarction in the rat. *Biomaterials*. 2010;31:7012-20.
- [33] Ma HL, Hung SC, Lin SY, Chen YL, Lo WH. Chondrogenesis of human mesenchymal stem cells encapsulated in alginate beads. *Journal of Biomedical Materials Research Part A*. 2003;64:273-81.
- [34] Kavalkovich KW, Boynton RE, Murphy JM, Barry F. Chondrogenic differentiation of human mesenchymal stem cells within an alginate layer culture system. *In Vitro Cellular & Developmental Biology-Animal*. 2002;38:457-66.

- [35] Mehlhorn A, Schmal H, Kaiser S, Lepski G, Finkenzeller G, Stark G, et al. Mesenchymal stem cells maintain TGF- β -mediated chondrogenic phenotype in alginate bead culture. *Tissue Engineering*. 2006;12:1393-403.
- [36] Hynes RO. Integrins: versatility, modulation, and signaling in cell adhesion. *Cell*. 1992;69:11-25.
- [37] Dalby MJ, Gadegaard N, Oreffo RO. Harnessing nanotopography and integrin-matrix interactions to influence stem cell fate. *Nature materials*. 2014;13:558-69.
- [38] Discher DE, Janmey P, Wang YL. Tissue cells feel and respond to the stiffness of their substrate. *Science*. 2005;310:1139-43.
- [39] Yagi K, Tsuda K, Serada M, Yamada C, Kondoh A, Miura Y. Rapid formation of multicellular spheroids of adult rat hepatocytes by rotation culture and their immobilization within calcium alginate. *Artificial organs*. 1993;17:929-34.
- [40] Mano J, Reis R, Cunha A. Dynamic mechanical analysis in polymers for medical applications. *Polymer based systems on tissue engineering, replacement and regeneration*: Springer; 2002. p. 139-64.
- [41] Awad HA, Wickham MQ, Leddy HA, Gimble JM, Guilak F. Chondrogenic differentiation of adipose-derived adult stem cells in agarose, alginate, and gelatin scaffolds. *Biomaterials*. 2004;25:3211-22.
- [42] Kong HJ, Smith MK, Mooney DJ. Designing alginate hydrogels to maintain viability of immobilized cells. *Biomaterials*. 2003;24:4023-9.
- [43] Jeon O, Bouhadir KH, Mansour JM, Alsberg E. Photocrosslinked alginate hydrogels with tunable biodegradation rates and mechanical properties. *Biomaterials*. 2009;30:2724-34.
- [44] Phisalaphong M, Suwanmajo T, Tammarate P. Synthesis and characterization of bacterial cellulose/alginate blend membranes. *Journal of Applied Polymer Science*. 2008;107:3419-24.
- [45] Kanjanamosit N, Muangnapoh C, Phisalaphong M. Biosynthesis and characterization of bacteria cellulose–alginate film. *Journal of Applied Polymer Science*. 2010;115:1581-8.
- [46] Abdollahi M, Alboofetileh M, Rezaei M, Behrooz R. Comparing physico-mechanical and thermal properties of alginate nanocomposite films reinforced with organic and/or inorganic nanofillers. *Food Hydrocolloids*. 2013;32:416-24.
- [47] Li Z, Ramay HR, Hauch KD, Xiao D, Zhang M. Chitosan–alginate hybrid scaffolds for bone tissue engineering. *Biomaterials*. 2005;26:3919-28.
- [48] Caridade SG, Merino EG, Alves NM, Mano JF. Bioactivity and viscoelastic characterization of chitosan/bioglass® composite membranes. *Macromolecular bioscience*. 2012;12:1106-13.

- [49] Caridade SG, Merino EG, Alves NM, de Zea Bermudez V, Boccaccini AR, Mano JF. Chitosan membranes containing micro or nano-size bioactive glass particles: evolution of biomineralization followed by in situ dynamic mechanical analysis. *Journal of the mechanical behavior of biomedical materials*. 2013;20:173-83.
- [50] Malheiro VN, Caridade SG, Alves NM, Mano JF. New poly (ϵ -caprolactone)/chitosan blend fibers for tissue engineering applications. *Acta biomaterialia*. 2010;6:418-28.
- [51] Silva JM, Duarte ARC, Caridade SG, Picart C, Reis RL, Mano JoF. Tailored freestanding multilayered membranes based on chitosan and alginate. *Biomacromolecules*. 2014;15:3817.
- [52] Grant GT, Morris ER, Rees DA, Smith PJ, Thom D. Biological interactions between polysaccharides and divalent cations: the egg-box model. *FEBS Letters*. 1973;32:195-8.

Chapter 4.2 Tunable Structural and Mechanical Properties of Cellulose Nanofiber Substrates in Liquid for Stem Cell Culture

This subchapter is based on *Tuning of Mechanical Properties of Cellulose Nanofiber Films in Aqueous Conditions for Cell Culture*. **Biomacromolecules**. (2017)

Abstract	257
1. Introduction.....	257
2. Materials and Methods	260
2.1 Materials	260
2.2 Methods	260
2.2.1 Production of CNF Films	260
2.2.2 CNF Film Characterization.....	261
2.2.3 MSC Cell Culture on CNF Films	263
2.3.4 Statistical Analysis	264
3. Results and Discussion.....	265
3.1 Tuning the Nanostructure Organization of CNF Substrate	265
3.2 Tuning Mechanical Properties of CNF Substrate.....	271
3.3 Influence of Tunable CNF Substrate on Cell Adhesion and Morphology	272
3.4 Influence of Tunable CNF Substrate on Cell Metabolic Activity	275
4. Conclusion	277
5. Acknowledgements.....	278
6. References	278

Tunable Structural and Mechanical Properties of Cellulose Nanofiber Substrates in Liquid for Stem Cell Culture

Megan Smyth^{a,b}, Carole Fournier^{c,d}, Carlos Driemeier^e, Catherine Picart^{c,d}, E. Johan Foster^f,
Julien Bras^{a,b,g}

a. CNRS, LGP2, 461 Rue de la Papeterie, 38402, Saint-Martin-d'Hères, France

b. Université Grenoble Alpes, LGP2, 38000 Grenoble, France

c. CNRS, UMR 5628, LMGP, 38016 Grenoble, France

d. Université Grenoble Alpes, Grenoble Institute of Technology, 38016 Grenoble, France

e. Centro Nacional de Pesquisa em Energia e Materiais (CNPEM), Laboratório Nacional de Ciência e Tecnologia do Bioetanol (CTBE), 13083-970 Campinas, São Paulo, Brazil

f. Virginia Polytechnic Institute and State University (Virginia Tech), Macromolecules Innovation Institute (MII), Department of Materials Science and Engineering, Blacksburg, Virginia 24061, USA

g. Institut Universitaire de France, 75005 Paris, France

Abstract

Thin cellulose nanofiber (CNF) nanostructured substrates with varying roughness, stiffness (Young's modulus), porosity, and swelling properties were produced, by varying the conditions used during fabrication. It was shown that with increased heat exposure, CNF substrate porosity in an aqueous state decreased while Young's modulus in a water submerged state increased. In this study, the adhesion and viability of mesenchymal stem cells (MSCs) cultured on this CNF substrate will be presented. Viability of D1/BALBc MSCs were assessed for 24 and 48 hours, and it was shown that depending on the CNF substrate the viability varied significantly. The adhesion of MSCs after 6 and 24 hours was conditional on material mechanical properties and porosity of the CNF in cell culture conditions. These results suggest that material properties of CNF nanostructured substrate within the aqueous state can be easily tuned with curing step without any chemical modification to the CNF, and that these changes can affect MSC viability in cell culture.

1. Introduction

With being the most abundant polymer on earth, interest in the use of cellulose for a variety of applications from paper or polymer composites to biomedical applications has increased annually since the 1980s [1]. Cellulose has favorable properties for biomedical researchers such as biocompatibility,

renewability, and low cytotoxicity [2]. The use of cellulose in biomedical applications such as drug delivery, tissue engineering, and wound healing has become more of an interest to researchers who want to use natural polymers [3]. Since the 2000's, a special focus on nanoscale cellulose has been observed for such applications. For example, bacterial nanocellulose (BNC) is commonly used in biomedical applications and is readily available on the market, especially in the field of wound healing [4]. Unfortunately, such material is expensive, its production is difficult to upscale since such membranes are processed with difficulties. The use of other forms of nanoscaled cellulose, cellulose nanocrystals (CNC) or microfibrillated cellulose (MFC, also called CNF), has gained greater interest with the announcement of industrialization the last 5 years. Respectively, discovered in the 50's [5] and the 80's [6], they are obtained from any cellulose fibers [7] either by a chemical hydrolysis for CNCs or by a mechanical disintegration, mostly after a pre-treatment, for CNF. Books [8] and reviews [9, 10] detail their production [11] and properties [12-14], but very recently they have been used in the field of biomedical engineering with a focus on using cellulose as a scaffold for tissue engineering or cell culture [2, 15].

CNCs are mostly used to impart specific chemical properties to promote cell adhesion and direct cell growth [16, 17] or to provide a structure for cell adhesion in a particular direction [18]. CNF has been used as a tissue engineering scaffold in as an additive to a matrix, and most commonly hydrogels [19-22]. Other processing techniques can be used to create cellulose based substrates such as electrospinning [23, 24] and aerogels [25]. Both of these techniques have been employed in biomedical applications. It is worth noting that most of these scientific papers are very recent (less than 2-3 years), proving by itself the novelty of our study.

Indeed microfibrillated cellulose has been first extensively studied for its use in composites and as barrier films [26] [12]. Compared to cellulose nanocrystals, CNF is less crystalline, flexible and has diameter of approximately 20-60 nm and length of several microns [12]. The morphological properties of CNF can vary depending on the source of the CNF, and the means of production. Enzymatic pre-treatment, mechanical fibrillation, homogenization, and chemical treatment are common ways to produce CNF. Each production technique imparts different characteristics to the CNF, such as surface groups, charge, and crystallinity [11]. CNF has numerous hydrogen bonds on the surface of the fiber, and because of these bonds and the entanglement of these flexible nanofibers, they can produce a nanostructured substrate, also called films or nanopaper. Such substrates present very good barrier or mechanical properties, and can also be transparent. There are different means to produce such nanopaper [27, 28], and their large scale production process is still an issue in spite of announcement

of pilot scale roll of such films from VTT Technical Research Centre of Finland. Depending on the manufacturing procedure, their properties might change as recently shown for barriers applications [29]. Others have shown that the structural properties, which influence barrier properties of the CNF film might differ based on drying techniques [29-31], but there has been no research conducted to fine tune the mechanical properties for biomedical applications.

The use of mesenchymal stem cells was first discovered by Friedenstein in the 1970s [32]. Further research on the work of Friedenstein showed that cells isolated from bone marrow had the ability to differentiate into osteoblasts, adipocytes, and chondrocytes [33]. MSC viability is dependent on many factors including adhesion and proliferation. It has been shown that without adhesion stem cells will undergo apoptosis, since stem cells are reliant on substrate attachment, or are anchorage dependent [34, 35]. This anchorage of the cells at the cellular level occurs when cells probe their microenvironment leading to contractility and reorganization of the actin filaments within the cytoskeleton into filopodia [35, 36]. The adhesion of stem cells can be dependent on various factors such as surface chemistry [37], stiffness [35], and topography [34, 36, 38]. In seminal work conducted by Engler and colleagues it was shown that MSCs can present different morphologies and spreading patterns dependent on substrate stiffness, and that these differences in morphology were indicative of various differentiation pathways [39]. The variation of the mechanical properties of polymer based substrates such as polyacrylamide [39] and the effect on MSC adhesion and viability has been studied extensively, but to the best of the authors' knowledge never on nanocellulose based materials with tunable material properties.

Culturing of MSCs onto cellulose based substrates has been performed by a variety of researchers. Most of the work is recent and focuses on bacterial nanocellulose substrates, not CNF produced from wood, which is the focus of this study. Krontiras and colleagues used murine MSCs for adipogenic differentiation using bacterial nanocellulose and alginate scaffolds. It was shown that after 4 weeks in culture, adipocytes displayed lipid formation [40]. BNC has been used alone as a scaffold in work by Favi et al. Favi showed that BNC scaffolds seeded with equine MSCs and differentiated *in vitro* promoted cell viability, proliferation, adhesion, and supported chondrogenic and osteogenic differentiation [41]. For plant-based nanocellulose, limited work has been completed using MSCs with both CNCs and CNF. CNCs were dispersed in a poly(lactic acid), followed by electrospinning to create a scaffold, and tested with human MSCs for basic cytocompatibility by Zhou et al. [42]. Xing and colleagues created a CNF hydrogel with gelatin and tested with human MSCs and determined that MSCs maintained differentiation potential and secreted extracellular matrix, but did not form cellular

colonies on the CNF [19]. Even if others have checked the cytotoxicity of purely CNF aerogels or other substrates [22, 43] or performed human cell culture [25], to the best of the authors' knowledge, there has been no reported research on only CNF based substrates with tunable mechanical properties and mesenchymal stem cells.

Thin CNF substrate mechanical and material properties were easily tuned by exposing the solvent casted CNF films to elevated temperatures. This facile curing step created a change in the material properties without any complicated chemical processes, or the addition of a polymer matrix or filler. Mechanical and material measurements were analyzed in cell culture like conditions to have a better understanding how the properties of CNF thin films are effected by hydration and how these properties could impact future cell based studies. The influence of surface roughness, porosity, and Young's modulus on MSC adhesion and viability will be reported.

2. Materials and Methods

2.1 Materials

A 2 % wt suspension of enzymatically pre-treated CNF from wood pulp (Domsjo) was purchased from Centre Technique du Papier (CTP) (France). Phosphate buffer solution (PBS), Minimum Essential Medium Eagle (α MEM), 4,6-diaminidino-2-phenylindole-dilactate (DAPI), phalloidintetramethylrhod B isothiocyanate dyes (Phalloidin), glycerol, mowiol 4-88, tris buffer saline (TBS), thiazolyl blue tetrazolium bromide (MTT), and dimethyl sulfoxide (DMSO) were purchased from Sigma-Aldrich (USA). BALB/c D1 murine bone marrow mesenchymal stem cells were purchased from American Type Culture Collection (ATCC, France). 10% heat-inactivated fetal bovine serum (FBS) was acquired from PAA Laboratories (Austria), and penicillin streptomycin mixture and L-Glutamine were purchased from Invitrogen (USA). All materials were used as delivered without any chemical modification.

2.2 Methods

2.2.1 Production of CNF Films

CNF was characterized to determine the cellulose content following the protocol of Rowell et al.[44], and zeta potential was measured a Malvern Zetasizer 2000 (Malvern, United Kingdom). 10 mL of approximately 0.001% suspension of CNF was measured in triplicate. Results are reported in mean \pm standard deviation. CNF membranes were produced by casting 1% wt solution of CNF onto teflon mold and allowed to dry at ambient conditions for 5 days (AC-CNF) followed by curing for 1 (1hC-

CNF) or 2 (2hC-CNF) hours at 150°C following a modified protocol by Bardet et al. [29, 31]. Basis weight was determined by the following equation:

$$\text{Basis Weight} \left(\frac{g}{m^2} \right) = \frac{\text{Mass of CNF film}}{\text{Area of CNF film}} \quad (\text{Eq. 1})$$

2.2.2 CNF Film Characterization

Transmittance

To measure the transparency of the CNF films, the transmittance from 300-800 nm was measured with ten scans in spectrum mode with a UV Spectrometer (Shimadzu, Japan) with a normal incidence and repeated in triplicate.

Atomic Force Microscopy (AFM) Imaging

Images of the surface of CNF films were acquired using tapping mode with a Nanoscope IIA microscope from Veeco Instruments (USA) at a frequency of ~265-340 Hz. Silicon cantilevers with a curvature of 10-15 nm were used (OTESPA®, Bruker, USA). For surface roughness measurements 10x10 μm images were acquired to analyze the surface roughness. All measurements were analyzed using Nanoscope Analysis (USA). ImageJ software (NIH) was used to analyze materials dimensions and at least 50 measurements have been performed on at least 5 different images and averages are presented.

Scanning Electron Microscopy (SEM) Imaging

SEM images of the CNF films for thickness measurements were obtained using a Quanta200® (Netherlands). Samples were attached to a holder, coated with a thin layer of Au/Pb to create a conductive charge, and scanned using an accelerated voltage of 10 kV and a working distance of 10.3 mm. An Everhart Thornley-Secondary electron detector (ETD) was employed. For thickness measurements at least 25 measurements were taken from each sample using ImageJ software (U.S National Institutes of Health, USA).

Water Content Measurement

To determine the amount of water remaining in each CNF film, a modified protocol by Fukuzumi was performed [45]. Films were prepared, cured, and conditioned for 1 hour at 23°C and 50%

relative humidity in a desiccator. Following conditioning, each film was weighted to determine the mass and placed in an oven for 24 hours at 105°C to evaporate all remaining water entrapped within the film. Following drying films were once again conditioned for 48 hours and weighed. The water content of the film was determined using the following equation, where M_i is the initial mass and M_d is the dried mass of the film. Each measurement was done in triplicate and averaged.

$$\text{Water Content (\%)} = \frac{M_i - M_d}{M_d} \times 100 \text{ (Eq. 2)}$$

PBS Uptake

Films were dried and conditioned at least 24 hours before analysis in a temperature and humidity controlled room at 35°C and 50% relative humidity. The swelling of films was determined by cutting the films into circles with a diameter of 15 mm and placed in 20 mL of PBS for 24 hours at 37°C. The wet film was removed from the PBS and weighed after excess PBS was removed from the surface of the film using filter paper. The uptake of PBS by the film was calculated using the following formula, where M_0 is the initial mass and M_t is the mass of the film following 24 hours of submersion in PBS.

$$\text{PBS Uptake (\%)} = \frac{M_0 - M_t}{M_t} \times 100 \text{ (Eq. 3)}$$

An average of three replicates for each sample was calculated.

Thermoporometry

Calorimetric thermoporometry was performed following a protocol developed by Driemeier et al. [46]. Thermoporometry employed a differential scanning calorimeter DSC-Q200 (TA Instruments, USA) with a RCS90 (TA Instruments, USA) cooling unit and an autosampler. CNF samples were pre-conditioned by soaking in deionized water (DI-H₂O) for 24 hours. The water-saturated samples were inserted into aluminum Tzero® pans later sealed with hermetic lids. The DSC temperature program freezes samples to -70°C followed by 18 heating steps, each one made of a heating ramp (1°C/min) followed by an equilibrating isotherm. Measured calorimetric signal is analyzed to quantify the amount of ice melting below 0°C, termed Freezing Bound Water (FBW). The temperature depression ΔT of ice melting is related to pore diameter d through the Gibbs-Thomson equation, $d = -2 K_c / \Delta T$, with $K_c = 19.8 \text{ nm/K}$. The reported thermoporometry profiles are the cumulative distributions of FBW (given in units of g water per g dry matter) as function of d in the 1-200 nm range of pore size.

Thermogravimetric Analysis

Thermogravimetric analysis (TGA) was used to determine the amount of water remaining in the CNF film following solvent casting and curing. Thermogravimetric measurements were performed with a Perkin Elmer STA 6000 (USA). The temperature ranged from 30°C to 200°C with a heating rate of 10°C/min. The tests were carried out under atmospheric conditions. All results were analyzed with Pyris Series software (Perkin Elmer, USA).

Mechanical Tests

Tensile tests and dynamic mechanical analysis (DMA) were measured using a TA Instruments RSA 3 (USA) with a submersion clamp system designed internally. CNF films were tested in physiological-like conditions, i.e. in aqueous environment. For physiological-like conditions, CNF films were conditioned for 24 hours in PBS prior to mechanical tests. Samples underwent rectangular tension measurements and compression testing. The distance between the clamps for the tension was 10 mm, and the films had a width of approximately 5 mm and thickness of 0.2 mm. Samples underwent rectangular tension measurements at a rate of 0.001 mm/s at 37°C. For compression, films were tested with an angular frequency from 0-20 Hz at 37°C with a constant strain of 10%. Samples had dimensions of 15 mm in diameter and thickness of approximately 0.2 mm. The stress vs strain and frequency dependent curves were measured and analyzed using TA Orchestrator (USA). Results were done in triplicate.

2.2.3 MSC Cell Culture on CNF Films

Cell culture studies were performed with BALB/c D1 murine bone marrow mesenchymal stem cells (MSCs) (American Type Culture Collection, ATCC, France). Cells were cultured in α MEM supplemented with 10% heat-inactivated fetal bovine serum, 1% penicillin streptomycin mixture and 2 mM L-Glutamine. CNF films were sterilized with UV exposure prior to cell seeding and rinsed twice with DI H₂O. Cells were seeded at a density of 20,000 cells/cm² for 6 hours and 24 hours for DAPI-phalloidin assay, and 24 hours and 48 hours for MTT analysis in a humidified atmosphere of 5% CO₂ at 37 °C.

DAPI-Phalloidin Assay

4,6-Diaminidino-2-phenylindole-dilactate (DAPI, 20 mg/mL, Sigma-Aldrich, USA) and phalloidintetramethylrhod B isothiocyanate dyes (phalloidin, 10 mg/mL, Sigma-Aldrich, USA) were used to determine the adhesion of cells at 6 hours and 24 hours following seeding on CNF substrates and a glass control. At each time point, the culture media was moved and the samples were fixed with 3.7% paraformaldehyde. The paraformaldehyde was removed after 20 min at room temperature and washed twice with PBS. The phalloidin/DAPI solution was added for 45 min at room temperature (12.5 µg/mL phalloidin, 10 µg/mL DAPI). The samples were then washed three times with PBS, mounted with anti-fade reagent, which is 24% glycerol, 9.6% mowiol 4-88 in tris buffered saline (TBS). Followed by analysis by inverted fluorescent microscopy (Zeiss, Germany) or confocal laser scanning microscopy (Zeiss, Germany) 24 hours later. The cell surface area and aspect ratio were analyzed using ImageJ with a sample size of 150 cells per condition using at least 12 different microscopy images from 4 samples from two independent experiments. Cell surface area and aspect ratio measurements were done by measuring clearly defined individual cells using the tracing tool in ImageJ after calibrating the scale and thresholding each image.

MTT Assay

Thiazolyl blue tetrazolium bromide (MTT, 2.5 mg/mL, Sigma Aldrich, USA) was used to perform a MTT assay on five independent experiments to measure the mitochondrial activity of MSCs after 24 hours and 48 hours post seeding on CNF substrates or tissue culture polystyrene (TCPS) control. MTT solution was added to the cells and incubated in media for 1 hour. After 1 hour, the growth media was removed and 500 µL of dimethyl sulfoxide (DMSO) was added to solubilize the formazan crystals formed in the reduction of MTT. 100 µL of the formazan solution was added to a microplate reader and diluted with 100 µL of DMSO. The absorbance of each sample was read at 550 nm. The samples were imaged using optical microscopy (Zeiss, Germany).

2.3.4 Statistical Analysis

All experiments were carried out in triplicate unless otherwise noted. All results are presented with mean \pm standard deviation unless otherwise noted. The R^2 value of thermoporosity vs. Young's modulus was performed by Originlab using a linear-regression test. Statistical analysis of cell studies (DAPI-Phalloidin Assay/MTT Assay) were performed in Originlab using a Kolmogorov-Smirnov test for normality. For the cell area and aspect ratio results following the DAPI-Phalloidin assay, the

samples did not follow a normal distribution and were normalized using a Box-Cox transformation. Following the normalization transformation, a Kolmogorov-Smirnov test was repeated. Normalized results were analyzed by two-way ANOVA with post-hoc testing using a Bonferroni test.

3. Results and Discussion

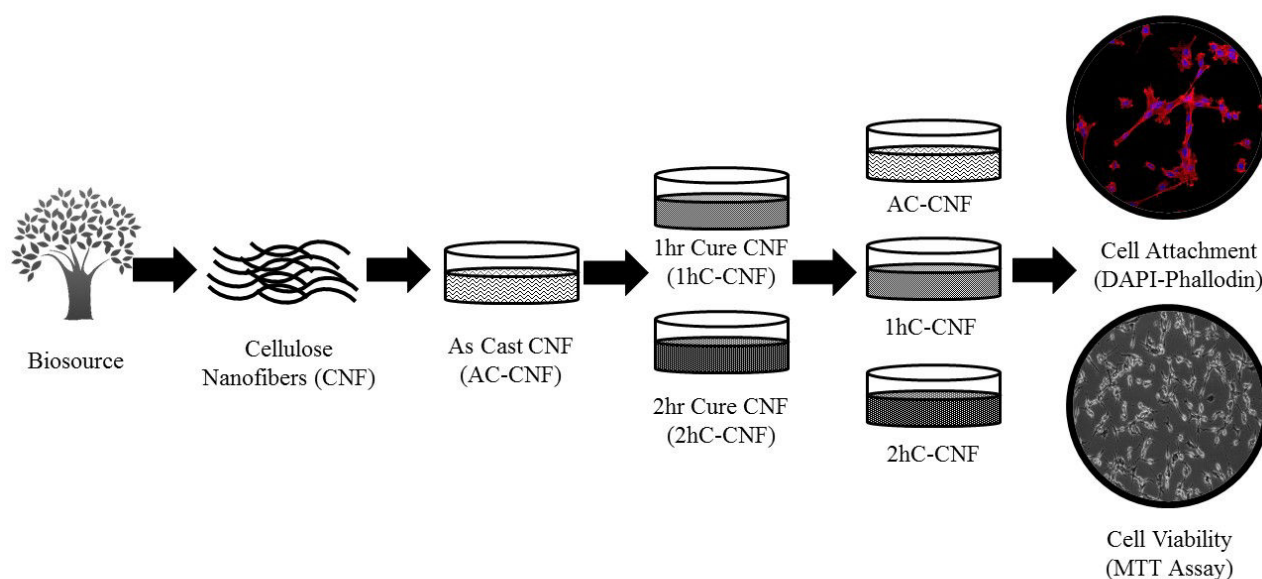


Figure 1. Schematic of the experimental set-up. From raw material of CNF suspension to CNF films and sequential curing of films and eventual cellular testing of CNF films for cell attachment and viability

3.1 Tuning the Nanostructure Organization of CNF Substrate

CNF films were produced with same mass of fiber following a protocol outlined in Section 3.4, but the drying time was varied for tuning the intrinsic properties of such CNF films. The table below summarizes the properties of such substrates.

Table 1. Summary of CNF films properties as measured by 1) UV spectroscopy (S1), 2) Root Mean Squared Roughness values from AFM images of CNF films, as measured by nanoscope analysis AFM, 3) drying of films at 105°C for 24 hours (S2), 4) submersion of films for 24 hours in PBS at 37°C (S2), 5) Basis Weight of CNF Films, 6) thermoporometry, 7) tensile testing at 37°C in PBS, 8) compression DMA at 37°C in PBS.

Sample	Transmittance (%) 300-800 nm ¹	Surface Roughness (RMS) (nm) ²	Water Content (%) (w/w) ³	PBS Uptake (%) (w/w%) ⁴	Basis Weight (g/m ²) ⁵	Freezing Bound Water at < 200 nm (g/g) ⁶	Elongation at Break (%) ⁷	Young's Modulus (E) (MPa) ⁷	Storage Modulus (E') (MPa) from 0.05-20 Hz ⁸
AC- CNF	4.0-10.1	4.71±1.55	13.1±4.0	103.5±2.8	38.6±1.1	0.44± 0.006	4.2 ± 1.3	5.6 ± 0.6	0.022±0.003– 0.305±0.120
1hC- CNF	3.8 -11.5	4.71±1.53	6.6±1.8	70.6±9.5	29.5±3.1	0.38± 0.02	3.4 ± 1.3	52.2 ± 26.3	0.026 ± 0.011– 0.329 ± 0.085
2hC- CNF	2.0 -8.2	4.34±0.48	3.4±1.4	65.3±3.7	28.1±2.8	0.36± 0.02	2.5 ± 0.6	116 ± 29.1	0.050± 0.028– 0.342 ± 0.194

The transmittance of the CNF films was measured using UV spectroscopy with a film holder. As shown in Table 1, there is no clear relationship between the drying time and transmittance of the CNF films. Further images of the films and transmittance graphs are reported in Figure 2. The transmittance of the films is an important measurement in regards to imaging and cell staining; if the transmittance of the films is too low, it is difficult to acquire fluorescent microscopy images and reproducibility of measurement might become a concern. Even though there are slight differences in the transmittance of the samples, the transmittance is high enough to allow for staining and microscope imaging following cell culture.

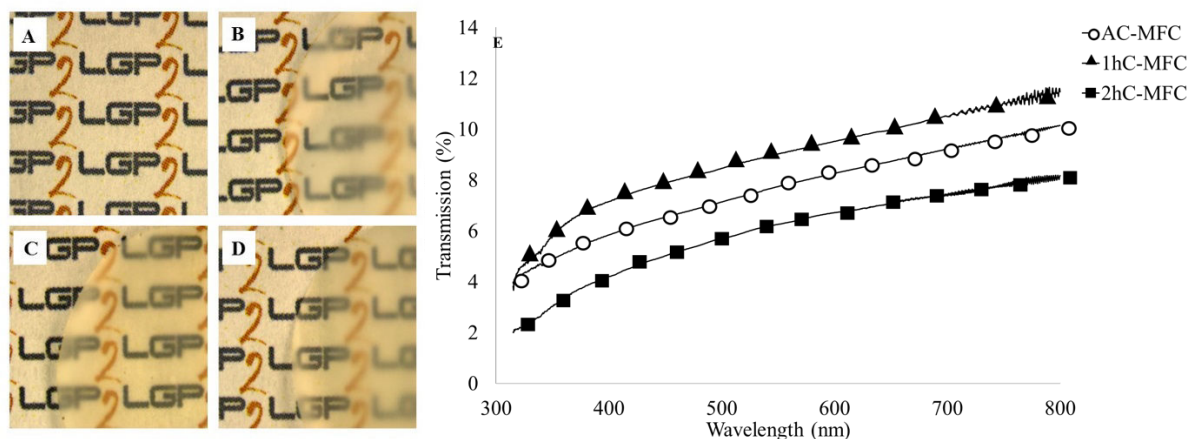


Figure 2. Optical images of A) Polystyrene (PS), B) as cast MFC film without any modification (AC-MFC), C) solvent casted films followed by 1 hour of curing at 150 °C (1hC-MFC) and D) followed by 2 hours of curing at 150°C (2hC-MFC). E) Transmittance of MFC films as a function of wavelength, measured using UV spectroscopy from 300-800 nm.

As shown in the images the transparency of the MFC films is much lower than the PS plate, which is a control for cell culture. LGP2 logo is used with permission from Didier Chaussy, 2017

The structural characteristics of the CNF substrates were measured using AFM, SEM, water content, PBS uptake, and thermoporometry. It was important to analyze the structure of the CNF substrates to investigate if there is any relationship between structural changes caused by curing at high temperature and the mechanical properties of these films.

Atomic force microscopy was performed on the CNF nanopaper to characterize their surface roughness. Figure 3 shows the AFM images of the film surface acquired following drying and curing. The reported roughness values from root-mean-square analysis of AFM images of AC-CNF, 1hC-CNF, and 2hC-CNF (Table 1.) shows that for micro scale roughness there is no significant difference between the roughness. Compared to glass, which was used as a control in the cell aspect ratio and surface area measurements, CNF has higher surface roughness (~ 4.7 nm), while glass is about 0.5 nm as reported by Domke et al. with the same scan size by AFM [47].

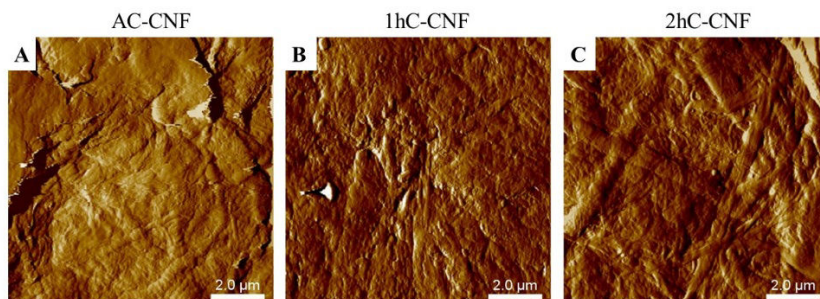


Figure 3. Atomic force microscopy images (10x10 μm) of the surface of the CNF films A) AC-CNF, B) 1hC-CNF, and C) 2hC-CNF taken by tapping mode in air

Scanning electron microscopy was performed to determine the thickness and image the porosity of each CNF film as shown in Figure 4. As shown in the figure, the thicknesses of the CNF substrates are similar, but there is a noticeable difference in porosity within the samples, most notably porosity in micrometric scale that can be visualized in the SEM images.

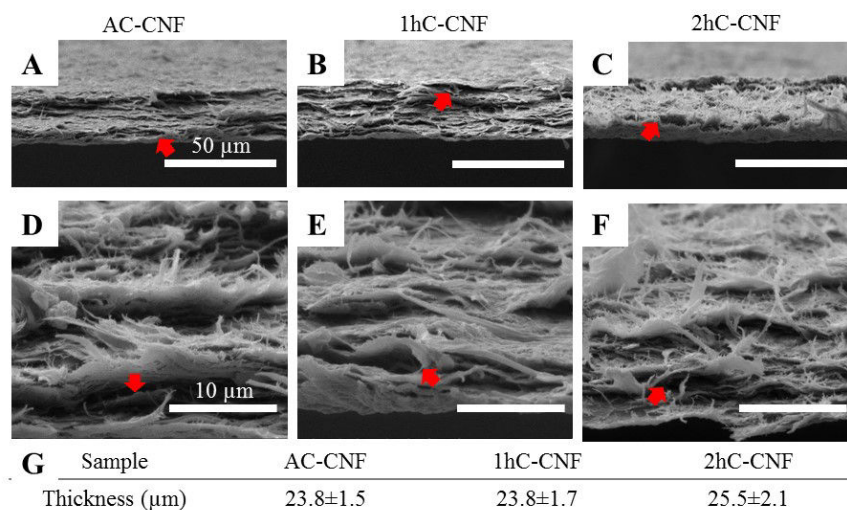


Figure 4. SEM images of the thickness with different magnifications A,B,C) 600x and D,E,F) 5000x A,D) AC-CNF, B,E) 1hC-CNF, and C,F) 2hC-CNF with different magnifications and G) measurements of thickness using Image J (mean + SD of 35 membrane section)

These differences in layer formation could influence the cell adhesion and viability on CNF. The direct nanoscale porosities of the CNF films were measured using thermoporometry, which will be reported later, and the CNF images supports those results with pore size and number decreasing with increased curing time at 150°C. AC-CNF and 1hC-CNF have a more porous structure, while 2hC-CNF is denser with less pores, but still a similar thickness. The direct measurement of this qualitative observation will be discussed later.

The water content of the CNF films was determined following conditioning and evaporation of the films at 105°C for 24 hours as outlined in the methods section. This method is commonly used to determine the water content within paper pulp and was adapted for CNF films. As shown in Table 1 curing of CNF films at 150°C for 1 or 2 hours lessens the water content within the film compared to casted CNF (AC-CNF), with maximum loss experienced by 2hC-CNF. This loss of water causes a change in the porosity and the basis weight of the CNF films but have not influenced mechanical properties of the CNF films which are obtained in an aqueous state. PBS absorption of CNF films is

dependent on the morphology and structure of the film. Also since the CNF will be tested in liquid conditions and culturing requires the films to be exposed to media, the differences in PBS uptake between the samples can change cell attachment and viability. Since 2hC-CNF has lower porosity compared to AC-CNF and 1hC-CNF the PBS solution cannot easily infiltrate the film and cause swelling. Water content and PBS uptake results are reported Figure 5.

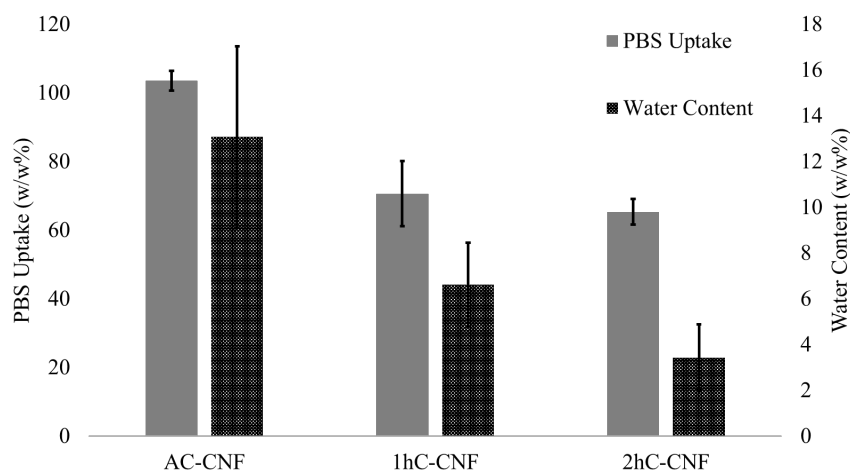


Figure 5. The percentage of water in CNF films following conditioning, drying for 24 hours at 105°C, and conditioning for 48 hours, as calculated using Equation 2. The percentage of PBS uptake in CNF films following incubation in PBS after 24 hours at 37°C, as calculated using Equation 3

Nanoscale porosity of the CNF films in aqueous conditions were determined using thermoporometry. This technique has been employed to characterize cellulosic fibers [48, 49]. The method was recently improved by Driemeier et al. [46], and is here for the first time used to analyze the nanoscale porosity of CNF films. As expected, with curing at 150°C for either 1 or 2 hours the nanoscale porosity of the films decreased compared to AC-CNF, and further decreased with increased curing time (AC-CNF > 1hC-CNF > 2hC-CNF). The observed loss of porosity is distributed in the measured 1-200 nm pore size range, without special behavior in any specific window of pore size. The maxima of the profiles (FBW read at 200 nm in Figure 7) is also reported in Table 1. The changes in porosity are caused by water evaporation during curing, which causes a decrease in the basis weight of the CNF films. Noteworthy, the changes are irreversible, since the AC-CNF porosity does not recover after 1hC-CNF and 2hC-CNF rehydrate in aqueous conditions. The measured reduction of nanoscale porosity (Figure

6) manifests the cohesive action of drying, which likely impacts other properties, such as CNF film mechanics and PBS uptake, as well as cell growth and viability.

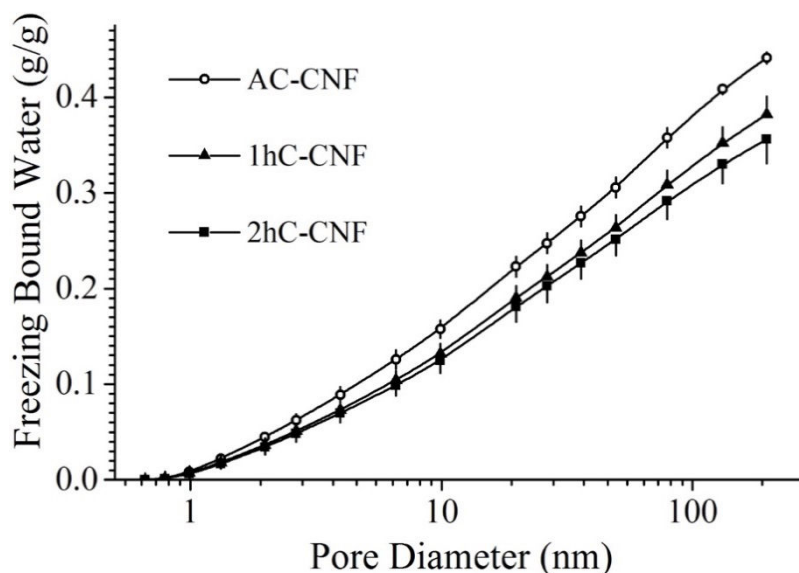


Figure 6. Cumulative distribution of Freezing Bound Water (FBW) (g/g) vs. pore diameter (nm) as measured by thermoporometry for CNF films. For 1hC-CNF and 2hC-CNF, respectively the low and the high branches of the symmetric error bars are omitted for better visualization. With curing the amount of FBW in pores between 1-200 nm decreases.

In order to attribute the changes in porosity and mechanical properties of the film only to the evaporation of water within the CNF alone, TGA measurements were conducted from 30°C until 900°C. Changes in residual mass percentage above 150°C for the samples would indicate a chemical modification of the CNF. As shown in the thermograms, which are reported in Figure 7, there are no differences. This lack of change or shift in the thermograms indicates that the curing of CNF does not produce any chemical change. Therefore, it can be noted that the mechanical properties and porosity changes are only dependent on the curing of the CNF with no chemical modification of the nanocellulose.

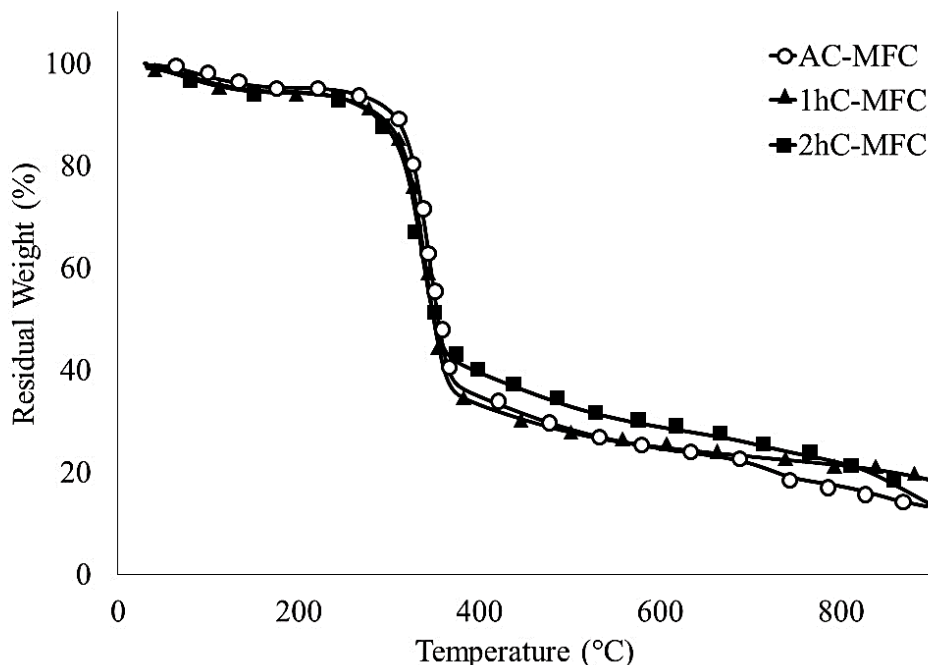


Figure 7. Thermograms of AC-MFC, 1hC-MFC, 2hC-MFC measured by TGA from 30-900°C at a rate of 10 °C/min. The traces of the curves from approximately 250-400°C show that there was no chemical modification of the films.

3.2 Tuning Mechanical Properties of CNF Substrate

Mechanical properties of the CNF films, as well as the viscoelastic properties were determined using tensile tests and DMA with a submersion clamp system. DMA is commonly used to determine if a material used for biomedical applications is suitable, while applying conditions that mimic a physiological environment [50]. Tensile tests and compression testing were conducted in a reservoir filled with PBS at 37°C to assess the mechanical properties in cell culture conditions. The stress-strain curve and the storage modulus (E') for the films were measured in hydrated conditions. The stress-strain curves show a significant increase in the Young's modulus (E) with increase in drying time, and a decrease in elongation at break. These variations in values show that the samples become more brittle following drying at elevated temperature. The storage modulus was measured using compression from 0.05-20 Hz, which mimics physiological conditions. As shown in Table 1, there was an increase in the storage modulus from 0.05 Hz to 20 Hz from AC-CNF to 2hC-CNF with a 56% increase in E' at 0.05 Hz and 10% increase at 20 Hz for AC-CNF vs. 2hC-CNF. The change in mechanical properties can be attributed to the new nanostructures (described previously) of the CNF substrate since the fiber content and preparation of the films were the same. The only differences occurring in the same trend

of increasing mechanical properties is the decrease of porosity with increased drying time, which implies that mechanical performance of CNF films and porosity are related with an R^2 value of 0.88.

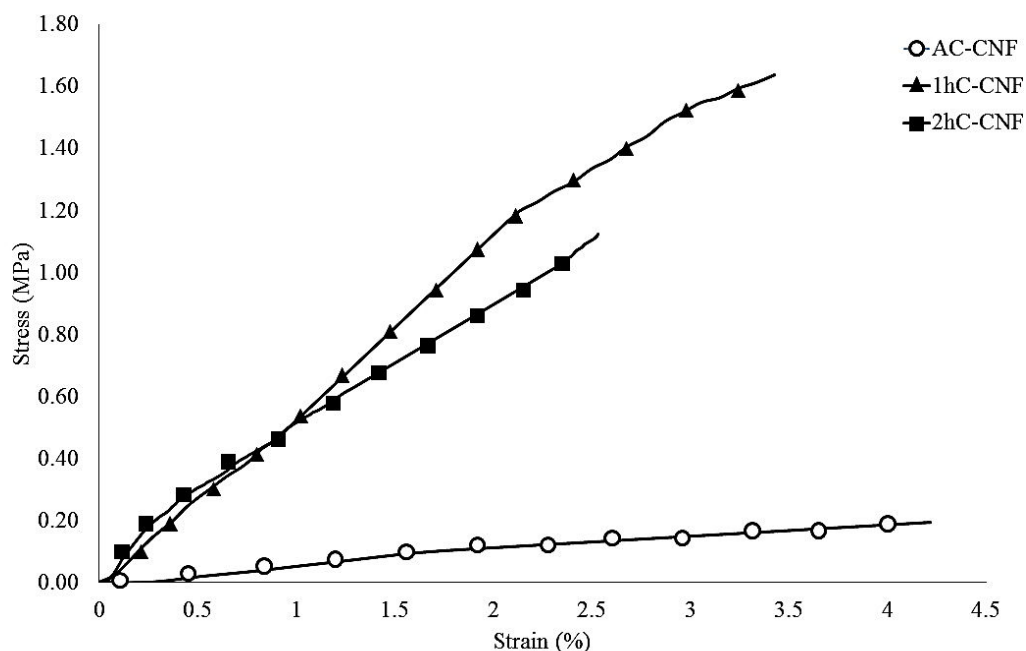


Figure 8. A) Stress-Strain curves for CNF films tested in phosphate buffer solution at 37°C. The films were either tested as casted (AC-CNF) or after curing (1hC-CNF, 2hC-CNF) with (N=3).

The results of mechanical testing in conjunction with CNF film structure characterization (i.e. surface roughness, thickness, porosity) shows that there is a direct relationship between the drying of films for extended periods of time and the material properties. Such results are innovative in regards to CNF substrate material properties, and this tenability has not been studied in details in other scientific paper up to our knowledge. These properties can be tuned depending on the amount of drying time, without any further chemical modification.

3.3 Influence of Tunable CNF Substrate on Cell Adhesion and Morphology

Since cell adherence and spreading is the first essential step to study the biocompatibility of a material, our next step was to study the adhesion and morphology of MSCs on the tunable CNF substrates. The cell morphology, surface area, and aspect ratio were determined by DAPI-Phalloidin staining of MSCs at 6 h and 24 h following cell seeding. Cells cultured on CNF with different curing conditions displayed different morphologies (Figure 9). Independently the culture time, MSCs seeded on CNF show more

elongation and cytoplasmic extension when compared to when seeded on glass (Figure 9 A-H). While cell area at 6 h was not affected by culturing MSCs on any CNF, at 24h only 1hC-CNF and 2hC-CNF showed a higher value when compared to glass (+33%, +28% $p < 0.05$), and interestingly to AC-CNF as well (+39%, +34% $p < 0.05$) (Figure 9I). This difference in cell area can be possibly explained by the differences in porosity and mechanical properties of 1hC-CNF and 2hC-CNF in comparison to AC-CNF. 6 and 24 hours post-seeding on AC-CNF, 1hC-CNF and 2hC-CNF, significant higher aspect ratios were observed when compared to the control group (+69%, +70% and +61% $p < 0.05$ for 6h and +37%, +29% and +41% $p < 0.05$ for 24h) (Figure 9J). With AC-CNF and 1hC-CNF the aspect ratio of the cells remains similar between 6 and 24 hours. This lack of change in the aspect ratio suggests that the cells maintain the same shape, and do not further increase their cytoplasmic extensions. Cells on 2hC-CNF developed long cytoplasmic extensions attached to the cellulose surface between 6 and 24 hours which is supported by an increase of the cell aspect ratio with time (+18% $p < 0.05$ 24 vs. 6 hours) (Figure 9J). The changes in cell area and aspect ratio on cellulose compared to the control suggests that CNF has properties that allows MSCs to more quickly spread and form cytoplasmic extension compared to the control when their structure is less porous or with higher mechanical properties.

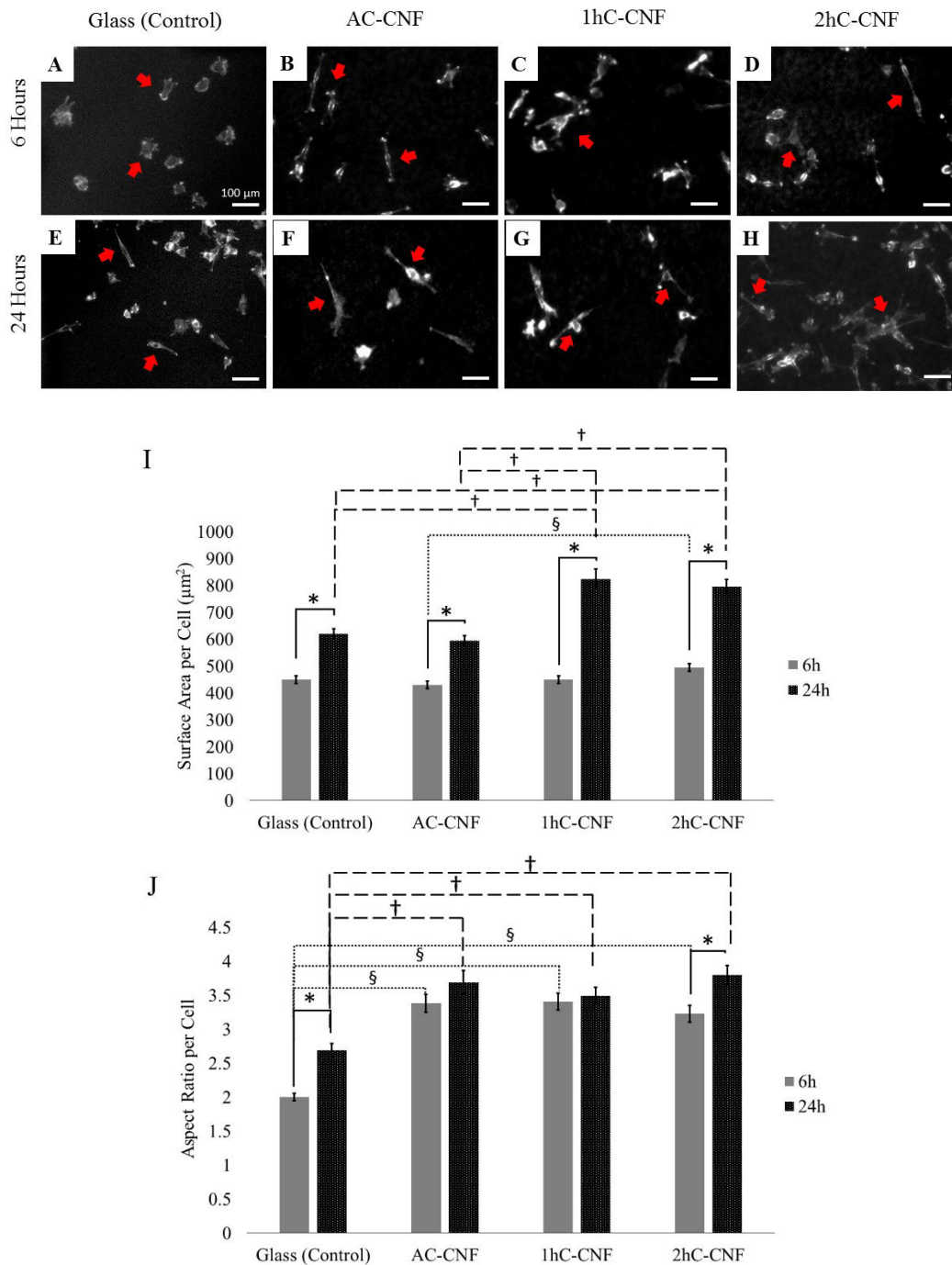


Figure 9. Fluorescent microscopy images of D1 MSCs stained for actin seeded on A, E) Glass (Control), B, F) AC-CNF, C, G) 1hC-CNF, and D, H) 2hC-CNF at A, B, C, D) at 6h and E, F, G, H) 24h post-seeding taken by inverted fluorescent microscopy with a scale bar of 100 μm . I) surface area per cell and J) cell aspect ratio as measured by ImageJ (N=300) for two independent experiments. * $p < 0.05$ significance between 6h and 24h for same substrate, § $p < 0.05$ significance between substrates at 6h, † $p < 0.05$ significance between substrates at 24h. All results are reported as mean \pm standard error of the mean.

3.4 Influence of Tunable CNF Substrate on Cell Metabolic Activity

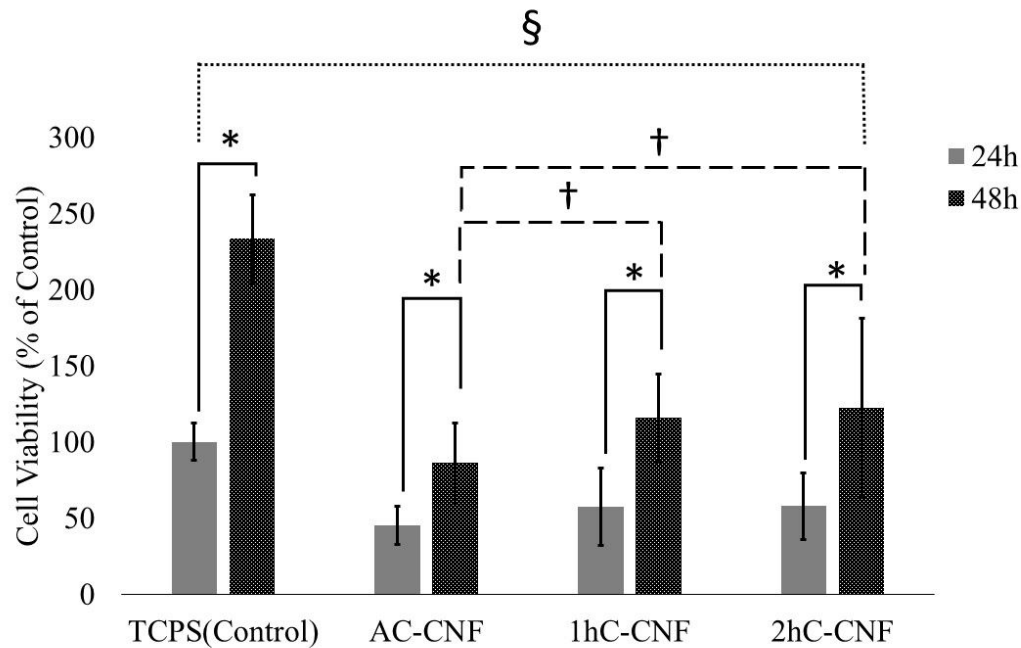


Figure 10. MTT assay results reported in % of control to monitor cell proliferation and viability following 24h and 48h incubation of 20,000 cells/cm² on TCPS (Control), AC-CNF, 1hC-CNF, and 2hC-CNF (N=11-17 per group) from 5 independent experiments. * $p < 0.05$ significance between 24h and 48h for same substrate, † $p < 0.05$ significance between substrates at 24h, ‡ $p < 0.05$ control vs all cellulose substrates at 24 hours, and § $p < 0.05$ control vs all cellulose substrates at 48 hours.

The effect of CNF on the mitochondrial activity of D1 MSCs was evaluated *in vitro* using an MTT assay. Cell viability was measured 24 and 48 hours post seeding. There is no significant difference between the cellulose substrates 24 hours post-seeding, but all cellulose substrates had a significant lower viability compared to the control (-55% for AC-CNF; -43% for 1hC-CNF; -42% for 2hC-CNF vs. control; $p < 0.05$) (Figure 10). The percent of viable cells increased between 24 and 48 hours for AC-CNF, 1hC-CNF, 2hC-CNF, and the control (+91%, +104%, +110%, +133% respectively; $p < 0.05$). The increased viability of MSCs with time shows that the cells remain viable. Interestingly, compared to AC-CNF, cells cultured on 1hC-CNF and 2hC-CNF had a significant higher viability at 48 hours post seeding (+35% $p < 0.05$; +42% $p < 0.05$ respectively vs. AC-CNF). These differences indicate that MSC viability is dependent on the mechanical and structural properties of the cellulose substrate.

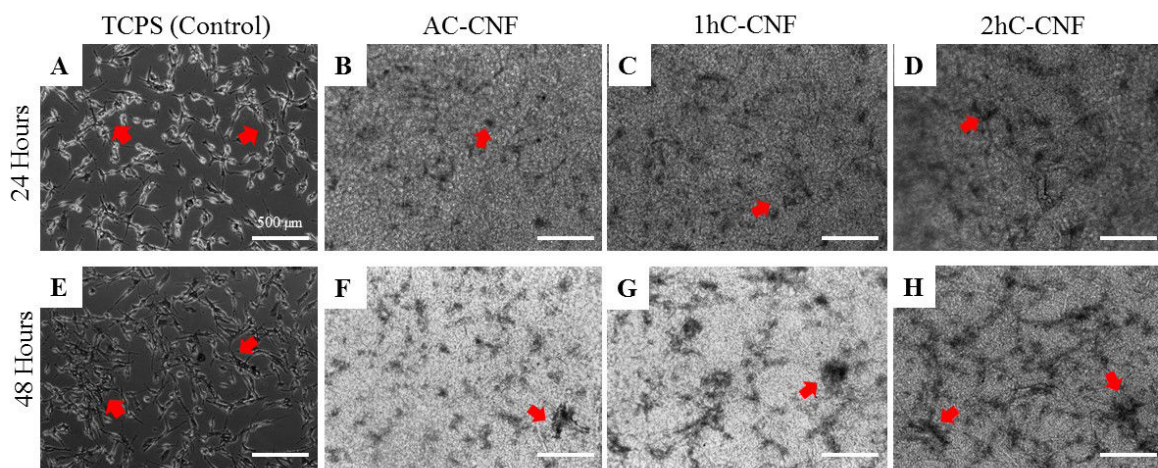


Figure 11. Optical microscopy images of D1 MSC seeded on A, E) PS, B, F) AC-CNF, C, G) 1hC-CNF, and D, H) 2hC-CNF 24h and 48h post-seeding.

The differences in cell viability on the control compared to cellulose can be related back to the mechanical properties of the specific substrate on which cells are cultured, and the resulting cell area and cell aspect ratio. The lower quantity of formazan we observed may result from a lower number of viable cells, but for cell culturing for longer periods of time compared to here (24h and 48h) form a lower rate of cell proliferation as well. The changes in cell shape show that there are more long cytoplasmic extensions for cells cultured on cellulose and this configuration may modulate cell division. Because of the rigid, flat, and uniform environments, 2D cultures on glass or plastic fail to represent well the features of cell-matrix interactions that occur *in vivo*. Cellulose substrates are softer than plastic or glass and show a fibrous texture that may influence cell division as previously shown on other type of substrates [51]. Physical forces, cell-matrix interactions, and the resulting cellular protrusions have been shown to be key regulators of cell division [52] and this concept may be greatly linked to our current results. Moreover, as shown in Figure 11, there is formation of cell clusters on the cellulose substrates which shows increased cell-cell interactions within the cluster, but not the formation of a cell sheet, which could hinder the number of cells that are viable. This is the first time such results are presented, proving strong interest in a CNF substrate.

If we compare with literature, CNF substrates have not been extensively used for MSC culture. Previous studies reported on CNF as a matrix filler as with gelatin substrates for MSC culture with results focused on creating a 3D highly porous gelatin, CNF composite for cell culture as well as inducing differentiation of human MSCs with osteo- or adipogenic media without any mention of

MSC adhesion [19]. In regards to cell culture on pure CNF substrates, only few studies have been published which are more focused on CNF hydrogels for tissue engineering scaffolds and not thin cell culture substrates. Nordli et al. has studied cell viability on TEMPO-oxidized CNF substrates of human fibroblasts and keratinocytes, but it must be noted that different cell species (i.e. human vs. murine) and cell types (i.e. fibroblasts/keratinocytes vs. MSCs) will produce different results and cannot be directly compared. Even if cell species and type within this reported study are different, it can be noted that the ultrapure TEMPO-oxidized CNF aerogels cultured with human fibroblasts and keratinocytes produced a lower metabolic activity of the cells when compared to the control at 6, 24, and 48 hours similar to what was reported in this study. Cell death was also reported by lactate dehydrogenase assay, and it was shown that TEMPO oxidized CNF aerogels and fibers did not significantly impact cell death [25]. While it was displayed that TEMPO oxidized CNF or aerogel did not implicit a negative response on fibroblasts and keratinocytes cell viability, death, and cytokine release it must be noted that only one type of CNF based structure was studied without any mechanical property variation with the aerogel like in this study, and there was no report on the mechanical properties of this CNF aerogel.

4. Conclusion

We showed that CNF films with varying mechanical properties can be easily created with only the application of an extra curing step, and no further chemical modification. With such treatment, the porosity decreases and the mechanical properties in cell culture conditions significantly increase. This curing step causes structural changes within the CNF that influence the mechanical characteristics. The viability and adhesion of MSCs onto the CNF films were measured and shown to have significant differences in comparison to as-casted CNF substrates and cured CNF films (1hC-CNF, 2hC-CNF). The differences in cell adhesion and viability can be attributed to the differences in mechanical properties of each CNF substrate, which is related to the structural changes. The facile design of CNF films of varying material properties has promising results for future applications in tissue engineering and stem cell differentiation.

5. Acknowledgments

ANR-11-LABX- 0030), the Fondation Nanoscience for a postdoctoral fellowship Grant FCSN 2-1302CE for C.F., and by FAPESP Grant13/07932-6. LGP2 is part of the PolyNat Carnot Institut (Investissements d'Avenir, Grant Agreement ANR-16-CARN-0025-01). LMGP is part of the LabEx Centre of Excellence of Multifunctional Architected Materials “CEMAM” (ANR 10-LABX-44-01). C.P. and J.B. are members of the Institute Universitaire de France whose support is acknowledged. The confocal laser microscope was bought on a European Research Council grant (FP7/2007-2013) / ERC GA259370. The authors would like to thank Isabelle Paintrand of LMGP for her assistance with the confocal microscope.

6. References

- [1] Klemm D, Heublein B, Fink HP, Bohn A. Cellulose: fascinating biopolymer and sustainable raw material. *Angewandte Chemie International Edition*. 2005;44:3358-93.
- [2] Jorfi M, Foster EJ. Recent advances in nanocellulose for biomedical applications. *Journal of Applied Polymer Science*. 2015;132:41719.
- [3] Reis RL, Neves NM, Mano JF, Gomes ME, Marques AP, Azevedo HS. Natural-based polymers for biomedical applications. Cambridge, England Woodhead Publishing Limited 2008.
- [4] Petersen N, Gatenholm P. Bacterial cellulose-based materials and medical devices: current state and perspectives. *Applied Microbiology and Biotechnology*. 2011;91:1277-86.
- [5] Rånby B, Ribi E. Über den feinebau der zellulose. *Experientia*. 1950;6:12-4.
- [6] Turbak AF, Snyder FW, Sandberg KR. Microfibrillated cellulose, a new cellulose product: properties, uses, and commercial potential. *Journal Applied Polymer Science: Applied Polymer Symposium*. Syracuse, NY, USA1983. p. 815-27.
- [7] García A, Gandini A, Labidi J, Belgacem N, Bras J. Industrial and crop wastes: A new source for nanocellulose biorefinery. *Industrial Crops and Products*. 2016;93:26-38.
- [8] Dufresne A. Nanocellulose: from nature to high performance tailored materials: Walter de Gruyter; 2013.
- [9] Moon RJ, Martini A, Nairn J, Simonsen J, Youngblood J. Cellulose nanomaterials review: structure, properties and nanocomposites. *Chemical Society Reviews*. 2011;40:3941-94.
- [10] Eichhorn SJ, Dufresne A, Aranguren M, Marcovich NE, Capadona JR, Rowan SJ, et al. Review: current international research into cellulose nanofibres and nanocomposites. *Journal of Materials Science*. 2010;45:1-33.

- [11] Nechyporchuk O, Belgacem MN, Bras J. Production of cellulose nanofibrils: a review of recent advances. *Industrial Crops and Products*. 2016;93:2-25.
- [12] Lavoine N, Desloges I, Dufresne A, Bras J. Microfibrillated cellulose - its barrier properties and applications in cellulosic materials: a review. *Carbohydrate Polymers*. 2012;90:735-64.
- [13] Mariano M, El Kissi N, Dufresne A. Cellulose nanocrystals and related nanocomposites: review of some properties and challenges. *Journal of Polymer Science Part B: Polymer Physics*. 2014;52:791-806.
- [14] Hoeng F, Denneulin A, Bras J. Use of nanocellulose in printed electronics: a review. *Nanoscale*. 2016;8:13131-54.
- [15] Lin N, Dufresne A. Nanocellulose in biomedicine: Current status and future prospect. *European Polymer Journal*. 2014;59:302-25.
- [16] Hossain KM, Hasan MS, Boyd D, Rudd CD, Ahmed I, Thielemans W. Effect of cellulose nanowhiskers on surface morphology, mechanical properties, and cell adhesion of melt-drawn polylactic Acid fibers. *Biomacromolecules*. 2014;15:1498-506.
- [17] Camarero-Espinosa S, Rothen-Rutishauser B, Weder C, Foster EJ. Directed cell growth in multi-zonal scaffolds for cartilage tissue engineering. *Biomaterials*. 2016;74:42-52.
- [18] Dugan JM, Collins RF, Gough JE, Eichhorn SJ. Oriented surfaces of adsorbed cellulose nanowhiskers promote skeletal muscle myogenesis. *Acta biomaterialia*. 2013;9:4707-15.
- [19] Xing Q, Zhao F, Chen S, McNamara J, DeCoster MA, Lvov YM. Porous biocompatible three-dimensional scaffolds of cellulose microfiber/gelatin composites for cell culture. *Acta biomaterialia*. 2010;6:2132-9.
- [20] Lou YR, Kanninen L, Kuisma T, Niklander J, Noon LA, Burks D, et al. The use of nanofibrillar cellulose hydrogel as a flexible three-dimensional model to culture human pluripotent stem cells. *Stem Cells Dev*. 2014;23:380-92.
- [21] Bhattacharya M, Malinen MM, Lauren P, Lou YR, Kuisma SW, Kanninen L, et al. Nanofibrillar cellulose hydrogel promotes three-dimensional liver cell culture. *J Control Release*. 2012;164:291-8.
- [22] Syverud K, Pettersen SR, Draget K, Chinga-Carrasco G. Controlling the elastic modulus of cellulose nanofibril hydrogels—scaffolds with potential in tissue engineering. *Cellulose*. 2015;22:473-81.
- [23] Rodríguez K, Gatenholm P, Renneckar S. Electrospinning cellulosic nanofibers for biomedical applications: structure and in vitro biocompatibility. *Cellulose*. 2012;19:1583-98.

- [24] He X, Xiao Q, Lu C, Wang Y, Zhang X, Zhao J, et al. Uniaxially aligned electrospun all-cellulose nanocomposite nanofibers reinforced with cellulose nanocrystals: scaffold for tissue engineering. *Biomacromolecules*. 2014;15:618-27.
- [25] Nordli HR, Chinga-Carrasco G, Rokstad AM, Pukstad B. Producing ultrapure wood cellulose nanofibrils and evaluating the cytotoxicity using human skin cells. *Carbohydrate Polymers*. 2016;150:65-73.
- [26] Siró I, Plackett D. Microfibrillated cellulose and new nanocomposite materials: a review. *Cellulose*. 2010;17:459-94.
- [27] Schaquí H, Morimune S, Nishino T, Berglund LA. Stretchable and strong cellulose nanopaper structures based on polymer-coated nanofiber networks: An alternative to nonwoven porous membranes from electrospinning. *Biomacromolecules*. 2012;13:3661-7.
- [28] Schaquí H, Ezekiel Mushi N, Morimune S, Salajkova M, Nishino T, Berglund LA. Cellulose nanofiber orientation in nanopaper and nanocomposites by cold drawing. *ACS Applied Materials & Interfaces*. 2012;4:1043-9.
- [29] Bardet R, Reverdy C, Belgacem N, Leirset I, Syverud K, Bardet M, et al. Substitution of nanoclay in high gas barrier films of cellulose nanofibrils with cellulose nanocrystals and thermal treatment. *Cellulose*. 2015;22:1227-41.
- [30] Bardet R, Belgacem N, Bras J. Flexibility and color monitoring of cellulose nanocrystal iridescent solid films using anionic or neutral polymers. *ACS Appl Mater Interfaces*. 2015;7:4010-8.
- [31] Bardet R, Belgacem MN, Bras J. Different strategies for obtaining high opacity films of MFC with TiO₂ pigments. *Cellulose*. 2013;20:3025-37.
- [32] Friedenstein AJ, Gorskaja J, Kulagina N. Fibroblast precursors in normal and irradiated mouse hematopoietic organs. *Experimental hematology*. 1976;4:267-74.
- [33] Prockop DJ. Marrow stromal cells as stem cells for nonhematopoietic tissues. *Science*. 1997;276:71-4.
- [34] Dalby MJ, Gadegaard N, Oreffo RO. Harnessing nanotopography and integrin-matrix interactions to influence stem cell fate. *Nature materials*. 2014;13:558-69.
- [35] Discher DE, Janmey P, Wang YL. Tissue cells feel and respond to the stiffness of their substrate. *Science*. 2005;310:1139-43.
- [36] Dalby MJ, Gadegaard N, Riehle MO, Wilkinson CD, Curtis AS. Investigating filopodia sensing using arrays of defined nano-pits down to 35 nm diameter in size. *The international journal of biochemistry & cell biology*. 2004;36:2005-15.

- [37] Anderson HJ, Dalby MJ, Sahoo JK, Ulijn RV. Mesenchymal Stem Cell Fate: Applying Biomaterials for Control of Stem Cell Behavior. *Frontiers in Bioengineering and Biotechnology*. 2016;4:38.
- [38] Dalby MJ, Gadegaard N, Tare R, Andar A, Riehle MO, Herzyk P, et al. The control of human mesenchymal cell differentiation using nanoscale symmetry and disorder. *Nature materials*. 2007;6:997-1003.
- [39] Engler AJ, Sen S, Sweeney HL, Discher DE. Matrix elasticity directs stem cell lineage specification. *Cell*. 2006;126:677-89.
- [40] Krontiras P, Gatenholm P, Hagg DA. Adipogenic differentiation of stem cells in three-dimensional porous bacterial nanocellulose scaffolds. *J Biomed Mater Res B Appl Biomater*. 2015;103:195-203.
- [41] Favi PM, Benson RS, Neilsen NR, Hammonds RL, Bates CC, Stephens CP, et al. Cell proliferation, viability, and in vitro differentiation of equine mesenchymal stem cells seeded on bacterial cellulose hydrogel scaffolds. *Materials Science and Engineering: C*. 2013;33:1935-44.
- [42] Zhou C, Shi Q, Guo W, Terrell L, Qureshi AT, Hayes DJ, et al. Electrospun Bio-Nanocomposite Scaffolds for Bone Tissue Engineering by Cellulose Nanocrystals Reinforcing Maleic Anhydride Grafted PLA. *ACS Applied Materials & Interfaces*. 2013;5:3847-54.
- [43] Alexandrescu L, Syverud K, Gatti A, Chinga-Carrasco G. Cytotoxicity tests of cellulose nanofibril-based structures. *Cellulose*. 2013;20:1765-75.
- [44] Rowell R. *The Chemistry of Solid Wood* 185th Meeting of the American Chemical Society. Seattle, Washington 1983.
- [45] Fukuzumi S, et al. . Transparent and High Gas Barrier Films of Cellulose Nanofibers Prepared by TEMPO-Mediated Oxidation. *Biomacromolecules*. 2008;10:162-5.
- [46] Driemeier C, Mendes FM, Oliveira MM. Dynamic vapor sorption and thermoporometry to probe water in celluloses. *Cellulose*. 2012;19:1051-63.
- [47] Domke J, Dannöhl S, Parak WJ, Müller O, Aicher WK, Radmacher M. Substrate dependent differences in morphology and elasticity of living osteoblasts investigated by atomic force microscopy. *Colloids and Surfaces B: Biointerfaces*. 2000;19:367-79.
- [48] Park S, Venditti RA, Jameel H, Pawlak JJ. Changes in pore size distribution during the drying of cellulose fibers as measured by differential scanning calorimetry. *Carbohydrate Polymers*. 2006;66:97-103.
- [49] Fahlén J, Salmén L. Ultrastructural changes in a holocellulose pulp revealed by enzymes, thermoporosimetry and atomic force microscopy. *Holzforschung*. 2005;59:589-97.

- [50] Mano JF. Viscoelastic properties of chitosan with different hydration degrees as studied by dynamic mechanical analysis. *Macromolecular bioscience*. 2008;8:69-76.
- [51] Skardal A, Mack D, Atala A, Soker S. Substrate elasticity controls cell proliferation, surface marker expression and motile phenotype in amniotic fluid-derived stem cells. *Journal of the mechanical behavior of biomedical materials*. 2013;17:307-16.
- [52] Lesman A, Notbohm J, Tirrell DA, Ravichandran G. Contractile forces regulate cell division in three-dimensional environments. *The Journal of cell biology*. 2014;205:155-62.

Figures and Tables

Figures

Chapter 4.1

Figure 1. Schematic Representation of Nanocomposite Fabrication and Characterization

Figure 2. Atomic force microscopy images of the surface of the CNC:Alginate composites A) Alginate, B) 10:90 CNC:Alginate, C) 30:70 CNC:Alginate, D) 50:50 CNC:Alginate and CNC-T:Alginate composites F) 10:90 CNC-T:Alginate, G) 30:70 CNC-T:Alginate, H) 50:50 CNC-T:Alginate, and I) 70:30 CNC-T:Alginate. J) root mean square roughness measurements of the surface of the composite films.

Figure 3. Frequency dependent dynamic mechanical analysis from 0.5-20 Hz with 3% applied strain in aqueous conditions in D-PBS at 37°C for CNC:Alginate composites (A) and CNC-T:Alginate composites (B)

Figure 4. Compression Frequency dependent dynamic mechanical analysis from 0.5-20 Hz with 3% applied strain in aqueous conditions in D-PBS at 37°C for CNC:Alginate composites (A) and CNC-T:Alginate composites (B)

Figure 5. Confocal microscopy images of D1 MSCs stained for actin seeded on A, K) Control (Glass) B, L) Alginate, C, M) 10:90 CNC:Alginate, D, N) 30:90 CNC:Alginate, E, O) 50:50 CNC:Alginate, F, P) 70:30 CNC:Alginate, G, Q) 10:90 CNC-T:Alginate, H, R) 30:70 CNC-T:Alginate, I, S) 50:50 CNC-T:Alginate, and J, T) 70:30 CNC-T:Alginate at A-J) at 6h and K-T) 24h post-seeding.

Figure 6. A) surface area per cell and B) cell aspect ratio as measured by ImageJ (N=300) for two independent experiments. * $p < 0.05$ significance between 6h and 24h for same substrate, # $p < 0.05$ significance between composites with same ratio of nanocellulose at the same time point, ✧ $p < 0.05$ significance between control (glass) and composite at same time point, § $p < 0.05$ significance between alginate and composite at same time point

Figure 7. Area fraction of well surface area covered by D1 MSCs seeded at a density of 10,000 cells/cm² on TCPS (Control), Alginate, CNC:Alginate composites, and CNC-T:Alginate composites (N=3 per group). * $p < 0.05$ significance between 6h and 24h for same substrate, # $p < 0.05$ significance between composites with same ratio of nanocellulose at the same time point, § $p < 0.05$ significance between alginate and composite at same time point

Figure 8. Microscopy images of D1 MSCs following formazan crystal formation A, K) Control (TCPS), B, L) Alginate, C, M) 10:90 CNC:Alginate, D, N) 30:90 CNC:Alginate, E, O) 50:50 CNC:Alginate, F, P) 70:30 CNC:Alginate, G, Q) 10:90 CNC-T:Alginate, H, R) 30:70 CNC-T:Alginate, I, S) 50:50 CNC-T:Alginate, and J, T) 70:30 CNC-T:Alginate at A-J) at 24h and K-T) 48h post-seeding.

Figure 9. MTT assay results reported in % of control to monitor cell proliferation and viability following 24h and 48h incubation of 10,000 cells/cm² on TCPS (Control), Alginate, CNC:Alginate composites, and CNC-T:Alginate composites (N=12 per group) from 2 independent experiments. *p<0.05 significance between 24h and 48h for same substrate, #p<0.05 significance between composites with same ratio of nanocellulose at the same time point, § p<0.05 significance between alginate and composite at same time point. All samples (alginate and composites) have 24h and 48h significance with the TCPS control

Chapter 4.2

Figure 1. Schematic of the experimental set-up. From raw material of CNF suspension to CNF films and sequential curing of films and eventual cellular testing of CNF films for cell attachment and viability

Figure 2. Optical images of A) Polystyrene (PS), B) as cast MFC film without any modification (AC-MFC), C) solvent casted films followed by 1 hour of curing at 150 °C (1hC-MFC) and D) followed by 2 hours of curing at 150°C (2hC-MFC). E) Transmittance of MFC films as a function of wavelength, measured using UV spectroscopy from 300-800 nm. As shown in the images the transparency of the MFC films is much lower than the PS plate, which is a control for cell culture. LGP2 logo is used with permission from Didier Chaussy, 2017

Figure 3. Atomic force microscopy images (10x10 µm) of the surface of the CNF films A) AC-CNF, B) 1hC-CNF, and C) 2hC-CNF taken by tapping mode in air

Figure 4. SEM images of the thickness with different magnifications A,B,C) 600x and D,E,F) 5000x A,D) AC-CNF, B,E) 1hC-CNF, and C,F) 2hC-CNF with different magnifications and G) measurements of thickness using Image J (mean + SD of 35 membrane section)

Figure 5. The percentage of water in CNF films following conditioning, drying for 24 hours at 105°C, and conditioning for 48 hours, as calculated using Equation 2. The percentage of PBS uptake in CNF films following incubation in PBS after 24 hours at 37°C, as calculated using Equation 3

Figure 6. Cumulative distribution of Freezing Bound Water (FBW) (g/g) vs. pore diameter (nm) as measured by thermoporometry for CNF films. For 1hC-CNF and 2hC-CNF, respectively the low and the high branches of the symmetric error bars are omitted for better visualization. With curing the amount of FBW in pores between 1-200 nm decreases.

Figure 7. Thermograms of AC-MFC, 1hC-MFC, 2hC-MFC measured by TGA from 30-900°C at a rate of 10 °C/min. The traces of the curves from approximately 250-400°C show that there was no chemical modification of the films.

Figure 8. A) Stress-Strain curves for CNF films tested in phosphate buffer solution at 37°C. The films were either tested as casted (AC-CNF) or after curing (1hC-CNF, 2hC-CNF) with (N=3).

Figure 9. Fluorescent microscopy images of D1 MSCs stained for actin seeded on A, E) Glass (Control), B, F) AC-CNF, C, G) 1hC-CNF, and D, H) 2hC-CNF at A, B, C, D) at 6h and E, F, G, H) 24h post-seeding taken by inverted fluorescent microscopy with a scale bar of 100µm. I) surface area per cell and J) cell aspect ratio as measured by ImageJ (N=300) for two independent experiments. *p<0.05 significance between 6h and 24h for same substrate, §p<0.05 significance between substrates at 6h, †p<0.05 significance between substrates at 24h. All results are reported as mean ± standard error of the mean

Figure 10. MTT assay results reported in % of control to monitor cell proliferation and viability following 24h and 48h incubation of 20,000 cells/cm² on TCPS (Control), AC-CNF, 1hC-CNF, and 2hC-CNF (N=11-17 per group) from 5 independent experiments. * p<0.05 significance between 24h and 48h for same substrate, †p<0.05 significance between substrates at 24h. §p<0.05 control vs all cellulose substrates at 24 hours, and control vs all cellulose substrates at 48 hours.

Figure 11. Optical microscopy images of D1 MSC seeded on A, E) PS, B, F) AC-CNF, C, G) 1hC-CNF, and D, H) 2hC-CNF 24h and 48h post-seeding.

Tables

Chapter 4.1

Table 1. Amounts of CNC, CNC-T, and sodium alginate for fabrication of composites

Chapter 4.2

Table 1. Summary of CNF films properties as measured by 1) UV spectroscopy (S1), 2) Root Mean Squared Roughness values from AFM images of CNF films, as measured by nanoscope analysis AFM, 3) drying of films at 105°C for 24 hours (S2), 4) submersion of films for 24 hours in PBS at 37°C (S2),

5) Basis Weight of CNF Films, 6) thermoporometry, 7) tensile testing at 37°C in PBS, 8) compression DMA at 37°C in PBS.

Conclusions and Perspectives

Conclusions

The scope of this Ph.D. was to develop a nanocellulose based substrate for use in stem cell culture for potential differentiation applications. Since the use of nanocellulose as a material for biomedical applications is limited, it was important to first understand the impact cellulose nanocrystals (CNCs) and cellulose nanofibers (CNFs) had on cell behavior. The first chapter outlines the development and use of functionalized cellulose nanocellulose as a biomaterial and the few instances in which nanocellulose (CNCs and CNFs) have been used to influence mesenchymal stem cell behavior.

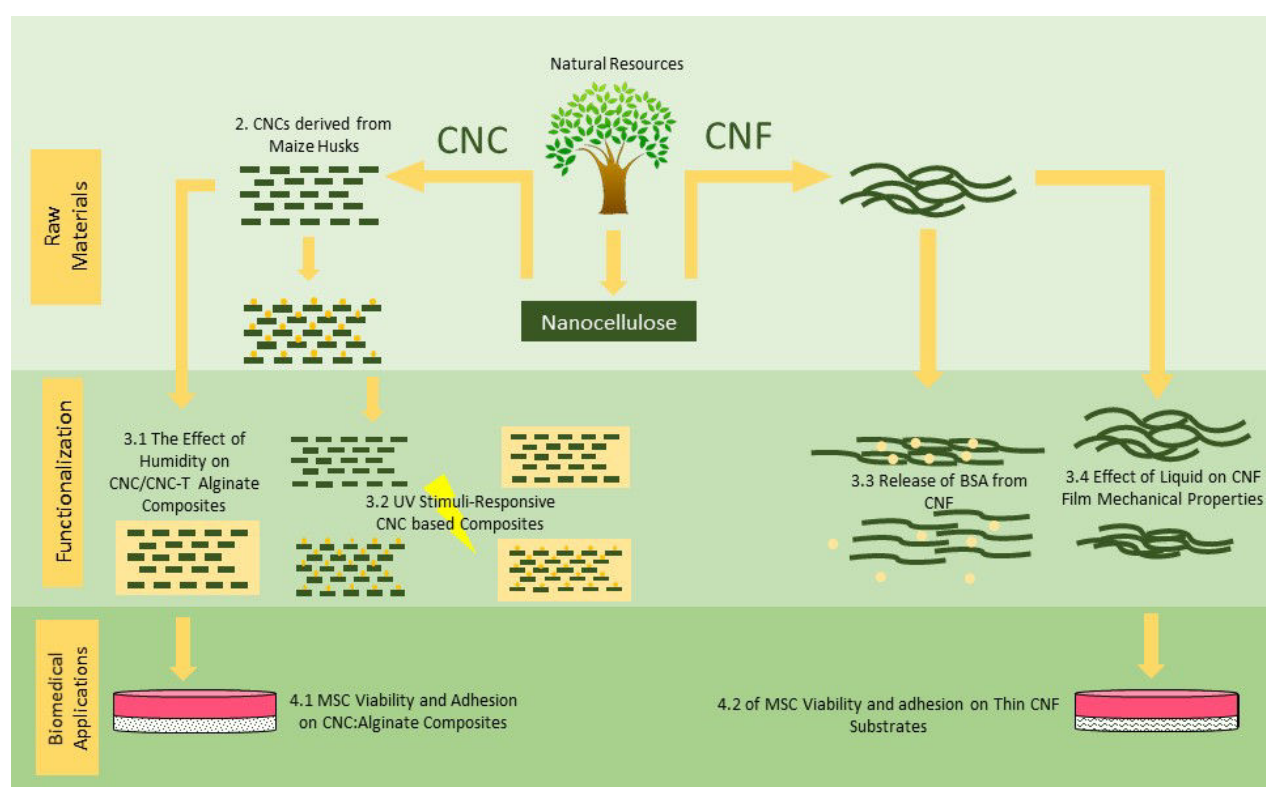


Figure 1. Schematic representation of thesis outline

As noted in **Chapter 1**, previous studies focused on the possible cytotoxicity of nanocellulose not how mechanically-adaptive materials could cause differences in cell viability and adhesion, which are necessary steps for stem cell differentiation. Through the research of this Ph.D. the development and valorization of nanocellulose-based biomaterial from material extraction (**Chapter 2**) to development and characterization of CNC and CNF-based substrates with varying mechanical properties and high-value added applications (**Chapter 3**) and finally the use of these materials in cell culture (**Chapter 4**)

was completed. These chapters illustrate the numerous steps necessary to create a functionalized nanocellulose-based material for use in biomedical studies.

The main objective of this research was to develop a nanocellulose-based material which was mechanically-adaptive in cell culture conditions, meaning in liquid conditions. The following are the main conclusions and results from each study conducted through the course of this Ph.D. thesis.

Chapter 2. Extraction and Process Analysis of High Aspect Ratio Cellulose Nanocrystals from Corn (*Zea mays*) Agricultural Residue

- Isolation of high quality and high aspect ratio CNCs from a common agricultural residue
- Determined maize CNCs have lower cost impact compared to other high quality CNCs (tunicate) based on process engineering
- Improved mechanical properties of natural rubber composites compared to commercially available CNCs with low filler content

Chapter 3. Nanocellulose-Based Materials in Physiological Conditions

Chapter 3.1 Effect of Hydration on the Material and Mechanical Properties of Cellulose Nanocrystal-Alginate Composites

- CNCs and TEMPO-oxidized CNCs (CNC-Ts) can be used as a filler within an alginate matrix to modulate mechanical properties in physiological aqueous conditions
- CNCs composites have greater sensitivity to liquid exposure (DI-H₂O or D-PBS) compared to CNC-Ts composites as illustrated by complexometric titration and changes in mechanical properties when tested in each liquid
- CNC-Ts improve the mechanical properties of alginate when exposed to D-PBS

Chapter 3.2 Characterization and Mechanical Properties of Ultraviolet Stimuli-Responsive Functionalized Cellulose Nanocrystal Alginate Composites

- CNCs underwent an esterification reaction with 4-pentenoic acid using the SolReact method, which is based on *in situ* solvent exchange where 4-pentenoic acid was the solvent
- Esterification of CNCs (PA-g-CNCs) was proven through bulk characterization by TGA, FTIR, and ¹³C NMR

- PA-g-CNCs were crosslinked with an azo-initiator and was proven through indirect methods and mechanical testing in DI-H₂O
- There was not a linear relationship between improvement of mechanical properties and addition of PA-g-CNCs or time of UV exposure
- 10:90 PA-g-CNCs had the highest level of mechanical improvement (+175%)

Chapter 3.3 Incorporation and Release of Bovine Serum Albumin from Cellulose Nanofiber Films for Growth Factor Release Applications

- Thin CNF films can be used as a release carrier for bovine serum albumin (BSA), which is a model protein
- Entrapment of BSA by diffusion or mixing affected the release properties of BSA
- BSA release can be controlled by fabrication technique and amount of BSA added

Chapter 3.4 Mechanical Properties of Thin Cellulose Nanofiber Films in Liquid

- Mechanical properties of CNF films tested in PBS can be tuned depending on fiber content and an additional curing step (2 hours, 150°C)
- 2-2hC-CNF films displayed an increase in the Young's modulus from 6 to 90 MPa following curing
- It was shown that changes in the mechanical properties of CNF films could cause differences in mesenchymal stem cell (MSCs) behavior as indicated by actin staining qualitative test

Chapter 4. The Influence of Nanocellulose on Stem Cell Behavior in Culture

Perspectives

Chapter 4.1 Modulation of Mechanical Properties of Cellulose Nanocrystal Composites for use in Stem Cell Culture

- Surface roughness of nanocomposites are similar to unmodified alginate
- The addition of CNCs and CNC-Ts to alginate can improve stem cell viability and adhesion compared to alginate

Chapter 4.2 Tunable Structural and Mechanical Properties of Cellulose Nanofiber Substrates in Liquid for Stem Cell Culture

- CNF films with differing mechanical and material properties were created through a simple curing step without any chemical modifications
- MSC viability and adhesion was dependent on the material properties of the CNF films
- MSCs showed significant changes in viability and morphology on stiffer films (cured) compared to low mechanical properties films (as cast)

These results suggest that nanocellulose, both CNCs and CNFs, have tunable mechanical properties when tested in cell culture-like conditions, and that these mechanical and material properties can influence stem cell viability and adhesion. Future studies can be conducted using these substrates to determine if the modulus of these nanocellulose-based substrates can cause a change in the differentiation of MSCs. This could be of high interest to researchers within the nanocellulose and biomaterial fields. Preliminary results on the effect of CNF films on the differentiation of MSCs have been conducted and will be presented below as a perspective.

Perspectives

The use of nanocellulose for biomedical applications has been limited in recent years, but interest has been gaining. The results produced during the course of this Ph.D. can be of interest for researchers because of the indication that MSCs can be influenced by the mechanical properties of nanocellulose, and that the testing conditions of all materials took place in cell culture like conditions (liquid conditions). This was an important distinction to make since previous research with nanocellulose has not focused on the material and mechanical properties of CNCs and CNFs within a liquid state. Overall, the changes in the mechanical and material properties of functionalized nanocellulose-based materials can be easily tuned for use in cell culture.

Table 1. Main Evolutions of Nanocellulose-Based Materials for Biomedical Applications

Scientific Theme	Before Ph.D. (June 2014)	End of Ph.D. (June 2017)
Bio-Sourced (alginate, collagen) Matrices for CNC-Based Nanocomposites	Determined if the addition of nanocellulose could improve mechanical properties <i>14 articles</i>	Testing and characterization focused for biomedical applications <i>18 articles</i>
Mechanical Testing of Nanocellulose-Based Materials in Aqueous Conditions	Previous research of nanocellulose-based materials were done in ambient conditions	Determined the effect of liquid on the mechanical properties of CNF films and CNC-based nanocomposites for biomedical applications
Tuning of Mechanical Properties of CNF Films	Mechanical properties thought to be changed through crosslinking or other chemical methods	Mechanical properties can be changed through a simple curing step at high temperature (150°C)
Use of Nanocomposites for Biomedical Applications	Focused on creating hydrogels and other composites with limited cell studies <i>1 review article</i>	Determined that the addition of CNCs to alginate can improve adhesion of stem cells <i>1 review article</i>
CNF Films use in Biomedical Applications	Focused on work with hydrogels or bacterial nanocellulose <i>1 patent</i> <i>1 review article</i> <i>1 article</i>	CNF films mostly tested with fibroblasts or other non-stem cells. CNF films can influence stem cell behavior <i>6 articles</i> <i>1 review article</i>

For all of the research conducted during the course of Ph.D. studies the most promising results were obtained for CNF films with tunable mechanical properties within liquid as reported in **Chapter 4.2**. Because of the differences in MSC viability and morphology that occurred for short time points (i.e. 6-48 hours) it was hypothesized that the mechanical properties of these CNF films could have an effect on MSC differentiation. To determine this, MSCs were seeded onto CNF films for 4, 7, and 14 days and analyzed. While the results are not fully complete, what has been obtained (detailed below) is of interest.

To determine if MSCs were viable after 4 and 7 days in culture a MTT assay was conducted. As seen in Figure 2., the viability has a slight increase from 4 to 7 days. This lack of drastic change in viability can be attributed to the maximum proliferation and confluence of the MSCs.

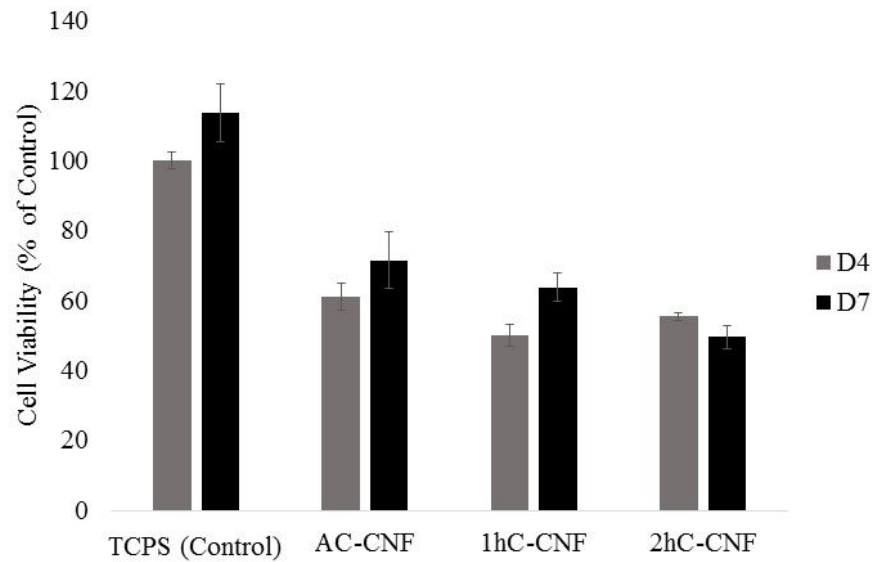


Figure 2. MTT assay results reported in % of control to monitor cell proliferation and viability following 4 days and 7 days of incubation of 20,000 cells/cm² on TCPS (Control), AC-CNF, 1hC-CNF, and 2hC-CNF (N=6) from 2 independent experiments.

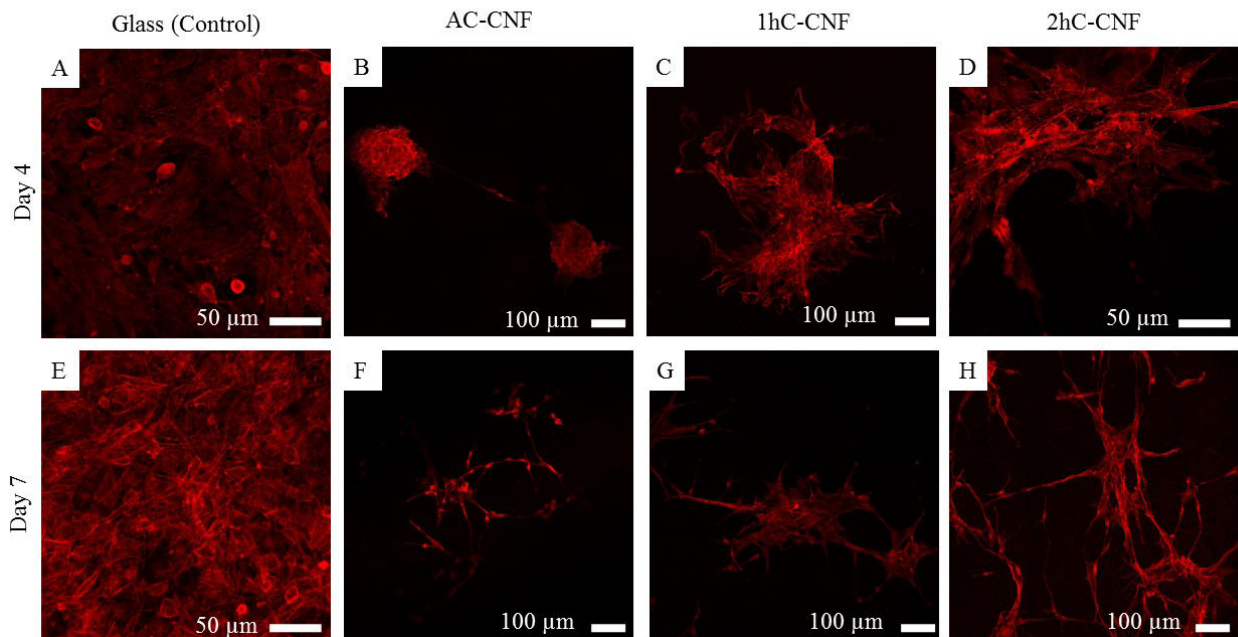


Figure 3. Inverted confocal images of D1 MSCs stained for actin seeded on A, E) Glass (Control), B, F) AC-CNF, C, G) 1hC-CNF, and D, H) 2hC-CNF at A, B, C, D) at 4 days and E, F, G, H) 7 days post-seeding.

The formation of MSC clusters or colonies were observed after immunofluorescent staining after 4 and 7 days in culture and SEM imaging after 7 days. Compared to the glass control, which caused the MSCs to produce a cell sheet, CNF substrates influenced the MSCs to form colonies on the surface. This difference in behavior can possibly be attributed to the differences in mechanical properties of the CNF and the glass since it has been reported that CNF has a similar surface roughness to glass. Also all experiments were conducted without the use of osteogenic media to determine if the mechanical properties alone caused differences in differentiation. These changes in morphology, secretion of ECM as seen in the SEM images (Figure 4.), could be promising in regards to differentiation towards osteogenesis [1].

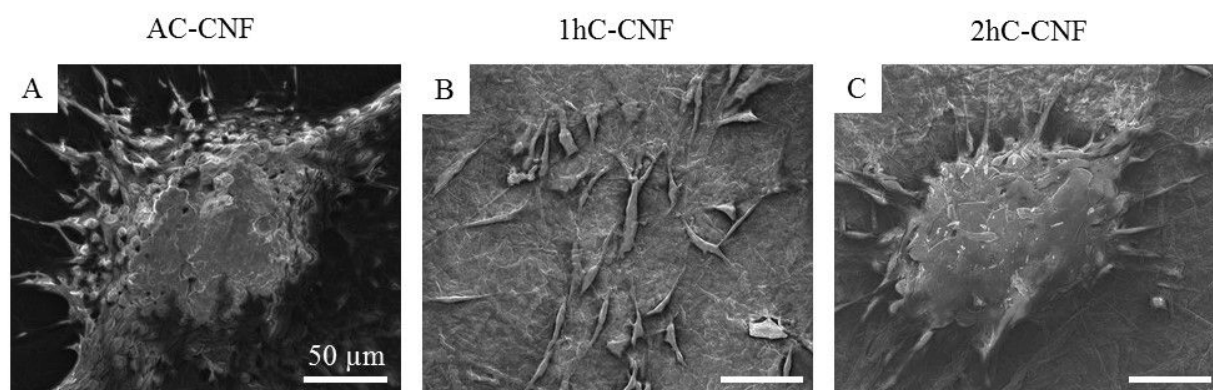


Figure 4. Scanning electron microscope images of fixed D1 MSCs seeded on A) AC-CNF, B) 1hC-CNF, and C) 2hC-CNF 7 days post-seeding with a scale bar of 50 μm .

The aggregation of the surface of the CNF films, especially in AC-CNF and 2hC-CNF as indicated in Figure 4., is the precursor to osteogenesis. Following aggregation the MSCs the cells will in turn increase expression of alkaline phosphatase and also form calcium [1, 2].

To determine if that is what is occurring with the MSCs on the surface of CNF films, MSCs were stained with alizarin red to determine if mineralization occurred. In order to aid in mineralization, but not induce differentiation, α MEM medium was supplemented with 10 mM β -glycerol phosphate disodium salt pentahydrate. As seen in Figure 5., all conditions with CNF did not produce any mineralization. While only the control cultured with low osteogenic media displayed some mineralization.

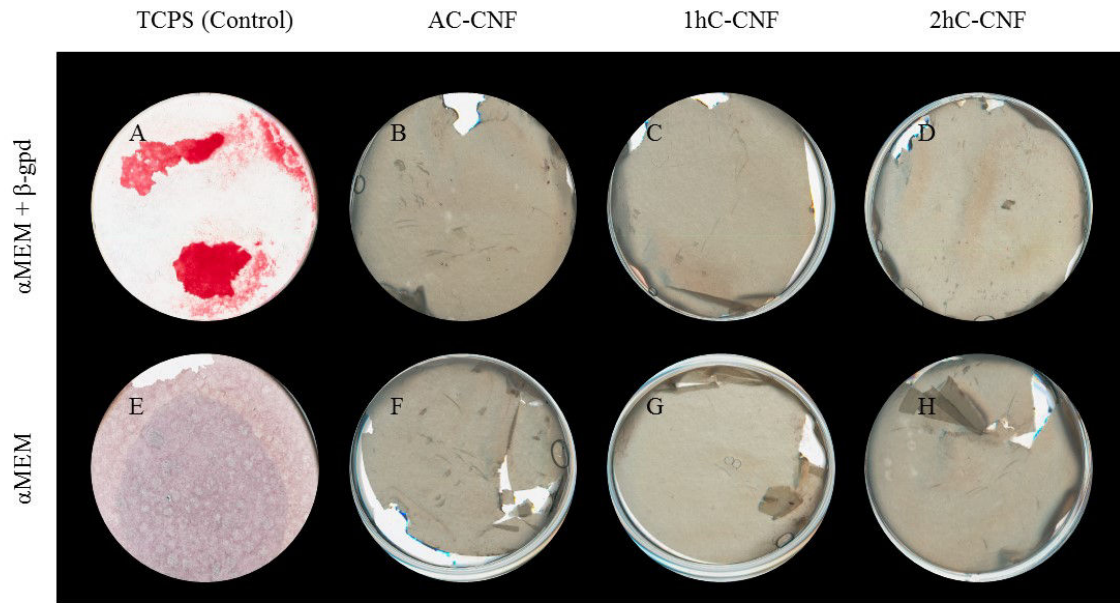


Figure 5. Images of D1 MSCs stained for calcium phosphate seeded on A, E) TCPS (Control), B, F) AC-CNF, C, G) 1hC-CNF, and D, H) 2hC-CNF at A, B, C, D) with low osteogenic medium and E, F, G, H) α MEM medium.

While all the results presented in these perspectives are promising, definitive conclusions cannot be drawn. It is obvious by the staining and SEM imaging of MSCs that CNF does have some effect on the phenotype displayed by MSCs, but without any definitive results besides a lack of mineralization. In order to determine if CNF does induce another differentiation pathway, or just not provide a favorable environment for mineralization qPCR will take place. With these results it can be determined if CNF promotes MSC differentiation along a certain lineage.

Table 2. Proposed Future Work and Perspectives based on results from Ph.D studies

Scientific Theme	Future Work and Perspectives
Bio-Sourced Matrices for CNC-Based Nanocomposites	<ul style="list-style-type: none"> • Explore the use of other polymers (e.g. collagen) to determine if CNCs can provide improved mechanical properties • Use alternative grafting techniques and materials to create more pronounced crosslinking in stimuli-responsive materials
Mechanical Testing of Nanocellulose-Based Materials in Aqueous Conditions	<ul style="list-style-type: none"> • Continue to test nanocellulose-based materials envisioned for biomedical applications or cell culture within physiological conditions • Apply results to other fields with high water contact such as packaging
Tuning of Mechanical Properties of CNF Films	<ul style="list-style-type: none"> • Research if same curing principle can be applied to other CNF-based materials such as aerogels
Use of Nanocomposites for Biomedical Applications	<ul style="list-style-type: none"> • Use other polymer matrices with known cell adhesion properties (e.g. collagen, fibrin) to improve cell adhesion and possibly induce differentiation • Conjugate CNCs or alginate with peptides such as RGD to improve protein deposition and adhesion • Create CNC-based nanocomposites for tissue engineering scaffolds for regenerative medicine
CNF Films within Biomedical Applications	<ul style="list-style-type: none"> • Determine if CNF films with differing mechanical properties can influence stem cell differentiation • Fabricate CNF films with varying surface chemistry and determine the effect on cell behavior • Generate stimuli-responsive CNF films, or films with gradient properties to influence stem cell differentiation or cell attachment

Other perspectives like *in vitro* cell treatment using a nanocellulose-based scaffold for degenerative diseases could be possible in the future with a collaboration with a medical research team. Regarding material design, several perspectives are proposed: (i) creating crosslinked CNF films with tunable or stimuli-responsive mechanical properties [3, 4] (ii) proposing active (e.g. antimicrobial) CNF-based structure which can be used in other biomedical applications, such as soft tissue repair, (iii) the use of

another biopolymer (e.g. collagen) to determine if there is increased improvement of the mechanical properties when compared to alginate. Continued research on stimuli-responsive system would also be of interest for monitoring the stiffness of the biomaterial before and during cell culture. This multidisciplinary Ph. D. proposes a first step in a new field of interest, and will be followed by other projects in coming years.

References

- [1] Pittenger MF, Mackay AM, Beck SC, Jaiswal RK, Douglas R, Mosca JD, et al. Multilineage potential of adult human mesenchymal stem cells. *Science*. 1999;284:143-7.
- [2] Chamberlain G, Fox J, Ashton B, Middleton J. Concise review: mesenchymal stem cells: their phenotype, differentiation capacity, immunological features, and potential for homing. *Stem Cells*. 2007;25:2739-49.
- [3] Syverud K, Pettersen SR, Draget K, Chinga-Carrasco G. Controlling the elastic modulus of cellulose nanofibril hydrogels—scaffolds with potential in tissue engineering. *Cellulose*. 2015;22:473-81.
- [4] De France KJ, Chan KJ, Cranston ED, Hoare T. Enhanced mechanical properties in cellulose nanocrystal–poly (oligoethylene glycol methacrylate) injectable nanocomposite hydrogels through control of physical and chemical cross-linking. *Biomacromolecules*. 2016;17:649-60.

Abstract

The research field of biocompatible materials also called biomaterials, or materials that come into contact with any microorganisms, organisms, or living tissue [1], encompasses many aspects and types of materials from polymers and metals to bio-sourced materials like alginate and collagen. Studied since the 1950s, biomaterials are now used in a variety of applications such as: artificial joint implants, tissue engineering, drug release monitoring, and cell therapy. One of the most important aspects in biomaterial research is determining if a biomaterial is biocompatible. A biomaterial can be deemed biocompatible if it performs adequately within the host in a particular application [2]. This requires numerous levels of research from determining the immunological response of the host caused by the introduction of the biomaterial to if the biomaterial has appropriate properties like mechanical, drug release, scaffold structure, etc. Biocompatibility is dependent on numerous factors such as: surface chemistry, porosity, mechanical properties, and other material properties. These properties of biomaterials can be modified by researchers to induce certain cell behavior such as limited immunological response, increased protein adhesion to the biomaterial surface, or even directed differentiation [3]. Figure 1 gives an exhausted list of possible cell response to a biomaterial.

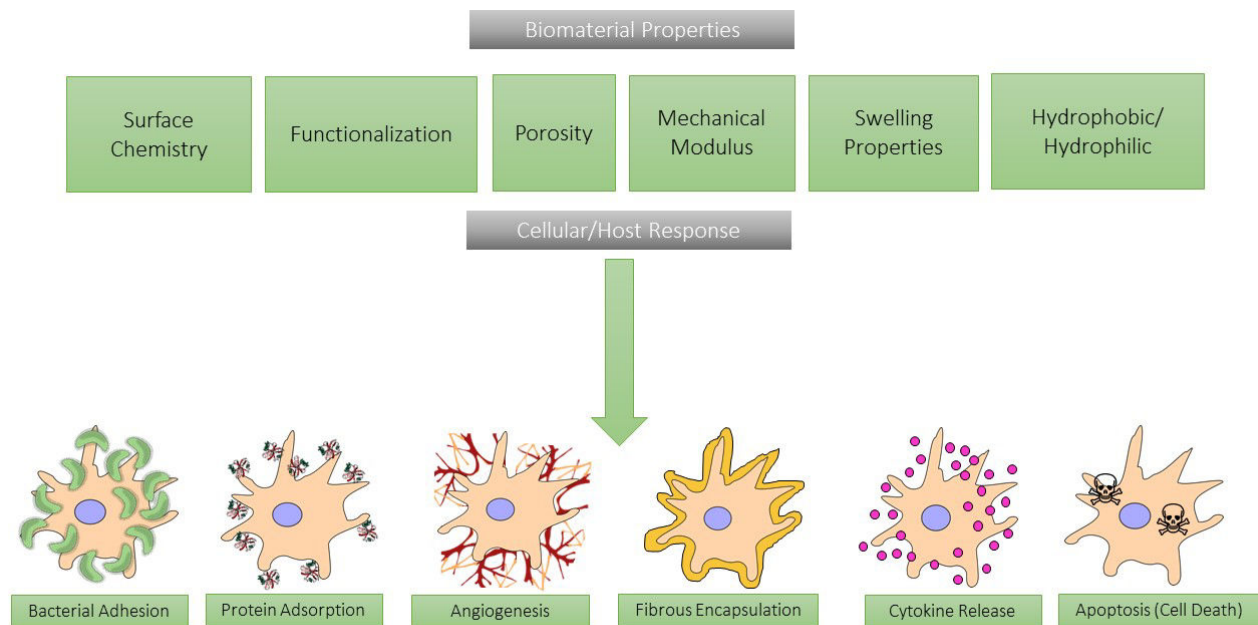


Figure 1. Cell or host response to physical biomaterial properties

One of the most common motifs to influence cell behavior in the presence of biomaterials is to change the mechanical properties of the biomaterial substrate. This recent approach was first proposed by

Engler et al. in 2006, which displayed that by changing the elastic modulus of polyacrylamide gels, mesenchymal stem cells (MSCs), could follow differing differentiation patterns [4]. At the start of this Ph.D. thesis (entitled CellDiff (2014-2017) and funded by lab of excellence Tec21 [5]) it was hypothesized that nanocellulose-based substrates could be fabricated with various elastic modulus to change the characteristics of MSCs.

The use of nanocellulose in biomedical applications has been very limited, but interest in using nanocellulose as a biocompatible material has increased in recent years as indicated by recent the review articles focusing on this topic [6-8]. Nanocellulose, which is obtained from the most abundant polymer on earth – cellulose [9], can be extracted from numerous sources from bacteria to vegetal biomass. Nanocellulose is commonly grouped into three categories: bacterial nanocellulose (BNC), cellulose nanocrystals (CNCs), and cellulose nanofibers (CNFs). All three types of nanocellulose have differing properties and even within each type, depending on the source the properties can change [10]. Previous studies of the use of nanocellulose in biomedical applications has especially focused on BNC because of its purity and lack of lignin or hemicellulose contamination [11], but BNC is known to be difficult and expensive to produce because of a limited source and production requirements [12]. BNC is known to have difficulties with maintaining the nanoscaled structure when producing materials as illustrated by Klemm et al [10]. The use of CNCs and CNFs in biomedical research has been mostly contained within the fields of drug delivery and wound healing or external application. The novelty of the research proposed in this Ph.D. was to consider that nanocellulose can have considerable research potential for tissue engineering applications or for the modulation of stem cell behavior during culture since previous research has mainly focused on determining the biocompatibility of CNC based materials with stem cells [13], but some results have shown the differentiation potential of pluripotent stem cells with CNF [14]. This project will focus on the use of nanocellulose within culture and the relationship between the material mechanical properties and cell behavior through a collaboration between experts in the fields of nanocellulose (LGP2), smart materials (Virginia Tech), and biomimetic materials (LMGP-BIOMIM).

As stated previously, the use of CNCs and CNFs in biomedical applications is limited. In order to have a thorough understanding of the necessary steps of biomaterial fabrication and characterization, all stages of material development from obtaining nanocellulose from a vegetal agricultural waste (**Chapter 2**) to creating high-value added nanocomposites (**Chapter 3**) and their effect on stem cell behavior in culture (**Chapter 4**) were researched during the course of the Ph.D. research. The main

innovation of this research is the relationship between tunable nanocellulose-based material properties within cell culture (**Chapter 4**).

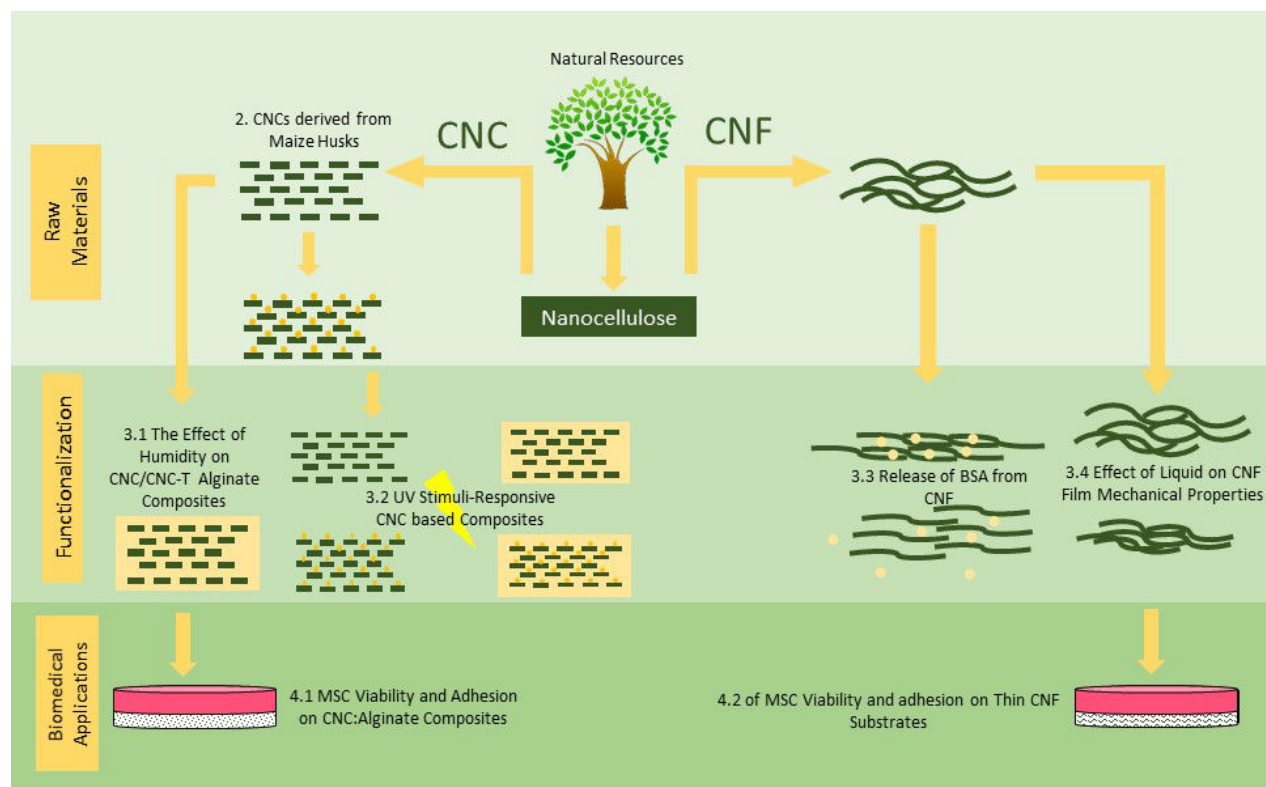


Figure 2. Schematic of Thesis Organization

- CNCs, which are known to have exceptional mechanical properties as well as being relatively inexpensive and renewable and can be produced from numerous sources with differing properties such as aspect ratio and network mechanical properties [15]. In **Chapter 2**, CNCs were extracted from maize (*Zea mays*) husk, which is a common agricultural residue. Current uses of maize husk residue are for the prevention of erosion [16], or the production of chemicals, paper, or insulating materials [17]. CNCs with high aspect ratio were produced through common sulfuric acid hydrolysis following alkali and bleaching treatment.

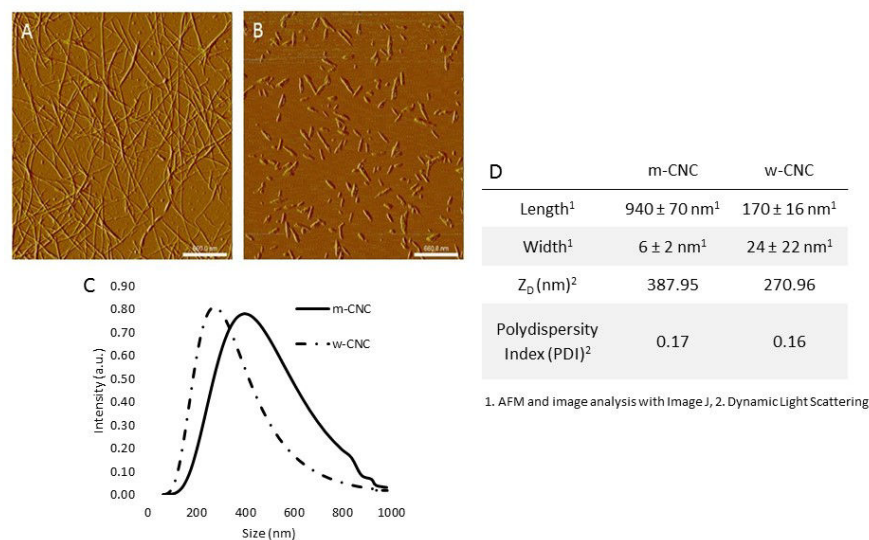


Figure 3. CNC AFM images from suspensions of 0.0001 wt% of A) m-CNC, B) w-CNC. C) Size distribution of m-CNC and w-CNC nanoparticles as determined by DLS. D) Length and width measurements m-CNCs and w-CNCs as determined by AFM, and Hydrodynamic diameter (Z_D), polydispersity index (PDI) determined by DLS.

It was found that the dimensions of these CNCs were to be 940 nm in length and 6 nm in width. These dimensions are found to be comparable to high quality CNCs extracted from tunicates (length = 1187 nm, width = 9 nm) [18], but with lowering processing requirements. m-CNCs were added to natural rubber to make composites and it was shown that the addition of m-CNCs had higher reinforcement compared to wood-commercial CNCs. This chapter confirms that CNCs can be produce high quality nanocellulose from one of the world's largest supplies of agricultural waste, which can be used in high-value added applications such as biomedical applications.

• **Chapter 3** highlights the use of nanocellulose-based materials in liquid or mimicking physiological conditions. Both CNCs and CNFs were employed to create high-value added materials for biomedical applications. Because of this, there was a special consideration for testing in physiological conditions for mechanical testing in **Chapter 3.1** and **Chapter 3.2**; while **Chapter 3.3** focuses on a CNF-based release system for bovine serum albumin (BSA).

Chapters 3.1 and 3.2 explores the use of an alginate-based nanocomposite with CNCs, CNC-Ts (oxidized CNCs with high COOH content) (**Chapter 3.1**) and 4-pentenoic acid grafted-CNCs (**Chapter 3.2**). Alginate was chosen as a matrix because of its extensive use as a hydrogel in biomedical applications. Alginate is known to be highly sensitive to degradation when exposed to liquid or

humidity. The effect of humidity and immersion in differing liquids on the material and mechanical properties of alginate films and nanocomposites with CNCs and CNC-Ts were studied in **Chapter 3.1**. CNCs and CNC-Ts were added to alginate in varying ratios, and was shown that the addition of nanocellulose can enhance the mechanical properties when immersed in liquid. This is especially true for the addition of TEMPO-oxidized CNCs tested in phosphate buffer solution (PBS) at 37°C as shown in Figure 5.

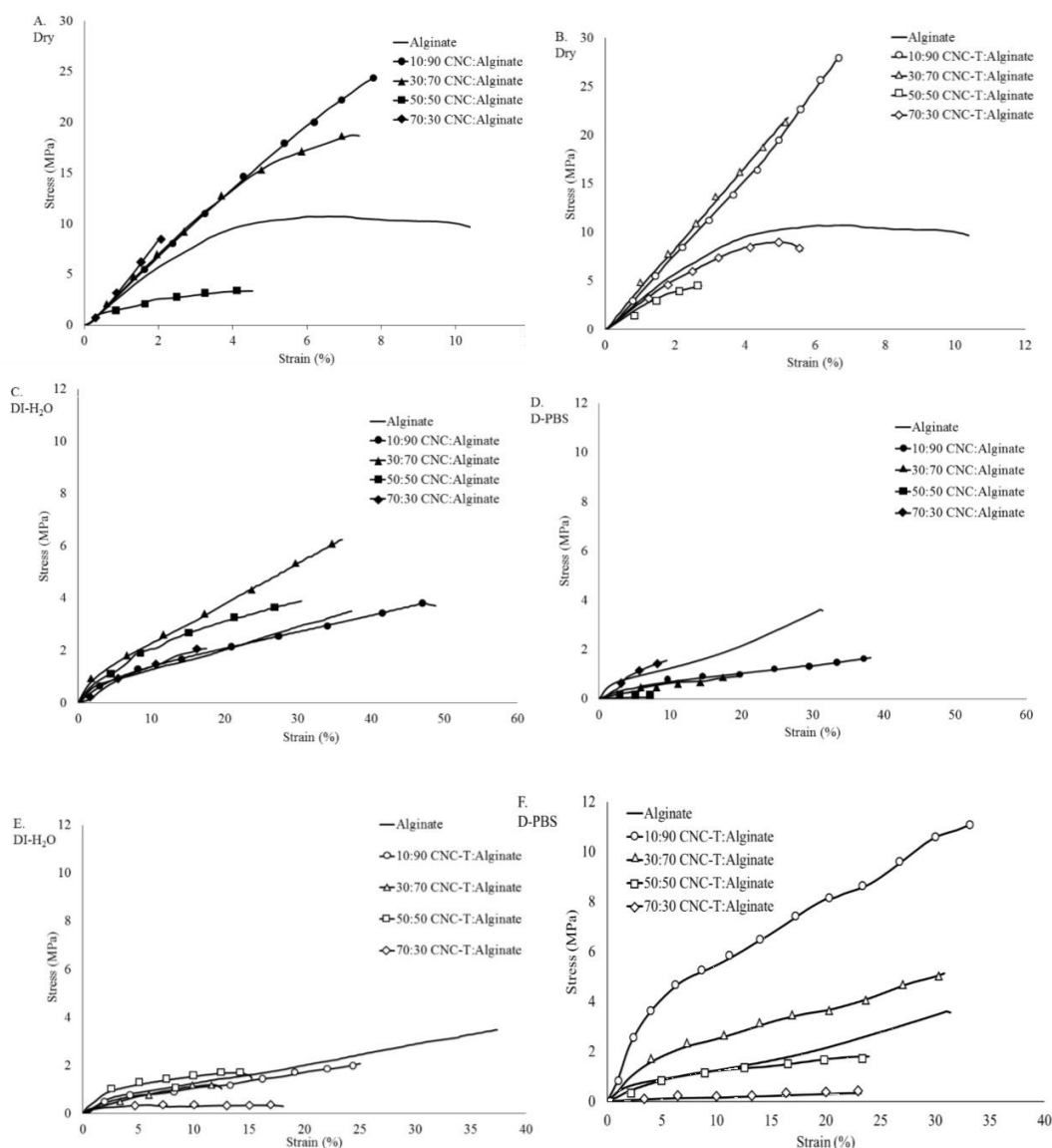


Figure 5. Stress-strain curves of in ambient conditions (A, B), in aqueous conditions in DI-H₂O (C, E) and D-PBS (D, F) at 37°C for CNC:Alginate composites (A, C, D) and CNC-T:Alginate composites (B, E, F)

A stimuli-responsive alginate nanocomposite was characterized and analyzed in **Chapter 3.2**. CNCs were grafted with 4-pentenoic acid through an esterification reaction using a green chemical process called SolReact and developed by Espino Perez [19].

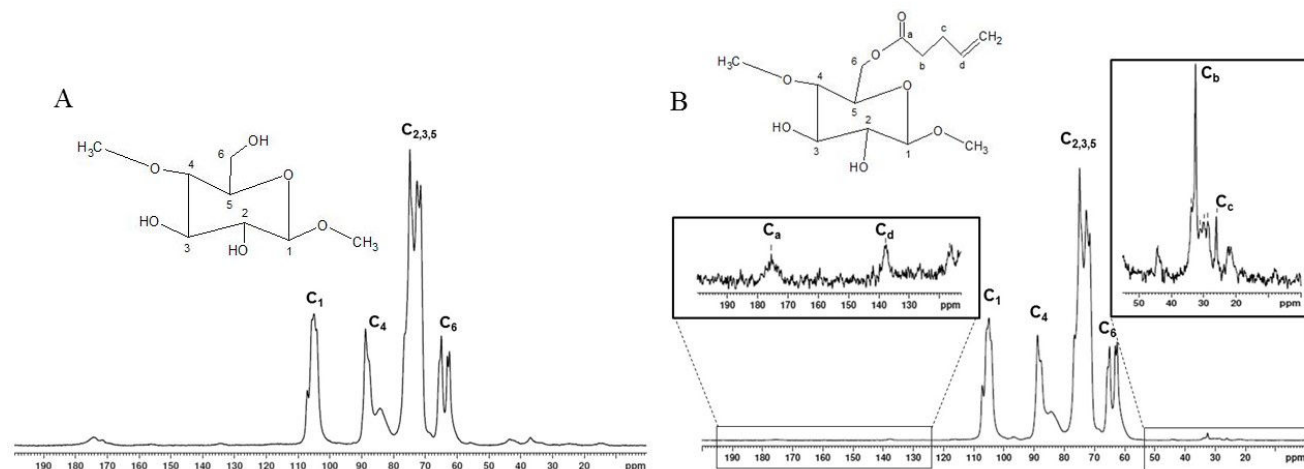


Figure 6. ^{13}C solid state NMR of A) CNC and B) PA-g-CNC

The 4-pentenoic acid functionalized CNCs (PA-g-CNCs) and 4,4'-Azobis(4-cyanovaleric acid) (ACVA) were added to alginate within the same ratios presented in **Chapter 3.1** and also tested in physiological conditions. ACVA, an azo-initiator, induced free-radical polymerization between the free allyl group on the PA-g-CNCs when exposed to UV radiation. The effect of UV exposure time on the efficacy of crosslinking was analyzed. It was determined through indirect and direct methods that crosslinking was dependent on the amount of PA-g-CNC within the nanocomposite and UV exposure time. Significant differences in the crosslinking efficacy was more pronounced for nanocomposites with higher amounts of PA-g-CNC and exposure time as determined by swelling of the nanocomposites and tensile testing in dry and wet conditions.

Conversely, CNF can be used as an active molecule carrier system because of the nanoporous structure that forms during fabrication, as well as the general reactivity or adsorption properties of the nanocellulose surface. Recently, these properties have made CNF films a highly attractive material to researchers for use in drug release systems. The nanoporous structure can be employed to entrap

particles, proteins, or molecules that can then be released. Since the 2010s, the most common uses of CNF as an active molecule carrier are for use in antibacterial or drug release systems. To our knowledge, the use of CNF for the release of model proteins, like BSA, has not been studied previously. The only reported use of BSA with nanocellulose was conducted by Müller et al. 2012 with bacterial nanocellulose aerogels. It was shown that the release of BSA from BNC aerogels was dependent on a variety of factors including: temperature, pH, concentration of BSA, pre-swelling conditions, and BNC drying processes. BNC that was freeze-dried had a lower capacity for the uptake of BSA within solution because of the morphological changes that occur during freeze-drying [20].

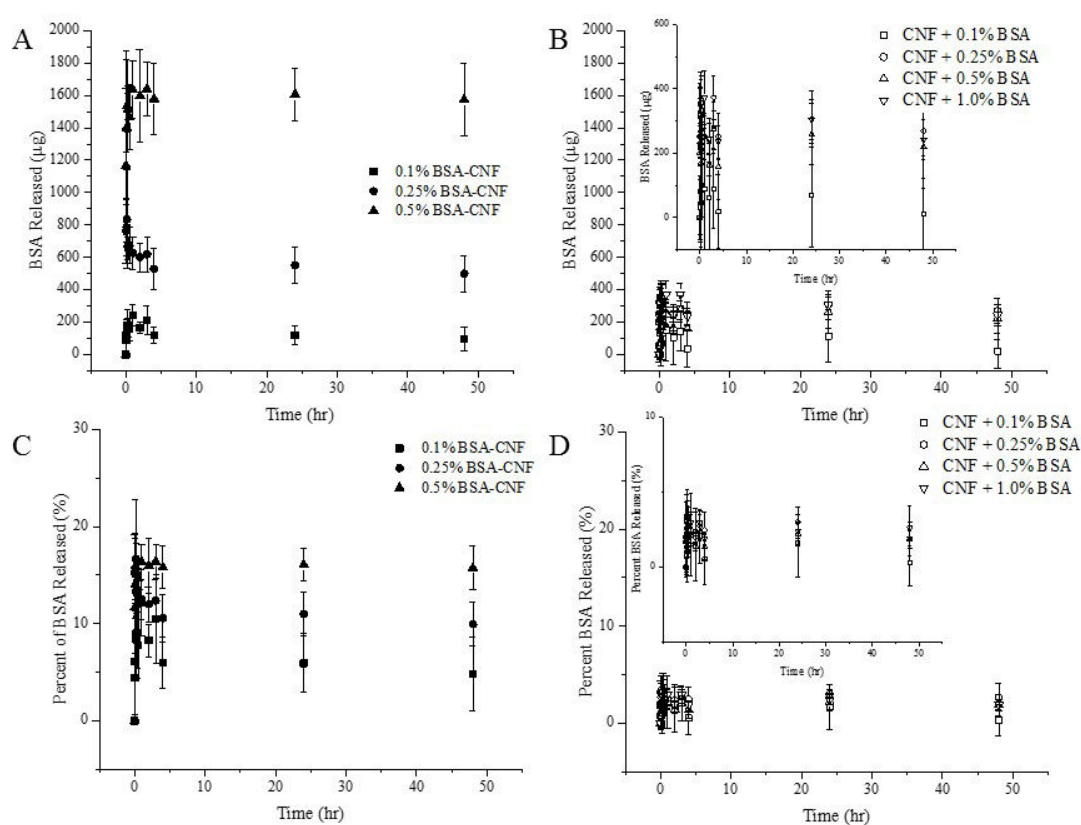


Figure 7. Release of BSA from CNF in A, B) micrograms, C, D) percentage of CNF added for A, C) BSA-CNF composites and B, D) BSA added by diffusion for 48 hours in PBS at 37°C as determined by BCA assay

In **Chapter 3.3**, BSA was incorporated into CNF through two different fabrication methods: diffusion or incorporation. CNF films with or without BSA were characterized to determine their water vapor permeability, which could affect the release of BSA. Incorporation of BSA through nanocomposite

formation was further characterized by scanning electron microscopy (SEM) and Fourier transform infrared spectroscopy (FTIR). Release of BSA was conducted for 48 hours in PBS and at physiological temperature. It was shown that the release profile of BSA from CNF is dependent on the loading technique with incorporation releasing more BSA, and the amount of BSA added to CNF. This was chosen because of the potential use of a CNF release system of growth factors in future cell culture experiments in order to influence cell differentiation.

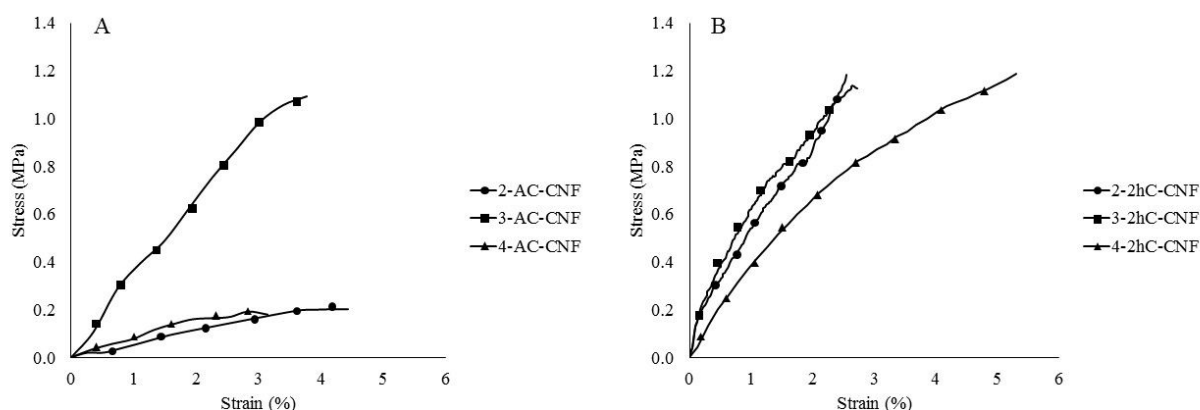


Figure 8. Stress-strain testing of (A) AC-CNF films and (B) 2hC-CNF films in aqueous conditions in PBS at 37°C.

Chapter 3.4 explores the effect of liquid on the mechanical properties of CNF films with differing basis weight and additional curing step. It was shown that when tested in conditions that mimic physiological conditions (i.e. in PBS at 37°C) the Young's modulus and storage modulus can vary. With some nanopapers exhibiting an increase of E from 6 to 90 MPa after curing at 150°C. With increased fiber content there is a trend of decreased mechanical properties in tensile tests and dynamic mechanical analysis. This can be attributed to possible disruption of hydrogen bonds that occur once exposed to an ionic liquid like PBS. It is suggested that the mechanical properties of CNF within a liquid state can be easily tuned in regards to Young's modulus and storage modulus, and could be of interest for use in stem cell culture.

• **Chapter 4**, entitled “The Influence of Nanocellulose on Stem Cell Behavior in Culture,” explores the use of nanocellulose on the viability and adhesion of mesenchymal stem cells (MSCs). This interaction is especially of importance with MSCs because they are anchorage dependent, or undergo

programmed cell death if they do not attach to a biomaterial surface [21, 22]. MSC attachment occurs when the cell reorganizes the actin filaments of the cytoskeleton into filopodia to adhere to the surface [22, 23]. This adhesion can be influenced by the properties of the biomaterial such as material topography [21, 23, 24], surface chemistry [25], and most importantly in this case, mechanical properties [4, 22]. The basis of this work was to determine if mechanically-adaptive nanocellulose substrates could influence stem cell behavior. This concept was first proposed with the use of a different polymer by Engler et al, which stated that the mechanical properties of a biomaterial could influence stem cell differentiation without any other external factors [4]. This finding was the basis of the thesis to determine if mechanically adaptive nanocellulose substrates could influence stem cells in a similar manner.

In **Chapter 4.1**, CNC:Alginate and CNC-T:Alginate nanocomposites that were extensively characterized in **Chapter 3.1**, will be analyzed for their effect on the adhesion and viability of MSCs. The attachment of MSCs to the surface is of importance in alginate-based systems because alginate is not a favorable material for MSC adhesion because its hydrophilic nature prevents the deposition of proteins onto the surface [26]. It is well-known by researchers that when cultured in the presence of alginate in a 2D system cells form clusters, which are not a favorable morphology for proliferation and viability [27]. Since it has been shown that the addition of CNCs or CNC-Ts can improve the mechanical properties of alginate in a physiological system (**Chapter 3.1**), it was hypothesized that nanocomposites could improve the adhesion and viability of MSCs. The adhesion of MSCs after 6 and 24 hours was conditional on the amount of CNCs added to the alginate in cell culture conditions as measured by cell area, cell aspect ratio, and also area fraction of cells adhered to the culture surface as seen in Figure 8. Viability of D1/BALBc MSCs were assessed for 24 and 48 hours, and it was shown that the viability varied significantly, with higher levels of significance for nanocomposites with unmodified CNCs. These results suggest the addition of CNCs or CNC-Ts can affect MSC behavior in cell culture, and that CNC-Alginate and CNC-T-Alginate composites are promising materials for future cell studies.

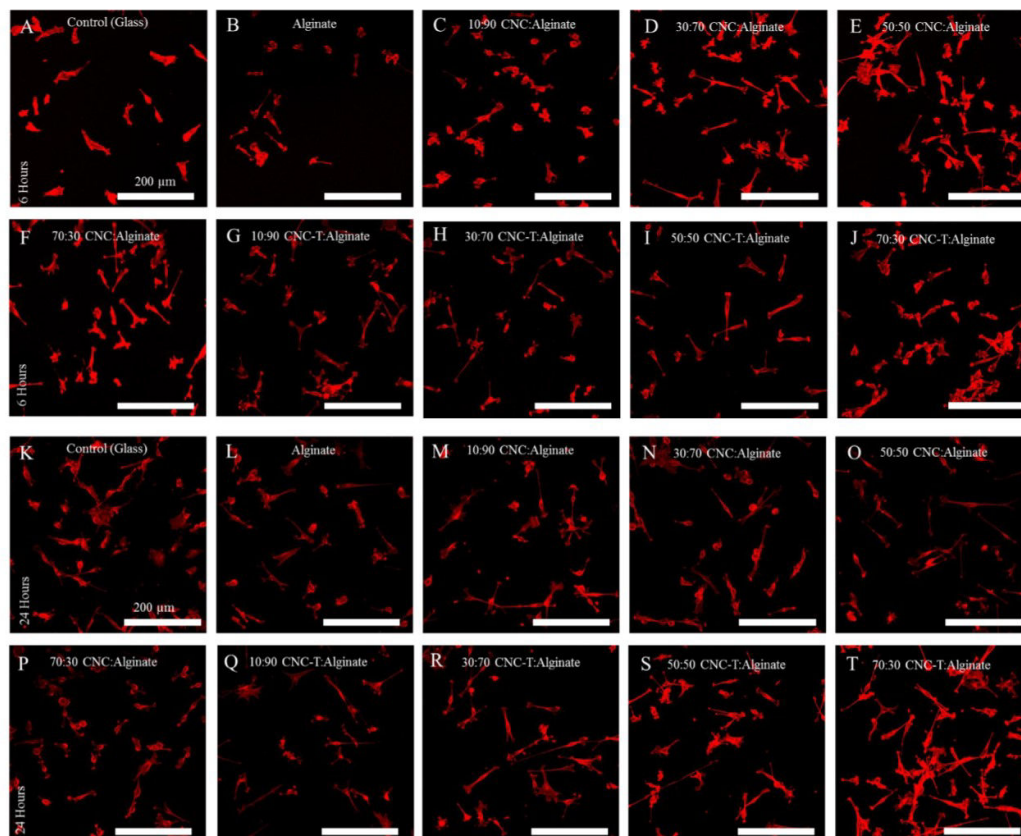


Figure 9. Confocal microscopy images of D1 MSCs stained for actin seeded on A, K) Control (Glass) B, L) Alginate, C, M) 10:90 CNC:Alginate, D, N) 30:90 CNC:Alginate, E, O) 50:50 CNC:Alginate, F, P) 70:30 CNC:Alginate, G, Q) 10:90 CNC-T:Alginate, H, R) 30:70 CNC-T:Alginate, I, S) 50:50 CNC-T:Alginate, and J, T) 70:30 CNC-T:Alginate at A-J) at 6h and K-T) 24h post-seeding with a scale bar of 200 μm .

For the use of CNF as a biomaterial, a differing approach to the CNC:Alginate system was employed and outlined in **Chapter 4.2**. Thin CNF nanostructured substrates were fabricated by different processes with varying roughness, Young's modulus, porosity, and swelling. The properties of the CNF films in liquid were strongly dependent on the curing at 150°C they underwent.

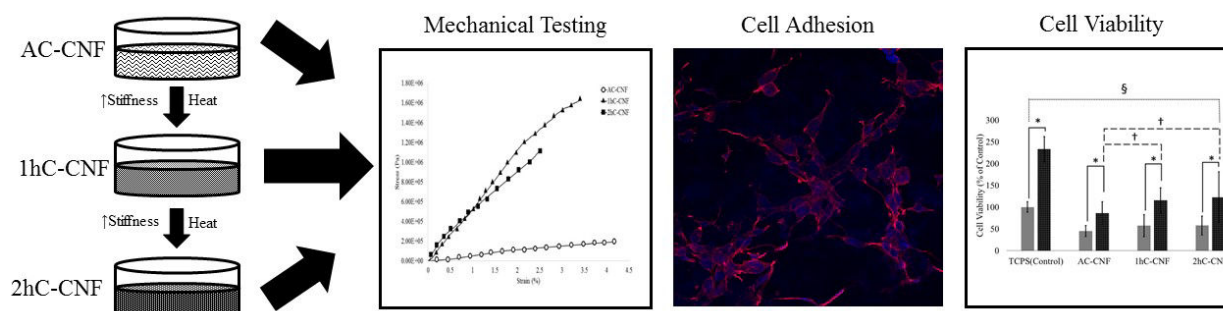


Figure 10. Schematic representation of CNF substrate fabrication and characterization for use in cell culture

With increased heat exposure, the porosity decreased and Young's modulus clearly increased when tested in an aqueous state. These material property changes were tested to determine if they influenced stem cell adhesion and viability. It was determined that MSC viability and adhesion was dependent on the CNF material and mechanical properties with significant differences reported, especially in the case of CNF substrates with high mechanical properties. These results suggest that the tuning of the nanocellulose material and mechanical properties without any chemical crosslinking or modification can strongly affect MSC viability and adhesion in culture.

The research presented in this thesis displays that nanocellulose, both CNCs and CNFs, are appropriate materials for biomedical applications with characterization and implementation of nanocellulose in a variety of ways: from production of CNCs, using CNF films as active carriers, creating and characterizing mechanically adaptive CNC-alginate nanocomposites in physiological conditions, and the effect nanocellulose-based substrate properties on stem cells. The main results show that nanocellulose, which has been extensively characterized in liquid, physiological conditions, can be mechanically modified by a drying process and induce differences in stem cell adhesion and viability. Both of which are the basis for future research on the differentiation of stem cells. Proving that nanocellulose is an innovative material for future tissue engineering constructs.

References

- [1] Vert M, Hellwich K-H, Hess M, Hodge P, Kubisa P, Rinaudo M, et al. Terminology for biorelated polymers and applications (IUPAC Recommendations 2012). *Pure and Applied Chemistry*. 2012;84:377-410.
- [2] Black J, Hastings G. *Handbook of biomaterial properties*: Springer Science & Business Media; 2013.
- [3] Palsson BØ, Bhatia SN. *Tissue Engineering*: Pearson Education; 2004.
- [4] Engler AJ, Sen S, Sweeney HL, Discher DE. Matrix elasticity directs stem cell lineage specification. *Cell*. 2006;126:677-89.
- [5] Tec21.
- [6] Jorfi M, Foster EJ. Recent advances in nanocellulose for biomedical applications. *Journal of Applied Polymer Science*. 2015;132:41719.
- [7] Lin N, Dufresne A. Nanocellulose in biomedicine: Current status and future prospect. *European Polymer Journal*. 2014;59:302-25.
- [8] Domingues RM, Gomes ME, Reis RL. The potential of cellulose nanocrystals in tissue engineering strategies. *Biomacromolecules*. 2014;15:2327-46.
- [9] Urruzola I, Robles E, Serrano L, Labidi J. Nanopaper from almond (*Prunus dulcis*) shell. *Cellulose*. 2014;21:1619-29.
- [10] Klemm D, Schumann D, Kramer F, Heßler N, Koth D, Sultanova B. Nanocellulose materials—Different cellulose, different functionality. *Macromolecular symposia*: Wiley Online Library; 2009. p. 60-71.
- [11] Gatenholm P, Klemm D. Bacterial nanocellulose as a renewable material for biomedical applications. *MRS Bulletin*. 2010;35:208-13.
- [12] Dufresne A. Nanocellulose: a new ageless bionanomaterial. *Materials Today*. 2013;16:220-7.
- [13] Zhou C, Shi Q, Guo W, Terrell L, Qureshi AT, Hayes DJ, et al. Electrospun Bio-Nanocomposite Scaffolds for Bone Tissue Engineering by Cellulose Nanocrystals Reinforcing Maleic Anhydride Grafted PLA. *ACS Applied Materials & Interfaces*. 2013;5:3847-54.
- [14] Lou YR, Kanninen L, Kuisma T, Niklander J, Noon LA, Burks D, et al. The use of nanofibrillar cellulose hydrogel as a flexible three-dimensional model to culture human pluripotent stem cells. *Stem Cells Dev*. 2014;23:380-92.
- [15] Bras J, Viet D, Bruzzese C, Dufresne A. Correlation between stiffness of sheets prepared from cellulose whiskers and nanoparticles dimensions. *Carbohydrate Polymers*. 2011;84:211-5.
- [16] Padgett M, et al. . Production practices for major crops in US agriculture, 1990-97. *Growth*. 2000.

- [17] Gogerty R. Crop leftovers: More uses, more value. Resource: Engineering & Technology for Sustainable World. 1996;3:6-9.
- [18] Sacui IA, Nieuwendaal RC, Burnett DJ, Stranick SJ, Jorfi M, Weder C, et al. Comparison of the properties of cellulose nanocrystals and cellulose nanofibrils isolated from bacteria, tunicate, and wood processed using acid, enzymatic, mechanical, and oxidative methods. ACS Applied Materials & Interfaces. 2014;6:6127-38.
- [19] Espino-Perez E, Domenek S, Belgacem N, Sillard C, Bras J. Green process for chemical functionalization of nanocellulose with carboxylic acids. Biomacromolecules. 2014;15:4551-60.
- [20] Müller A, Ni Z, Hessler N, Wesarg F, Müller FA, Kralisch D, et al. The biopolymer bacterial nanocellulose as drug delivery system: investigation of drug loading and release using the model protein albumin. Journal of Pharmaceutical Sciences. 2013;102:579-92.
- [21] Dalby MJ, Gadegaard N, Oreffo RO. Harnessing nanotopography and integrin-matrix interactions to influence stem cell fate. Nature materials. 2014;13:558-69.
- [22] Discher DE, Janmey P, Wang YL. Tissue cells feel and respond to the stiffness of their substrate. Science. 2005;310:1139-43.
- [23] Dalby MJ, Gadegaard N, Riehle MO, Wilkinson CD, Curtis AS. Investigating filopodia sensing using arrays of defined nano-pits down to 35 nm diameter in size. The international journal of biochemistry & cell biology. 2004;36:2005-15.
- [24] Dalby MJ, Gadegaard N, Tare R, Andar A, Riehle MO, Herzyk P, et al. The control of human mesenchymal cell differentiation using nanoscale symmetry and disorder. Nature materials. 2007;6:997-1003.
- [25] Anderson HJ, Dalby MJ, Sahoo JK, Ulijn RV. Mesenchymal Stem Cell Fate: Applying Biomaterials for Control of Stem Cell Behavior. Frontiers in Bioengineering and Biotechnology. 2016;4:38.
- [26] Yagi K, Tsuda K, Serada M, Yamada C, Kondoh A, Miura Y. Rapid formation of multicellular spheroids of adult rat hepatocytes by rotation culture and their immobilization within calcium alginate. Artificial organs. 1993;17:929-34.
- [27] Rowley JA, Madlambayan G, Mooney DJ. Alginate hydrogels as synthetic extracellular matrix materials. Biomaterials. 1999;20:45-53.

Résumé

Le domaine de recherche de matériaux biocompatibles, appelés également biomatériaux, ou matériaux qui entrent en contact avec des microorganismes, organismes ou tissus vivants [1], englobe de nombreux applications et types de matériaux (des polymères, des métaux aux matériaux biosourcés comme l'alginate et le collagène). Étudiés depuis les années 1950, les biomatériaux sont maintenant utilisés dans une variété d'applications telles que : les implants articulaires artificiels, l'ingénierie tissulaire, la libération contrôlée de médicament ou la thérapie cellulaire. L'un des aspects les plus importants d'un biomatériau est de déterminer s'il est biocompatible. Un biomatériau peut être considéré comme biocompatible s'il se comporte de manière adéquate au sein de l'hôte dans une application particulière [2]. Cela nécessite de déterminer la réponse immunologique de l'hôte causée par l'introduction du biomatériau et de vérifier si le biomatériau possède des propriétés appropriées à l'application comme la résistance mécanique, la libération de médicament, la structure des prothèses, etc. La biocompatibilité dépend de nombreux facteurs tels que la chimie de surface, la porosité ou les propriétés mécaniques. Ces propriétés des biomatériaux peuvent être modifiées par des chercheurs pour induire certains comportements cellulaires tels qu'une réponse immunologique limitée, une adhérence protéique accrue ou même une différenciation cellulaire dirigée [3]. La figure 1 donne une liste exhaustive de la réponse cellulaire possible à un biomatériau.

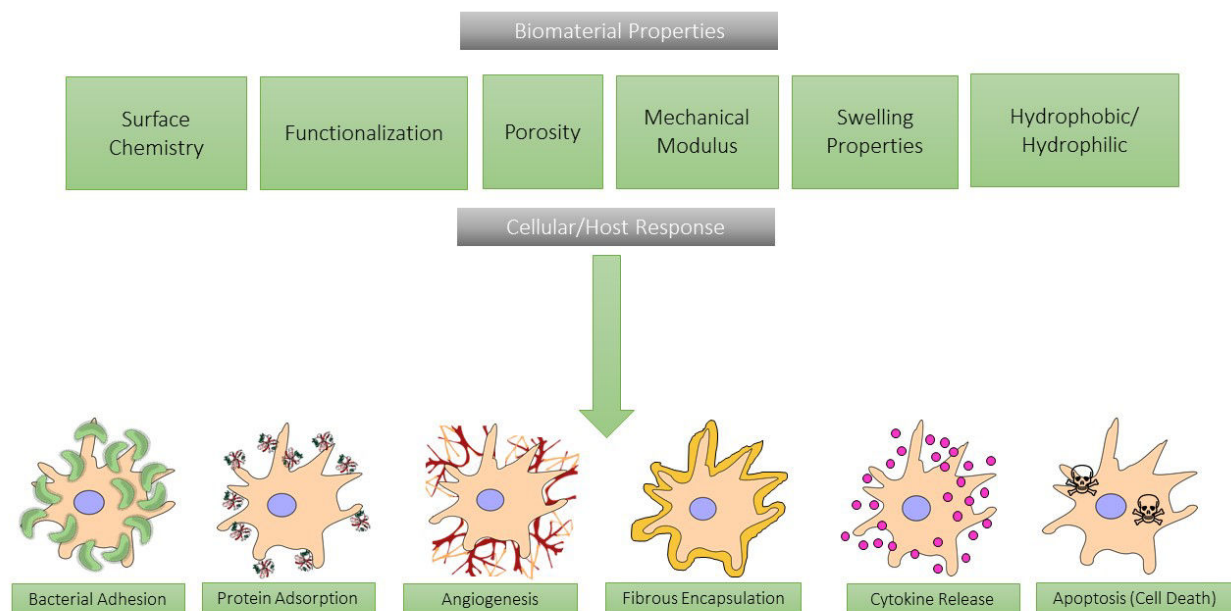


Figure 1. Réponse de la cellule ou de l'hôte aux propriétés du biomatériau physique

L'un des moyens pour influencer le comportement des cellules en présence des biomatériaux consiste à modifier leurs propriétés mécaniques. Cette approche récente a d'abord été proposée par

Engler et al. en 2006, il a montré qu'en changeant le module élastique des gels de polyacrylamide, les cellules souches mésenchymateuses (MSC), pourraient suivre des modèles de différenciation différents [4]. Au début de ce doctorat intitulé CellDiff (2014-2017) et financée par le laboratoire d'excellence Tec21 [5], il a été supposé que les substrats à base des nanocelluloses pourraient être fabriqués avec divers modules élastiques pour modifier ainsi les caractéristiques des MSC lors de leur culture.

L'utilisation des nanocelluloses dans les applications biomédicales a été jusqu'à présent très limitée, même si l'intérêt pour leur utilisation en tant que matériau biocompatible a fortement augmenté ces dernières années, comme l'ont indiqué récemment les articles de revue portant sur ce sujet [6-8]. Les nanocelluloses, obtenues à partir du polymère le plus abondant sur terre – la cellulose [9], peuvent être extraites de nombreuses sources. Les nanocelluloses sont généralement regroupées en trois catégories : la nanocellulose bactérienne (BCN), les nanocristaux de cellulose (CNC) et les nanofibres de cellulose (CNF). Entre parenthèse sont les abréviations selon les récents standards proposés par la communauté. Les trois types des nanocelluloses ont des propriétés différentes et même dans chaque type, selon la source et le procédé, les propriétés peuvent changer [10]. Des études antérieures sur l'utilisation des nanocelluloses dans les applications biomédicales ont surtout porté sur la BCN en raison de sa pureté et de son manque de contamination par la lignine ou l'hémicellulose [11], mais la BCN est aussi connue comme difficile à produire en raison d'une source limitée et d'un procédé de production difficilement industrialisable à grande échelle [12]. On sait que la BCN a des difficultés à maintenir la structure nanométrique lors de la production de matériaux, comme l'ont illustré Klemm et al [10]. L'utilisation des CNC et des CNF dans la recherche biomédicale a été principalement contenue dans les domaines de la délivrance de médicaments et de la guérison des plaies en application externe. La nouveauté de la recherche proposée dans ce doctorat était de considérer que les nanocelluloses peuvent avoir un potentiel de recherche considérable pour les applications d'ingénierie tissulaire ou pour la modulation du comportement des cellules souches pendant leur culture. Les recherches précédentes ont surtout porté sur la détermination de la biocompatibilité des matériaux à base de CNC avec des cellules souches [13], mais certains résultats ont montré le potentiel de différenciation des cellules souches pluripotentes avec les CNF [14]. Ce projet portera donc sur l'utilisation des nanocelluloses dans la culture cellulaire et la relation entre les propriétés mécaniques des matériaux cellulosique et le comportement des cellules en croissance grâce à une collaboration entre plusieurs équipes complémentaires et expertes dans les domaines des nanocelluloses (LGP2), des matériaux intelligents (Virginia Tech) et des matériaux biocompatibles (LMGP-BIOMIM).

Comme indiqué précédemment, l'utilisation des CNC et des CNF dans les applications biomédicales est limitée. Afin d'avoir une compréhension approfondie, les différentes étapes dans le développement de biomatériaux cellulotiques ont été étudiées au cours de ce projet, en partant de l'obtention des nanocelluloses à partir d'un déchet agricole végétal (**chapitre 2**), puis la création de nanomatériaux à forte valeur ajoutée (**chapitre 3**) et enfin le comportement des cellules en culture sur ces matériaux (**chapitre 4**). L'innovation principale de cette recherche est la relation entre les propriétés de matériaux à base des nanocelluloses et la culture cellulaire (**chapitre 4**).

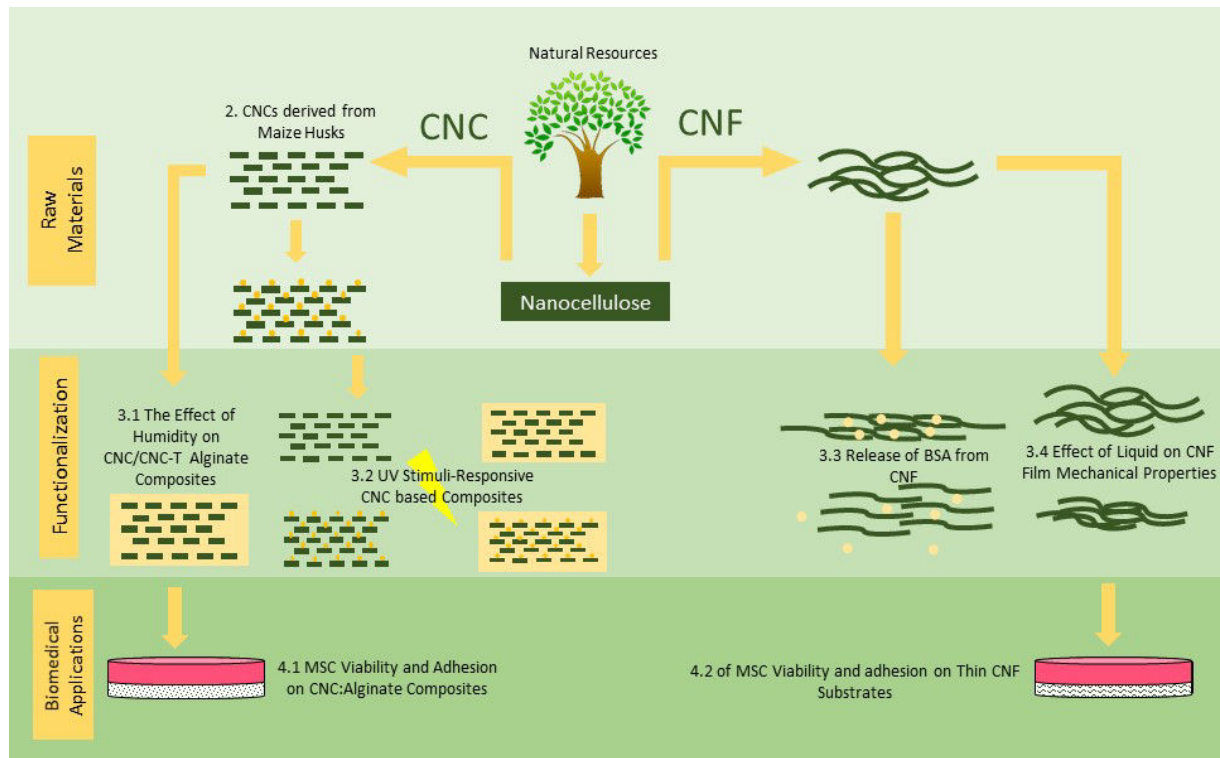


Figure 2. Schéma d'organisation du projet de thèse

- Les CNC, connues pour avoir des propriétés mécaniques exceptionnelles, sont relativement peu coûteux, renouvelables et peuvent être produits à partir de nombreuses sources avec des propriétés différentes telles que les dimensions et les propriétés mécaniques du réseau [15]. Au **chapitre 2**, les CNC ont été extraits de l'épis de maïs (*Zea mays*), qui est un résidu agricole commun. Les utilisations actuelles de ces résidus de maïs sont destinées à prévenir l'érosion [16], ou à la production de produits chimiques, de papier ou d'isolants [17]. Des CNC avec un facteur Longueur/Diamètre élevé ont été produits grâce à une hydrolyse classique d'acide sulfurique suite à un traitement alcalin et de blanchiment de la matière première.

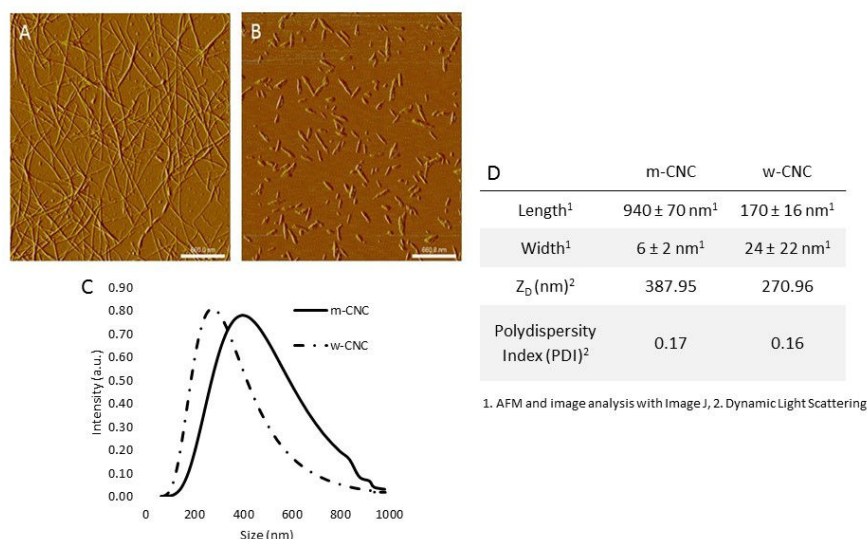


Figure 3. Images CNC AFM à partir de suspensions de 0,0001% en poids de A) m-CNC, B) w-CNC. C) Distribution de taille des nanoparticules m-CNC et w-CNC telles que déterminées par DLS. D) Mesures en longueur et en largeur m-CNC et w-CNC déterminés par AFM, et diamètre hydrodynamique (ZD), indice de polydispersité (PDI).

On a constaté que les dimensions de ces CNC avaient une longueur de 940 nm et une largeur de 6 nm. Ces dimensions se révèlent être comparables aux CNC de haute qualité extraits des tuniciers (longueur = 1187 nm, largeur = 9 nm) [18], mais avec des exigences de traitement inférieures. Les m-CNC ont été ajoutés au caoutchouc naturel pour fabriquer des composites et il a été démontré que l'ajout de m-CNC avait un renforcement plus élevé par rapport aux CNC commercialisés issus de bois. Ce chapitre confirme que peuvent être produits des nanocelluloses de haute qualité à partir d'un des déchets agricoles les plus courant au monde et qu'ils peuvent être utilisées dans des applications à forte valeur ajoutée telles que des applications nanocomposites ou biomédicales.

- Le **chapitre 3** met en évidence l'utilisation et la caractérisation de matériaux à base des nanocelluloses dans des conditions physiologiques liquides. Les CNC et les CNF ont été utilisées récemment pour créer des matériaux à forte valeur ajoutée dans le domaine du biomédical. Pour cette raison, il a été décidé de tester les propriétés mécaniques de ces matériaux dans les conditions physiologiques au **chapitre 3.1** et au **chapitre 3.2**; tandis que le **chapitre 3.3** se concentre sur un système de libération en liquide à base de CNF pour l'albumine de sérum bovin (BSA).

Les **chapitres 3.1 et 3.2** explorent l'utilisation d'un nanocomposite à base d'alginate avec des CNC, CNC-T (CNC oxydés à teneur élevée en COOH) (**chapitre 3.1**) et CNC greffés avec l'acide 4-penténoïque (**chapitre 3.2**). L'alginate a été choisi comme matrice en raison de son utilisation intensive en hydrogel dans les applications biomédicales. L'alginate est connu pour être très sensible à la dégradation lorsqu'il est exposé au liquide ou à l'humidité. L'effet de l'humidité ou de

l'immersion dans différents liquides sur les propriétés mécaniques des films d'alginate et des nanocomposites avec CNC et CNC-T a été étudié au **chapitre 3.1**. Les CNC et les CNC-T ont été ajoutés à l'alginate dans des rapports variables, et il a été montré que l'ajout de nanocellulose peut améliorer les propriétés mécaniques lors de l'immersion dans un liquide. Cela est particulièrement vrai pour l'addition de CNC TEMPO-oxydés testés dans une solution tampon phosphate (PBS) à 37 °C comme le montre la figure 5.

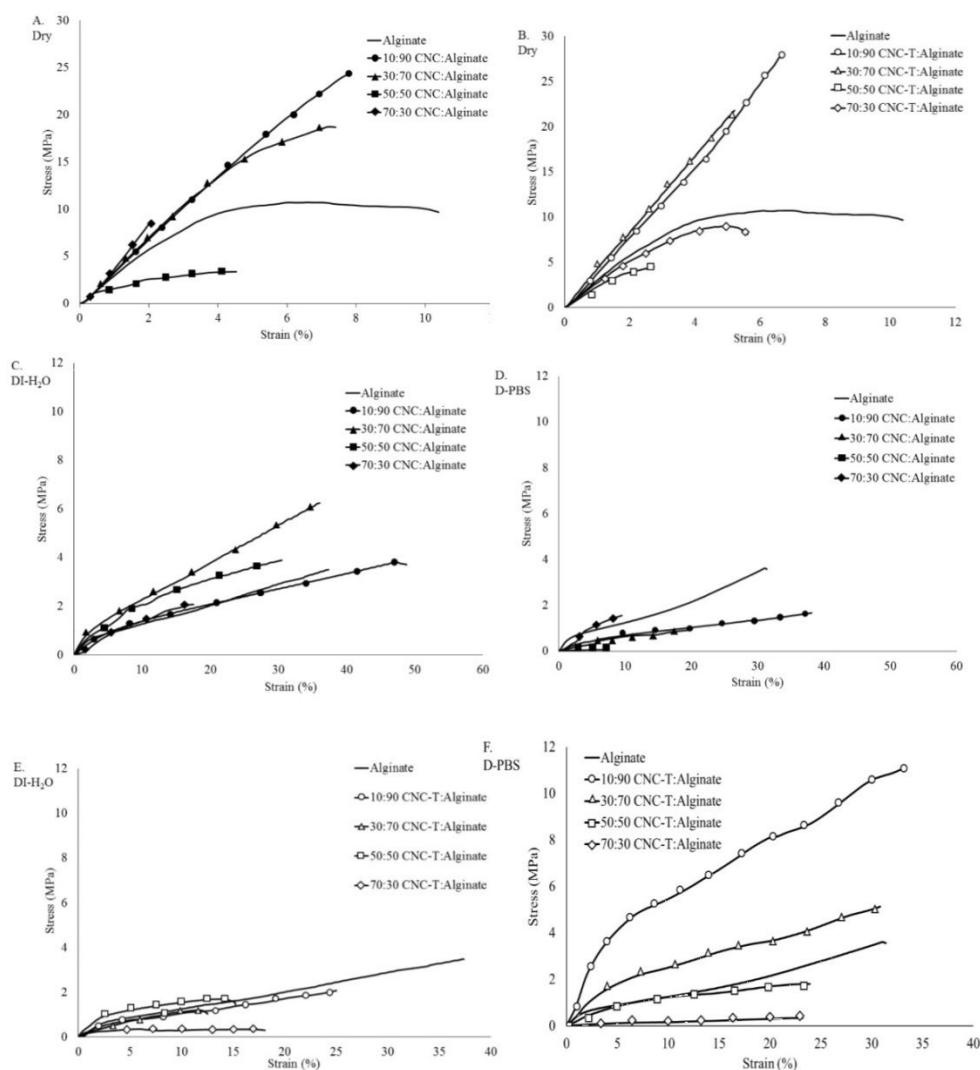


Figure 5. Courbes contrainte-déformation dans les conditions ambiantes (A, B), en conditions aqueuses dans DI-H₂O (C, E) ou dans D-PBS (D, F) à 37 °C pour des composites CNC: alginate (A, C, D) et CNC-T: alginate (B, E, F).

Un nanocomposite d'alginate réticulable par UV a ensuite été préparé et caractérisé au **chapitre 3.2**. Les CNC ont été greffés avec de l'acide 4-penténoïque par une réaction d'estérification en

utilisant un processus chimique « vert » appelé SolReact et récemment développé par Espino Perez [19]. La qualité du greffage a été vérifiée par plusieurs moyens et notamment la RMN (figure 6)

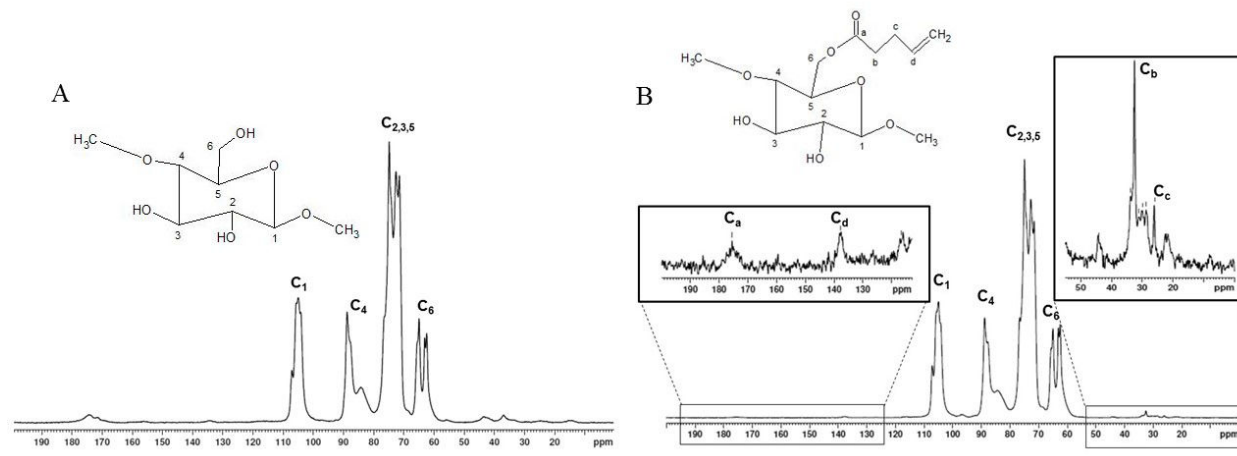


Figure 6. RMN du ^{13}C à l'état solide de A) CNC et B) PA-g-CNC

Les CNC fonctionnalisés à l'acide 4-penténoïque (PA-g-CNC) et le 4,4'-Azobis (acide 4-cyanovalérique) (ACVA) ont été ajoutés à l'alginate dans les mêmes proportions présentés au **chapitre 3.1** et également testés dans des conditions physiologiques. L'ACVA est un amorceur azoïque qui peut induire une réticulation radicalaire entre le groupe allyle libre sur les CNC-PAs lorsqu'ils sont exposés aux rayonnements UV. L'effet du temps d'exposition aux UV sur l'efficacité de la réticulation a été analysé. Il a été déterminé par des méthodes indirectes et directes selon lesquelles la réticulation dépendait de la quantité de PA-g-CNC dans le nanocomposite et le temps d'exposition aux UV. Des différences significatives dans l'efficacité de réticulation ont été plus prononcées pour les nanocomposites avec des quantités plus élevées de PA-g-CNC et des temps d'exposition déterminées, comme indiqué par le gonflement des nanocomposites et les essais de traction dans des conditions sèches et humides.

En ce qui concerne les CNF, elles peuvent être utilisées comme un système de support puis de relargage de molécules actifs en raison de la structure nanoporeuse qui se forme pendant la fabrication de films de CNF (aussi appelé nanopapier), mais aussi grâce à la réactivité générale ou aux propriétés d'adsorption de la surface des nanocelluloses. Récemment, ces propriétés ont permis aux films CNF de devenir un matériau très intéressant pour les chercheurs dans les systèmes de libération de médicaments. La structure nanoporeuse peut être employée pour piéger des particules, des protéines ou des molécules qui peuvent ensuite être relarguées. Depuis les années 2010, les usages les plus courants du CNF en tant que support moléculaire actif concernent les systèmes

antibactériens ou la libération de médicaments. À notre connaissance, l'utilisation de CNF pour la libération de protéines modèles, comme la BSA, n'a pas été étudiée précédemment. La seule utilisation déclarée de BSA avec la nanocellulose a été menée par Müller et al. En 2012 avec des aérogels de nanocellulose bactérienne. Il a été démontré que la libération de BSA à partir d'aérogels de BCN dépendait d'une variété de facteurs, tels que: la température, le pH, la concentration de BSA, les conditions de pré-gonflement et les processus de séchage. La BCN qui a été lyophilisée avait une capacité inférieure pour l'absorption de BSA dans la solution en raison des changements morphologiques qui se produisent pendant la lyophilisation [20].

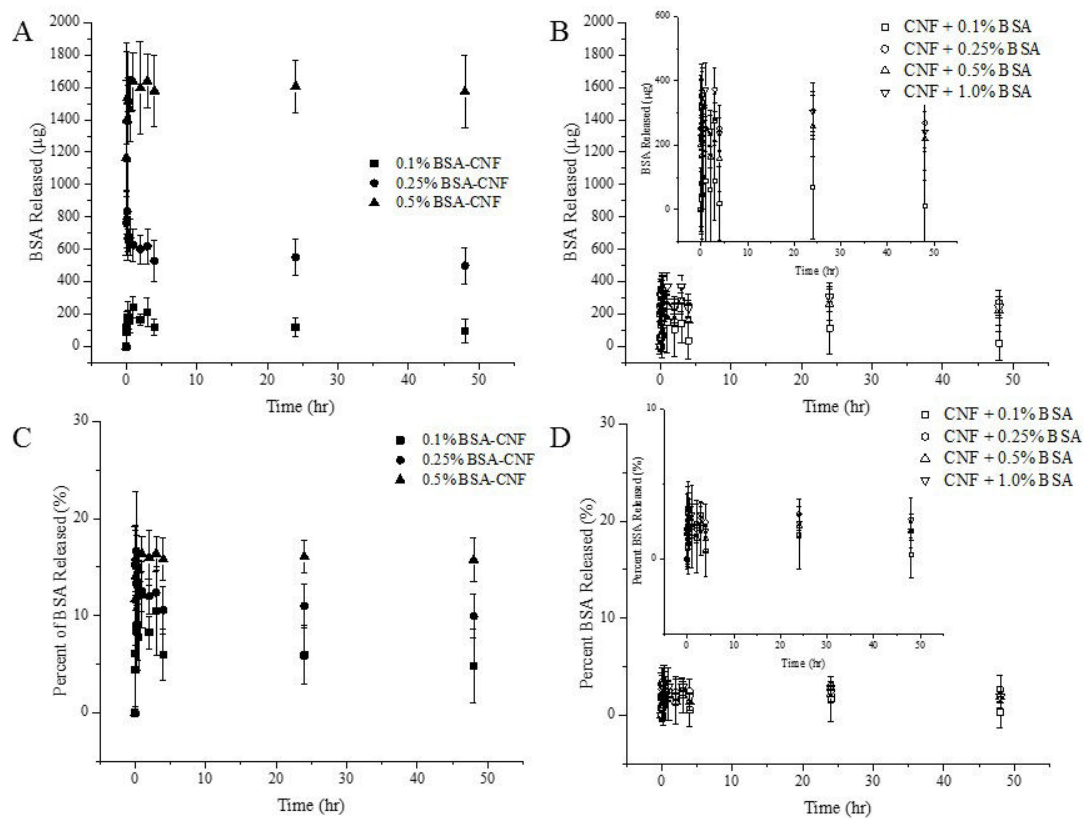


Figure 7. Libération de BSA de CNF en A, B) microgrammes, C, D) pourcentage de CNF ajouté pour A, C) Composés BSA-CNF et B, D) BSA ajoutée par diffusion pendant 48 heures dans du PBS à 37 ° C tel que déterminé par un dosage de l'acide bicinchoninique

Au **chapitre 3.3**, la BSA a été incorporée dans des films de CNF à travers deux méthodes de fabrication différentes : diffusion ou incorporation. Les films de CNF avec ou sans BSA ont été caractérisés pour déterminer leur perméabilité à la vapeur d'eau, ce qui pourrait affecter la libération de BSA. L'impact de l'incorporation de BSA sur la formation des nanocomposites a été caractérisé par microscopie électronique à balayage (MEB) et spectroscopie infrarouge à transformée de Fourier (FTIR). La libération de BSA a été effectuée pendant 48 heures dans du PBS et à la

température physiologique. Il a été démontré que le profil de libération de BSA de CNF dépend de la technique d'incorporation et la quantité de BSA ajoutée. Cette étude a été réalisée en raison de l'utilisation potentielle d'un système mélangeant des CNF et des facteurs de croissance (proche de la BSA) dans de futures expériences de culture cellulaire afin d'influencer la différenciation cellulaire.

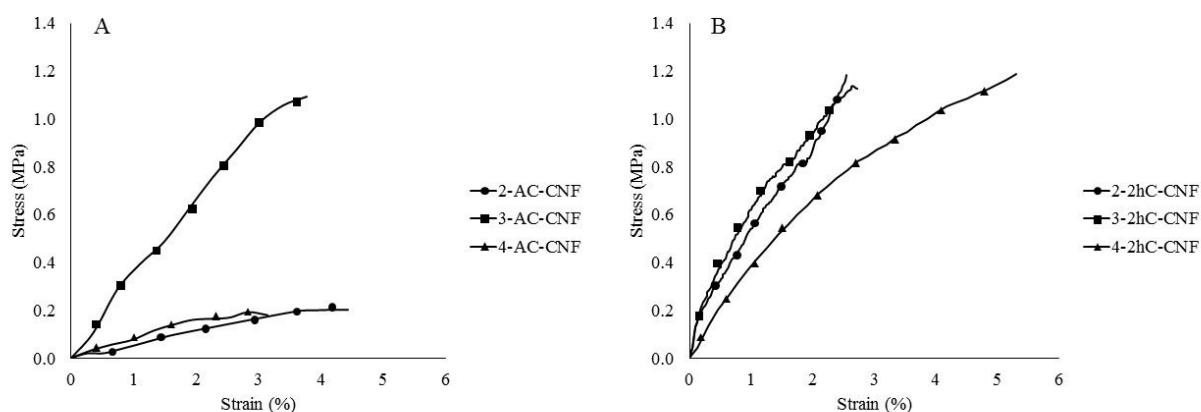


Figure 8. Essai de contrainte de contrainte de (A) films AC-CNF et (B) films 2hC-CNF en conditions aqueuses dans du PBS à 37 ° C.

Le **chapitre 3.4** explore l'effet du liquide sur les propriétés mécaniques des films CNF ayant un grammage différent et une étape de séchage supplémentaire favorisant la réticulation par hornification de la cellulose. Il a été démontré que dans des conditions qui imitent les conditions physiologiques (c'est-à-dire dans le PBS à 37 ° C), le module d'Young et le module de stockage peuvent varier en fonctions des échantillons. Certains nanopapiers présentent une augmentation de E de 6 à 90 MPa après un séchage à 150 ° C. Avec une teneur accrue en fibres, il existe une tendance à la diminution des propriétés mécaniques dans les essais de traction et l'analyse mécanique dynamique. Ceci peut être attribué à une modification possible des liaisons hydrogène une fois exposées à un liquide comme le PBS. Il est suggéré que les propriétés mécaniques du CNF à l'état liquide peuvent être facilement réglées en ce qui concerne le module de Young et le module de stockage, ce qui pourrait être utile pour la culture de cellules souches.

- Le **chapitre 4**, intitulé « L'influence des nanocelluloses sur le comportement des cellules souches dans la culture », explore l'utilisation des nanocelluloses sur la viabilité et l'adhésion des cellules souches mésenchymateuses (MSC). Cette interaction est particulièrement importante avec les MSC car leur culture dépende de l'ancrage et elles subissent une mort cellulaire programmée si elles ne s'attachent pas à une surface de biomatériau [21, 22]. L'attachement des MSC se produit lorsque la

cellule réorganise les filaments d'actine du cytosquelette dans filopodia pour adhérer à la surface [22, 23]. Cette adhésion peut être influencée par les propriétés du biomatériau telles que la topographie des matériaux [21, 23, 24], la chimie de surface [25], et surtout dans ce cas, les propriétés mécaniques [4, 22]. La base de ce travail était de déterminer si les substrats de nanocelluloses mécaniquement adaptables (décrit précédemment) pouvaient influencer le comportement des cellules souches. Ce concept a d'abord été proposé avec l'utilisation d'un polymère différent par Engler et al, qui a déclaré que les propriétés mécaniques d'un biomatériau pourraient influencer la différenciation des cellules souches sans d'autres facteurs externes [4]. Cette constatation a été la base de la thèse pour déterminer si les substrats des nanocelluloses mécaniquement adaptables pourraient influencer les cellules souches d'une manière similaire.

Au **chapitre 4.1**, les nanocomposites d'alginate qui ont été largement caractérisés au **chapitre 3.1**, ont été analysés pour leur effet sur l'adhésion et la viabilité des MSC. La fixation de MSC à la surface est un point important dans les systèmes à base d'alginate parce que l'alginate n'est pas un matériau favorable à l'adhésion MSC car sa nature hydrophile empêche généralement le dépôt de protéines sur la surface [26]. Il est bien connu des chercheurs que lorsque les MSC sont cultivés en présence d'alginate dans un système 2D, les cellules forment des grappes, ce qui n'est pas une morphologie favorable pour leur prolifération et viabilité [27]. Comme il a été démontré que l'addition de CNC ou de CNC-T peut améliorer les propriétés mécaniques de l'alginate dans un système physiologique (**chapitre 3.1**), on a émis l'hypothèse que les nanocomposites pourraient améliorer l'adhérence et la viabilité des MSC. L'adhésion des MSC après 6 et 24 heures est proportionnelle à la quantité de CNC ajoutée à l'alginate dans les conditions de culture cellulaire, mesurée par la surface cellulaire, le rapport d'aspect de la cellule, et aussi la fraction de surface des cellules adhérant à la surface de culture comme on le voit sur la Figure 8. La viabilité des MSC D1 / BALBc a été évaluée pendant 24 et 48 heures, et il a été démontré que la viabilité variait de manière significative, avec des niveaux plus élevés pour les nanocomposites avec des CNC non modifiés. Ces résultats suggèrent que l'addition de CNC ou CNC-T peut affecter le comportement du MSC dans la culture cellulaire et que les composites CNC-Alginate et CNC-T-Alginate sont des matériaux prometteurs pour de futures études cellulaires.

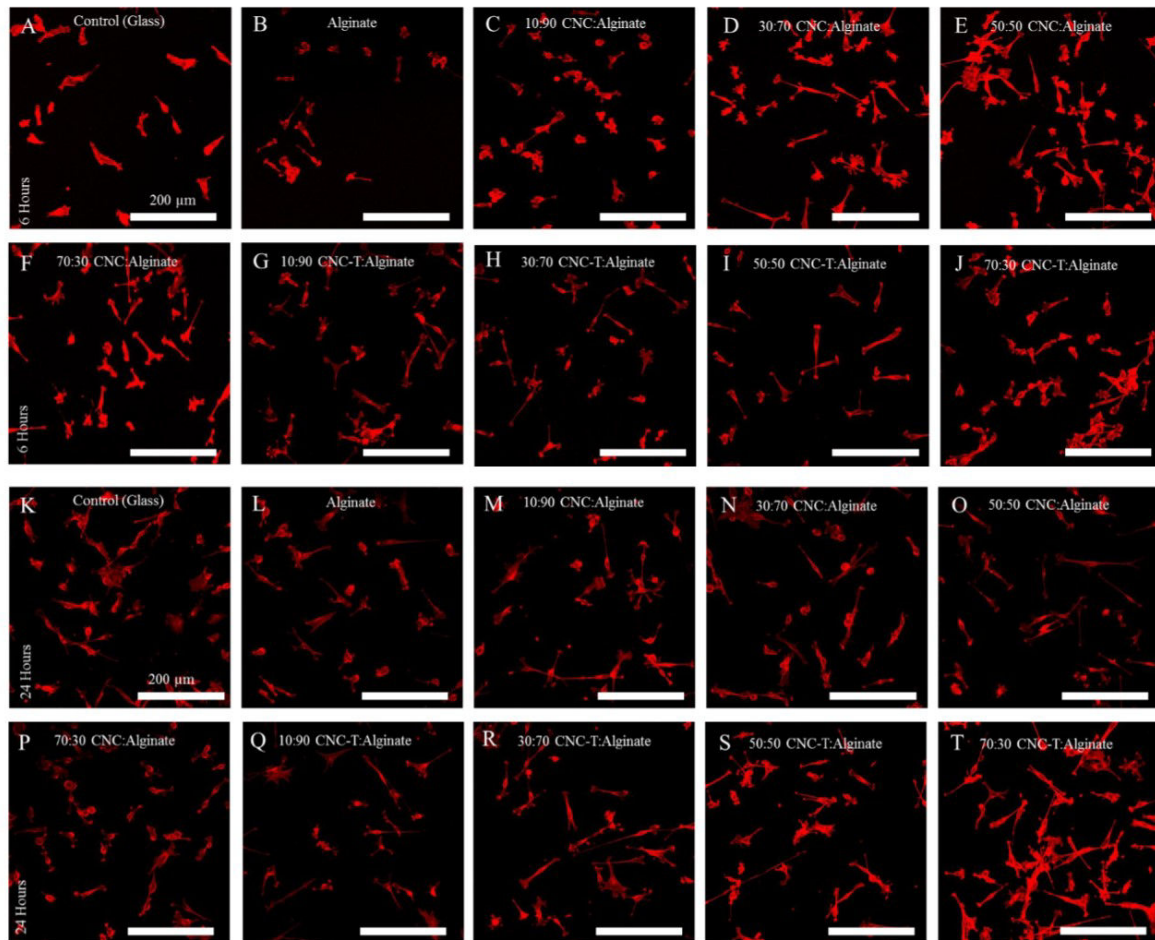


Figure 9. Images microscopiques confocales des MSC D1 colorées pour l'actine ensemencée sur A, K) Contrôle (verre) B, L) Alginate, C, M) 10:90 CNC: Alginate, D, N) 30:90 CNC: Alginate, E, O) 50:50 CNC: Alginate, F, P) 70:30 CNC: Alginate, G, Q) 10:90 CNC-T: Alginate, H, R) 30:70 CNC-T: Alginate, I, S) 50:50 CNC-T: Alginate, et J, T) 70:30 CNC-T: Alginate à A) à 6h et K) à 24h post-ensemencement avec une barre d'échelle de 200 μm .

Pour l'utilisation du CNF en tant que biomatériau, une approche différente du système d'alginate a été utilisée et décrit au **chapitre 4.2**. Les substrats nanostructurés CNF minces ont été fabriqués par différents procédés avec une rugosité variable, le module d'Young, la porosité et le gonflement. Les propriétés des films CNF en liquide dépendaient fortement du durcissement lors du séchage à 150 °C.

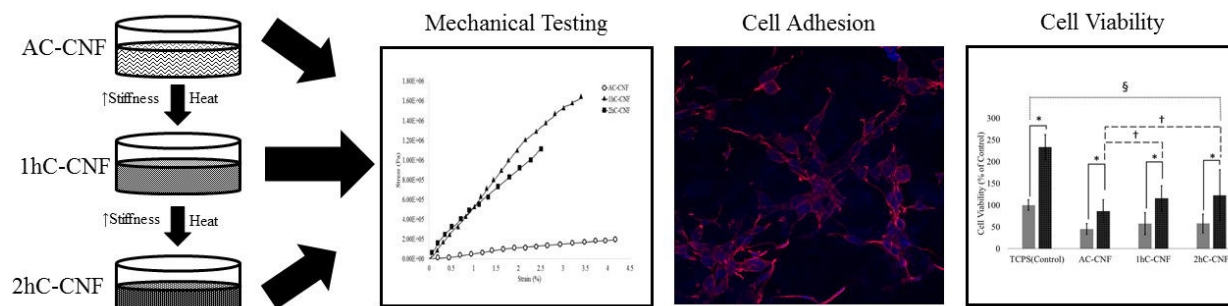


Figure 10. Représentation schématique de la fabrication et de la caractérisation du substrat du CNF à utiliser dans la culture cellulaire

Avec une exposition accrue à la chaleur, la porosité a diminué et le module d'Young a nettement augmenté lorsqu'il a été testé dans un état aqueux. Ces changements de propriétés matérielles ont été testés pour déterminer s'ils peuvent influencer l'adhésion et la viabilité des cellules souches. Il a été montré que la viabilité et l'adhérence du MSC dépendaient du matériau CNF et des propriétés mécaniques avec des différences significatives signalées, en particulier dans le cas de substrats CNF à propriétés mécaniques élevées. Ces résultats suggèrent que l'ajustement du matériau nanocellulose et des propriétés mécaniques sans modification chimique peut fortement affecter la viabilité du MSC et l'adhésion en culture. Ce résultat est considéré comme le plus innovant de nos travaux.

La recherche présentée dans cette thèse montre donc que les nanocelluloses, à la fois CNC et CNF, sont des matériaux appropriés pour les applications biomédicales avec la caractérisation et la mise en œuvre des nanocelluloses de diverses manières: en partant de la production de CNC, en utilisant des films CNF comme supports actifs, en créant une adaptation mécanique des nanocomposites de CNC-alginate dans des conditions physiologiques.

Les principaux résultats montrent que les matériaux à base de nanocelluloses, qui ont été largement caractérisés en conditions physiologiques liquides, peuvent être mécaniquement modifiés par un processus de séchage ou réticulation et induire ainsi des différences dans l'adhérence et la viabilité des cellules souches. Ces résultats seront à la base de recherches futures sur la différenciation des cellules souches et prouvent que les nanocelluloses sont des matériaux novateurs dans l'ingénierie tissulaire.

Références

- [1] Vert M, Hellwich K-H, Hess M, Hodge P, Kubisa P, Rinaudo M, et al. Terminology for biorelated polymers and applications (IUPAC Recommendations 2012). *Pure and Applied Chemistry*. 2012;84:377-410.
- [2] Black J, Hastings G. *Handbook of biomaterial properties*: Springer Science & Business Media; 2013.
- [3] Palsson BØ, Bhatia SN. *Tissue Engineering*: Pearson Education; 2004.
- [4] Engler AJ, Sen S, Sweeney HL, Discher DE. Matrix elasticity directs stem cell lineage specification. *Cell*. 2006;126:677-89.
- [5] Tec21.
- [6] Jorfi M, Foster EJ. Recent advances in nanocellulose for biomedical applications. *Journal of Applied Polymer Science*. 2015;132:41719.
- [7] Lin N, Dufresne A. Nanocellulose in biomedicine: Current status and future prospect. *European Polymer Journal*. 2014;59:302-25.
- [8] Domingues RM, Gomes ME, Reis RL. The potential of cellulose nanocrystals in tissue engineering strategies. *Biomacromolecules*. 2014;15:2327-46.
- [9] Urruzola I, Robles E, Serrano L, Labidi J. Nanopaper from almond (*Prunus dulcis*) shell. *Cellulose*. 2014;21:1619-29.
- [10] Klemm D, Schumann D, Kramer F, Heßler N, Koth D, Sultanova B. Nanocellulose materials—Different cellulose, different functionality. *Macromolecular symposia*: Wiley Online Library; 2009. p. 60-71.
- [11] Gatenholm P, Klemm D. Bacterial nanocellulose as a renewable material for biomedical applications. *MRS Bulletin*. 2010;35:208-13.
- [12] Dufresne A. Nanocellulose: a new ageless bionanomaterial. *Materials Today*. 2013;16:220-7.
- [13] Zhou C, Shi Q, Guo W, Terrell L, Qureshi AT, Hayes DJ, et al. Electrospun Bio-Nanocomposite Scaffolds for Bone Tissue Engineering by Cellulose Nanocrystals Reinforcing Maleic Anhydride Grafted PLA. *ACS Applied Materials & Interfaces*. 2013;5:3847-54.
- [14] Lou YR, Kanninen L, Kuisma T, Niklander J, Noon LA, Burks D, et al. The use of nanofibrillar cellulose hydrogel as a flexible three-dimensional model to culture human pluripotent stem cells. *Stem Cells Dev*. 2014;23:380-92.
- [15] Bras J, Viet D, Bruzzese C, Dufresne A. Correlation between stiffness of sheets prepared from cellulose whiskers and nanoparticles dimensions. *Carbohydrate Polymers*. 2011;84:211-5.
- [16] Padgitt M, et al. . Production practices for major crops in US agriculture, 1990-97. *Growth*. 2000.

- [17] Gogerty R. Crop leftovers: More uses, more value. *Resource: Engineering & Technology for Sustainable World*. 1996;3:6-9.
- [18] Sacui IA, Nieuwendaal RC, Burnett DJ, Stranick SJ, Jorfi M, Weder C, et al. Comparison of the properties of cellulose nanocrystals and cellulose nanofibrils isolated from bacteria, tunicate, and wood processed using acid, enzymatic, mechanical, and oxidative methods. *ACS Applied Materials & Interfaces*. 2014;6:6127-38.
- [19] Espino-Perez E, Domenek S, Belgacem N, Sillard C, Bras J. Green process for chemical functionalization of nanocellulose with carboxylic acids. *Biomacromolecules*. 2014;15:4551-60.
- [20] Müller A, Ni Z, Hessler N, Wesarg F, Müller FA, Kralisch D, et al. The biopolymer bacterial nanocellulose as drug delivery system: investigation of drug loading and release using the model protein albumin. *Journal of Pharmaceutical Sciences*. 2013;102:579-92.
- [21] Dalby MJ, Gadegaard N, Oreffo RO. Harnessing nanotopography and integrin-matrix interactions to influence stem cell fate. *Nature materials*. 2014;13:558-69.
- [22] Discher DE, Janmey P, Wang YL. Tissue cells feel and respond to the stiffness of their substrate. *Science*. 2005;310:1139-43.
- [23] Dalby MJ, Gadegaard N, Tare R, Andar A, Riehle MO, Herzyk P, et al. The control of human mesenchymal cell differentiation using nanoscale symmetry and disorder. *Nature materials*. 2007;6:997-1003.
- [24] Dalby MJ, Gadegaard N, Riehle MO, Wilkinson CD, Curtis AS. Investigating filopodia sensing using arrays of defined nano-pits down to 35 nm diameter in size. *The international journal of biochemistry & cell biology*. 2004;36:2005-15.
- [25] Anderson HJ, Sahoo JK, Ulijn RV, Dalby MJ. Mesenchymal Stem Cell Fate: Applying Biomaterials for Control of Stem Cell Behavior. *Frontiers in Bioengineering and Biotechnology*. 2016;4.
- [26] Yagi K, Tsuda K, Serada M, Yamada C, Kondoh A, Miura Y. Rapid formation of multicellular spheroids of adult rat hepatocytes by rotation culture and their immobilization within calcium alginate. *Artificial organs*. 1993;17:929-34.
- [27] Rowley JA, Madlambayan G, Mooney DJ. Alginate hydrogels as synthetic extracellular matrix materials. *Biomaterials*. 1999;20:45-53.

Comparison of cellulose nanocrystals properties extracted from agricultural residues

Smyth Megan^{1,2}, Pereira Novo Lísias^{1,2,3}, García Araceli^{1,2,4}, Bras Julien^{1,2}

1. CNRS, LGP2, 461 Rue de la Papeterie, 38402, Saint-Martin-d'Hères, France

2. Univ. Grenoble Alpes, LGP2, 38000 Grenoble, France

3. Univ. de São Paulo, Departamento de Física-química, Instituto de Química de São Carlos, Av. Trabalhador São Carlense 400, 13560-970, São Carlos, São Paulo, Brazil

4. Univ. of the Basque Country UPV/EHU, Department of Chemical and Environmental Engineering, Plaza Europa, 1, 20018 Donostia-San Sebastián, Spain

Abstract: Cellulose nanocrystals (NCCs) have long been an interest of researchers because of their exceptional mechanical properties as well as being sourced from natural, inexpensive, and renewable materials. In this work, NCCs were obtained from four different agricultural residues, maize (*Zea mays*) husk, bean (*Phaseolus vulgaris*) shell, and sugarcane (*Saccharum officinarum*) bagasse core and bark. These materials are common waste products from agricultural production in different parts of the world, and of potential value if NCCs with advantageous properties are extracted from them. For example, maize husk is a major agricultural waste in the United States and is used for erosion prevention, [1] or to produce insulating materials, paper, and other chemicals [2]. Dried materials were alkali treated, bleached, and hydrolyzed to NCCs using sulfuric acid. The extracted NCCs from each source were characterized by atomic force microscopy (AFM), dynamic light scattering (DLS), conductometry, thermal gravimetric analysis (TGA), and x-ray powder diffraction (XRD). The morphology, surface charge, thermal stability, and crystallinity were measured and compared for NCCs acquired from each material. As result, NCCs with different properties were obtained from agricultural residues. Maize husks provided high aspect ratio type I NCCs whereas sugarcane produces small type II NCCs. This study could provide assistance for selecting the best raw materials for NCC production from agricultural residues.

MATERIALS & METHODS



Figure 1. Dried material before mercerization, bleaching, and hydrolysis. A) maize husk, B) bean shell, C) Bagasse bark, and D) Bagasse core

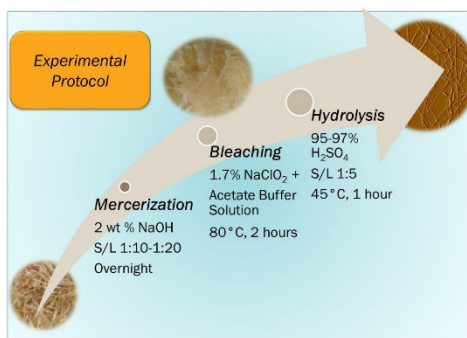


Figure 2. Schematic of experimental protocol of NCC production

Characterization Technique	Specifications
Dynamic Light Scattering (DLS)	Dynamic Light Scattering to determine the size of the nanoparticles was carried out using a Vasco Particle Size Meter (Coultron Technologies, Pessac, France). Ten measurements with 60 time step and a noise ratio of 1.06 were carried out for each sample in triplicate.
Atomic Force Microscopy (AFM)	Images were acquired using tapping mode with a Nanoscope IIIA microscope from Veeco Instruments (Plainville, New York, USA) at a frequency of ~265-340 Hz. Silicon cantilevers with a curvature of 10-15 nm were used (OTESPAH, Bruker, Billerica, Massachusetts, USA).
Conductometry	Sulfate groups content in NCCs were determined by classical conductometric titration [3], using a conductivity meter (Ithome Scientific Orion 4 star) and a calibrated conductivity cell (Orion U13005MD).
X-Ray Diffraction (XRD)	The XRD diffractogram patterns were recorded on a PW 1720 X-ray generator (Philips) operated at 45 kV and 40 mA with Cu K α radiation ($\lambda = 0.154$ nm) in the range $2\theta = 5 - 50^\circ$ with a fixed step interval. The crystallinity index was calculated according to the equation proposed by Segal et al. [4] as the ratio between the interference of the (200) crystal planes subtracted by the amorphous contribution and the total peak height of the (200) crystal planes.
Thermogravimetric Analysis (TGA)	Thermogravimetric measurements were performed with a Perkin Elmer STA 6000 (Waltham, Massachusetts, USA) (the temperature ranged from 30 °C to 500 °C with a heating rate of 10 °C/min). The tests were carried out under air (20 mL/min) for comparison of thermogravimetric degradation. All results were analyzed with Pyris Software (Perkin Elmer, Waltham, Massachusetts, USA).

RESULTS & DISCUSSION

	DLS Dimensions (Z_{avg}) (nm)	AFM Dimensions (L x W) (nm)	Sulfate Content (mol/g)	Crystallinity Index (%)	Max. Degradation Temperature (°C)
Comm. NCC	271	168 \pm 16 x 24 \pm 2	2.06E-06	78.6	356.7
Maize Husk	388	937 \pm 66 x 6 \pm 0.2	1.01E-06	59.5	405.3
Bean Shell	291	171 \pm 64 x 136 \pm 45	1.20E-07	28.8	482.3
Bagasse Bark	185	80 \pm 46 x 63 \pm 39	2.65E-06	35.8	287.7
Bagasse Core	286	101 \pm 41 x 11 \pm 5	9.57E-07	44.0	368.1

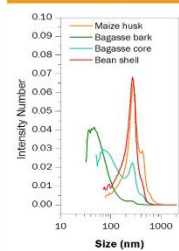


Figure 3. Dynamic light scattering measurements of maize husk, bean shell, bagasse bark, and bagasse core.

Morphology
As seen in the AFM images (Figure 3), bagasse core exhibits the most traditional, rod-like NCC shape. While bean shell and Bagasse bark NCCs are small and spherical. Maize husk NCCs are thin, long, and have a high aspect ratio. This high aspect ratio can be attractive for applications that currently use tunicate derived NCCs. DLS measurements (Figure 4) indicate that Bagasse bark NCCs have the lowest diameter and can be confirmed by AFM. Other DLS measurements can not be confirmed because of the nonspherical shape of the NCCs.

Conductometry

Sulfuric acid hydrolysis extraction of cellulose nanocrystals causes sulfate groups ($-SO_3^-$) to be on the surface of the crystals. The charge density of $-SO_3^-$ groups varied between the materials (see Table) with bean shell having the least amount of sulfate groups imparted on the surface, and bagasse bark with the most. This variance in charge density can be attributed to the source material since hydrolysis conditions were consistent between samples.

Thermal stability of these residues are of interest because of potential melt-processing applications of cellulose nanocrystals. As shown in the thermogravimetric analysis of the NCCs derived from agricultural residue (Figure 6), bean shell residues have the highest maximum temperature of degradation, while Bagasse bark has the lowest with 297.7 °C. The weight loss observed below 100 °C can be contributed to the presence of residual water in the samples. Two weight loss events occurred in these samples, which is indicative of samples treated with sulfuric acid, and have beginning degradation temperatures lower than pure cellulose.



Figure 4. AFM images of NCCs isolated by acid hydrolysis

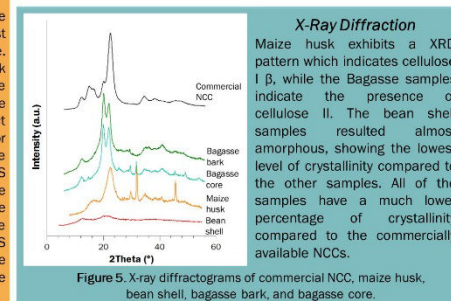


Figure 5. X-ray diffractograms of commercial NCC, maize husk, bean shell, bagasse bark, and bagasse core.

Thermogravimetric Analysis

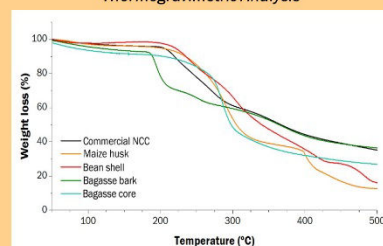


Figure 6. Thermograms of commercial NCC, maize husk, bean shell, bagasse bark, and bagasse core.

CONCLUSIONS & PERSPECTIVES

In this work we have presented the properties of nanocellulose crystals derived from four different agricultural residue sources. It has been shown that depending on the source the properties can differ immensely. This difference in properties can be advantageous depending on what property researchers want to exploit.

- Maize husk NCCs are long, thin with a high aspect ratio, cellulose I β crystallinity patterns, and relative thermal stability
- Bagasse bark and bean shell NCCs exhibit some NCC degradation as shown in the AFM images and low crystallinity
- A mixture of degraded cellulose and NCCs were derived from Bagasse core and displayed the highest amount of added sulfate groups.

Further investigation is needed in order to optimize the conditions for NCCs isolation from each agricultural residue to prevent cellulose degradation.

References

1. Padgett, M., et al., "Production practices for major crops in US agriculture, 1990-97. Growth, 2000.
2. Gogerty, J., et al., "Crop leftovers: More uses, more value." Resource Engineering & Technology for Sustainable World 3 (1) (1996): 6-9.
3. Romdhane, A., et al., Effect of pH and ionic strength on the electrical charge and particle size distribution of starch nanocrystal suspensions. Starch (2013) 64 (3-4): 319-327.
4. Segal, L., et al., An Empirical Method for Estimating the Degree of Crystallinity of Native Cellulose Using the X-Ray Diffractometer. Text. Res. J. (1959); 29 (10): 786-794.

Acknowledgements

XRD measurements were conducted by Thierry Encheas at Grenoble INP - CMIC. LGP2 is part of the LabEx Tec 21 (Investissements d'Avenir - grant agreement n°ANR-11-LABX-0030) and of the Energies du Futur and PolyNat Carnot Institutes (Investissements d'Avenir - grant agreements n°ANR-11-CARN-007-01 and ANR-11-CARN-030-01). This work was partially supported by the LabEx Tec 21 (Investissements d'Avenir - grant agreement n°ANR-11-LABX-0030). The authors would like to thank Fundação de Amparo à Pesquisa do Estado de São Paulo (FAPESP) and the Basque Government (Research Development Program) for providing scholarships to the researchers involved.

LGP2, 461 rue de la papeterie, CS10065,
38402 Saint-Martin-d'Hères
<http://pagora.grenoble-inp.fr/recherche/>



Email: Megan.Smyth@lgp2.grenoble-inp.fr

Tuning of Mechanical Properties of Cellulose Nanofiber Films for Cell Culture

Megan Smyth^{1,2}, Carole Fournier³, Carlos Driemeier⁴, Catherine Picart³, Johan Foster⁵, and Julien Bras^{1,2}

1. CNRS, LGP2, 461 Rue de la Papeterie, 38402, Saint-Martin-d'Hères, France

2. Université Grenoble Alpes, LGP2, 38000 Grenoble, France

3. CNRS, UMR 5628, LMGP, 38016 Grenoble, France

4. Laboratório Nacional de Ciência e Tecnologia do Biotecnológico - CTBE, Campinas, São Paulo 13083-970, Brazil

5. Virginia Tech, Department of Materials Science & Engineering, Blacksburg, VA 24061, USA

Abstract: Stem cells are a natural part of the human body's regenerative processes, having the capability to self-renew and differentiate into many different types of tissue, depending on their environment. The mechanical properties (e.g. stiffness and texture) of the cell culture substrate have important implications on proliferation, migration, apoptosis, and differentiation during cell growth. Meanwhile, nanocellulose appears to be a next generation biofriendly high-value added product. Cellulose nanofibers (CNF) differs from the other forms of nanocellulose because of the differences in morphology, crystallinity, and mechanical properties compared to cellulose nanocrystals^{1,2}. Previous studies using CNF in biomedical applications focused on CNF hydrogels or scaffolds for tissue engineering applications^{3,6}. The aim of this study is to modulate various material properties of thin CNF films without chemical modification, and to study these changes in conditions necessary for cell culture. The effect of these changes on the viability, cell surface area, and cell aspect ratio of mesenchymal stem cells will be presented.

Materials & Methods

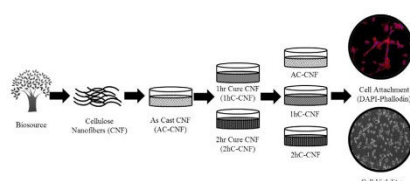


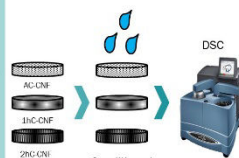
Figure 1. Schematic of the experimental set-up. From raw material of CNF suspension to CNF films and sequential curing of films and eventual cellular testing of CNF films for cell attachment and viability

CNF films were solvent casted from a 1 % wt solution of CNF at ambient conditions for 5 days (AC-CNF) followed by curing at 150 °C for 1 hour (1hC-CNF) or 2 hours (2hC-CNF). These samples underwent material property characterization (SEM, Thermoporometry, Tensile Testing) and cell adhesion and viability of BALB/c D1 murine mesenchymal stem cells. Cells were seeded at a density of 20,000 cells/cm² for 6 and 24 hours for DAPI/Phalloidin staining and 24 and 48 hours for MTT viability assay.

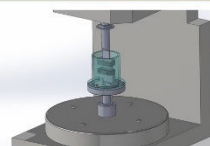
Material Characterization Techniques

Thermoporometry

To determine the porosity of the CNF films that are similar to cell culture conditions thermoporometry was employed. This technique measures the pore size in an aqueous state by differential scanning calorimetry from -70 °C to 5 °C after submerging the CNF films in DI H₂O in 24 hours. The pore size is measured by determining the freezing bound water (g/g).



Aqueous Tensile Testing



Experimental Conditions

- Height: ≈10 mm
- Width: ≈5 mm
- Rate: 0.001 mm/s

To mimic cell culture conditions, mechanical testing was done in phosphate buffer solution (PBS) at physiological temperature (37 °C). Samples were conditioned for 24 hours in PBS at 37 °C prior to testing.

Results & Discussion

Tuning of Material Properties

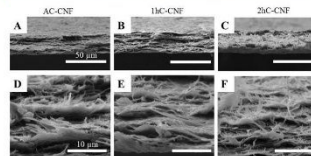


Figure 2. SEM images of the thickness A,D) AC-CNF, B,E) 1hC-CNF, and C,F) 2hC-CNF

There is apparent layer formation for each sample and porosity between the samples with less pores present in 2hC-CNF. These images in coordination with the results obtained from thermoporometry support the conclusion that an additional curing step at 150 °C causes the material properties to change.

Thermoporometry

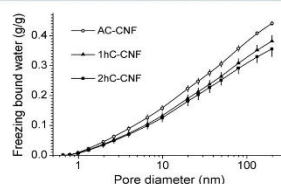


Figure 3. The amount of freezing bound water (g/g) vs. of pore diameter (nm) as measured by thermoporometry for CNF films.

Figure 3 shows that the CNF substrate with no curing (AC-CNF) has a higher number of pores with diameter above 10 compared to 1hC-CNF and 2hC-CNF when tested by thermoporometry. It can be said that with increased curing the amount of pores within the CNF sample decreases.

Aqueous Tensile Testing

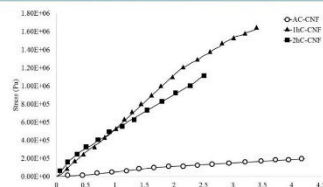


Figure 4. Stress-Strain curves for CNF films tested in phosphate buffer solution at 37 °C. The films were either tested as casted (AC-CNF) or after curing (1hC-CNF, 2hC-CNF).

With increased curing time the Young's modulus of the sample increased (2hC-CNF > 1hC-CNF > AC-CNF), while elongation at break decreased. These results are concurrent with the results reported with the SEM and thermoporometry; that increased curing changes the material properties of the CNF in dry and physiological conditions.

Effect of Material Properties on Cell Adhesion and Viability

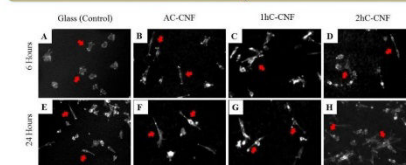


Figure 5. Fluorescent microscopy images of BALB/c D1 murine cells stained for actin seeded on A,E) PS, B,F) AC-CNF, C,G) 1hC-CNF, and D,H) 2hC-CNF 6h and 24h post-seeding. Cell surface area and aspect ratio was determined using these images and ImageJ and are reported in the table below.

Sample	Surface Area per Cell (μm ²)		Aspect Ratio per Cell	
	6 Hours	24 Hours	6 Hours	24 Hours
Control (Glass)	406±120	487±207	1.9±0.9	4.4±3.1
AC-CNF*	768±323†	1019±619†	4.6±3.2†	4.8±2.3
1hC-CNF*†	953±503†	616±320	5.0±2.7†	4.0±2.5
2hC-CNF*††	847±367†	858±411†	5.2±2.6†	8.1±4.6†§

Cell surface area and cell aspect ratio measurements for BALB/c D1 cells cultured on CNF films and control as measured by ImageJ for 6 and 24 hours (N=50). *p<0.05 for cell area, cell aspect ratio interaction between substrate and time. †p<0.05 significance between control of same time point and CNF. ‡p<0.05 significance between 6-hour and 24-hour within same CNF substrate for cell area. ††p<0.05 significance between 6-hour and 24-hour within same CNF substrate for cell aspect ratio. §p<0.05 significance between 2hC-CNF and AC-CNF, 1hC-CNF for cell aspect ratio

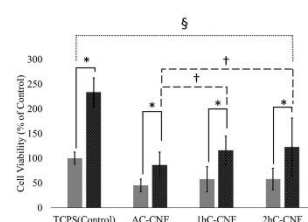


Figure 6. MTT assay results reported in % of control to monitor cell proliferation and viability (after 24h and 48h incubation of 20,000 cells/cm² on PS (Control), AC-CNF, 1hC-CNF, and 2hC-CNF (N=11-17 per group)). *p<0.05 for same substrate between 24 and 48 hours, †p<0.05 for same time point of 48 hours and different substrates. §p<0.05 control vs cellulose substrates at 24 hours, and control vs cellulose substrates at 48 hours.

Conclusions & Perspectives

Conclusions

- The material properties of CNF films can be easily changed without any chemical modification by a simple curing step at 150 °C
- With increased curing time the porosity of the CNF films decreases, while the Young's modulus increases as measured in an aqueous state
- With the changes in material properties the cell shape and adhesion changes with significant differences reported between CNF substrates
- There are significant differences in cell viability for murine MSCs cultured for 48 hours on AC-CNF vs. 1hC-CNF and AC-CNF vs. 2hC-CNF with cell viability increasing for 1hC-CNF and 2hC-CNF compared to AC-CNF

Perspectives

- Future studies will determine if CNF substrates with differing mechanical and material properties influence differentiation of MSCs following 7 days in culture

References

1. Sjö, L.; Plackett, D. Microfibrillated cellulose and new nanocomposite materials: a review. *Cellulose* **2010**, *17* (3), 459-494.
2. Lavoie, N.; Desjardins, I.; Dufresne, A.; Bras, J. Microfibrillated cellulose - Its barrier properties and applications in cellulosic materials: a review. *Carbohydr Polym* **2012**, *90* (2), 735-64.
3. Xing, Q.; Zhao, F.; Chen, S.; Mehmanna, I.; Decker, M. A.; Luby, Y. M. Porous biocompatible three dimensional scaffolds of cellulose microfibril/polymer composites for cell culture. *Acta Biomater* **2010**, *6* (6), 2152-2159.
4. Lou, Y. R.; Kanninen, L.; Kusama, T.; Nikander, J.; Noon, L. A.; Burks, D.; Urttilä, A.; Yliperttula, M. The use of nanofibrillar cellulose hydrogel as a flexible three-dimensional model to culture human pluripotent stem cells. *Stem Cells* **2014**, *32* (4), 580-592.
5. Bhattacharya, M.; Mäkelä, M. M.; Lauren, P.; Lou, Y. R.; Kusama, S. W.; Kanninen, L.; Lalle, M.; Corlu, A.; Guo, Z.; Guller, C.; Nikula, O.; Laakkonen, A.; Urttilä, A.; Yliperttula, M. Nanofibrillar cellulose hydrogel promotes three-dimensional liver cell culture. *J Control Release* **2012**, *154* (2), 292-8.
6. Sørensen, K.; Petersen, S. R.; Dräger, K.; Chinga-Carrasco, G. Controlling the elastic modulus of cellulose nanofiber hydrogels—scaffolds with potential in tissue engineering. *Cellulose* **2015**, *22* (1), 473-481.

Acknowledgements

LGP2 is part of the Lab'X Tec 21 (Investissements d'Avenir - grant agreement n°ANR-11-LABX-0030) and of the Fingéris du Futur and PolyMat Carot Institutes (Investissements d'Avenir - grant agreements n°ANR-11-CARR-007-01 and ANR-11-CARR-003-01). This work has been partially supported by the Lab'X Tec 21 (Investissements d'Avenir - grant agreement n°ANR-11-LABX-0030).



LGP2, 461 rue de la papeterie,
CS10065, 38402 Saint-Martin-
d'Hères, France
<http://pagora.grenoble-inp.fr/recherche/>



Email: Megan.Smyth@lgp2.grenoble-inp.fr